3-18-2019

The Modern Mississippi: Provenance Indicators and Human Impact

Brittney Anne Gregory
Louisiana State University and Agricultural and Mechanical College

THE MODERN MISSISSIPPI: PROVENANCE INDICATORS AND HUMAN IMPACT

A Dissertation

Submitted to the Graduate Faculty of the
Louisiana State University and
Agricultural and Mechanical College
in partial fulfillment of the
requirements for the degree of
Doctor of Philosophy

in

The Department of Geology and Geophysics

by
Brittney Anne Gregory
M.S. University of North Texas 2011
B.A. University of North Texas 2006
May 2019

ACKNOWLEDGEMENTS

I would like to thank all of my advisors as well as friends and family, without which this degree would not have been possible. I also want to thank my daughter for keeping me company during the final writing process. Special consideration to the McCord Chair in an effort to fund many key analyses essential to this project. I would also like to show appreciation for the Coastal Institute Fellowship and Moffet Scholarships for financial academic support throughout this process.

TABLE OF CONTENTS

ABSTRACT

Given the significant degree to which the modern Mississippi River and its tributaries have been altered through dams, levees, and diversions, it is important to understand how sediment is transported from source to sink. The objective of this dissertation is to explore how the modern Mississippi River transports sediment from its tributaries to its delta using three independent proxies. Provenance indicators have traditionally been an effective way with which to characterize sediment transport in large river systems. First, detrital U-Pb zircon dating is used to investigate modern flux and possible anthropogenic influences on coarse-grained sediment within the modern Mississippi River. Overall, results indicate that samples taken from the modern river show regional flux and possible repercussions of the Red River diversion into the Atchafalaya basin. Secondly, apatite geochemistry is used to determine its viability as an independent provenance indicator when used on detrital populations with large samples sizes. In the end, it is concluded that when quantitative analysis is used to enhance variability between samples, these results compare closely with detrital zircon U-Pb spectra. Finally, Nd and Sr samples are evaluated from a core taken within the modern Mississippi River delta. From this data, it is concluded that εNd values from the Mississippi River remain relatively stable until modern human alterations shift the geochemical signature in the top of the core.

CHAPTER 1. INTRODUCTION

1.1 Overview

Rivers are the cornerstones of many geologic sediment transport systems, with drainages that range from small scales to those that cover continents. They erode and weather terranes and transport sediment from source to sink. They carry sediment within suspended or bedload through the river until it is eventually delivered into the marine basin. This transport process can be stalled as sediment is temporarily stored within the floodplain, delta, and sometimes within the river channel itself. Recently, the natural order of this geologic process has been altered due to intensive human engineering projects which have fundamentally changed the dynamics of sediment transport through rivers (Rogers, 2005). In general, the alterations humans have made to the fluvial landscapes in which they live have resulted in dire consequences for floodplain nourishment, delta progradation, beach nourishment, and land subsidence in coastal landscapes (M. D. Blum & Roberts, 2009; Boesch et al., 1994)

The Mississippi River and its tributaries drain 2/3 of the eastern continental United States. For decades, this major fluvial thoroughfare has experienced concentrated artificial engineering, which has profoundly changed the way in which the river transports sediment from its headwaters to the coast. The intensified construction of dams, locks, river control structures, and levees has not only curtailed sediment flux, it has cut the Mississippi River off from its floodplain and deltas. In the case of the Red River, human diversion projects have completely cut off sediment supply from one of the Mississippi's main tributaries to the main trunk and delta.

Recent studies by Blum and Roberts (M. D. Blum & Roberts, 2009) estimate a 60% decrease in sediment flux in the last ~60 years, while Bouche et al. (1994) show a 25% loss of wetland environments within the Mississippi delta. The problem is seen as so dire that

restoration projects in starting the 1990s (culminating in the 2017 a Coastal Master Plan) have been implemented to help curtail loss and damage to coastal wetland environments, making it the first of its kind in the world to address the colossal human-induced changes to coastal Louisiana on the Mississippi Delta. It is because of these problems that this research seeks to understand the modern sediment transport dynamic of the Mississippi River using a suite of provenance indicators to determine the way in which the modern river moves material from source to sink.

Provenance indicators have traditionally been an effective way to characterize sediment transport in large river systems. They can be used in both geologically ancient and modern systems; however, they must follow a few criteria in order to be effective. A provenance indicator must directly represent the bedrock from which it is sourced and it must be relatively robust, i.e., resistant to chemical and physical weathering. Another stipulation for using provenance indicators is that the geologic terrane from which the sediment is sourced must be diverse enough to be able to distinguish source signatures. In this dissertation, zircon, apatite, and Nd-Sr isotopes are used to interpret sediment provenance from in the modern Mississippi River.

Zircon is a robust provenance indicator. It has been shown to be useful in a variety of dynamic continental-scale rivers such as the Pearl River, the Indus River, and a series of ancestral geologic basins (Alizai et al., 2011; Amidon, Burbank, & Gehrels, 2005; Zhao, Shao, & Qiao, 2015). In this study, zircon is used as a provenance tool to better understand how the coarse fraction (63-125 um) of the Mississippi and its tributaries is transported from source to sink. To do this, detrital zircon U-Pb age spectra are analyzed from grab samples taken from each of the main tributaries of the Mississippi River and downstream in the main trunk throughout the river. This creates a downstream sediment contribution map for the Mississippi

and its tributaries, which can be assembled to understand the flux of the sand-sized fraction throughout the system. Given the possible lag of sand sized heavy minerals during fluvial transport, this study seeks to determine not only where the Mississippi River zircon are derived from, but whether or not modern alteration of the catchments has fundamentally changed the U-Pb age spectra of the system. The first chapter explores variability or flux within the modern system by comparing new data with previously dated modern samples (M. Blum & Pecha, 2014). Final tributary contributions are consequently unmixed to determine relative drainage contribution using the DZmix program to determine relative percent contributions of each tributary to the overall system (Sundell & Saylor, 2017).

The second part of this study investigates the viability of apatite Rare Earth Elements (REE) and trace element compositions as a provenance indicator in continental scale drainage systems. While previous studies on generalized source rock type groups and the Paleo-Volga show the promise of using apatite for provenance, this study takes these analyses a step further by introducing quantitative methods to identify both variability and source contribution in the Mississippi River drainage (Belousova, Griffin, O'Reilly, & Fisher, 2002; Morton & Yaxley, 2007). Large detrital samples can often mask data patterns due to the diversity in the sample; however, using smaller sample sizes often does not capture all variability found within samples with extensive geologic range (Pullen, Ibanez-Mejıa, Gehrels, Ibanez-Mejıa, & Pecha, 2014; Vermeesch, 2004). This study uses the Belousova et al. (2002) cladogram and known elements which correlate with apatite fractionation to discriminate between drainage sources. By doing so, we are able to create plots that inherently highlight the diversity between geochemical data for major Mississippi River tributaries. These data are then used in an inverse Monte Carlo to infer

percent contribution from each tributary to the main Mississippi River downstream from its southernmost confluence.

In the final chapter, Nd and Sr isotopes are used to explore shifts in provenance throughout the last 3 thousand years in the Mississippi River delta. A core from the Modern/Plaquemines delta is examined in concurrence with grab samples taken from the modern Mississippi River and its tributaries in an effort to determine if humans have altered the εNd signature of delta sediment, specifically within the last 150 years. Samples from the modern Mississippi and its tributaries were taken to identify general Nd-Sr signatures for different regions of the Mississippi catchment. These values are then applied to samples taken from a 5 m core extracted from the delta, dated with radiocarbon, OSL, and ^{210}Pb along with ^{137}Cs in effort to investigate the variability of Nd through time.

The goal of this dissertation is to explore how the modern Mississippi River transports sediment from its tributaries to its delta using three independent proxies. By using a multi-proxy approach a more comprehensive picture of the Mississippi River and its transport pathways can be drawn and possible anthropogenic influence can be explored. It is important that we study these kind of broad questions given the rapid alterations being made to the fluvial environments in which humans occupy(J. P. M. Syvitski & Kettner, 2011). Given rising populations around the world and the increasing demands for water, hydroelectric power and flood control, human engineered structures are already having a significant global effect on coastal environments. This is especially important in deltas and coastal regions with high population densities. By understanding the modern dynamics of the large modern river systems, it might be possible to curtail or alter the changes to help rescue the disappearance of these coastal environments and communities.

1.2 References Cited

Alizai, A., Carter, A., Clift, P. D., VanLaningham, S., Williams, J. C., & Kumar, R. (2011). Sediment provenance, reworking and transport processes in the Indus River by U-Pb dating of detrital zircon grains. *Global and Planetary Change, 76*, 33-55. doi:doi:10.1016/j.gloplacha.2010.11.008

Amidon, W. H., Burbank, D. W., & Gehrels, G. E. (2005). Construction of detrital mineral populations: insights from mixing of U-Pb zircon ages in Himalayan rivers. *Basin Research, 17*(4), 463-485.

Belousova, E., Griffin, W., O'Reilly, S. Y., & Fisher, N. (2002). Apatite as an indicator mineral for mineral exploration: trace-element compositions and their relationship to host rock type. *Journal of Geochemical Exploration, 76*(1), 45-69.

Blum, M., & Pecha, M. (2014). Mid-Cretaceous to Paleocene North American drainage reorganization from detrital zircons. *Geology*. doi:10.1130/g35513.1

Blum, M. D., & Roberts, H. H. (2009). Drowning of the Mississippi Delta due to insufficient sediment supply and global sea-level rise. *Nature Geoscience, 2*(7), 488-491. doi:10.1038/ngeo553

Boesch, D. F., Josselyn, M. N., Mehta, A. J., Morris, J. T., Nuttle, W. K., Simenstad, C. A., & Swift, D. J. (1994). Scientific assessment of coastal wetland loss, restoration and management in Louisiana. *Journal of Coastal Research*, i-103.

Morton, A., & Yaxley, G. (2007). Detrital apatite geochemistry and its application in provenance studies. *Special Papers-Geological Society of America, 420*, 319.

Pullen, A., Ibanez-Mejıa, M., Gehrels, G. E., Ibanez-Mejıa, J. C., & Pecha, M. (2014). What happens when n¼ 1000? Creating large-n geochronological datasets with LA-ICP-MS for geologic investigations. *Journal of Analytical Atomic Spectrometry, 29*, 971-980. doi:doi:10.1039/c4ja00024b

Rogers, D. (2005). History of the New Orleans flood protection system. *Investigation of the performance of the New Orleans flood protection systems in Hurricane Katrina on August 29*.

Sundell, K., & Saylor, J. E. (2017). Unmixing detrital geochronology age distributions. *Geochemistry Geophysics Geosystems, 18*, 2872–2886.

Syvitski, J. P. M., & Kettner, A. J. (2011). Sediment flux and the Anthropocene. *Philosophical Transactions of the Royal Society of London, Series A: Mathematical and Physical Sciences, 369*, 957–975. doi:doi:10.1098/rsta.2010.0329

Vermeesch, P. (2004). How many grains are needed for a provenance study? *Earth and Planetary Science Letters, 224*, 351–441.

Zhao, M., Shao, L., & Qiao, P. (2015). Characteristics of detrital zircon U-Pb geochronology of the Pearl River sands and its implication on provenances. *Journal of Tongji University (Natural sciences), 43*(6), 915-923. doi:doi:10.11908/j.issn.0253-374x.2015.06.018

CHAPTER 2. ZIRCON U-PB DATING COMPARISONS IN A HIGHLY ALTERED RIVER SYSTEM, MISSISSIPPI RIVER,USA

2.1.Introduction

Tectonic and climatic factors shape and develop river drainages by influencing the transport of sediment from source to sink within a given system. Analyzing sediment from within river basins can provide useful information about sediment provenance and constrain the relative contribution of source tributaries to the net load of the river. Data from modern river systems often serve as an analogue for interpreting ancient systems; however, recently humans have altered drainage basins, inherently changing the way in which rivers access and deliver sediment to the coast (J. P. M. Syvitski & Kettner, 2011; J.P.M. Syvitski & Milliman, 2007). The Mississippi River is the largest river in North America, with constant human occupation of the catchment for at least the last five thousand years. Blum and Roberts (2009) estimated a reduction in sediment delivery to the delta of 60% due in large part to damming of the upstream tributaries over the last 60 years. Given the degree of anthropogenic alteration to the modern sediment transport regime, it is important to understand 1) if U-Pb zircon dating results can be reproduced in large rivers and 2) if erosional signals in the form of zircon age population variability propagates from source to sink in historic times.

This study compares previously reported detrital zircon U-Pb ages to new data to elucidate the degree to which resolvable U-Pb age populations that are used for provenance studies fluctuate in anthropogenically altered systems. These ages are paired with both grain size analysis and bulk geochemistry to understand the possible causes of variation found between samples taken throughout the basin.

2.2. Regional Basement Rock Provinces

The use of zircon grains as provenance tools is based on the large-scale tectonic heterogeneity of the continental source areas, which in turn is related to the progressive accretion of these blocks through geologic time through phases of magmatism and crustal accretion. The Superior Province (2500–2700 Ma) formed as a result of several cratonic blocks colliding, specifically the Slave-Rae-Hearn and the Superior, to eventually form the North American craton (Hoffman, 1988)}. Zircon dates for the longest continuous greenstone belt in the Superior Province largely fall between 2600 and 2800 Ma (Corfu, Krogh, Kwok, & Jensen, 1989). Later the Trans-Hudson Province (1800-1900 Ma) accumulated the Hearn, Wyoming, and Superior Blocks to form the core of the Laurentian continent, which can be seen in the Black Hills of Dakota (Hoffman, 1988; Ross & Villeneuve, 2003; Dahl, Holm, Gardner, Hubacher, & Foland, 1999)

The Penokean province is comprised of a series of Archean and Paleoproterozoic rocks that reach from central Minnesota to Canada (Van Schmus, 1976), (Dahl, Holm, Gardner, Hubacher, & Foland, 1999; Davidson, 1995). This terrane contains igneous and metasedimentary rocks which later experienced metamorphism and deformation from arc accretion events and plutonic activity. These provinces have been regionally dated through both Nd and zircon to approximately 1800-1900 Ma (Bickford & Van Schmus, 1985) (Nelson & DePaolo, 1985).

The Yavapai/Mazatzal Province (1600-1800 Ma) is the basement terrane that underlies much of the western and mid-continental regions of North America. The Yavapai Province runs from Arizona to Minnesota and was formed as a result of multiple pulses of arc accretion (Bowring & Karlstrom, 1990; K. Karlstrom, Bowring, & Reed, 1993; K. E. Karlstrom & Humphreys, 1998). According to Nd isotope data, this block shows little to no reworking of

Archean or Paleoproterozoic older crustal units (Donald J DePaolo, 1981). The Mazatzal Province formed directly after the Yavapai and stretches from northern Mexico, through the southwest United States into Canada. This terrane formed in a continental active margin which and was affected by arc accretion and the accumulation of back arc supracrustal sequences (Heslop et al., 1999; K. Karlstrom et al., 1993).

The Granite-Rhyolite and Grenville Provinces can be found at depth from the Southwest and across the eastern United States. The Granite-Rhyolite Province is focused in the Midwest but may extend further into areas of New York (Bickford & Van Schmus, 1985; Muehlberger, Denison, & Lidiak, 1967). It is dominated by intrusive A-type granites which may have been orogenic in origin (McLelland, Daly, & McLelland, 1996), (Corrigan & Hanmer, 1997), (K. E. Karlstrom et al., 2001). The Grenville Province (1000–1200 Ma) stretches from Texas and parts of Mexico across eastern North America. This terrane is the result of prolonged collisions which assembled the Rodinia Supercontinent (Moores, 1991);(Dalziel, 1991).

The Appalachian/Suwannee/Wichita Block as defined here represents several terranes that date to a similar time period. The Appalachian Province was constructed as a series of collisional events fused terranes onto Laurentia (Drake Jr, Sinha, Laird, & Guy, 1989; Horton, Drake, & Rankin, 1989). While there is strong evidence for recycling of zircon in these areas, a signature of about 500-700 Ma characterizes the Acadian clastic wedge (Park, Barbeau Jr, Rickenbaker, Bachmann-Krug, & Gehrels, 2010). The Suwannee Province accounts for Gondwanan accumulations that make up the basement of the Florida Peninsula and yield a zircon population of ages from 515 to 637 Ma (Mueller et al., 1994). While the Mississippi drainage does not venture as far south as the Suwannee Province it does capture the Wichita Igneous

Province in Southern Oklahoma. This province is associated with rifting that created the Southern Iapetus Ocean during the breakup of Rodinia 539-530 Ma (Hanson et al., 2013).

In this paper, we define the Cenozoic/Laramide region to represent the Laramide and Sevier mountain building events, which yield young zircon ages (<275 Ma), despite also affecting much older tectonic basement blocks. It is important to note that there are several regions from which <400 Ma zircons could be derived within the Mississippi basin. However, Whitmeyer and Karlstrom (Whitmeyer & Karlstrom) recognize that a Northern Rocky Sevier/Laramide Basin zircon signature, dominated by 30–275 Ma grains, overlies the Wyoming Block in the upper reaches of the Missouri River (Fan et al., 2011) (Fuentes, DeCelles, Constenius, & Gehrels, 2011) (May et al., 2013), (Craddock & Kylander-Clark, 2013). We demonstrate that this area is the primary source of <300 Ma grains in the catchment.

2.3. Geologic Setting

The Mississippi River is the fourth longest drainage system in the world, reaching from Canada and flowing southward for almost 4000 km, before eventually emptying into the Gulf of Mexico (J.P.M. Syvitski & Saito, 2007). It is the largest drainage basin in North America with five main tributary systems that reach from the Appalachian Mountains in the east to the Laramide Orogeny in the west (Fig 2.1). Because the Mississippi River spans a variety of geologic terrains, it is ideal for understanding both continental-scale geologic and anthropogenic processes.

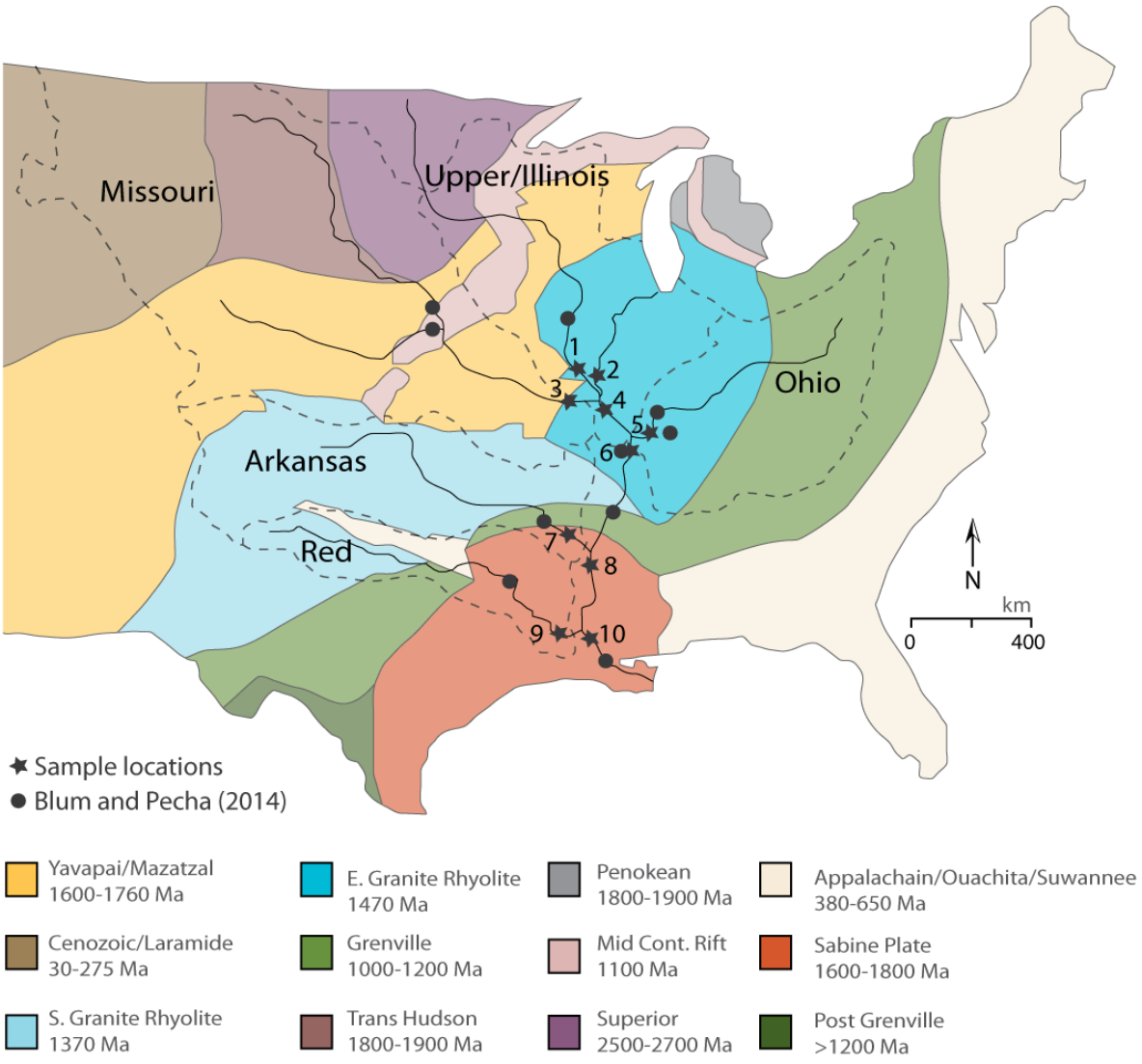

Figure 2. 1 Map of the basement tectonic blocks and associated zircon ages of North America. The major tributary catchments are outlined with dashed black lines, while sample locations are indicated by stars. 1) Upper Mississippi sampled above St. Louis (Upper), 2) Illinois River (Illinois), 3) Missouri River (Missouri), 4) Mississippi sampled south of Missouri, Illinois, and Upper Mississippi confluence (S. of Missouri), 5) Ohio River (Ohio), 6) Mississippi sampled south of the Ohio confluence (S. of Ohio), 7) Arkansas River (Arkansas), 8) Mississippi sampled south of Arkansas confluence (S. of Arkansas), 9) Red River (Red), 10) Mississippi River sampled south of confluence with Red River (S. of Red). Map modified from Gehrels (2014).

The Upper Mississippi River constitutes that stretch of the river that runs from Minnesota to Cairo, Illinois (Fig 2. 1), while the Illinois River drains parts of Illinois, Ohio, and Wisconsin and connects with the Upper Mississippi just north of St. Louis. The Upper Mississippi River

drains basement rocks from the Superior Province (2500–2700 Ma), Yavapai/Mazatzal Province (1600–1760 Ma), and Eastern Granite-Rhyolite Province (~1470 Ma) while the Illinois River exclusively drains the Eastern Granite-Rhyolite Province (Fig 2. 1).

The Missouri River is the longest river in North America and, in the past, has supplied the most suspended sediment to the Mississippi (Meade & Moody, 2010). The Missouri drains from Canada and the western United States to St. Louis, Missouri, and was formed following the Last Glacial Maximum (LGM. The retreat of the Pleistocene ice sheets blanketed the area with loess and glacial deposits, which contribute greatly to the sediment fertility of the river valley and its extensive agricultural development (Andrea Fildani, Hessler, Mason, McKay, & Stockli, 2018; Otvos, 1975). In general, the Missouri River contains a cornucopia of basement rock types including those of Mesozoic-Cenozoic magmatic provinces and the Laramide orogeny to older Archean crust (Gehrels, 2014; Iizuka et al., 2005). Prior to the LGM the Missouri River contributed much less material to the net flow into the Gulf of Mexico as a result of ice damming and stream rerouting (Andrea Fildani et al., 2018). During the LGM erosion and sediment flux from Cordilleran magmatic provinces and the Canadian Shield was more important compared to the modern drainage (A. Fildani et al., 2016).

The Ohio River and its tributaries drain most of the eastern and southeastern United Sates. It joins the Mississippi River at Cairo, Illinois and is, by water volume, the largest tributary of the Mississippi. The Ohio River formed in the Pliocene after ice dam failures around 3 Ma (Wayne, 1952). The basement rocks that the Ohio derives its sediment from mainly comprise those of the Grenville (1000–1200 Ma) and the Eastern Granite Rhyolite terranes (Fig. 2.1).

The Arkansas and Red Rivers derive their headwaters from the Rocky Mountains and flow from west to east across the continental North America. The Arkansas River headwaters lie in the Rocky Mountains and then flows across the northern edge of the Paleozoic Ouachita Orogen eventually joining the Mississippi near Napoleon, Arkansas. The source of the modern Red River lies near Harmon, Oklahoma and has ceased being a tributary to the Mississippi since the construction of the Old River Control Structure in 1963 (Meade & Moody, 2010). The sediment for the Red River is now diverted to the Atchafalaya Basin, along with 30% of the Mississippi River discharge, forming the Wax Lake delta (Roberts, Coleman, Bentley, & Walker, 2003).

2.4. Sediment Transport and Provenance

Determining the provenance of sediment in large drainage basins can often be an arduous and complicated process. Large river systems, such as the Mississippi, often buffer sediment through temporary storage, erosion and intermittent transport (Nittrouer, 2011)}. Buffering in this context means the stabilization of the net flux to the ocean due to temporary storage and recycling of sediment between source and sink, eliminating short-term fluctuations and direct transfer to the basin of the erosional signal (Allen, 2008a, 2008b; Romans, Castelltort, Covault, Fildani, & Walsh, 2016).

In an unaltered system, sediment would be eroded from the upper basin and subsequently delivered to the delta. During transport, sediment would be captured and stored in large floodplain and point bar systems. The terrestrial delta would also provide storage for large amounts of sediment through distributary systems along the coast (H.H. Roberts, 1997). Transport and storage of sediment through a large river system can be complicated by the

behavior of different grain size in suspension and bedload. Fine grained clay, silt, and sand are usually transported as the suspended sediment load; however, zircon largely travels by bedload transport, and thus moves more slowly between source and sink. For example, U-series isotopic work in the Ganges suggests that the coarse-grained part of the sediment load takes approximately 80,000 years to travel from the source to the delta (Granet, Chabaux, Stille, France-Lanord, & Pelt, 2007). Studies of detrital zircon U-Pb ages in the Mississippi show responses times to environmental forcing of $10^{3–4}$ yrs (A. Fildani et al., 2016; Mason et al., 2017), implying rapid transport times of that order of magnitude within this system and contrasting with model prediction (Castelltort & Van Den Driessche, 2003; Paola, Heller, & Angevine, 1992). This lag effect may be curtailed in modern river systems where levees confine and shuttle sediment more efficiently through the river channel.

In the modern Mississippi, previous studies have argued that most of the sediment is derived from the Missouri River (56.9 Mt/yr, 40.5% of total), while the largest portion of the water discharge is from the Ohio (24000 m^3/s compared to 8000 m^3/s in the Missouri) (Alexander, Wilson, & Green, 2012; Meade & Moody, 2010). Despite this high discharge, the Ohio accounts for only 32.5 Mt/yr of sediment flux, 23.1% of the total. Resolving the contribution of the Ohio in the final depocenter of the Mississippi River is, however, complicated since the dominant Grenville U-Pb population is also shared with the Upper Mississippi and Illinois River in particular. The last hundred years have seen the Mississippi River effectively cut off from its floodplains and distributaries due to the construction of large levee systems that span from the Upper Mississippi to the coast. Evidence presented by Heimann et al. (2011) shows a sharp decrease in the total suspended river sediment load after damming, largely in the 1950s (Fig. 2.2). This along with the construction of the Old River Control Structure coincides with a

60% reduction in sediment delivered to the delta (M. D. Blum & Roberts, 2009). While the data points to a significant reduction in fine-grained sediment transport, it does not appear that the sand is affected in the same way. Nittrouer and Viparelli (2014) show that sand impoundment behind dams is not affecting the coarse bedload supply because the Mississippi River scours enough of its own bed to maintain a constant supply. While dams are not seen to affect the overall sand supply of the Mississippi, the Old River Control Structure has completely cut off the Red River as a tributary, which must have impacted the provenance of the sediment downstream of this former confluence. Given the intense amount of anthropogenic alteration, it is important to understand if zircon U-Pb data taken from rivers like the Mississippi are representative of the stream over long time spans and if they are reproducible.

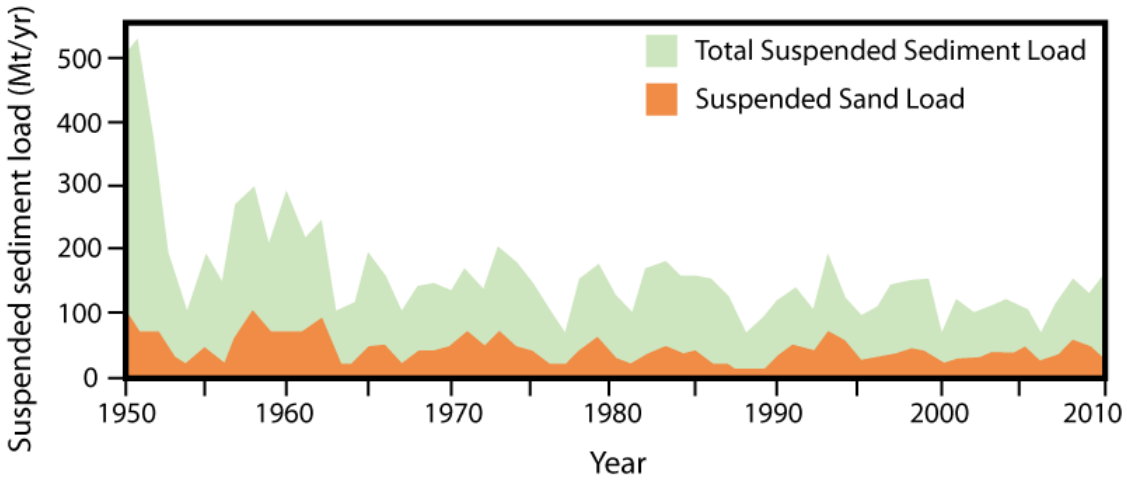

Figure 2. 2 History of suspended total sediment and sand loads in the Mississippi in the upper reaches from 1950 to 2010 after Heimann et al. (2011).

2.5. Sampling

Ten samples were taken from within the modern artificial levees of the Mississippi and its tributaries. Both coarse- and fine-grained facies were sampled across multiple beds to

counteract the effects of hydrodynamic sorting that can affect the concentration of zircons in any given sample (Fig. 2.1). Tributaries were sampled upstream of their confluences with the main trunk of the river, outside of the Modern/Holocene Mississippi river valley. Samples were also taken downstream from each tributary joining the Mississippi, to evaluate not only the input from each tributary but also the downstream transport and mixing of zircon in the modern system.

2.6. Methods

2.6.1 Bulk geochemistry and grain size

Hydrodynamic sorting can affect zircon age spectra, although studies to date suggest that there is no effect of the typically analyzed size fraction (63–125 μm) as a result of current sorting (Yang, Zhang, & Wang, 2012). To assess the impact of the sorting, bulk geochemistry was undertaken on all samples (Lawrence, Cox, Mapes, & Coleman, 2011). Zirconium concentrations have been used as a proxy for the relative abundance of zircon sand grains in any given sample (Amidon, Burbank, & Gehrels, 2005). These analyses can be used to compare the different samples in an effort to quantify outside factors that may be affecting zircon grain age populations.

The major element composition of the bulk sediment (all grain sizes) was analyzed by Inductively Coupled Plasma Emission Spectrometry (ICP-ES) at Boston University (BU), USA. Sediment samples were decarbonated with 30% acetic acid, washed with distilled and deionized water with a purity of 9–12 megaohms, and hand powdered at Louisiana State University (LSU) before total fusion preparation at BU. Glass beads for each sample were made in a muffle furnace at 1050˚C by fusing 100 ± 0.5 mg of sample mixed with 400 ± 0.5 mg lithium

metaborate ($LiBO_2$). The melted mixture was then dissolved in 5% HNO_3, sonicated, manually shaken until no visible grains were observed, and further diluted for analysis (Dunlea et al., 2015). Precision for all elements was better than 1% of the measured value, and accuracy was confirmed by repeated analyses of International Standard Reference Materials (Basalt, Hawaiian Volcano Observatory, BHVO-2)(Wilson, 1997). Results of the geochemical measurements are shown in Table 1.

Table 1. Major Element Concentrations in wt % Oxide and Trace Elements in ppm

Sample Location	P_2O_5	SiO_2	MnO	Fe_2O_3	MgO	Al_2O_3	TiO_2	CaO	Na_2O	K_2O	Ba	Zr	Sr
South of Red	0.03	76.4	0.01	0.66	-0.03	4.77	0.06	0.4	0.94	1.43	329	19	99
Red River	0.02	80.6	0	0.69	-0.07	3.66	0.27	0.1	0.56	1.31	278	791	46
South of Arkansas	0.1	79.2	0.01	1.66	0.24	7.81	0.33	0.8	1.42	2.01	534	294	186
Arkansas River	0.04	75.1	0.01	0.9	-0.06	5.37	0.24	0.2	1.03	2.16	507	530	85
South of Ohio	0.06	77.6	0.02	1.18	0.09	7.11	0.19	0.8	1.33	1.96	635	143	192
Upper Mississippi	0.04	77	0.01	0.74	-0.02	4.98	0.09	0.6	1.12	1.21	248	58	115
Missouri River	0.07	79.5	0.01	1.36	0.2	7.79	0.31	1	1.5	2.01	661	355	221
South of Missouri	0.09	80.8	0.01	1.47	0.21	7.84	0.33	1	1.62	1.94	784	467	227
Illinois River	0.12	73.8	0.02	2.06	0.33	7.38	0.53	0.8	1.22	1.87	364	397	114
Ohio River	0.15	77.1	0.03	2.45	0.2	6.45	0.52	0.4	0.81	1.35	253	566	78

2.6.2 Grain size Analysis

Grain size analysis followed the procedures of Hülse and Bentley (2012) and was completed on the bulk sediment sample (all grain sizes). A small amount of a sample was placed into a cleaned 50 ml plastic centrifuge tube and 5–7 ml of sodium metaphosphate solution was added. The tube was capped and vortexed to deflocculate clay-sized sediment and separate organic particles. The sample was poured through an 850 μm sieve and funneled into a 15 ml glass test tube. After centrifuging and removing the clear supernatant, 2–3 ml of sodium metaphosphate and 5 ml of 30% H_2O_2 were added. Tubes were vortexed again and then put into a hot bath that was heated to 70˚C. This step requires persistent monitoring to prevent loss of

reactant by spraying with acetone until the reaction stabilized. Reactants sat overnight in an effort to completely oxidize any organic matter. Reacted supernatant was then removed and 5 ml of sodium metaphosphate were added. Samples were then rinsed with deionized water, transferred into 50 ml plastic centrifuge tubes, and topped with sodium metaphosphate into a sample solution of up to 40 ml. Samples were vortexed again prior to grain size analysis. Grain size analysis was conducted on a Beckmann Coulter LS13 320 laser diffraction particle size analyzer at LSU. The obscuration of all running samples in the aqueous liquid module (ALM) was between 8–12 %.

2.6.3 Zircon Dating

Zircons were concentrated using heavy liquid methods; all age analysis for zircon was completed at LSU on an iCAP Q ICP-MS with a CETAC Technologies LSX-213 laser ablation system. Three standards were used: the Plešovice (337 Ma, (Sláma et al., 2008), Temora (417 Ma,(Black et al., 2003)), and 91500 (1065 Ma, (Wiedenbeck et al., 1995). For each sample, about 120 grains were analyzed in order to assure a statistically robust quantification of the age populations in a sediment derived from multiple sources (Vermeesch, 2004). Post-analytical processing of the data was completed in IGOR Pro using Iolite v.2.5 for data reduction. For zircon quality, a control of ±30% concordance was used, with $^{206}Pb/^{238}U$ ratios being used in grains younger than 1000 Ma and $^{207}Pb/^{235}U$ ratios being used in grains older than 1000 Ma(Ludwig & Probst, 1998). Further data processing for the zircon age data was completed in R with the Provenance package of Vermeesch et al. (2016). The deconstruction of the zircon populations to determine mixing inputs and to derive comparisons between data were completed using the detrital zircon statistical comparative and mixing software Sundell & Saylor (2017). Analytical data is provided in Appendix A.

2.7. Results

2.7.1 Bulk Geochemistry

Bulk geochemistry of the sediment samples shows that these are quartz-rich sands when plotted against average continental crust values (Fig. 2.3). Calculation of the CIA (Chemical Index of Alteration) using the following formula:

$$CIA = \frac{Al_2O_3}{(Al_2O_3 + CaO + Na_2O = K_2O)}$$

indicate moderate levels of alteration (between 56 and 70), with the Ohio River showing the highest values and the Arkansas the lowest (Fig. 2.4).

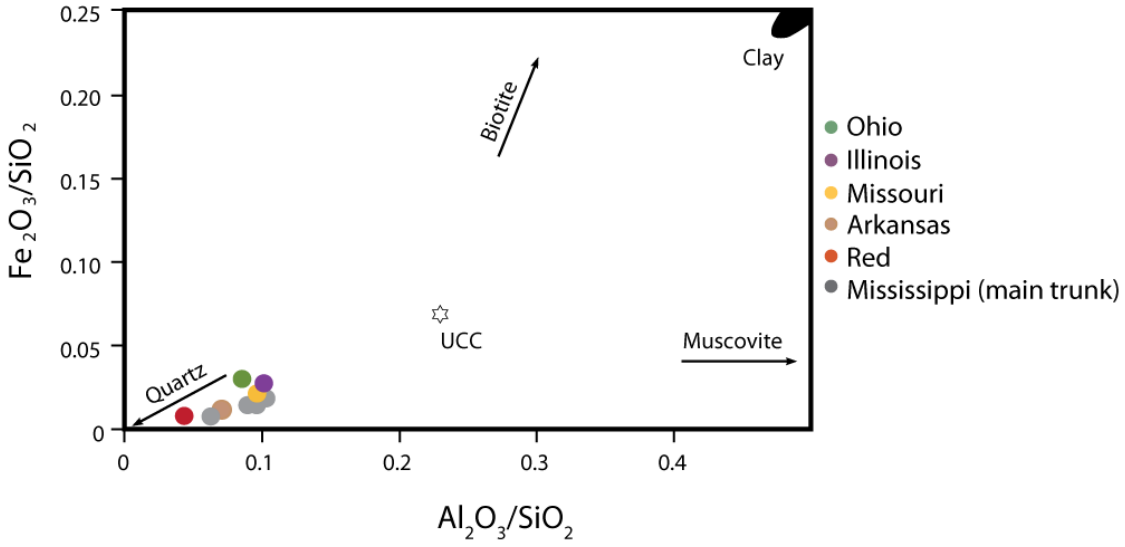

Figure 2. 3 Plot of Al2O3/SiO2 versus Fe2O3/SiO2 for sediments from the Mississippi River after Singh et al. (2005). Lower ratios indicate increase of the quartz proportion and depletion of phyllosilicates. Linear trend corresponds to mineralogical sorting of these sediments during fluvial transport. Star corresponds to average Upper Continental Crust (UCC) (Taylor & McLennan, 1995) (Taylor & McLennan, 1995) (Taylor & McLennan, 1995) (Taylor & McLennan, 1995).

Most of the trunk stream values for the Mississippi River plot around values found in the Missouri River. In addition, Principle Component Analysis (PCA) was performed on the major element geochemistry in an effort to compare differences between samples (Fig. 2.5). Most of the elements have little variation between samples, however Al_2O_3 and SiO_2 are highlighted as being the most variable. The Red and Illinois River samples show the most variation in this aspect, with the Red River displaying relative Al_2O_3 depletion and SiO_2 enrichment (Fig. 2.5). The Illinois River conversely is relatively Al_2O_3 rich and SiO_2 poor. Despite these minor variations, when viewed as a whole, the bulk geochemistry data is relatively uniform (Fig. 2.3), suggesting that the samples are comparable to one another in terms of their general mineralogy and do not show many major differences driven by hydrodynamic sorting.

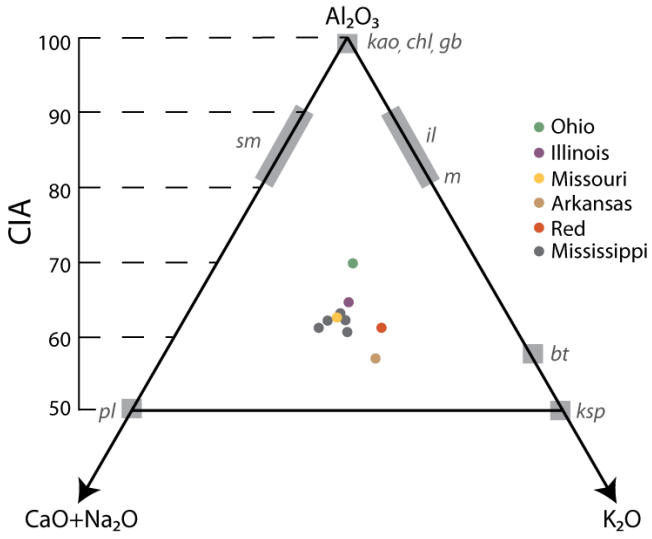

Figure 2. 4 Geochemical signature of the analyzed samples illustrated by a CN-A-K ternary diagram (Fedo et al., 1995). CN denotes the mole weight of Na2O and CaO* (CaO* represents the CaO associated with silicate, excluding all the carbonate). A and K indicate the content of Al_2O_3 and K_2O respectively. Samples closer to Al_2O_3 are rich in kaolinite, chlorite and/or gibbsite (represented by Kao, Chl and Gb). CIA values are also calculated and shown on the left side, with its values are correlated with the CN-A-K. Samples from the Arkansas River have the lowest values of CIA and indicates high contents of CaO and Na2O and plagioclase. Abbreviations: sm (smectite), pl (plagioclase), ksp (K-feldspar), il (illite), m (muscovite), bt (biotite).

Trace elements (Zr, Ba, and Sr) were also used to determine the heterogeneity of samples, because these too are often used as provenance tools (Bhatia & Crook, 1986; McLennan, Hemming, McDaniel, & Hanson, 1993). Water immobile elements in source bedrocks are transferred to the sediment and affect the bulk compositions of the mixed stream. Within this data set, Ba and Sr values are mostly stable, with the Zr values being the most variable (Table 1). South of the Red River, in particular, Zr content is low, implying a paucity of zircon content.

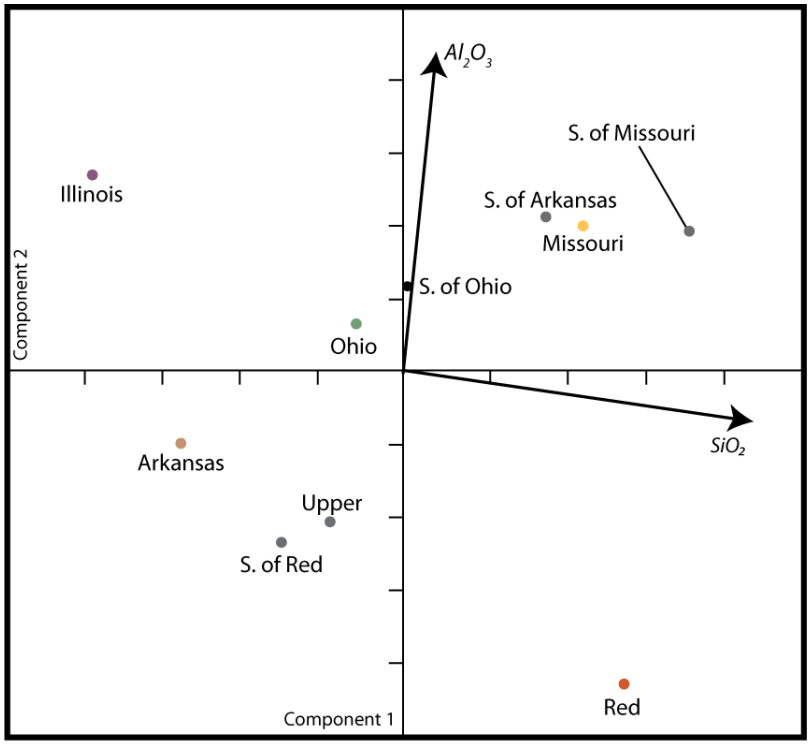

Figure 2. 5 Principal component analysis (PCA) based on the major and select trace element geochemistry of the bulk sediment samples considered in this study. The scatter in values shows that there is significant variability only for Al_2O_3 and SiO_2 in the sediments which we interpret to be largely driven by hydrodynamic sorting.

2.7.2 Grain size

Analysis of grain size also shows variation between samples (Fig. 2.6). Consequently, when Zr contents are plotted against mean grain size, there is an interesting link between the abundance of Zr and larger mean grain size (Fig. 2.7). Larger mean grain size is associated with lower Zr concentrations and thus fewer zircon grains in our sample set.

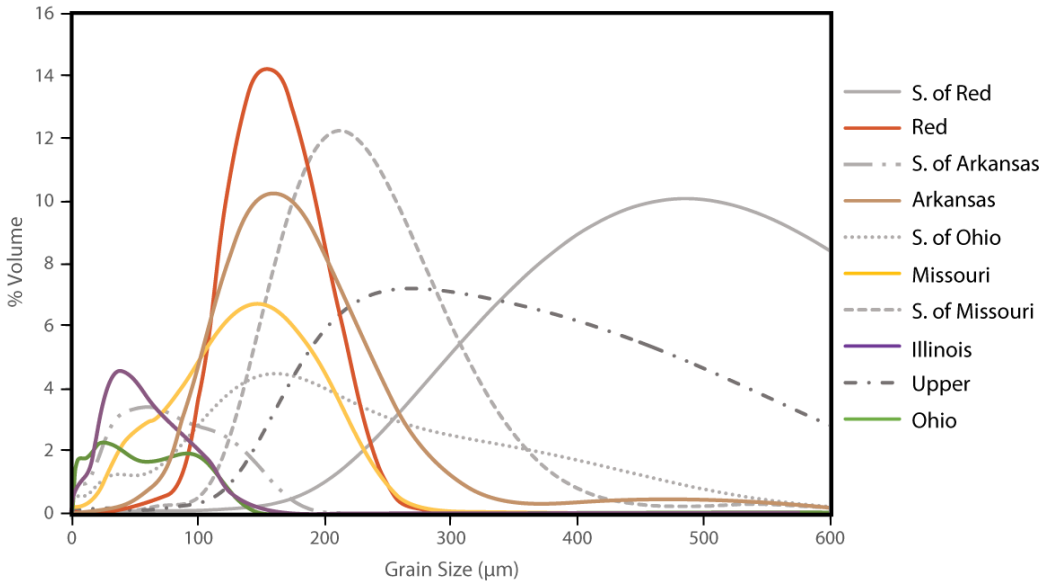

Figure 2. 6 Range of grain sizes as measured by laser particle size analysis methods for the samples analyzed for zircon U-Pb dates within the study (see Fig. 2.1 for sample locations).

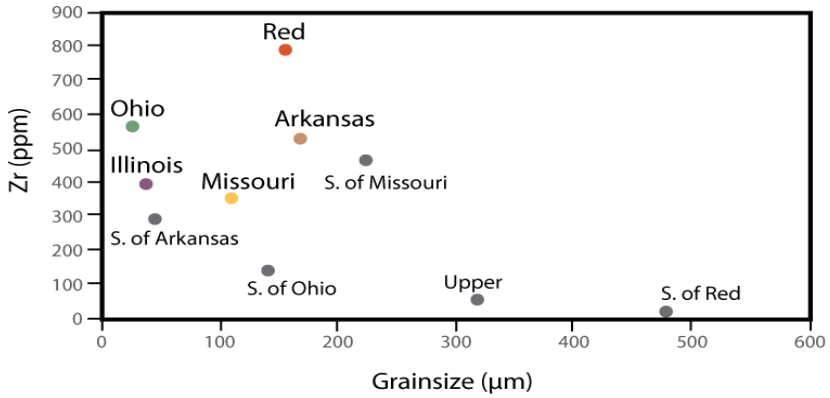

Figure 2.7 Plot of Zr concentrations against mean grain size showing that samples with mean grain size >300 µm have low Zr contents.

Taking both the bulk geochemistry and grain size into account, there is little variation of most major elements (Table. 1) or in the level of chemical alteration (Fig. 2.4) between the headwaters and the Gulf of Mexico. There is, however, variability in grain size and the abundance of zircon between samples (Fig. 2.7).

2.7.3 U-Pb Zircon Results

Following the earlier study of Mason et al. (2017) and Blum & Pecha (2014), the zircon ages are broken down into seven population groups, which are deemed to be of significance to the provenance. The youngest is the Cenozoic/Laramide group (30–275 Ma)(Iizuka et al., 2005), followed by the Appalachian/Wichita/Swannee (380-650), Grenville (1000–1200 Ma), South and East Granite Rhyolite (1370–1470 Ma), Yavapai/Mazatzal (1600–1760 Ma), Trans-Hudson (1800–1900 Ma) and the Penokean/Superior Group (2500–2700 Ma) (Fig. 2.8). We find here the Missouri tributary is dominated by the younger zircon populations found in the Rocky Mountains. In contrast, the Red and Arkansas Rivers have a relatively smaller abundance of young zircon (<300 Ma) and also contain substantial populations of Grenville, Granite Rhyolite and Yavapai affinity. The northern tributaries (Upper and Illinois) have a large number of older Penokean/Superior and Grenville zircons. The samples from the main trunk of the Mississippi River (4,6,8, and 10; Fig. 2.8) all have a dominant young (<300 Ma) population, showing a strong downward propagation of Missouri/Rocky Mountain zircons throughout the modern system.

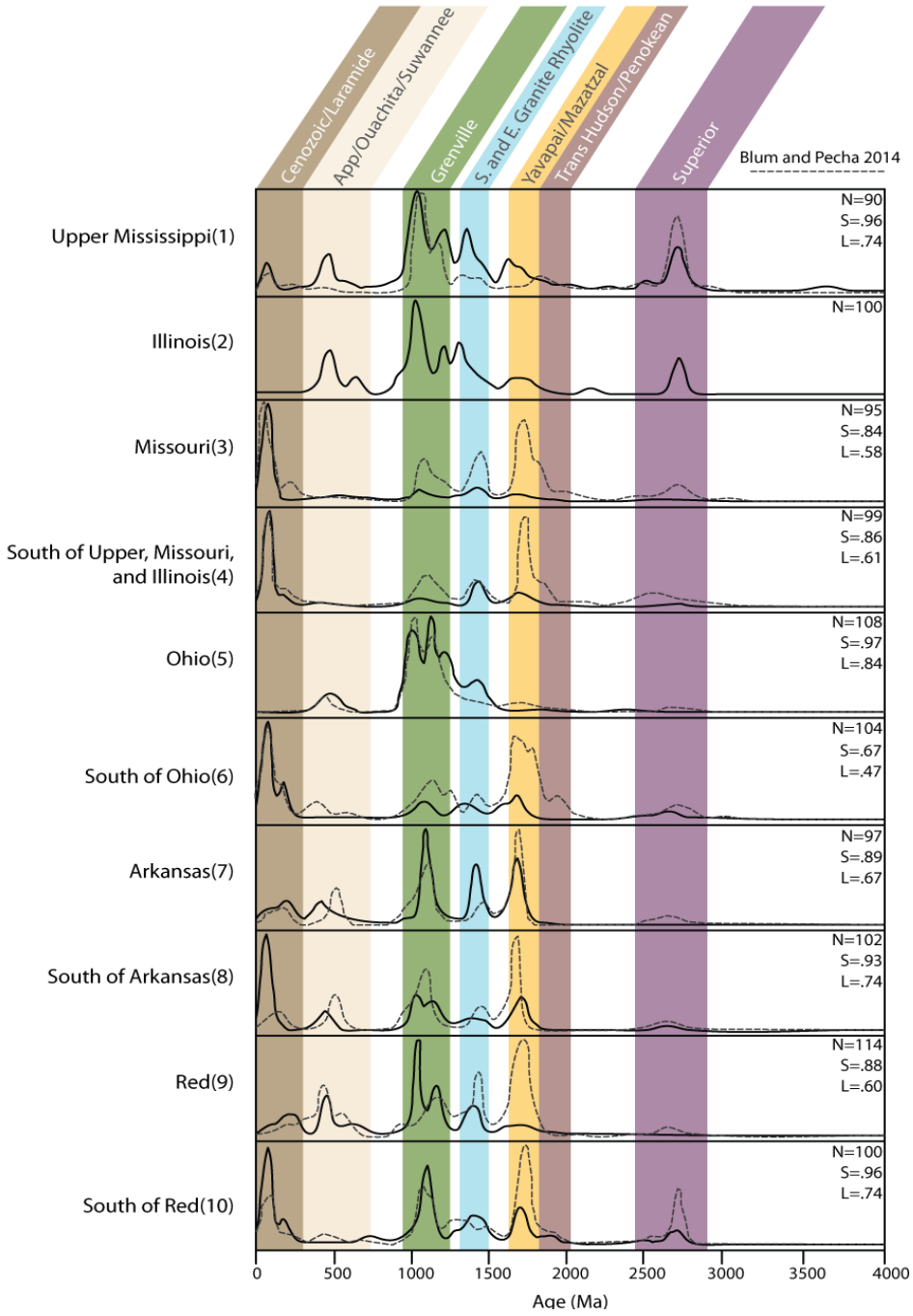

Figure 2. 8 Kernel density estimate (KDE) diagrams (Vermeesch et al., 2016) for the zircon U-Pb ages in the different samples considered in this study. Vertical colored bars show diagnostic ages associated with key tectonic blocks within North America and which form source terrains to the Mississippi. Also plotted are the data from Blum & Pecha (2014) as KDEs in dotted line next to our data to allow direct comparison.The similarity and likeness of the two samples were calculated using the Sundell & Saylor (2017) statistical package to show how the different analyses compare with one another.

2.8. Discussion

2.8.1 Bulk Geochemistry and Grain Size

The bulk geochemistry does not vary greatly between samples, as shown by the major element ratio (Fig. 2.3) and PCA plot (Fig. 2.5). Al_2O_3 and SiO_2 contents are the most variable, especially in the Illinois and the Red River (Fig. 2.5). If the samples were variably enriched in heavy minerals as a result of strong hydrodynamic sorting, they would show increased variability in TiO_2, Fe_2O_3, and MgO which are abundant in mafic minerals. The samples addressed by this study are neither greatly enriched nor depleted in these elements, which implies that there is no significant hydrodynamic sorting affecting the bulk geochemistry. This conclusion, however, is somewhat complicated by the concentration of Zr found within the samples, which does show significant variance. As mentioned above, there is a relationship between grain size and the concentration of Zr in these samples. Samples with a mean grain size of over 300 μm show significantly lower concentrations of Zr (Fig. 2.7). This specifically affects the samples from the Upper Mississippi and the Mississippi south of the Red River, which suggests that hydrodynamic sorting could be influencing the amount of zircon found within these samples. In general, these samples are relatively similar in bulk composition, but coarser in grain size, which is shown to have an effect on Zr content.

Although grain size may play some role in controlling zircon concentration, we also consider zircon fertility in the different source areas as a possible explanation for the discrepancy in Zr concentrations in the different tributaries. In some settings, such as the European Alps, the fertility of source rocks with regard to zircon can vary by up to three orders of magnitude (Malusa, Resentini, & Garzanti, 2016). However, in North America, it has been noted that Grenville age granites are especially rich in zircon (~520 ppm) and are not reset during later

orogenic events, leading to a bias in sediment budgets that do not account for this (David P. Moecher & Scott D. Samson, 2006). North American subduction-related granites are noted to have relatively low Zr (~150 ppm) in comparison (Dickinson, 2008). These differences should be reflected in the zircon concentrations in the tributaries. However, in this study the goal is to estimate the relative sediment budgets of the different tributaries, and, in particular, to determine the average zircon fertility of each catchment, which is achieved through analysis of Zr contents of the bulk sediment analyses.

Looking at fine-grained sediment, <200 μm, there is a wide variation in Zr contents, suggesting significant variability in zircon fertility within the bedrock of the different tributaries. These vary as low as 58 ppm in the Upper Mississippi and as high as 791 ppm in the Red River (Table 1). If these truly reflected the abundance of zircon in these source regions, then a correction would have to be made to any mixing calculations. However, it is noteworthy that the Mississippi south of its confluence with the Red River has one of the lowest abundances of Zr, which suggests that hydrodynamic sorting, at least of zircon, may be just as important as fertility in controlling the concentration of zircon in any given sample (Fig. 2.7). Consequently, we are reluctant to apply a simple correction based on Zr concentrations because this would introduce as many errors as it might resolve. Specifically the Upper Mississippi sample is affected by hydrodynamic sorting with a mean grainsize >300 μm, resulting in its low Zr content. If this was considered a good regional average, then correcting for apparent zircon fertility would result in overestimation of the flux from this part of the basin. The importance of hydrodynamic sorting is also emphasized by the fact that the trunk Mississippi River itself (Mississippi south of the Red River is generally lower in Zr compared to any of the tributaries from which it is derived.

2.8.2 Detrital U-Pb Zircon Populations

The different amounts of sand-sized sediment provided by the tributaries into the main Mississippi River can be assessed by looking at the relative proportions of the major populations of detrital zircon groups downstream of confluences between the headwaters and the Gulf of Mexico (Fig. 2.9). The upper reaches of the river are marked by mixing between the Missouri, the Upper Mississippi, and the Illinois, each with their own unique signature. Downstream of their confluence, there is a very large contribution from the Cenozoic/Laramide (30–275 Ma), which requires a dominant flux from the Missouri compared to the Upper Mississippi and the Illinois. Further downstream, as this mixes with the Ohio, which is dominated by Grenville-aged grains, there is comparatively little change downstream, suggesting that the Ohio's net contribution to the Mississippi is rather modest. Further downstream, mixing with the Arkansas River shows a marked increase in the proportion of Grenville (1000–1200 Ma) grains, which are also abundant in the Arkansas River. This implies significant sediment flux from the Arkansas tributary into the mainstream. In contrast, although the Red River also has a large proportion of Grenville grains, the net composition of the mainstream Mississippi does not change greatly downstream of this confluence (Fig. 2.9). This suggests the Red River is a relatively modest contributor to the total sediment flux, especially given the high Zr contents of the samples measured from this stream. A low flux from the Red River is consistent with the fact of the Red River is now separated from the main Mississippi by the Old River Control Structure, put in place in the 1960s, so that large volumes of sand are not expected to be added to the mainstream from that particular tributary since that time.

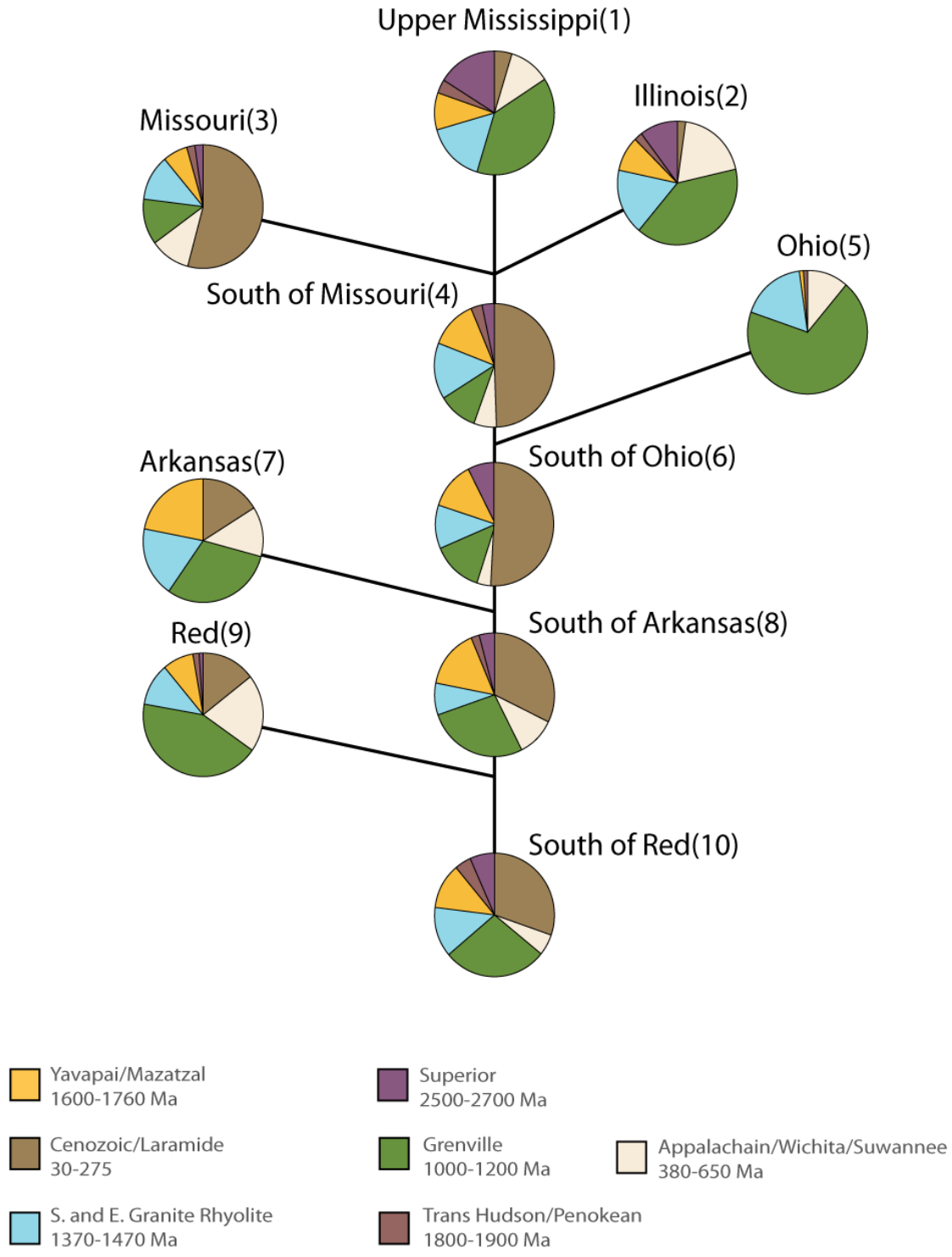

Figure 2. 9 Pie diagrams showing the breakdown of the zircon U-Pb ages for each of the samples considered in this study. Categories relate to age ranges considered diagnostic of key source terranes in the headwaters of the Mississippi. See Figure 2.1.

2.8.3 Sediment Mixing

The unmixing software of Sundell & Saylor (2017) allows for a statistical evaluation of the mixing process of the four tributaries downstream of each of the major confluences. This software uses the age composition of the individual tributaries upstream of the mixed sample in order to estimate the relative contributions from each river to generate the zircon population measured downstream of the confluence. Statistical calculations assume that each of the tributary samples is representative of the beadload flux from that particular branch of the river. The uppermost sample, just south of the Missouri, Illinois, and Upper Mississippi River confluence (Fig. 2.10A), shows a strong dominance of sediment derived from the Missouri River (73%) with very little being contributed from the Illinois (1%). It should be noted that the compositions measured in the Upper Mississippi and Illinois are very close to one another, making them hard to resolve (Fig. 2.8). Further downstream, as the Ohio River joins the Mississippi, the unmixing software estimates that only 2% of the bedload downstream of that confluence may be coming from the Ohio River. A slight increase in flux from the Illinois is not considered significant given the lack of separation between the Illinois and the Upper Mississippi, but with confidence assume both combined result in 26% bedload contribution. Figure 2.10C shows a much more significant change downstream of the Arkansas confluence. Here the model estimates up to 16% of the total load downstream of this point is derived from the Arkansas River. The Ohio and the Illinois both increase their relative flux downstream of the Arkansas-Mississippi confluence compared to upstream trunk river samples, which should not be possible. However, this calculation assumes that the river is in steady state and not susceptible to short-term variations, which would account for such variation.

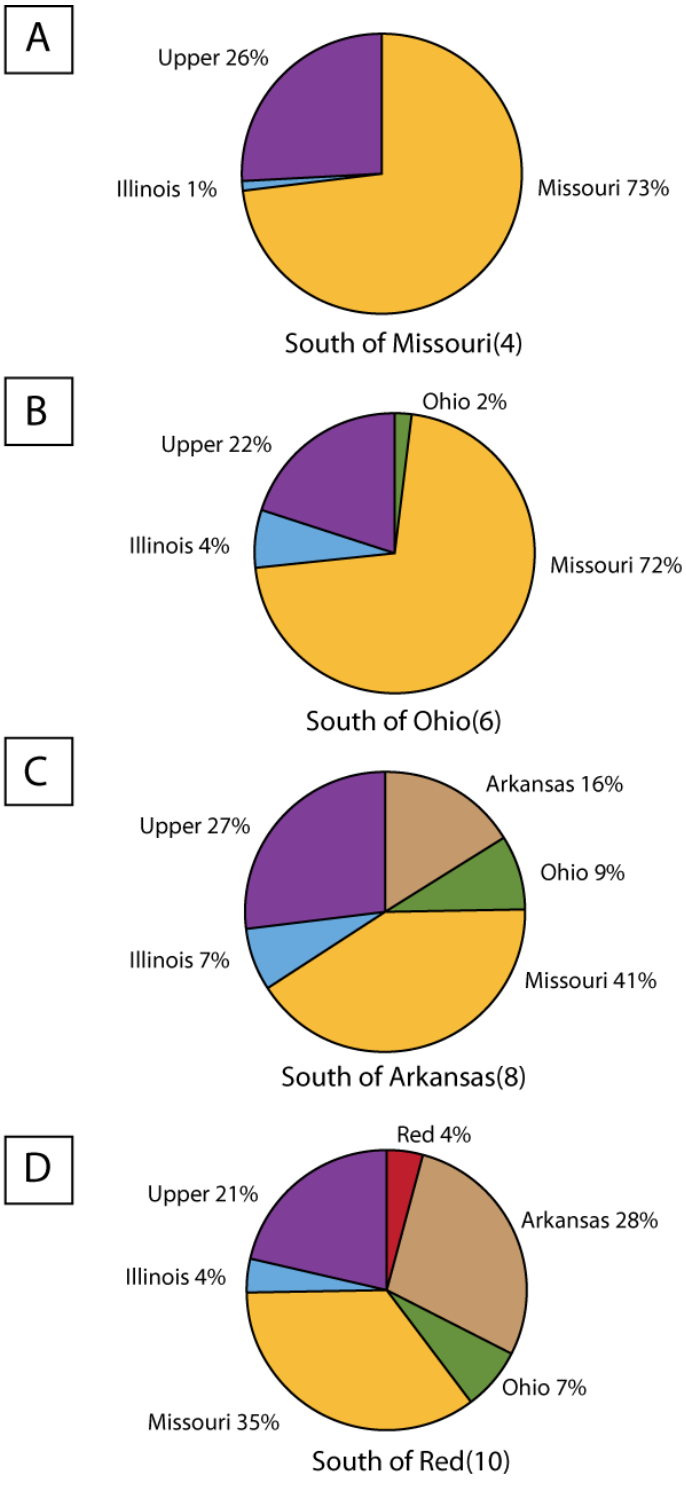

Figure 2. 10 Downstream variation in flux from the major tributaries to the trunk stream of the Mississippi showing the mixing as each tributary joins the mainstream. The calculated contributions are derived from the un-mixing software of Sundell & Saylor (2017) using zircon age spectra from samples. See Fig. 2.1 for sample locations.

Again, the lack of separation between the Illinois and Upper Mississippi in terms of its zircon U-Pb age spectra may also be a factor in the apparent increase in sediment derived from the Illinois. The large flux from the Arkansas is of particular importance in this mixing model compared to earlier budgets based on water discharge and zircon mixing models (Mason et al., 2017).

Finally, when considering the sediment downstream of the Red River confluence, the contribution from that particular tributary is estimated to be quite low (4%). Again the material flux from the Arkansas River is relatively great (28% Fig. 2.10D), and is somewhat more than immediately downstream from its own confluence (16%) (Fig. 2.10C). This may be suggestive of short-term variations in the flux within the mainstream. Regardless of uncertainty in the Red and Arkansas Rivers, these analyses show that the Missouri is the dominant contributor, even in the lower reaches the river. We, however, emphasize the low contributions from the Red River and significant flux from the Arkansas River well into the lower reaches of the Mississippi River (Fig 2.10D).

2.8.4 Controls on Continental Erosion

Having established the relative contributions of the different tributaries to the overall bedload flux into the Mississippi, it is important to consider why sediment production is distributed in this way. The Missouri River is, unsurprisingly, the most sediment-productive because it is also the largest tributary within the Mississippi basin and furthermore, it drains relatively high and steep topography in the Rocky Mountains. Erosion rates are known to increase sharply when local relief exceeds around 1 km (Burbank & Anderson, 2001). Because the Appalachian Mountains only locally exceed that value in total elevation above sea level, erosion rates might be expected to be consequently slow. In contrast, the Rocky Mountains are

much higher (>3 km) and have been more recently tectonically active, resulting in steep slopes in the headwaters and thus rapid erosion rates. The Missouri River further erodes easily mobilized glacial-era materials eroded from local bedrock and transported via rivers and wind to proximal plains in the form of loess and till (Otvos, 2015). It is significant that although the zircon budget for the Missouri River comprises around half Cenozoic/Laramide age grains, the area of its basin underlain by Laramide rocks is relatively small (Fig. 2.1). This requires that erosion in the Missouri River is focused in its uppermost (highest relief) reaches. The relative productivity of the Missouri River contrasts with that of the Ohio which, despite being a relatively large basin, is a small contributor to the overall flux. This is because the topography of the Appalachian Mountains is reduced and heavily eroded compared to that in the upper reaches of the Missouri. Although the average rainfall is much higher in the Ohio basin, this does not translate into higher erosion rates and this may partly reflect the widespread vegetated character of the basin, which reduces runoff and erosion, as well as the lack of high local relief (Burbank & Anderson, 2001). The Arkansas River, identified as being a significant source of sediment, also drains relatively steep source ranges in the central Rocky Mountains area, which is consistent with the greater contribution estimated here. It is not possible to assess the controls on erosion in the Red River basin because its influence has been curtailed by the installation of the Old River Control Structure. In general, steepness of topography in the sediment producing regions and size of the drainage basin are more important than climatic variability in controlling sediment flux within the Mississippi drainage. In addition, the erodibility of the sediment sources in west, particularly in the form of loose glacial era sediments, are subjected to seasonal rainfall and less vegetative cover, makes them even more susceptible to erosion. We further recognize that large areas within the Missouri and Arkansas basins have been cleared of the natural vegetation and are now

extensively utilized as agricultural land, which is susceptible to erosion through runoff and soil loss (Montgomery, 2007). The anthropogenic impact on the modern erosion pattern cannot be overstated.

2.8.5 Reproducibility of Zircon Age Populations

In order to assess the robustness of the zircon U-Pb method in modern anthropogenically altered systems and to measure the amount of erosion and sediment productivity through the Mississippi basin, we compare our results with previously published analyses. These new data are compared to zircon dated by Blum & Pecha (2014), who analyzed many of these same tributaries, with slight differences in location of sampling (Fig. 2.1, 8, and 11).

The Upper Mississippi shows a close similarity between the new and existing analyses (Fig. 2.8 and 2.11). A crucial difference is that zircon dated by Blum & Pecha (2014) emphasize more strongly the importance of the Granite Rhyolite and Yavapai terrains to sediment production in the upper reaches. The Missouri River shows greater differences between the earlier work and the data presented here (Fig. 2.8). Both studies emphasize a Laramide peak, but the older ages of Grenville, Granite Rhyolite and Yavapai origin seen in the earlier work are less well represented in the present study. A similar result can be seen south of the Missouri-Mississippi confluence where our new data emphasize flux from the Missouri River (Fig. 2.8). Analyses of the Ohio River are remarkably similar between the two studies. Likewise, the Arkansas River yields a close match between the different data sets. Analyses from the Red River show some of the biggest disparities in age population between the two studies (Fig. 2.8). The earlier work emphasized a strong peak of Yavapai provenance that is not prominent in this study. However, our sample was taken further downstream, close to the Mississippi confluence,

compared to those in the Blum & Pecha (2014) study. In the lower reaches the two data sets are broadly comparable, although the Yavapai population is more strongly represented in the Blum & Pecha (2014) study, whereas the new data presented here emphasize a greater contribution from the Laramide.

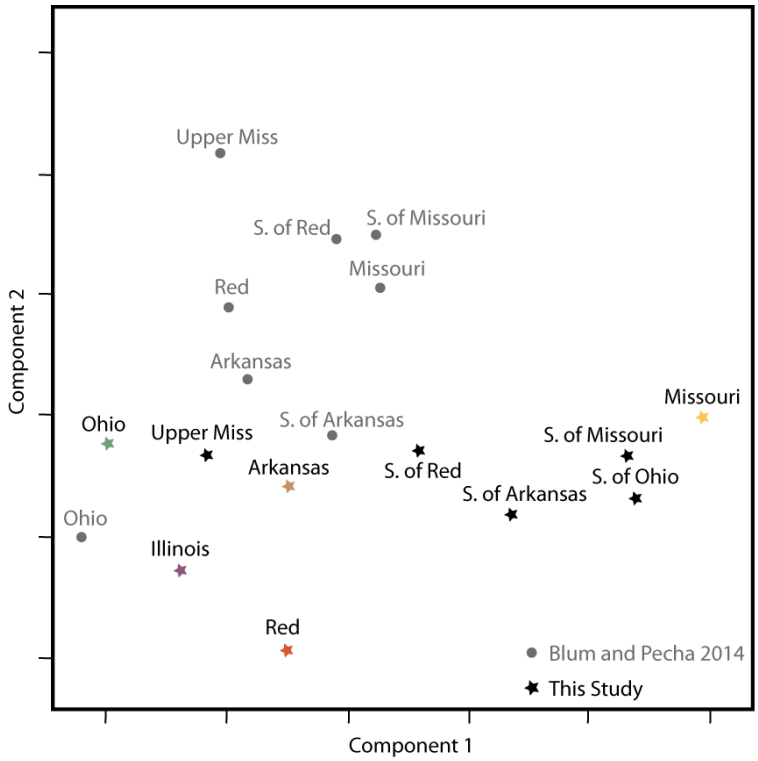

Figure 2. 11 Multidimensional scalar diagram (MDS) showing the characteristics of the zircon ages analyzed in this study together with those from the earlier work by Blum & Pecha (2014). Figure is generated using the R program software from Vermeesch et al. (2016). Note that significant differences are seen between some samples but that the Ohio and Arkansas rivers shows significant similarities between the different studies.

To further quantify the differences between our data sets and earlier work, a multidimensional scaling diagram (MDS) was generated using the software package of Vermeesch et al. (2016)(Fig. 2.11). This allows an objective comparison of the age spectrum for each of the samples. In this diagram, samples with comparable zircon age spectra plot close together. The two analyses from the Ohio River are very similar to one another, as are those from

the Arkansas River and the Mississippi River south of its confluence with the Arkansas (Fig. 2.11). The diagram highlights the significant differences between our new analyses from the Red and Missouri Rivers compared to earlier work. The Upper Mississippi also appears to have significant differences, although comparison using the Sundell & Saylor (2017) statistical package indicate a relatively high degree of similarity (Fig. 2.8). The MDS diagram exaggerates the differences between those samples.

The samples from the lower reaches, just south of the Red River, from this study and the earlier zircon dated by Blum & Pecha (2014) can be unmixed into their contributing tributaries using the Sundell & Saylor (2017) software package. These bedload results are presented alongside average suspended sediment load readings from the USGS for each major tributary found in Mason et al. (2017)(Fig. 2.12). For a more direct comparison the Illinois was omitted from source data for the unmixing because Blum & Pecha (2014) did not analyze this tributary. Furthermore, the Illinois zircon age spectrum is similar to the Upper Mississippi therefore making it difficult to distinguish between for unmixing given the similar age spectra (Fig. 2.8). Data are presented with and without the Red River as a source to better understand the effect of the Old River Control Structure on sediment flux in the Mississippi. The result of the inverse Monte Carlo (Saylor &Sundell, 2017; DZMIX) from samples derived just south of the former Red River confluence shows that in our data there is very little input from the Red (4%), while the sample dated by Blum & Pecha (2014) implies a significant contribution based on unmixing calculation (36%) (Fig. 2.12A). Although the USGS gauging data indicate high flux from the Red River (18%), this material is currently diverted into the Atchafalaya distributary, which now forms the Wax Lake and Atchafalaya delta.

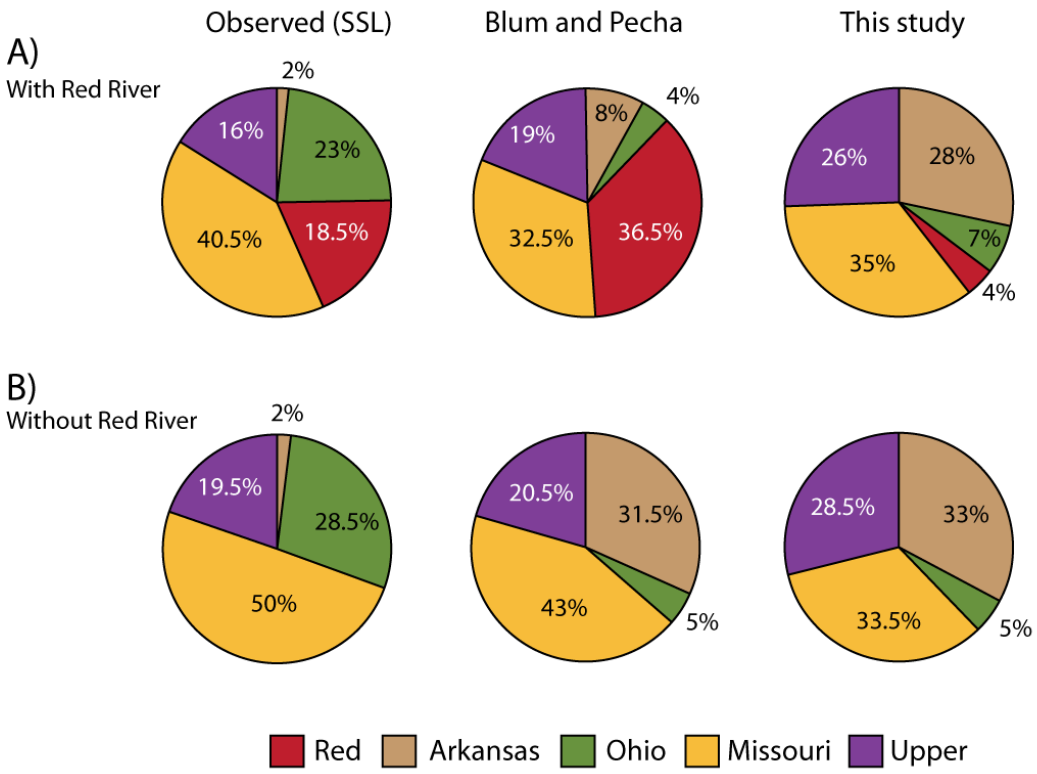

Figure 2. 12 Estimated budgets for the net flux from the Mississippi River to the Gulf of Mexico showing observational suspended sediment discharge data as reported by Mason et al. (2017) and the inverse Monte Carlo caluculated bedload contributions using the data from Blum and Pecha (2014) and this study. The upper row shows budgets including flux from the Red River, while those in the lower row are recalculated to exclude contributions from the source.

Although our data taken from immediately south of the confluence implies a rapid response to the sand load from the cutoff of the Red River, the Blum & Pecha (2014) sample taken further downstream near Baton Rouge does not. This implies that the river is either recycling older Red River material from its channel or that zircons from the Red River move relatively slowly through the Mississippi, delaying the downstream propagation of the cutoff to the Baton Rouge location. We further suggest that the very high apparent contribution from the Red River to the Mississippi, as estimated with the Monte Carlo from the zircon dated by Blum & Pecha (2014) could be a reflection of high zircon fertility, as estimated from the Zr content

(Table 1; Fig. 2.7). The Red River sample contains 791 ppm Zr compared to 294 ppm in the Mississippi upstream. If these values are representative, then the bulk sediment flux from the Red River would be ~2.7 times less than the zircon estimate of 36% reported here.

If we consider the river zircon budget excluding the Red River as a contributor, the relative percentages using the zircon dated by Blum & Pecha (2014) data are very similar to those derived from this study in respect to relative contributions of sand from the source tributaries (Fig. 2.12B). In this case, the major discrepancy with our budget is with the USGS gauging data, which shows a much greater flux of sediment from the Ohio than recognized by either of the zircon studies. We suggest that this is because the Ohio sediment load is dominated by finer grained suspended sediments measured by the USGS but not analyzed in this zircon study, which focuses on the sand fraction. In a similar way, the discrepancy between the zircon budgets and the gauging data in regards to the Arkansas River suggest that most of the sediment contributed by the Arkansas River is in the form of sand and not suspended material (Fig. 2.12A). This is not surprising given the strong contribution of sand provided by the young, mountainous western sources of the Mississippi basin.

2.9. Conclusions

This study shows the importance of hydrodynamic sorting in controlling the zircon populations and in particular the importance of grain size, as well as fertility. We recognize that the coarsest sands are relatively poor in Zr concentrations and thus in zircon grains. If the potential effects of sorting are to be properly accounted for, it is critical to measure grain size and bulk sediment geochemical analyses in addition to the U-Pb ages whenever considering this type of data.

Analysis of the zircon U-Pb ages in the Mississippi River system presented here show the importance of the Missouri River in controlling the total amount of bedload sediment reaching the Gulf of Mexico. We do, however, estimate that the Arkansas River is an important source of material, despite previous studies indicating a relatively modest contribution. In contrast, the Ohio River, despite its significant water discharge and suspended sediment load, is not a major contributor of zircon sand grains into the mainstream. This is highlighted even more by the fact that Grenville basement rock has such high zircon fertility, which should result in an increase of these detrital ages in the sample south of the Ohio confluence not seen in this study. Much of the sediment in the Missouri River is derived from Cenozoic/Laramide source rocks and this contribution is seen to propagate far downstream. While this Cenozoic/Laramide bedrock comprises only a small part of the Missouri basin, glacial reworking has provided a rich source terrane for the Missouri to access. This emphasizes the importance of young mountain building and glaciation events in controlling the sediment record in the final depocenter. Additionally, this pattern of sediment production could be compounded by the spread of agriculture across the western plains of the Missouri and Arkansas rivers, affecting the high contribution of these areas to the net sediment load of the Mississippi.

Comparison of our new data with earlier work on the Mississippi through KDE (Kernel Density Estimate) diagarms shows a reasonable comparison between the two (Fig. 2.8). This gives confidence that detrital zircon studies can be a valuable way of examining provenance in modern and ancient samples, even in significantly altered rivers. However, we recognize some important differences between the earlier work and our new data. In particular, our analyses have a much lower proportion of Yavapai grains and higher Cenozoic/Laramide content compared to modern zircon dated by Blum & Pecha (2014) . Since this trend can be seen along the entire

river, this is not attributed to damming effects, but most likely represents short-term instabilities in the sediment flux of the Mississippi.

Our study further emphasizes the importance of anthropogenic processes in controlling the sediment in the mainstream Mississippi. For example, large differences in the unmixing Monte Carlo preformed between our work and the zircon dated by Blum & Pecha (2014) (Fig. 2.12) indicate that installation of the Old River Control Structure has had a large influence on the bedload immediately downstream, but that this influence is slow in propagating further towards the Gulf of Mexico. This would imply relatively slow zircon transport rates, consistent with the high density of this mineral relative to many others in the sand fraction. Separating this influence from short-term pulses is not feasible based on the present data set alone. However, accounting for similar damming or river diversion effects in other drainage basins in other rivers could be critical for a realistic assessment of the sediment budget.

2.10 References Cited

Alexander, J. S., Wilson, R. C., & Green, W. R. (2012). *A brief history and summary of the effects of river engineering and dams on the Mississippi River system and delta*: US Department of the Interior, US Geological Survey.

Allen, P. A. (2008a). From landscapes into geological history. *Nature, 451*, 274. doi:doi:10.1038/nature06586

Allen, P. A. (2008b). Time scales of tectonic landscapes and their sediment routing systems. In K. Gallagher, S. J. Jones, & J. Wainwright (Eds.), *Landscape Evolution: Denudation, Climate and Tectonics over Different Time and Space Scales* (Vol. 296, pp. 7-28). London: Geological Society.

Amidon, W. H., Burbank, D. W., & Gehrels, G. E. (2005). Construction of detrital mineral populations: insights from mixing of U-Pb zircon ages in Himalayan rivers. *Basin Research, 17*(4), 463-485.

Bhatia, M. R., & Crook, K. A. (1986). Trace element characteristics of graywackes and tectonic setting discrimination of sedimentary basins. *Contributions to Mineralogy and Petrology, 92*(2), 181-193.

Bickford, M., & Van Schmus, W. (1985). Discovery of two Proterozoic granite-rhyolite terranes in the buried midcontinent basement: The case for shallow drill holes *Observation of the Continental Crust through Drilling I* (pp. 355-364): Springer.

Black, L. P., Kamo, S. L., Allen, C. M., Aleinikoff, J. N., Davis, D. W., Korsch, R. J., & Foudoulis, C. (2003). TEMORA 1: a new zircon standard for Phanerozoic U-Pb geochronology. *Chemical Geology, 200,* 155–170.

Blum, M., & Pecha, M. (2014). Mid-Cretaceous to Paleocene North American drainage reorganization from detrital zircons. *Geology*. doi:10.1130/g35513.1

Blum, M. D., & Roberts, H. H. (2009). Drowning of the Mississippi Delta due to insufficient sediment supply and global sea-level rise. *Nature Geoscience, 2*(7), 488-491. doi:10.1038/ngeo553

Bowring, S. A., & Karlstrom, K. E. (1990). Growth, stabilization, and reactivation of Proterozoic lithosphere in the southwestern United States. *Geology, 18*(12), 1203-1206.

Burbank, D. W., & Anderson, R. S. (2001). *Tectonic Geomorphology*. Oxford: Blackwell.

Castelltort, S., & Van Den Driessche, J. (2003). How plausible are high-frequency sediment supply-driven cycles in the stratigraphic record? *Sedimentary Geology, 157,* 3–13.

Corfu, F., Krogh, T., Kwok, Y., & Jensen, L. (1989). U–Pb zircon geochronology in the southwestern Abitibi greenstone belt, Superior Province. *Canadian Journal of Earth Sciences, 26*(9), 1747-1763.

Corrigan, D., & Hanmer, S. (1997). Anorthosites and related granitoids in the Grenville orogen: A product of convective thinning of the lithosphere? *Geology, 25*(1), 61-64.

Craddock, W. H., & Kylander-Clark, A. R. C. (2013). U-Pb ages of detrital zircons from the Tertiary Mississippi River Delta in central Louisiana: Insights into sediment provenance. *Geosphere, 9*(6), 1832-1851. doi:10.1130/GES00917.1

Dahl, P. S., Holm, D. K., Gardner, E. T., Hubacher, F. A., & Foland, K. A. (1999). New constraints on the timing of Early Proterozoic tectonism in the Black Hills (South Dakota), with implications for docking of the Wyoming province with Laurentia. *Geological Society of America Bulletin, 111*(9), 1335-1349.

Dalziel, I. W. (1991). Pacific margins of Laurentia and East Antarctica-Australia as a conjugate rift pair: Evidence and implications for an Eocambrian supercontinent. *Geology, 19*(6), 598-601.

Davidson, A. (1995). A review of the Grenville orogen in its North American type area. *AGSO Journal of Australian Geology and Geophysics, 16*(1), 3-24.

DePaolo, D. J. (1981). Neodymium isotopes in the Colorado Front Range and crust–mantle evolution in the Proterozoic. *Nature, 291*(5812), 193.

Dickinson, W. R. (2008). Impact of differential zircon fertility of granitoid basement rocks in North America on age populations of detrital zircons and implications for granite petrogenesis. *Earth and Planetary Science Letters, 275*(1-2), 80-92. doi:doi:10.1016/j.epsl.2008.08.003

Drake Jr, A. A., Sinha, A., Laird, J., & Guy, R. (1989). The taconic orogen. *The Appalachian-Ouachita orogen in the United States: Boulder, Colorado, Geological Society of America, Geology of North America, 2*, 101-177.

Dunlea, A. G., Murray, R. W., Sauvage, J., Spivack, A. J., Harris, R. N., & D'Hondt, S. (2015). Dust, volcanic ash, and the evolution of the South Pacific Gyre through the Cenozoic. *Paleoceanography, 30*(8), 1078-1099. doi:doi:10.1002/2015PA002829

Fan, M., DeCelles, P. G., Gehrels, G. E., Dettman, D. L., Quade, J., & Peyton, S. L. (2011). Sedimentology, detrital zircon geochronology, and stable isotope geochemistry of the lower Eocene strata in the Wind River Basin, central Wyoming. *Bulletin, 123*(5-6), 979-996.

Fedo, C. M., Nesbitt, H. W., & Young, G. M. (1995). Unraveling the effects of potassium metasomatism in sedimentary rocks and paleosols, with implications for paleoweathering conditions and provenance. *Geology, 23*, 921–924.

Fildani, A., Hessler, A. M., Mason, C. C., McKay, M. P., & Stockli, D. F. (2018). Late Pleistocene glacial transitions in North America altered major river drainages, as revealed by deep-sea sediment. *Scientific Reports, 8*(1), 13839.

Fildani, A., McKay, M. P., Stockli, D., Clark, J., Dykstra, M. L., Stockli, L., & Hessler, A. M. (2016). The ancestral Mississippi drainage archived in the late Wisconsin Mississippi deep-sea fan. *Geology*. doi:10.1130/g37657.1

Fuentes, F., DeCelles, P. G., Constenius, K. N., & Gehrels, G. E. (2011). Evolution of the Cordilleran foreland basin system in northwestern Montana, USA. *GSA Bulletin, 123*(3-4), 507-533.

Gehrels, G. E. (2014). Detrital Zircon U-Pb Geochronology Applied to Tectonics. *Annual Review of Earth and Planetary Sciences, 42*, 127-149. doi:DOI: 10.1146/annurev-earth-050212-124012

Granet, M., Chabaux, F., Stille, P., France-Lanord, C., & Pelt, E. (2007). Time-scales of sedimentary transfer and weathering processes from U-series nuclides: Clues from the Himalayan rivers. *Earth and Planetary Science Letters, 261*(3-4), 389-406.

Hanson, R. E., Puckett Jr, R. E., Keller, G. R., Brueseke, M. E., Bulen, C. L., Mertzman, S. A., . . . McCleery, D. A. (2013). Intraplate magmatism related to opening of the southern Iapetus Ocean: Cambrian Wichita igneous province in the Southern Oklahoma rift zone. *Lithos, 174*, 57-70.

Heimann, D. C., Sprague, L. A., & Blevins, D. W. (2011). *Trends in suspended-sediment loads and concentrations in the Mississippi River Basin, 1950-2009*: US Department of the Interior, US Geological Survey.

Heslop, D., Shaw, J., Bloemendal, J., Chen, F., Wang, J., & Parker, E. (1999). Sub-millennial scale variations in East Asian monsoon systems recorded by dust deposits from the north-western Chinese Loess Plateau. *Physics and Chemistry of the Earth, Part A: Solid Earth and Geodesy, 24*(9), 785-792. doi:doi:10.1016/S1464-1895(99)00115-5

Hoffman, P. F. (1988). United plates of America, the birth of a craton: Early Proterozoic assembly and growth of Laurentia. *Annual Review of Earth and Planetary Sciences, 16*(1), 543-603.

Horton, J. W., Drake, A. A., & Rankin, D. W. (1989). Tectonostratigraphic terranes and their Paleozoic boundaries in the central and southern Appalachians. *Geological Society of America Special Papers, 230*, 213-246.

Hülse, P., & Bentley, S. J. (2012). A 210Pb sediment budget and granulometric record of sediment fluxes in a subarctic deltaic system: the Great Whale River, Canada. *Estuarine and Coastal Shelf Science, 109*, 41–52. doi:doi:10.1016/j.ecss.2012.05.019

Iizuka, T., Hirata, T., Komiya, T., Rino, S., Katayama, I., Motoki, A., & Maruyama, S. (2005). U-Pb and Lu-Hf isotope systematics of zircons from the Mississippi River sand: Implications for reworking and growth of continental crust. *Geology, 33*(6), 485-488.

Karlstrom, K., Bowring, S. A., & Reed, J. (1993). Proterozoic orogenic history of Arizona. *Precambrian: Conterminous US: Boulder, Colorado, Geological Society of America, Geology of North America, 2*, 188-211.

Karlstrom, K. E., Åhäll, K.-I., Harlan, S. S., Williams, M. L., McLelland, J., & Geissman, J. W. (2001). Long-lived (1.8–1.0 Ga) convergent orogen in southern Laurentia, its extensions

to Australia and Baltica, and implications for refining Rodinia. *Precambrian Research, 111*(1-4), 5-30.

Karlstrom, K. E., & Humphreys, E. D. (1998). Persistent influence of Proterozoic accretionary boundaries in the tectonic evolution of southwestern North America: Interaction of cratonic grain and mantle modification events. *Rocky Mountain Geology, 33*(2), 161-179.

Lawrence, R. L., Cox, R., Mapes, R. W., & Coleman, D. S. (2011). Hydrodynamic fractionation of zircon age populations. *Geological Society of America Bulletin, 123*, 295–305.

Ludwig, W., & Probst, J. L. (1998). River sediment discharge to the oceans: present-day controls and global budgets. *American Journal of Science, 298*, 265–295.

Malusa, M. G., Resentini, A., & Garzanti, E. (2016). Hydraulic sorting and mineral fertility bias in detrital geochronology. *Gondwana Research, 31*, 1-19. doi:doi:10.1016/j.gr.2015.09.002

Mason, C. C., Fildani, A., Gerber, T., Blum, M. D., Clark, J. D., & Dykstra, M. (2017). Climatic and anthropogenic influences on sediment mixing in the Mississippi source-to-sink system using detrital zircons: Late Pleistocene to recent. *Earth and Planetary Science Letters, 466*, 70-79. doi:http://dx.doi.org/10.1016/j.epsl.2017.03.001

May, S. R., Gray, G. G., Summa, L. L., Stewart, N. R., Gehrels, G. E., & Pecha, M. E. (2013). Detrital zircon geochronology from the Bighorn Basin, Wyoming, USA: Implications for tectonostratigraphic evolution and paleogeography. *Bulletin, 125*(9-10), 1403-1422.

McLelland, J., Daly, J. S., & McLelland, J. M. (1996). The Grenville orogenic cycle (ca. 1350-1000 Ma); an Adirondack perspective. *Tectonophysics, 265*(1-2), 1-28.

McLennan, S., Hemming, S., McDaniel, D., & Hanson, G. (1993). Geochemical approaches to sedimentation, provenance, and tectonics. *Special Papers-Geological Society of America*, 21-21.

Meade, R. H., & Moody, J. A. (2010). Causes for the decline of suspended-sediment discharge in the Mississippi River system, 1940–2007. *Hydrological Processes: An International Journal, 24*(1), 35-49.

Moecher, D. P., & Samson, S. D. (2006). Differential zircon fertility of source terranes and natural bias in the detrital zircon record: Implications for sedimentary provenance analysis. *Earth and Planetary Science Letters, 247*(3), 252-266. doi:doi:10.1016/j.epsl.2006.04.035

Montgomery, D. R. (2007). *Dirt: The erosion of civilizations*. Berkeley: University of California Press.

Moores, E. (1991). Southwest US-East Antarctic (SWEAT) connection: a hypothesis. *Geology, 19*(5), 425-428.

Muehlberger, W. R., Denison, R. E., & Lidiak, E. G. (1967). Basement rocks in continental interior of United States. *AAPG Bulletin, 51*(12), 2351-2380.

Mueller, P. A., Heatherington, A. L., Wooden, J. L., Shuster, R. D., Nutman, A. P., & Williams, I. S. (1994). Precambrian zircons from the Florida basement: A Gondwanan connection. *Geology, 22*(2), 119-122.

Nelson, B. K., & DePaolo, D. J. (1985). Rapid production of continental crust 1.7 to 1.9 b.y. ago: Nd isotopic evidence from the basement of the North American mid-continent. *Geological Society of America Bulletin, 96*(6), 746-754. doi:doi: 10.1130/0016-7606(1985)96

Nittrouer, J. A., & Viparelli, E. (2014). Sand as a stable and sustainable resource for nourishing the Mississippi River delta. *Nature Geoscience, 7*(5), 350.

Otvos, E. G. (1975). Southern limits of Pleistocene loess, Mississippi valley. *Southeastern Geology, 17*, 27-38.

Otvos, E. G. (2015). The last interglacial stage: Definitions and marine highstand, North America and Eurasia. *Quaternary International, 383*, 158-173.

Paola, C., Heller, P. L., & Angevine, C. L. (1992). The large-scale dynamics of grain-size variation in alluvial basins, 1: Theory. *Basin Research, 4*(2), 73–90. doi:DOI: 10.1111/j.1365-2117.1992.tb00145.x

Park, H., Barbeau Jr, D. L., Rickenbaker, A., Bachmann-Krug, D., & Gehrels, G. (2010). Application of foreland basin detrital-zircon geochronology to the reconstruction of the southern and central Appalachian orogen. *The Journal of Geology, 118*(1), 23-44.

Roberts, H., Coleman, J., Bentley, S., & Walker, N. (2003). An embryonic major delta lobe: A new generation of delta studies in the Atchafalaya-Wax Lake Delta system.

Roberts, H. H. (1997). Dynamic changes of the Holocene Mississippi River delta plain: The delta cycle. *Journal of Coastal Research, 13*(3), 605-627.

Romans, B. W., Castelltort, S., Covault, J. A., Fildani, A., & Walsh, J. P. (2016). Environmental signal propagation in sedimentary systems across timescales. *Earth-Science Reviews, 153*, 7–29. doi:doi:10.1016/j.earscirev.2015.07.012

Ross, G. M., & Villeneuve, M. (2003). Provenance of the Mesoproterozoic (1.45 Ga) Belt basin (western North America): Another piece in the pre-Rodinia paleogeographic puzzle. *GSA Bulletin, 115*(10), 1191-1217.

Singh, M., Sharma, M., & Tobschall, H. J. (2005). Weathering of the Ganga alluvial plain, northern India: implications from fluvial geochemistry of the Gomati River. *Applied Geochemistry, 20*, 1-21.

Sláma, J., Košler, J., Condon, D. J., Crowley, J. L., Gerdes, A., Hanchar, J. M., . . . Whitehouse, M. J. (2008). Plezovice zircon A new natural reference material for U–Pb and Hf isotopic microanalysis. *Chemical Geology, 249*, 1-35. doi:doi:10.1016/j.chemgeo.2007.11.005

Sundell, K., & Saylor, J. E. (2017). Unmixing detrital geochronology age distributions. *Geochemistry Geophysics Geosystems, 18*, 2872–2886.

Syvitski, J. P. M., & Kettner, A. J. (2011). Sediment flux and the Anthropocene. *Philosophical Transactions of the Royal Society of London, Series A: Mathematical and Physical Sciences, 369*, 957–975. doi:doi:10.1098/rsta.2010.0329

Syvitski, J. P. M., & Milliman, J. D. (2007). Geology, geography and humans battle for dominance over the delivery of sediment to the coastal ocean. *Journal of Geology, 115*, 1-19.

Syvitski, J. P. M., & Saito, Y. (2007). Morphodynamics of deltas under the influence of humans. *Global and Planetary Change, 57*, 261–282.

Taylor, S. R., & McLennan, S. M. (1995). The geochemical evolution of the continental crust. *Reviews of Geophysics, 33*, 241–265.

Van Schmus, W. (1976). A Discussion on global tectonics in Proterozoic times-Early and Middle Proterozoic history of the Great Lakes area, North America. *Phil. Trans. R. Soc. Lond. A, 280*(1298), 605-628.

Vermeesch, P. (2004). How many grains are needed for a provenance study? *Earth and Planetary Science Letters, 224*, 351–441.

Vermeesch, P., Resentini, A., & Garzanti, E. (2016). An R package for statistical provenance analysis. *Sedimentary Geology, 336*, 14-25. doi:doi:10.1016/j.sedgeo.2016.01.009

Wayne, W. J. (1952). Pleistocene evolution of the Ohio and Wabash valleys. *The Journal of Geology, 60*(6), 575-585.

Whitmeyer, S. J., & Karlstrom, K. E. (2007). Tectonic model for the Proterozoic growth of North America. *Geosphere, 3*, 220–259.

Wiedenbeck, M., Allé, P., Corfu, F., Griffin, W. L., Meier, M., Oberli, F., . . . Spiegel, W. (1995). Three natural zircon standards for U-Th-Pb, Lu-Hf tarce element and REE analyses. *Geostandards Newsletter, 19*(1), 1-23. doi:doi:10.1111/j.1751-908X.1995.tb00147.x

Wilson, S. A. (1997). Data compilation for USGS reference material BHVO-2, Hawaiian Basalt. *U.S. Geological Survey Open-File Report*.

Yang, S., Zhang, F., & Wang, Z. (2012). Grain size distribution and age population of detrital zircons from the Changjiang (Yangtze) River system, China. *Chemical Geology, 296-297*, 26-38.

CHAPTER 3. REE AND TRACE ELEMENTS IN DETRITAL APATITE AS A PROVENANCE INDICATOR: A CASE STUDY OF THE MISSISSIPPI RIVER AND ITS TRIBUTARIES, USA

3.1 Introduction

Apatite is found as an accessory mineral in metamorphic rocks, and in igneous rocks as a primary mineral, as well as in sedimentary rocks both as a diagenetic cement and in a detrital context (Belousova, Griffin, O'Reilly, & Fisher, 2002; Chang, Howie, & Zussman, 1996). Apatite is relatively physically robust and ubiquitous in continental settings, thus it can be a useful as a tracer of the origin of detrital material based on its geochemistry. Apatite geochemistry has been useful as a provenance tool in a number of modern and ancient settings based on variability in both geochemical character and thermochronologic age (Belousova et al., 2002; Chew, Sylvester, & Tubrett, 2011; Fleischer & Altschuler, 1986; A. Morton & Yaxley, 2007; Naeser, Naeser, & McCulloh, 1989).

Popular provenance methods, such as U-Pb geochronology of detrital zircons, represent robust approaches for the determination of provenance; however, this method can be affected by significant source fertility and lack of source rock age variability (A. Fildani et al., 2016). In the Alps, zircon fertility of different source terranes has been shown to differ by 3 orders of magnitude (Malusa et al., 2016). Specifically in North America, granites associated with Grenville orogenic events have significantly more Zr concentrations than surrounding terranes (Dickinson, 2008; D.P. Moecher & S.D. Samson, 2006). Grenville zircon also suffer from recycling issues and have been redistributed across most of the eastern half of the North America, which has led to complications with interpreting source derivation (A. Fildani et al., 2016). In such settings, additional datasets need to be used to cross-check and interpret findings that are influenced by such complications (Gerdes & Zeh, 2006; Sevastjanova et al., 2011).

Apatite geochemistry has the potential to contribute to provenance analyses due to its distinct variability between host rock types and its ability to characterize specific source regions in independent ways (Belousova et al., 2002; Fleischer & Altschuler, 1986; A. Morton & Yaxley, 2007). Belousova et al. (2002) provided one of the groundbreaking studies for this kind of analysis, using geochemical data to independently determine specific rock types of igneous apatites through a series of geochemical concentration thresholds. Morton and Yaxley (2007) studied the Paleo-Volga, which has a comparable geographic scale to the Mississippi River drainage, and they derived some useful interpretations regarding the provenance by using a variety of methods and element thresholds from past studies. That study was one of the first to examine detrital apatite use in provenance and determine its effectiveness as an independent tool to interpret source contribution through time. Sample sizes Morton and Yaxley (2007), however, were small (n= 19-52) which has been shown to be detrimental for provenance studies using detrital zircon (Vermeesch, 2004).

This study seeks to further advance the methods used in Belousova (2002) and Morton and Yaxley (2007) through quantitative analysis in order to determine whether apatite can effectively be used to interpret provenance on a continental scale using the Mississippi River Valley drainage basin as a test (Fig. 2.1). By using a larger sample size (n=85-168) and applying a more quantitative approach, we seek to further the application of trace elements and Rare Earth Elements (REEs) as an independent provenance proxy for typical continental siliciclastic sediment. This new approach used both REEs and trace minerals to derive an apatite geochemical signature for each of the Mississippi's large tributaries. These signatures are then used to determine the provenance of a mixed sample taken from the Mississippi River just south of its last major confluence with the Red River and upstream of the river mouth. Using the

defined end members, we unmix the apatite population using a Monte Carlo approach and compare them with recent studies involving modern Mississippi River provenance.

3.2 Apatite Geochemistry

Previous studies have shown that apatite geochemistry is largely controlled by host rock type and the degree of fractionation (Belousova et al., 2002; Fleischer & Altschuler, 1986). Trace elements and rare earth elements (REEs) substitute for Ca in trace amounts with concentrations varying according to the whole rock SiO_2 content (Belousova et al., 2002; Chang et al., 1996). With increased fractionation Y, Mn, and heavy REEs (HREEs) content increases. Conversely, Sr, Th and light REEs (LREEs) deplete with greater amounts of fractionation (Belousova et al., 2002; Chang et al., 1996; Nash, 1984). Furthermore, negative Eu anomalies increase with fractionation due to the depletion of Eu through the crystallization of feldspar (Budzinski & Tischendorf, 1989).

Belousova et al. (2002) used laser ablation inductively coupled-mass spectrometry (LA-ICP-MS) to characterize apatite REE and trace element compositions by source bedrock type and devised an apatite classification cladogram to discriminate apatite by rock type based on concentration thresholds for different elements. Bouch et al. (2002) and Morton and Yaxley (2007) investigated the geochemical composition of apatites from sandstones to understand authigenic diagenetic processes and constrain detrital provenance. Earlier studies generally used cross-plots to compare Sr/Y, Sr/Mn and Th/U ratios in order to discriminate source rock type.

3.3 Methods

3.3.1 Laser ablation ICP-MS analysis

Sand samples were taken from each Mississippi River tributary and from the Mississippi River just south of its confluence with the Red River. They were then sieved and apatite grains between 63 and 150 micron in size were concentrated using heavy liquid methods and hand-picked. Laser ablation analysis of REE and trace elements was completed at in the Department of Geology and Geophysics at LSU on an iCAP Qc ICP-MS connected to a CETAC Technologies LSX-213 laser ablation system (Appendix B Supplemental Table 2.1). The NIST 612 glass standard (Pearce et al., 1997) was used for calibration. Due to the lack of international recognized apatite standards for REE and trace element concentrations, we used two in-house standards for assessing precision and reproducibility (Appendix B Supplemental Table 2.2). Post-analytical processing of the ICP-MS data was completed with IGOR Pro using the Iolite REE and Trace package. Results of the analyses are provided in Table 1 For each sample, approximately 120 grains were analyzed to account for lithologic variability found within each detrital sample and reflecting the potential multi-source origin, consistent with statistical methods used for interpreting detrital zircon (Vermeesch, 2004). REE data was chondrite normalized to account for the Otto-Harkins effect using the chondrite values from McDounough and Sun (1995). Eu anaomolies (Eu/Eu*) were calculated chondrite normalized values with the following formula:

$$Eu/Eu^* = Eu/((Sm+Gd)/2))$$

3.3.2 Belousova Cladogram

Following Belousova et al. (2002), a cladogram was used to differentiate apatite from different types of source rock to the using a series of discriminating elements and element ratios (supplementary material, Fig 3.1). Based on this cladogram, apatite grains were separated into seven source rock categories: Lherzolite, Larvikite, Jacupirangite, Iron Ore, Granitoid, Dolerite, Carbonatite and Granite Pegmatite.

3.3.3 Monte Carlo Unmixing

Monte Carlo population simulations are often used in unmixing models for detrital zircon U-Pb age spectra (Sundell & Saylor, 2017). These types of analysis have been found to be especially useful in continental scale highly recycled populations and while traditionally used in zircon have been modified to help interpret apatite data in this study. In general, this modeled simulation predicts a best fit mixing model through repeated iterations of random sampling within categorically organized data (Sundell & Saylor, 2017).

To further interpret the geochemical dataset of the detrital apatites, a Monte Carlo population simulation was completed in MATLAB. We use an inverse Monte Carlo to essentially unmix large numbers of detrital apatite grains based on 1) La-Y-Sr geochemical proportions and 2) categorical source rock data. A program was designed to retro-source detrital apatite samples from specific tributaries by creating randomly generated weighted populations that were then compared to a mixed sample a user specified number times (we use 1000). Each of these generated populations was then compared to the known values of the mixed sample with a KS (Kolmogorov-Smirnov) test with a failure cutoff at user set 0.05 to determine the best fit or optimal unmixing model producing percent contribution from each tributary.

3.4. Geologic Background

3.4.1 Precambrian shield

Apatite, like all provenance indicators, requires large-scale bedrock heterogeneity of the potential continental source areas to be useful in determining the geographical source of sediment to the final depocenter. The Mississippi drainage basin spans a variety of North American source regions that have complex geological histories. In particular, progressive accretion of tectonic blocks through geologic time led to different phases of magmatism and crustal accretion. This is reflected in a mosaic of different geological provinces in North America (Fig. 3.1) which potentially have unique apatite geochemical fingerprints.

The Superior Province (2500–2700 Ma) is part of the Archaean Craton and formed as a result of the Slave-Rae-Hearn and the Superior Blocks colliding and eventually forming the North American craton (P.F. Hoffman, 1989). Later the Trans-Hudson Province (1800–1900 Ma) amassed the Hearn, Wyoming and Superior Blocks to form the core of the Laurentian continent (Dahl et al., 1999; Paul F Hoffman, 1988; Ross et al., 2005). The Penokean Province is comprised of a series of Archean and Paleoproterozoic rocks that reach from the northern United States to Canada (Dahl et al., 1999; Davidson, 1995; Van Schmus, 1976). These terranes have been regionally dated through both Sm-Nd and zircon U-Pb methods to approximately 1800–1900 Ma (Bickford & Van Schmus, 1985; Nelson & DePaolo, 1985) and are drained by the northern reaches of the Ohio and Missouri Rivers, as well as the entirety of the Upper Mississippi River.

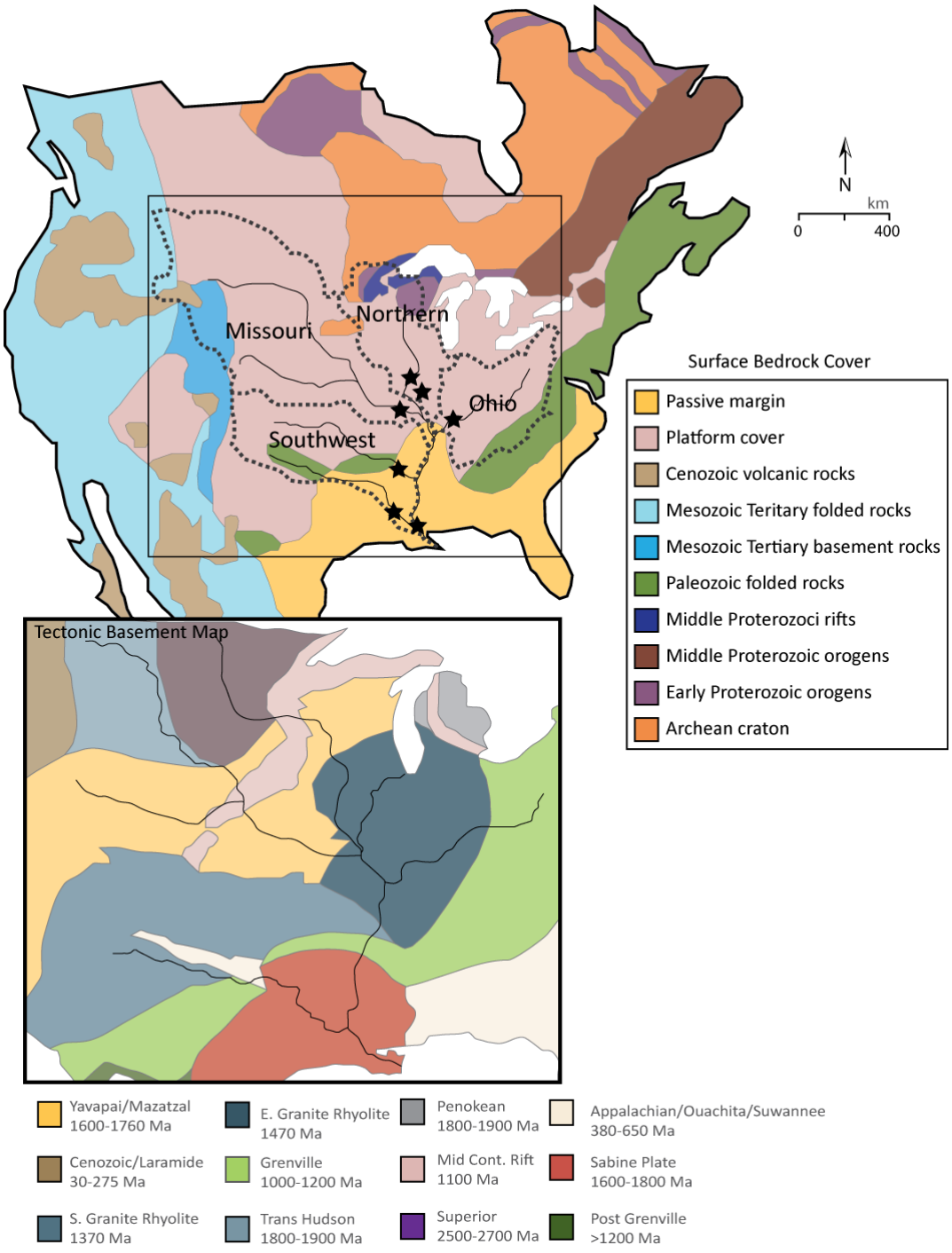

Figure 3. 1 Map of continental North America showing major surface crustal provinces of the bedrock divided by major age grouping. The outlines of the major tributary catchment defined in this paper are shown by dashed lines. Black stars show sample locations. Simplified and modified from (Garrity, 2009). The lower map indicates major continental block source terrane underlying surficial geology modified from Gehrels(2010).

3.4.2 Proterozoic midcontinent regions

The Yavapai and Mazatzal Province (1600–1800 Ma) is the basement terrane which underlies much of the western and mid-continental regions of North America. It spans from Arizona to Minnesota and formed as a result of multiple pulses of arc accretion (Bowring & Karlstrom, 1990; K. Karlstrom et al., 1993; K. E. Karlstrom & Humphreys, 1998). Nd isotope data indicate that the Yavapai Province experienced little to no reworking of Archean or Paleoproterozoic crustal units during its formation (Donald J DePaolo, 1981). The Mazatzal Province formed directly after the Yavapai and stretches from northern Mexico into Canada. This terrane formed in a continental active margin setting as a result of arc accretion and the accumulation of back-arc supracrustal sequences (K. Karlstrom et al., 1993; Shaw & Karlstrom, 1999). Rocks of this terrane are now largely covered by Cenozoic sequences.

The Granite-Rhyolite and Grenville Provinces are located in the Southwest and Eastern United States. The Granite-Rhyolite Province is extenisve in the Midwest but extends further into areas of Canada (Bickford & Van Schmus, 1985; Muehlberger et al., 1967). It is dominated by intrusive A-type granites which may have been orogenic in origin (Corrigan & Hanmer, 1997; K. E. Karlstrom et al., 2001; McLelland et al., 1996). The Grenville Province (1000–1200 Ma) stretches from the southwest and across eastern North America. This terrane is the product of prolonged collisions which assembled the Rodinia Supercontinent (Dalziel, 1991; Moores, 1991). It is now largely covered by sedimentary passive margin marine and clastic sedimentary rocks (Fig. 3.1).

3.4.3 Phanerozoic orogens

The Appalachian and Ouachita terranes represents several terranes that date to a similar time period from 500-700 Ma. The Appalachian terrane was constructed during a series of collisional events with Laurentia (Drake Jr et al., 1989; Horton et al., 1989). The Ouachita Igneous bedrock is associated with rifting that created the Southern Iapetus Ocean during the breakup of Rodinia at 539–530 Ma (Hanson et al., 2013). The Appalachian and Ouachita terranes are shown as Paleozoic folded rocks in Figure 3.1

The younger Mesozoic and Cenozoic rocks associated with the Western Cordilleran Province of North America are associated with the building of the Rocky Mountains and have been proposed to account for a large amount of the sediment in the Missouri and Mississippi Rivers (Gregory, Herrmann, Ireland, & Clift, 2018, in review; also see Ch.2).

3.5. Results

3.5.1 Apatite by Source Rock Type

The most abundant types of apatite found in our samples are assigned to the Granitoid, Dolerite, Carbonatite, Granite Pegmatite and Iron Ore source types (Fig. 3.2, 3, and 4). For this reason, only these were plotted because there are too few apatite analyses assigned to Lherzolite, Larvikite or Jacupirangite source rock types to be statistically meaningful. Nonetheless, these data are provided in Appendix B for reference.

3.5.1.1 Rare Earth element geochemistry

Chondrite-normalized REE plots of the different apatite source rock groups divided by the Belousova (2002) cladogram were created from a select few samples to demonstrate their general character, given the large sample size within each of the main categories (Fig. 3.2).

Trends in REE data are better expressed by plotting La/Yb, which represents the overall slope of the REE curve, against La/Sm which is a proxy for the relative enrichment of the LREEs (Fig. 3.3).

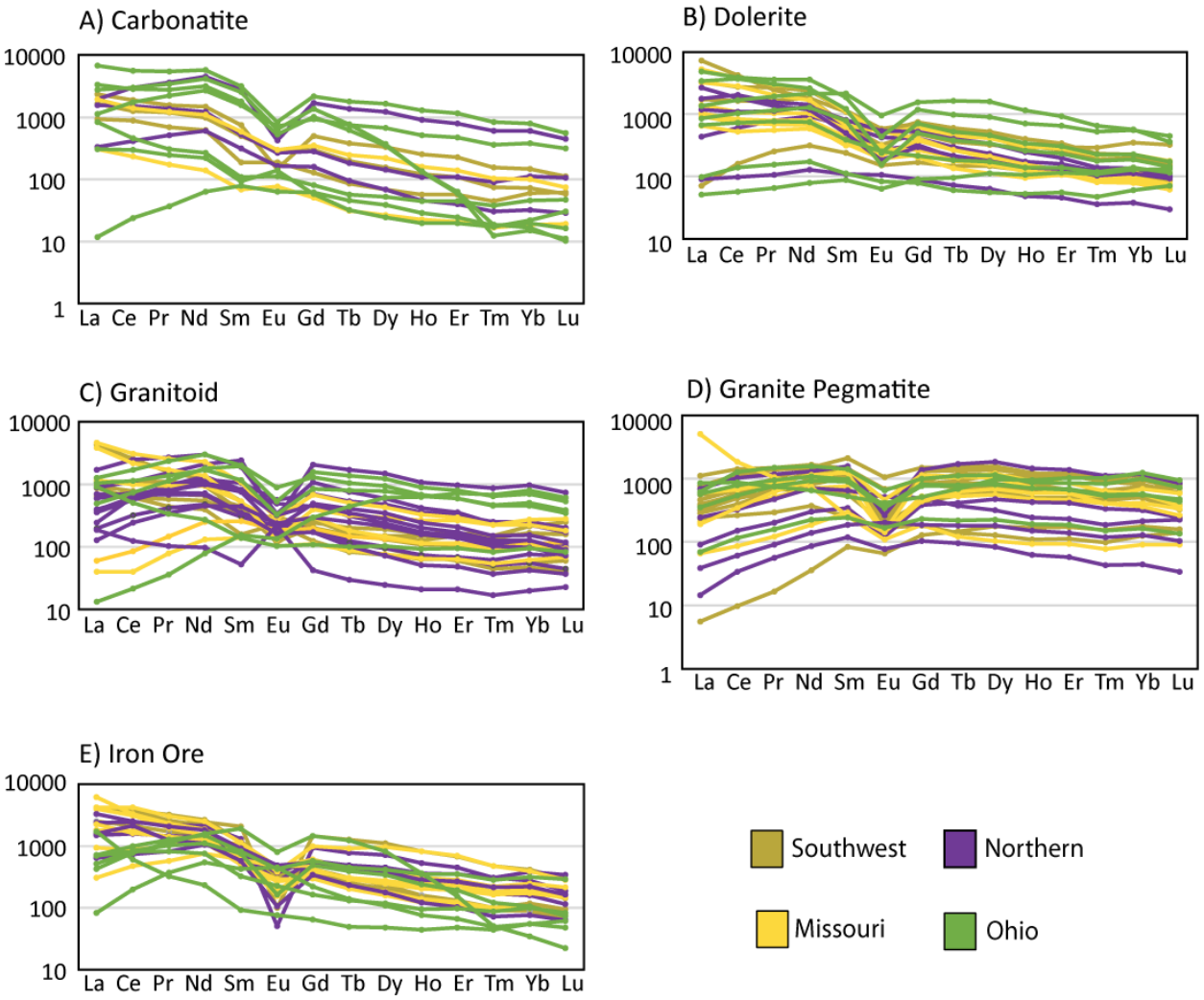

Figure 3. 2 REE plots from the population of apatite divided by Belousova (2002) apatite source rock type and colored by basin. Purple represents the northern/upper Mississippi apatites, yellow the Missouri River, Green the Ohio River, and brown the Southwestern tributaries.

Apatites classified as Carbonatites (Fig. 3.3A) show moderate to high HREE depletion (low La/Yb and La/Sm values) and LREE enrichment (high La/Yb and La/Sm values). Dolerite-

derived apatites (Fig. 3.3B) show modest to high levels of HREE depletion, with little LREE enrichment.

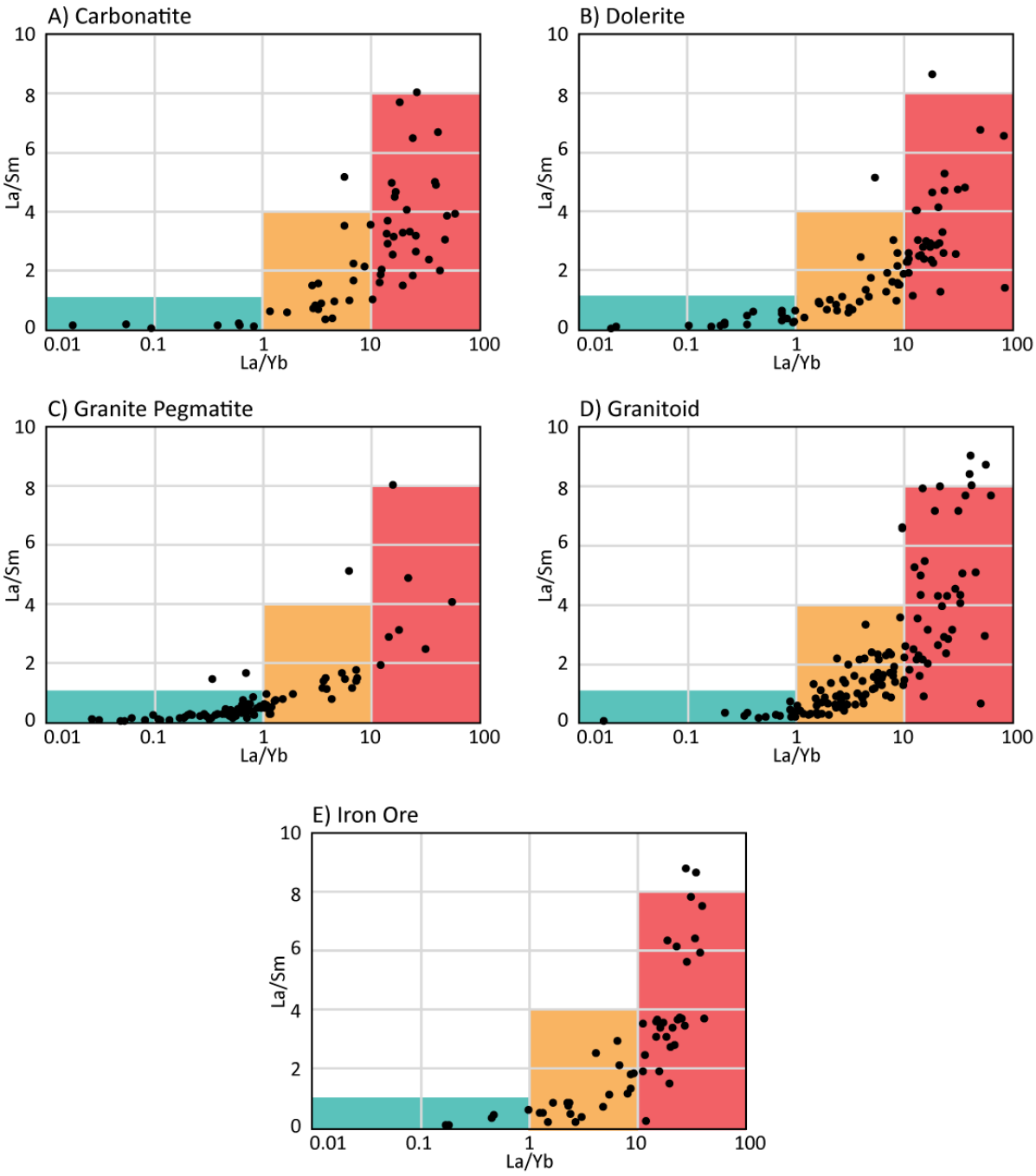

Figure 3. 3 Cross plots of La/Yb against La/Sm for apatite grains divided by source rock type. (A) Carbonatite, (B) Dolerite, (C) Granite pegmatite, (D) Iron ore, and (E) Granitoid. Blue, Orange, and Red boxes indicate increasing levels of LREE and HREE depletion.

Granite Pegmatites (Fig. 3.3C) have the most distinctive REE signature within their apatites, with the majority of samples showing LREE depletion and a depletion of HREEs, with a generalized negative slope to the REE plot. A few of the apatite grains in this group are found to have moderate HREE enrichment. Iron ore derived grains fall into three main groups (Fig. 3.3D). The first group are apatites with LREE depletion and moderate HREE depletion. A second group comprises apatites with moderate LREE enrichment and HREE depletion, while a third shows strongly negative REE slope (Fig. 3.2) with high HREE depletion. Finally, Granitoid apatites cluster between 1 and 10 along the La/Yb axis and 0 and 2 on the La/Sm axis (Fig. 3.3D), showing LREE depletion and moderate HREE depletion. A second group within the Granitoid population exhibits high HREE depletion.

3.5.1.2 Ternary Diagrams

Since previous studies have found that trace elements such as La, Y, Sr, Mn and REEs change in relative proportions in apatites from different source rocks. Three of these elements were chosen to demonstrate variability in source rock type within the sample (Belousova et al., 2002; Chang et al., 1996; Nash, 1984). Y and Sr were chosen to plot because they had the highest variability among the trace elements, and they should, in theory, inversely vary with changes in fractionation. La was also chosen because, within the REEs elements, it dsiplays the most variability and is therefore considered here as an analog for relative LREEs enrichment or depletion. Another reason for choosing these three elements is that, for the most part, La, Y and Sr have similar date ranges and generally plot well on a ternary diagram. Results were not normalized before plotting; however, plotting concentration values on a ternary diagram allows for in sample standardization between elements since they are scaled to relative proportions (Fig 3.4).

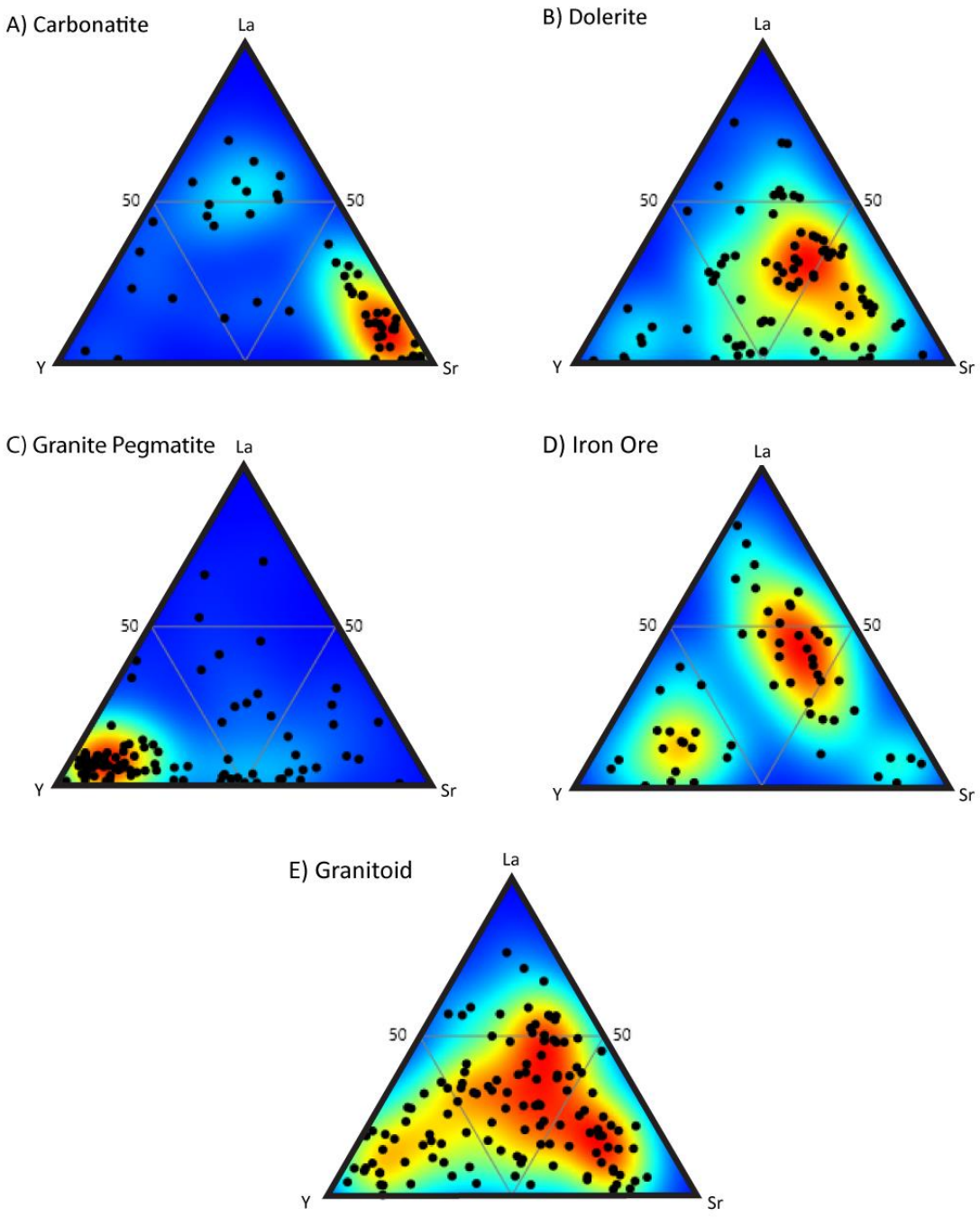

Figure 3. 4 Ternary diagrams plotting La, Y and Sr for apatite grains divided by rock type source. (A) Carbonatite, (B) Dolerite, (C) Granite pegmatite, (D) Iron ore, and (E) Granitoid. Red colors represent a high density of points while blue represents a low density.

Ternary plots show distinct differences in apatite by rock type (Fig. 3.4). Carbonatite apatites generally have high Sr concentrations and low concentrations of both La and Y (Fig.

3.4A). Dolerite apatites plot more in the center of the ternary diagram, with moderate to high concentrations of Sr and moderate levels of both La and Y (Fig. 3.4B). The Granite Pegmatite apatite population has a very distinctive signature showing enrichment in Y compared to La and Sr (Fig. 3.4C). There is another distinctive clustering within the Granite Pegmatite group that shows moderate levels of both Sr and Y, but overall granite pegmatite apatites are characterized by La depletion. Iron ore apatite grains (Fig. 3.4D) fall into three distinct groups with the largest group characterized by moderate levels of Sr and La, as well as Y depletion. While there is some overlap between Dolerite and Iron Ore apatites, the main Dolerite group tends to tighter clustering. A second group within the Iron Ore apatites has Y enrichment, with relatively low levels of La and Sr. Granitoid apatites (Fig. 3.4E), a catch-all felsic category, show the greatest degrees of variation and are harder to classify using this ternary plot.

3.5.2 Apatite Provenance

3.5.2.1 Apatite by Tributary

For this study, apatite grains were divided into four main provenance groups related to different geographic areas of the Mississippi River catchment (Fig. 3.1 and 5); Northern tributaries, Missouri River, Southwestern tributaries (i.e., the Red and Arkansas Rivers) and the Ohio River. Morton and Yaxley (2007) previously used a series of cross-plots to show geochemical differences between apatite grains.

However, these graphs often fail to identify distinctive populations, especially when dealing with numerous, highly geochemically variable detrital grains, which are common when the drainage system is at the continental scale (Fig. 3.5, 6; see also Supplementary Figs. 3.2 and 3.3). Within these graphs, apatite grains show too much geochemical variation to be able to distinguish

coherent patterns that can be used to constrain provenance (Fig. 3.5). The only exception in our dataset is the Missouri River, where it appears that the apatites tend to plot towards the alkaline field around the iron ore end member (Fig. 3.5).

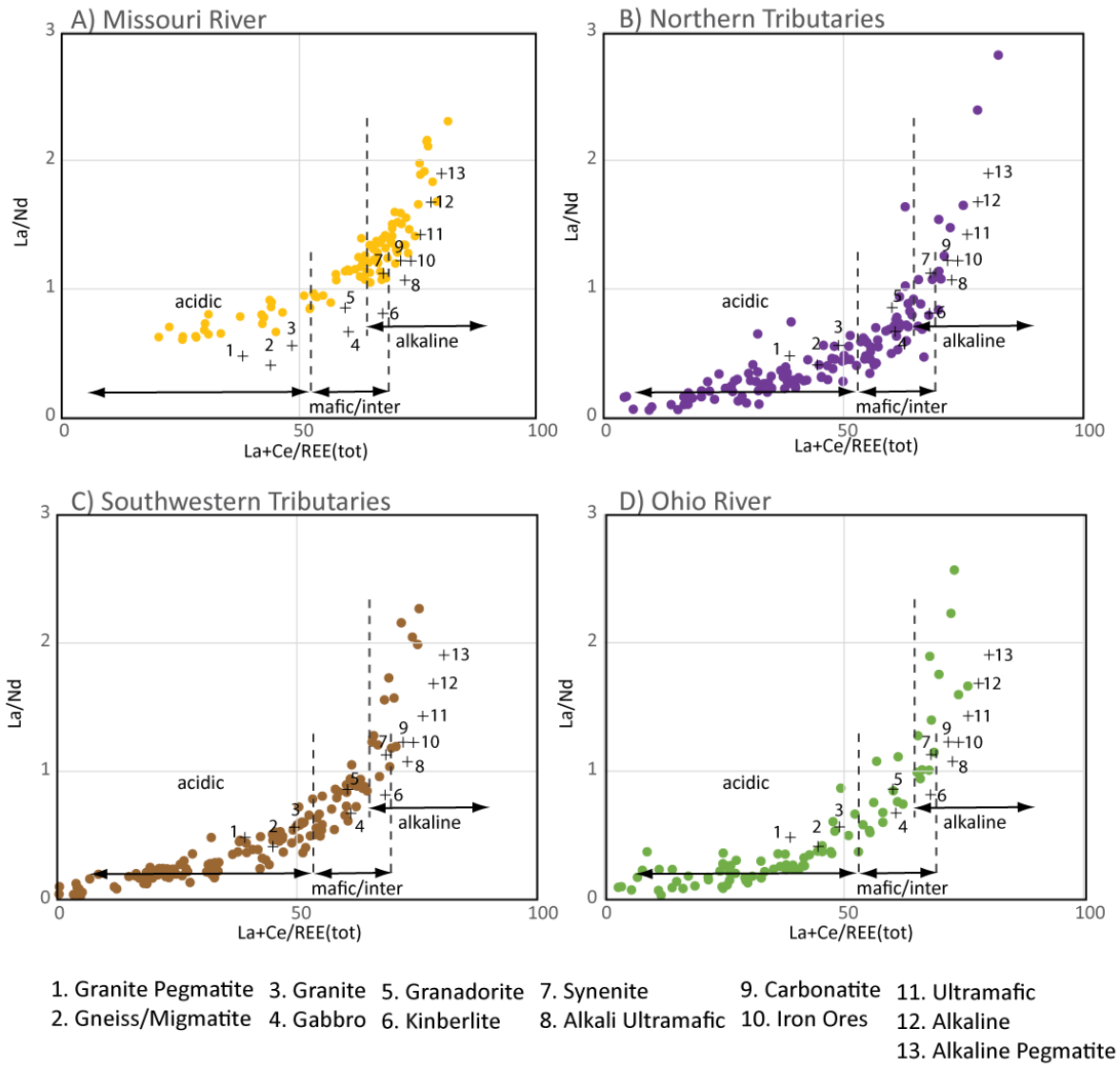

Figure 3. 5 Cross plots of La/Nd versus (La+Ce)/REE (total) divided by tributary. (A) Missouri, (B) Northern Tributaries, (C) Southwest Tributaries, and (D) Ohio. Numbers next to crosses represent average values of apatite from different rock type taken from (Belousova et al., 2002).

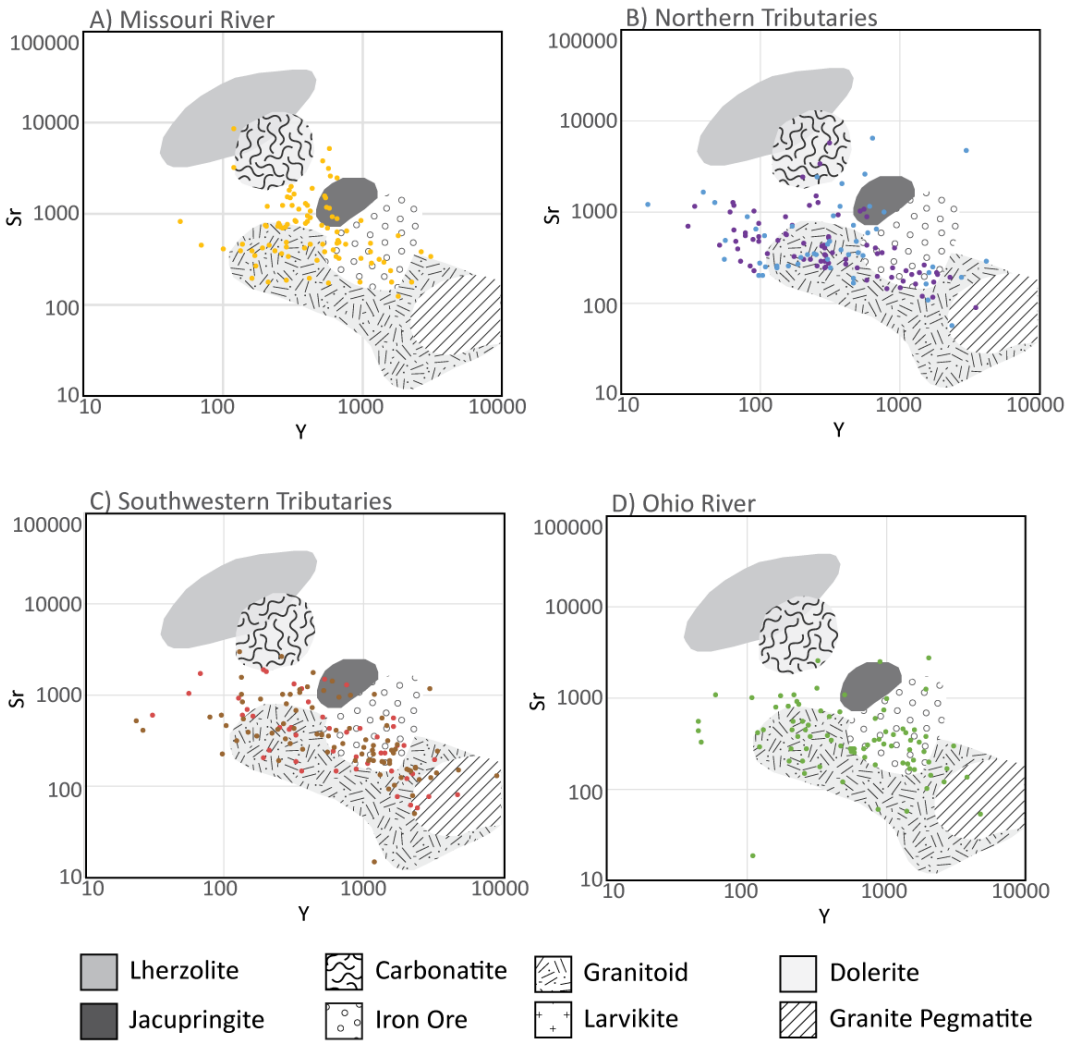

Figure 3. 6 Cross plots of Sr against Y concentrations for single apatite grains with fields showing the predicted source rock types from (A. Morton & Yaxley, 2007) and (Belousova et al., 2002), divided by tributary. (A) Missouri, (B) Northern Tributaries, (C) Southwest Tributaries, and (D) Ohio.

However, multidimensional statistical tools, such as PCA, appear to highlight differences within these detrital samples, especially when applied within the nomenclature framework of the Belosouva et al. (2002) cladogram. Based on this cladogram, the major tributary areas were separated by rock type and then plotted as pie graphs (Fig. 3.7). The Missouri River appears to derive most of its apatite grains from Iron Ore, Dolerite, and Granitoid sources. What is specific to this drainage is the large amount of Iron Ore-derived apatite within the population (Fig. 3.7A).

When divided into different types of source rocks, the Northern Tributaries and the Ohio River have almost identical populations (Fig. 3.7B,D). This is interesting given that their geochemical signatures mapped on the ternary plots (of La, Y, and Sr) show such striking differences (Fig. 3.8). The Southwest Tributaries are dominated by Granite Pegmatite grains, having twice as many as any of the other drainage (Fig. 3.7C).

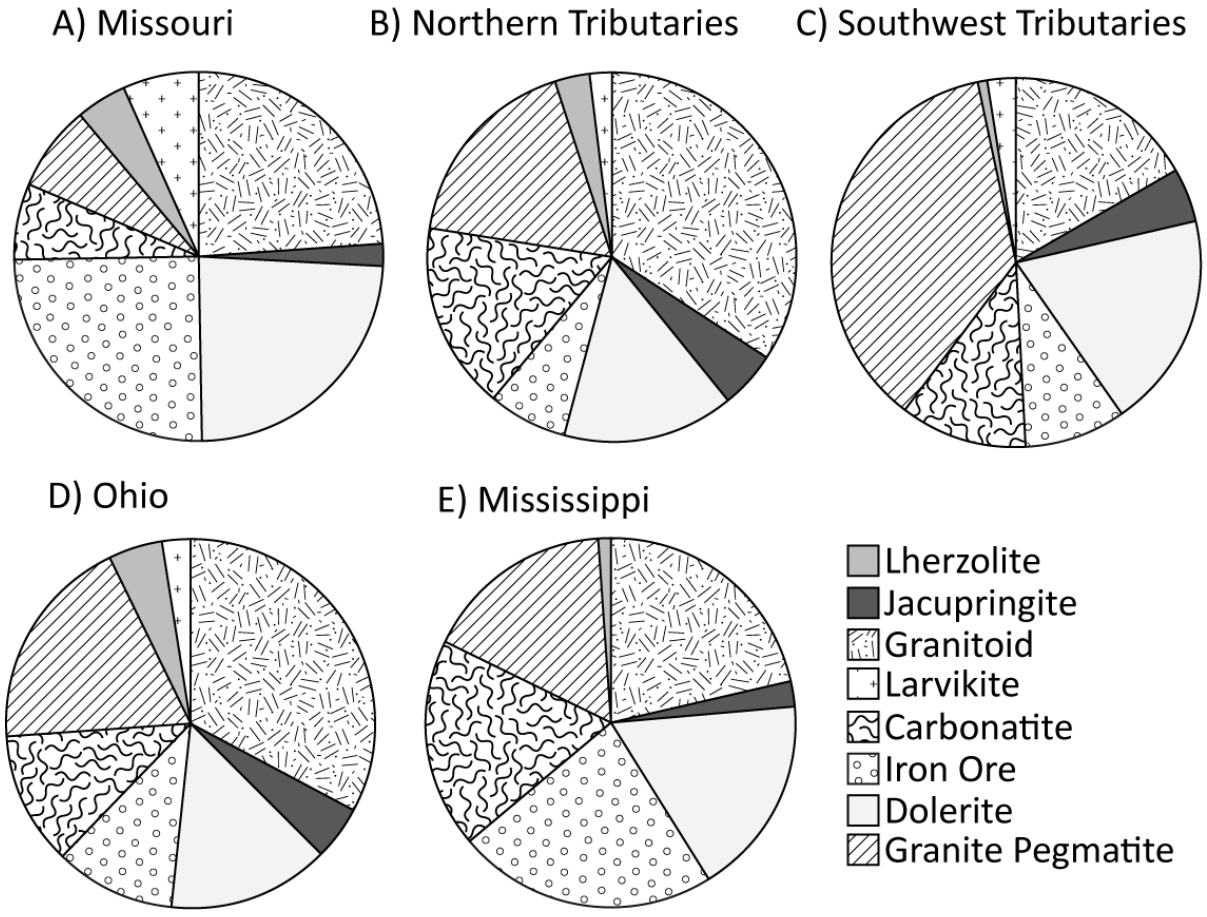

Figure 3. 7 Pie diagram showing the proportion of apatite grains derived from each rock type source divided by tributary, (A) Missouri, (B) Northern Tributaries, (C) Southwest Tributaries, (D) Ohio, and (E) Lower Mississippi.

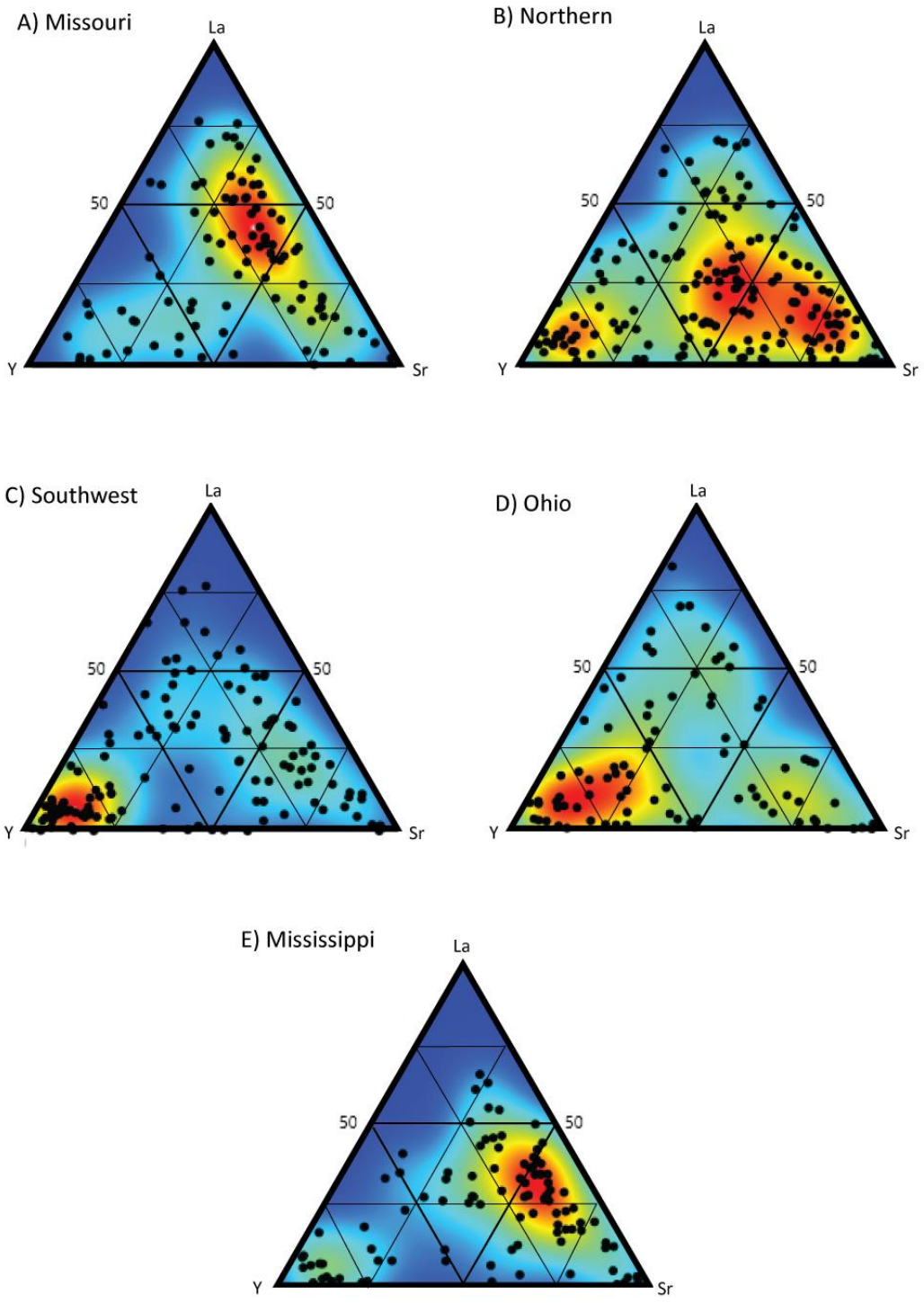

Figure 3. 8 Ternary diagrams plotting La, Y and Sr for individual apatite grains separated by tributary. (A) Missouri, (B) Northern Tributaries, (C) Southwest Tributaries, (D) Ohio, and (E) Lower Mississippi.Red colors represent a high density of points while blue represents a low density.

Ternary plots were created for each tributary showing distinct differences between the main drainage areas of the Mississippi. The Missouri River shows a distinct grouping of apatite grains that show Y depletion and moderate levels of both Sr and La (Fig. 3.8A). When we compare this to the ternary plots of apatites divided by source rock type (Fig. 3.4), the Missouri apatites tend to plot strongly towards Iron Ore and Dolerite end members. The Northern Tributaries are slightly more diverse in terms of their apatite chemistry but have two resolvable main groups (Fig. 3.8B): one with Sr enrichment with moderate to low levels of La and Y, while the secondary grouping has Y enrichment with La and Sr depletion. The diversity found within the population is likely attributed to the large degree of geochemical variability in the Granitoid-related apatite found within the sample. The data suggests a diverse source composition. Apatites from the Southwestern tributaries have a rather diverse population but with a distinctive grouping of apatite grains that are enriched in Y and depleted in both Sr and La (Fig. 3.8C). When this ternary plot is compared to those in Figure 3.4 it can be seen that granite pegmatite apatites dominate the population. The Ohio River has one major grouping of apatite grains which are enriched in Y and depleted in both La and Sr (Fig. 3.8D). If this ternary (Fig. 3.8D) is compared to the La-Y-Sr ternary plot divided by source rock types (Fig. 3.4) it implies that the majority of grains in the Ohio River should be derived from Granitoid or Granite Pegmatite sources. A map showing the possible sources for each major apatite grain classification shows the distribution by tributary of Iron Ore, Carbonatite, Dolerite, and Granite Pegmatite source areas are later used to compare these findings (Fig. 3.9).

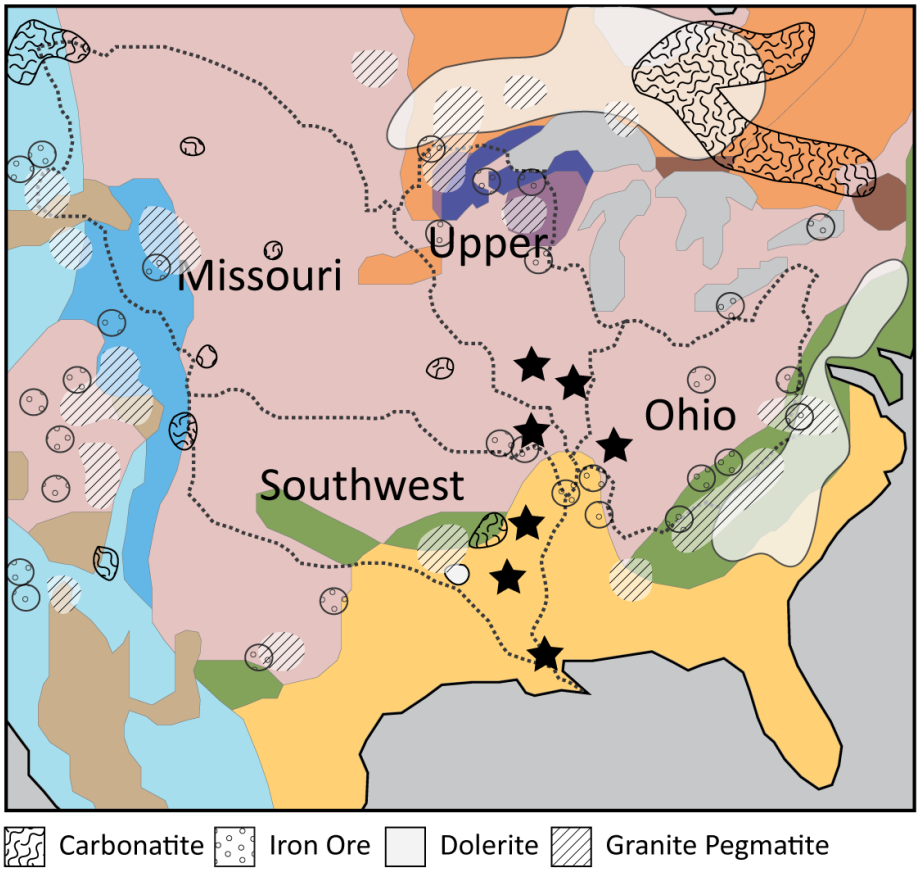

Figure 3. 9 Close-up map of the surficial bedrock cover found in Figure 3.1 showing possible apatite source rocks within each tributary catchment. Possible source rock locations complied from several different sources (Hamilton, Goutier, & Matthews 2001; Krevor, Graves, Van Gosen, & McCafferty 2009; Landes, 1935; Schlische, Withjack, & Olsen, 2003; Tarr & McMurry, 1922; Woolley & Kjarsgaard, 2008)

3.5.2.2 Apatite in the Mississippi River

To test whether or not apatite can be used to decipher geochemistry at a continental scale, a sample was taken just south of the Mississippi's southernmost confluence, close to the river mouth. This sample was then plotted as a La-Y-Sr ternary (Fig. 3.8E), and the apatites were then divided into source groups that are presented as a pie plot (Fig. 3.7E). The La-Y-Sr ternary shows that the lower Mississippi River apatite population is represented by two major groups. The first group has moderate to high levels of Sr and La in relation to Y. The second group has

both Sr and La depletion relative to Y. Furthermore when apatite grains are divided into discreet apatite groups using the Belousova et al. (2002) cladogram, the Mississippi apatite population contains almost even amounts of Carbonatite, Granitoid, and Granite Pegmatite derived grains (Fig. 3.7E). Most notably, the lower Mississippi River contains a high number of apatite grains derived from Iron Ore, which is only seen to be dominant in the Missouri River (Fig. 3.7).

To more thoroughly explore the provenance of apatite grains in the Mississippi River, a statistical Monte Carlo unmixing model was applied to the apatite grains in two ways: 1) unmixing using the Belousova et al. (2002) cladogram categories, and 2) unmixing using the distribution in the La-Y-Sr ternary plots. When the apatite grains were divided based on the cladogram categories shown in Supplementary Figure 3.1, the percentage of apatite grains contributed from the Missouri River dominates at ~53% (Fig. 3.10B). Secondary contributions from the SW tributaries are at 27% with minimal input from both the northern tributaries and the Ohio River.

The same inverse Monte Carlo was applied to the La-Y-Sr ternary plots since they provide the most separation between both apatite grain types and source tributary compositions (shown previously in Figs. 3.4 and 8. Each ternary diagram was divided into 16 categories according to the different percentages of La, Y and Sr, then each grain falling within the those divisions were counted (divisions noted in Fig. 3.8 with black lines).Those counts were then used to create categorical datasets from which the Monte Carlo was constructed. The result of this Monte Carlo unmixing is displayed in Figure 3.10A. This shows the Northern Tributaries,

Southwestern Tributaries and the Missouri River as roughly equal contributors to the mixed lower reaches Mississippi apatite population.

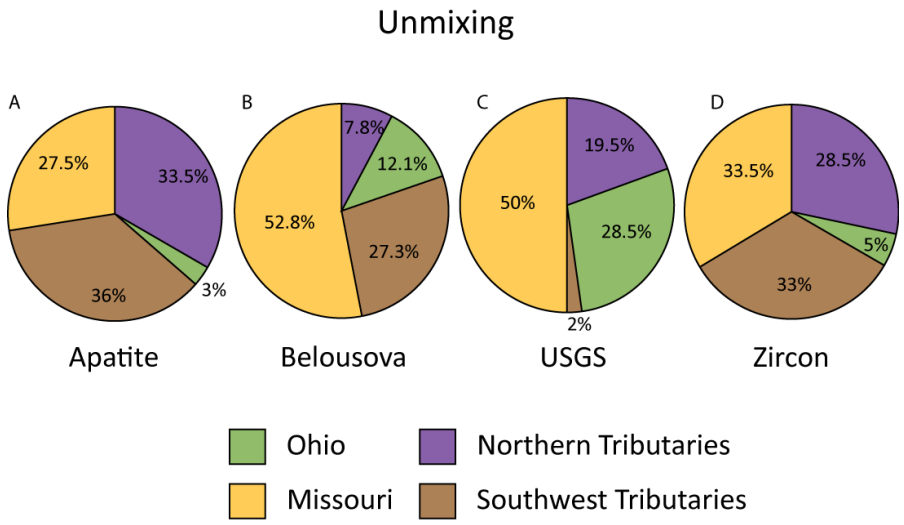

Figure 3. 10 Pie diagrams showing the estimated contributions from the major tributaries to the lower reaches of the Mississippi River based on (A) Monte Carlo results from 16 apatite ternary groups, (B) Monte Carlo results from seven source rock groups, (C) USGS suspended sediment from gauging measurements (Mason et al., 2017), and (D) from zircon U-Pb age spectra (Gregory et al., in review; See Ch. 2).

3.6. Discussion

3.6.1 Apatite Derived from Tributaries

The Missouri River has a distinctive cluster of apatites, as shown on the La-Y-Sr ternary plot (Fig. 3.8A). Furthermore, Missouri River apatites plot in the same part of the diagram as Iron Ore and Dolerite bedrock apatites (Fig. 3.4). The majority of the Missouri River apatites are Y-depleted with moderate levels of La, indicating less fractionated and more mafic/alkaline compositions (Figs. 3.8A and 3.5A). A recent study of zircon derived from the Missouri River catchment showed a relative lack of diversity in source rock that might explain the limited geochemical diversity seen in the ternary diagram (Fig. 3.8A) (Gregory et al., 2018, in review; see Ch. 2). Apatites from the Northern Tributaries of the Mississippi River show diversity in

their source compositions, with moderate to high levels of Sr for many of the grains and another minority cluster with high levels of Y (Fig. 3.8B). This pattern indicates erosion of apatites from a variety of sources. Both mafic and felsic sources are inferred from Figure 3.5B, but few grains are derived from alkaline sources. The mafic apatite grains in the Northern Tributaries are most likely derived from the Canadian Shield and Great Lakes region. We infer a high number of Granitoid-derived apatites based on the similarity between the ternary high density areas between the total population (Fig. 3.8B) and the granitoid only diagram (Fig. 3.11B). Given this association, it is apparent why many of the Northern Tributary apatites are classified as acidic on Figure 3.5B. The apatites from the Southwestern Tributaries of the Mississippi are dominated by a large group of grains with relative Sr and La depletions (Fig. 3.8C).

This is an indicator of high fractionation and erosion from felsic and metamorphic sources (Fig. 3.5C). The bulk of the apatite population from that part of the catchment is most likely derived from intrusive granite pegmatite sources within the southwest (Fig.3.9). However, apatite grains from these rivers do show a broad variety of geochemical compositions and thus source rock bulk compositions, despite the concentration towards high Y contents. Previous studies of zircon U-Pb ages from the same catchment indicate a diverse basement rock provenance (Gregory et al., 2018; in review, see Ch. 2). Apatites from the Ohio River show La and Sr depletions with high levels of Y, which again likely indicates felsic and metamorphic source rocks (Fig. 3.8D and Fig. 3.9). Given the distinctive grouping and limited range of the Ohio apatite compositions shown in Figures 3.8D and 3.5D we suggest that these apatites are not derived from a great variety of sources. This finding is supported by multiple zircon U-Pb dating studies in that region (Gregory et al., 2018; Mason et al., 2017; D.P. Moecher & S.D. Samson, 2006).

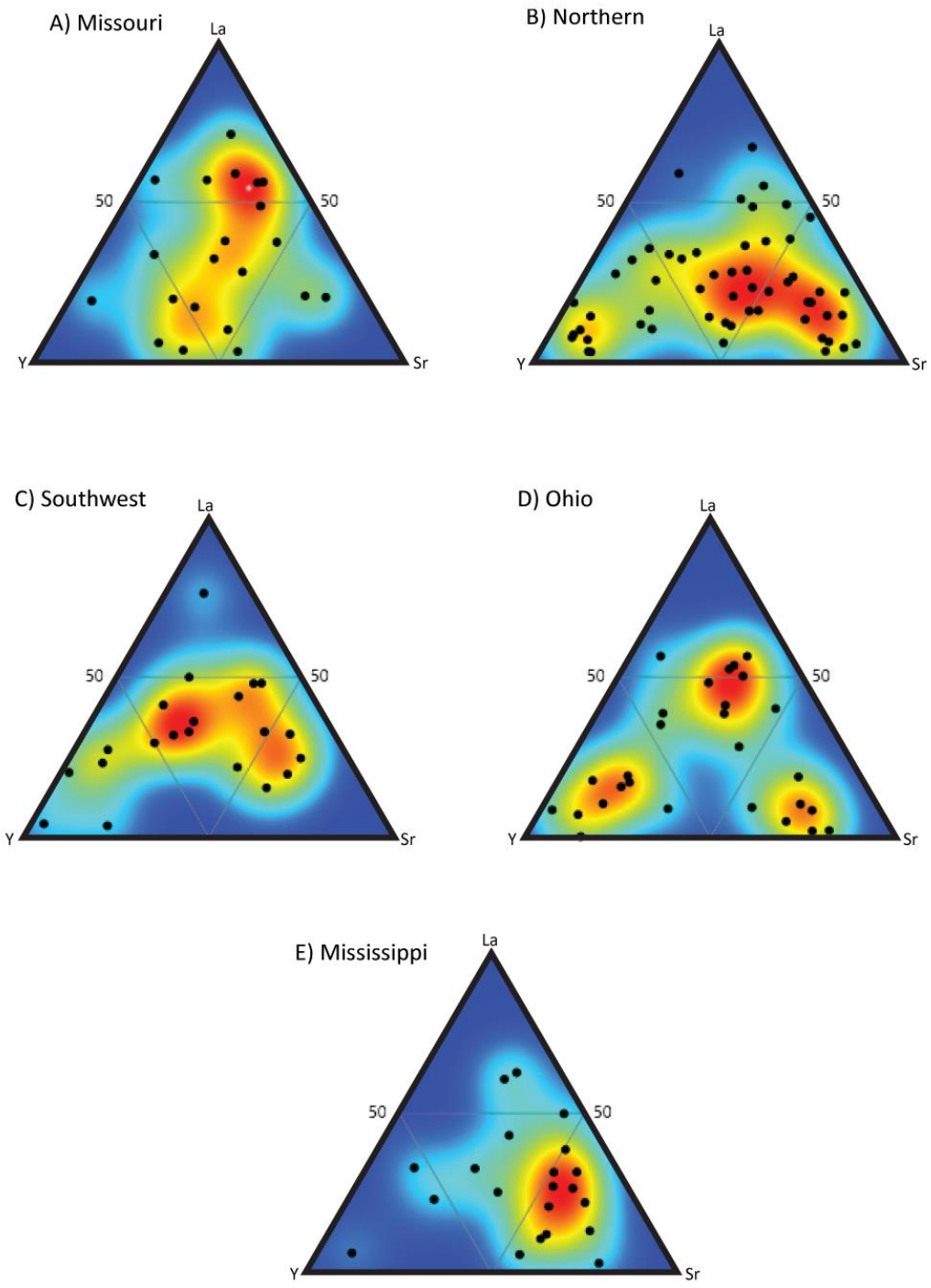

Figure 3. 11 A) Missouri, (B) Northern Tributaries, (C) Southwest Tributaries, and (D) Ohio (E) Mississippi. Red color indicate high point density while blue colors represent low.

3.6.2 Apatite within the Mississippi River

When viewing the results for the inverse Monte Carlo for the Belousova et al. (2002) categories (Fig. 3.10B), the implied dominant flux from the Missouri River into the main stream is consistent with measurements of suspended sediment taken from USGS gauging stations of suspended sediment (Fig. 3.10C) (Mason et al., 2017). The relative contributions from the tributaries, however do not correlate very well. The differences between the Belousova et al.(Belousova et al.) categorical Monte Carlo results and the USGS sediment gauging results can either be attributed to temporally variable flux within the system, or a disconnect between suspended sediment and coarser bedload (Fig. 3.10B and 3.10C). Another issue that arises from running the Monte Carlo simulation on the cladogram categories is that the categorical data for each tributary must be relatively distinct in order to discern between populations. Lack of diversity can lead to possible overestimations from source with significant overlap. As seen in Figure 3.7, the Northern Tributaries and the Ohio River apatite populations are practically identical based on this analytical approach. This could explain the variation seen in the Ohio and Northern Tributary percentages between the Belsousova et al. (Belousova et al.) unmixing pie diagram and those from the detrital zircon and Ternary (Fig. 3.10). It is for this reason that a second approach was applied by applying the inverse Monte Carlo to the results of the La-Y-Sr ternary diagrams.

When viewing the pie graph resulting from the inverse Monte Carlo applied to the La-Y-Sr ternary diagram (Fig. 3.10A), results closely resemble the relative contributions found in the detrital zircon U-Pb populations taken from the same grab sample and from detrital zircon studies in Mason et al. (Mason et al.). They, however, contrast with the USGS gauging data and results of the Belousova et al.(2002) categorical cladogram Monte Carlo results. The variability

between the two Monte Carlo unmixing models (Cladogram and Ternary) can best be explained by the limited variability resolvable between tributaries within the cladogram categorized apatite that were divided based on source rock type. The ternary diagrams were specifically designed to separate tributary populations and therefore produce a more region specific fingerprint with which the Monte Carlo can distinguish source contribution. What is interesting to note is the disconnect between the measured USGS suspended sediment flux and the apatite and zircon data (Fig. 3.10D) (Mason et al., 2017). It would seem that the suspended sediment within the Mississippi River is overwhelmingly dominated by the Missouri in comparison to the bedload sands. However, the bedload sands still account for a lion's share of the sediment flux, which can be seen in the deep sea fan both in the Pleistocene and Holocene (Andrea Fildani et al., 2018; A. Fildani et al., 2016; Mason et al., 2017).

Another important comparison is the difference that can be seen is between the detrital zircon and the ternary unmixing. The detrital zircon model estimates the Missouri contribution at 33.5% while the ternary slightly varies at 27.5% (Fig. 3.10D). This is one of the first provenance analyses of the Mississippi River bedload to show a less than dominant contribution from the Missouri River. The detrital apatite geochemical model may be capturing a decreased bedload flux from the Missouri due to the extensive damming of the river over the last 60 years (M. D. Blum & Roberts, 2009; Mason et al., 2017). This may have been missed by previous detrital zircon studies given the overlap of detrital zircon ages among the western tributaries of the Mississippi River.

Overall however, these methods seem to show that differences between the apatite U-Pb age analysis and apatite ternary unmixing are minimal and, going forward, could be used in tandem or independently to interpret provenance.

3.7 Conclusions

This study finds that apatite can be effectively used to interpret detrital apatite provenance based on the REE and trace element geochemistry chemistry from a population of grains. We found traditional methods of plotting the geochemistry of apatite grains to be limited when trying to fingerprint a detrital population with a large sample size. It is, however, interesting that, when plotting the 3 elements traditionally used to determine apatite variability (La-Y-Sr) in a ternary diagram, a geochemical fingerprint was able to be created for each tributary. This could then be linked to the Belousova et al. (2002) cladogram categories to define possible source rock within each tributary. By categorically dividing the data both with the traditional rock type categories from Belousova et al.(2002) and new ternary plot categories based on relative La-Y-Sr percentages, this study was able to produce mixing models that closely resembled those found from detrital zircon (Gregory, Herrmann, Ireland, & Clift, 2018). The Southwest tributaries are the largest contributor of bedload flux at 36%, with comparable contributions from the Northern Tributaries and Missouri at 33.5% and 27.5% respectively. As previously seen in other studies, the Ohio River contributes a modest amount at 3% (A. Fildani et al., 2016; Mason et al., 2017). Here we calculated a lower sediment flux from the Missouri River than previously reported, which could be one of the first provenance indicators showing the effect of damming on the Missouri River. By using a combination of both old and new methods, both trace elements and REEs are here confirmed as a useful tool for interpreting provenance of continental-scale detrital populations. This new approach can be used alongside or independent

of other provenance methods such as zircon and apatite U-Pb dating methods, and would be especially useful in situations where zircon is not a viable option,

3.8 References Cited

Belousova, E., Griffin, W., O'Reilly, S. Y., & Fisher, N. (2002). Apatite as an indicator mineral for mineral exploration: trace-element compositions and their relationship to host rock type. *Journal of Geochemical Exploration, 76*(1), 45-69.

Bickford, M., & Van Schmus, W. (1985). Discovery of two Proterozoic granite-rhyolite terranes in the buried midcontinent basement: The case for shallow drill holes *Observation of the Continental Crust through Drilling I* (pp. 355-364): Springer.

Blum, M. D., & Roberts, H. H. (2009). Drowning of the Mississippi Delta due to insufficient sediment supply and global sea-level rise. *Nature Geoscience, 2*(7), 488-491. doi:10.1038/ngeo553

Bouch, J. E., Hole, M. J., Trewin, N. H., Chenery, S., & Morton, A. C. (2002). Authigenic apatite in a fluvial sandstone sequence; evidence for rare-earth element mobility during diagenesis and a tool for diagenetic correlation. *Journal of Sedimentary Research, 72*(1), 59-67.

Bowring, S. A., & Karlstrom, K. E. (1990). Growth, stabilization, and reactivation of Proterozoic lithosphere in the southwestern United States. *Geology, 18*(12), 1203-1206.

Budzinski, H., & Tischendorf, G. (1989). Distribution of REE among minerals in the Hercynian postkinematic granites of Westerzgebirge-Vogtland, GDR. *Zeitschrift fur Geologische Wissenschaften, 17*(11), 1019-1031.

Chang, L., Howie, R., & Zussman, J. (1996). Rock-Forming Minerals, Volume 5B, Non-Silicates (pp. 383): Longman Group Harlow, UK.

Chew, D. M., Sylvester, P. J., & Tubrett, M. N. (2011). U–Pb and Th–Pb dating of apatite by LA-ICPMS. *Chemical Geology, 280*(1-2), 200-216.

Corrigan, D., & Hanmer, S. (1997). Anorthosites and related granitoids in the Grenville orogen: A product of convective thinning of the lithosphere? *Geology, 25*(1), 61-64.

Dahl, P. S., Holm, D. K., Gardner, E. T., Hubacher, F. A., & Foland, K. A. (1999). New constraints on the timing of Early Proterozoic tectonism in the Black Hills (South Dakota), with implications for docking of the Wyoming province with Laurentia. *Geological Society of America Bulletin, 111*(9), 1335-1349.

Dalziel, I. W. (1991). Pacific margins of Laurentia and East Antarctica-Australia as a conjugate rift pair: Evidence and implications for an Eocambrian supercontinent. *Geology, 19*(6), 598-601.

Davidson, A. (1995). A review of the Grenville orogen in its North American type area. *AGSO Journal of Australian Geology and Geophysics, 16*(1), 3-24.

DePaolo, D. J. (1981). Neodymium isotopes in the Colorado Front Range and crust–mantle evolution in the Proterozoic. *Nature, 291*(5812), 193.

Dickinson, W. R. (2008). Impact of differential zircon fertility of granitoid basement rocks in North America on age populations of detrital zircons and implications for granite petrogenesis. *Earth and Planetary Science Letters, 275*(1-2), 80-92. doi:doi:10.1016/j.epsl.2008.08.003

Drake Jr, A. A., Sinha, A., Laird, J., & Guy, R. (1989). The taconic orogen. *The Appalachian-Ouachita orogen in the United States: Boulder, Colorado, Geological Society of America, Geology of North America, 2*, 101-177.

Fildani, A., Hessler, A. M., Mason, C. C., McKay, M. P., & Stockli, D. F. (2018). Late Pleistocene glacial transitions in North America altered major river drainages, as revealed by deep-sea sediment. *Scientific Reports, 8*(1), 13839.

Fildani, A., McKay, M. P., Stockli, D., Clark, J., Dykstra, M. L., Stockli, L., & Hessler, A. M. (2016). The ancestral Mississippi drainage archived in the late Wisconsin Mississippi deep-sea fan. *Geology*. doi:10.1130/g37657.1

Fleischer, M., & Altschuler, Z. (1986). The lanthanides and yttrium in minerals of the apatite group-an analysis of the available data. *Neues Jahrbuch für Mineralogie, Monatshefte*, 467-480.

Garrity, C. P. (2009). Database of the Geologic Map of North America-Adapted from the Map by JC Reed, Jr. and others (2005).

Gehrels, G. E. (2014). Detrital Zircon U-Pb Geochronology Applied to Tectonics. *Annual Review of Earth and Planetary Sciences, 42*, 127-149. doi:DOI: 10.1146/annurev-earth-050212-124012

Gerdes, A., & Zeh, A. (2006). Combined U-Pb and Hf isotope LA-(MC-)ICP-MS analyses of detrital zircons: Comparison with SHRIMP and new constraints for the provenance and age of an Armorican metasediment in Central Germany. *Earth and Planetary Science Letters, 249*(1-2), 47-61.

Gregory, B., Herrmann, A. D., Ireland, T., & Clift, P. D. (2018). Zircon U-Pb Dating Comparisons in a Highly Altered River System, Mississippi River, USA. *Basin Research, in review*.

Hamilton, M., Goutier, J., & Matthews, W. (2001). *U-Pb baddeleyite age for the Paleoproterozoic Lac Esprit dyke swarm, James Bay region, Quebec*: Natural Resources Canada, Geological Survey of Canada.

Hanson, R. E., Puckett Jr, R. E., Keller, G. R., Brueseke, M. E., Bulen, C. L., Mertzman, S. A., . . . McCleery, D. A. (2013). Intraplate magmatism related to opening of the southern Iapetus Ocean: Cambrian Wichita igneous province in the Southern Oklahoma rift zone. *Lithos, 174*, 57-70.

Hoffman, P. F. (1988). United plates of America, the birth of a craton: Early Proterozoic assembly and growth of Laurentia. *Annual Review of Earth and Planetary Sciences, 16*(1), 543-603.

Hoffman, P. F. (1989). Precambrian geology and tectonic history of North America. In A. W. Bally & A. R. Palmer (Eds.), *The Geology of North America-An Overview* (pp. 447-511). Boulder, CO: Geological Society of America.

Horton, J. W., Drake, A. A., & Rankin, D. W. (1989). Tectonostratigraphic terranes and their Paleozoic boundaries in the central and southern Appalachians. *Geological Society of America Special Papers, 230*, 213-246.

Karlstrom, K., Bowring, S. A., & Reed, J. (1993). Proterozoic orogenic history of Arizona. *Precambrian: Conterminous US: Boulder, Colorado, Geological Society of America, Geology of North America, 2*, 188-211.

Karlstrom, K. E., Åhäll, K.-I., Harlan, S. S., Williams, M. L., McLelland, J., & Geissman, J. W. (2001). Long-lived (1.8–1.0 Ga) convergent orogen in southern Laurentia, its extensions to Australia and Baltica, and implications for refining Rodinia. *Precambrian Research, 111*(1-4), 5-30.

Karlstrom, K. E., & Humphreys, E. D. (1998). Persistent influence of Proterozoic accretionary boundaries in the tectonic evolution of southwestern North America: Interaction of cratonic grain and mantle modification events. *Rocky Mountain Geology, 33*(2), 161-179.

Krevor, S., Graves, C., Van Gosen, B., & McCafferty, A. (2009). *Mapping the mineral resource base for mineral carbon-dioxide sequestration in the conterminous United States*: US Geological Survey.

Landes, K. K. (1935). Age and distribution of pegmatites. *American Mineralogist: Journal of Earth and Planetary Materials, 20*(2), 81-175.

Malusa, M. G., Resentini, A., & Garzanti, E. (2016). Hydraulic sorting and mineral fertility bias in detrital geochronology. *Gondwana Research, 31*, 1-19. doi:doi:10.1016/j.gr.2015.09.002

Mason, C. C., Fildani, A., Gerber, T., Blum, M. D., Clark, J. D., & Dykstra, M. (2017). Climatic and anthropogenic influences on sediment mixing in the Mississippi source-to-sink system using detrital zircons: Late Pleistocene to recent. *Earth and Planetary Science Letters, 466*, 70-79. doi:http://dx.doi.org/10.1016/j.epsl.2017.03.001

McDonough, W. F., & Sun, S.-S. (1995). The composition of the Earth. *Chemical Geology, 120*(3-4), 223-253.

McLelland, J., Daly, J. S., & McLelland, J. M. (1996). The Grenville orogenic cycle (ca. 1350-1000 Ma); an Adirondack perspective. *Tectonophysics, 265*(1-2), 1-28.

Moecher, D. P., & Samson, S. D. (2006). Differential zircon fertility of source terranes and natural bias in the detrital record: implications for sedimentary provenance analysis. *Earth and Planetary Science Letters, 247*((3-4), 252–266.

Moores, E. (1991). Southwest US-East Antarctic (SWEAT) connection: a hypothesis. *Geology, 19*(5), 425-428.

Morton, A., & Yaxley, G. (2007). Detrital apatite geochemistry and its application in provenance studies. *Special Papers-Geological Society of America, 420*, 319.

Morton, A. C. (1991). Geochemical studies of detrital heavy minerals and their application to provenance research. In A. C. Morton, S. P. Todd, & P. D. W. Haughton (Eds.), *Developmentsin Sedimentary Provenance Studies* (Vol. 57, pp. 31-45). London: Geological Society.

Muehlberger, W. R., Denison, R. E., & Lidiak, E. G. (1967). Basement rocks in continental interior of United States. *AAPG Bulletin, 51*(12), 2351-2380.

Naeser, N. D., Naeser, C. W., & McCulloh, T. H. (1989). The application of fission-track dating to the depositional and thermal history of rocks in sedimentary basins *Thermal history of sedimentary basins* (pp. 157-180): Springer.

Nash, W. P. (1984). Phosphate minerals in terrestrial igneous and metamorphic rocks *Phosphate minerals* (pp. 215-241): Springer.

Nelson, B. K., & DePaolo, D. J. (1985). Rapid production of continental crust 1.7 to 1.9 b.y. ago: Nd isotopic evidence from the basement of the North American mid-continent. *Geological Society of America Bulletin, 96*(6), 746-754. doi:doi: 10.1130/0016-7606(1985)96

Pearce, N. J. G., Perkins, W. T., Westgate, J. A., Gorton, M. P., Jackson, S. E., Neal, C. R., & Chenery, S. P. (1997). A compilation of new and published major and trace element data for NIST SRM 610 and NIST SRM 612 glass reference materials. *Geostandards Newsletter-the Journal of Geostandards and Geoanalysis, 21*(1), 115-144.

Ross, G. M., Patchett, P. J., Hamilton, M., Heaman, L., DeCelles, P. G., Rosenberg, E., & Giovanni, M. K. (2005). Evolution of the Cordilleran Orogen (southwestern Alberta, Canada) inferred from detrital mineral geochronology, geochemistry, and Nd isotopes in the foreland basin. *Geological Society of America Bulletin, 117*(5-6), 747-763.

Schlische, R. W., Withjack, M. O., & Olsen, P. E. (2003). Relative timing of CAMP, rifting, continental breakup, and basin inversion: tectonic significance. *GEOPHYSICAL MONOGRAPH-AMERICAN GEOPHYSICAL UNION, 136*, 33-60.

Sevastjanova, I., Clements, B., Hall, R., Belousova, E. A., Griffin, W. L., & Pearson, N. (2011). Granitic magmatism, basement ages, and provenance indicators in the Malay Peninsula: insights from detrital zircon U–Pb and Hf-isotope data. *Gondwana Research, 19*(4), 1024-1039.

Shaw, C. A., & Karlstrom, K. E. (1999). The Yavapai-Mazatzal crustal boundary in the southern Rocky Mountains. *Rocky Mountain Geology, 34*(1), 37-52.

Sundell, K., & Saylor, J. E. (2017). Unmixing detrital geochronology age distributions. *Geochemistry Geophysics Geosystems, 18*, 2872–2886.

Tarr, R. S., & McMurry, F. M. (1922). *New Geographies: First [-second] Book* (Vol. 2): Macmillan.

Van Schmus, W. (1976). A Discussion on global tectonics in Proterozoic times-Early and Middle Proterozoic history of the Great Lakes area, North America. *Phil. Trans. R. Soc. Lond. A, 280*(1298), 605-628.

Vermeesch, P. (2004). How many grains are needed for a provenance study? *Earth and Planetary Science Letters, 224*, 351–441.

Woolley, A., & Kjarsgaard, B. (2008). Carbonatite occurrences of the world: map and database. Geological Survey of Canada. Open File 5796.—2008.

CHAPTER 4. PROVENANCE OF ND ISOTOPES IN THE LATE HOLOCENE MISSISSIPPI RIVER DELTA

4.1 Introduction

Humans have changed the world and landscape in which they live, especially within the last 200 years. Many different scientific disciplines have shown these alterations to both atmosphere and climate (Montgomery, 2007; Ruddiman, 2003). In more recent years, geologists have also started to study the dynamic way in which human interactions have changed earth processes (Zalasiewicz, Williams, Steffen, & Crutzen, 2010). These alterations to the landscape disrupt the processes of the geosphere and hydrosphere both locally and globally. In particular, rivers and delta systems have been subject to some of the most dramatic changes (J.P.M. Syvitski & Milliman, 2007), e.g., the Pearl River (Hu et al., 2013). The Mississippi River is the largest in North America and has been populated since at least 9 ka with intensive settlement starting around 200–300 BP. This paper uses a delta sediment record to understand the dynamics between the natural and human processes that have impacted the Mississippi River drainage over the last 3 ky. To do this, we use Neodymium and Strontium isotopes from the tributaries and main trunk of the Mississippi to interpret the evolving provenance of the clay fraction in a well-dated core from the Mississippi River delta.

4.2 Neodymium as a Provenance Indicator

Neodymium isotopic character is commonly used as a provenance indicator to understand siliciclastic dynamics within drainage basins. While other methods (such as U-Pb dating of zircon grains) are popular for coarse grained sediment, Sm-Nd and Rb-Sr radioisotopes have traditionally been used for the fine grained fraction (Bouquillon, France-Lanord, Michard, & Tiercelin, 1990; Clift & Giosan, 2012; France-Lanord, Derry, & Michard, 1993; Garzanti et al., 2011; Liu et al., 2017; Singh et al., 2008). Nd isotopes are particularly useful for provenance

studies because this isotope system does not fractionate during diagenetic processes or transport (S. L. Goldstein, O'Nions, & Hamilton, 1984). This means that Nd can be used as a direct representation of average source rock isotopic composition to interpret sediment provenance (S. J. Goldstein & Jacobsen, 1988; Steven L Goldstein & Hemming, 2003).

Nd isotope ratios ($^{143}Nd/^{144}Nd$), commonly expressed as εNd values (D. J. DePaolo & Wasserburg, 1976) are commonly used to distinguish between sediment eroded from terranes of different ages and/or petrogenesis. Rocks derived from the mantle in the deep geologic past have more negative εNd values, while younger rocks have less negative or positive εNd values. Younger rocks may also have negative values if they are formed by remelting of older material. Recent findings by Jonell et al. (2018) argued that the typical margin of uncertainty within bulk samples from the Himalayas resulted in a +/- 1 εNd error. While rather large, this uncertainty most likely reflects the great variability found within samples and bedrock sources from the region, as well as the wide range in grain sizes. Previous studies addressing uncertainties within Nd isotope analyses that involved repeat analyses concluded that there was a +/- 0.6 εNd uncertainty between samples (Chauvel, Bureau, & Poggi, 2010). When analyses have considered only the clay fraction, better reproducibility with smaller error has been achieved. Fine-grained sediments from South China Sea showed variations of ±0.1 εNd on repeat analyses (Liu et al., 2017). Given this, we expect that we can achieve a smaller scale of variability in the Mississippi, especially when considering only the clay (<2 μm) fraction.

4.2.1 Neodymium in North America

North America has a large database of Nd isotope compositions which, in general, correspond with the crystallization ages of the igneous/metamorphic bedrock (Fig. 4.1). The

oldest rocks, dating from the Archean, which comprise the Canadian Shield, have εNd signatures that range from -26 to -17 (Patchett, Ross, & Gleason, 1999). Younger rocks, which comprise the bedrock of much of the southwest and mid-continental United States, have εNd values that range from -17 to -13 (D. J. DePaolo & Wasserburg, 1976). Younger bedrocks from the Grenville region have εNd values from -13 to -3 (Bream et al., 2004; James D Gleason, Patchett, Dickinson, & Ruiz, 1994; J.D. Gleason, Patchett, Dickinson, & Ruiz, 1995). This signature dominates the rocks of the Appalachian orogeny through recycling of earlier rocks during that phase of magmatism and deformation. Studies have shown that this εNd signature propagates far westward and is present in most of the sedimentary rocks younger than 450 Ma (Patchett et al., 1999). Although bedrock sources formed or eroded from the Laramide and Corderillan (30 to 275 Ma) orogenic events (hashed area in Figure 4.1) have more positive εNd values, Patchett et al. (1999) did not see the impact of this change in chemistry in sedimentary rock postdating these events. However, they proposed that recent sediment eroded from these regions should show a shift in isotopic composition as a result of these new orogenic sources.

4.3. Mississippi River and Delta

The Mississippi River is the 4th largest drainage system in the world in terms of drainage area, reaching into Canada and flowing southward for almost 4000 km before eventually emptying into the Gulf of Mexico (J.P.M. Syvitski & Milliman, 2007). It is the largest river in North America comprised of five main drainage systems that flow across geologically diverse terrane and supply sediment from the headwaters down to the Mississippi delta. The Missouri, Arkansas, and Red Rivers drain the western part of North America, with their headwaters reaching the Rocky Mountains in the West. The Upper Mississippi, Illinois, and Ohio River

drain the Canadian Shield and Appalachian Mountains to the north and east of the United States, respectively (Fig. 4.1).

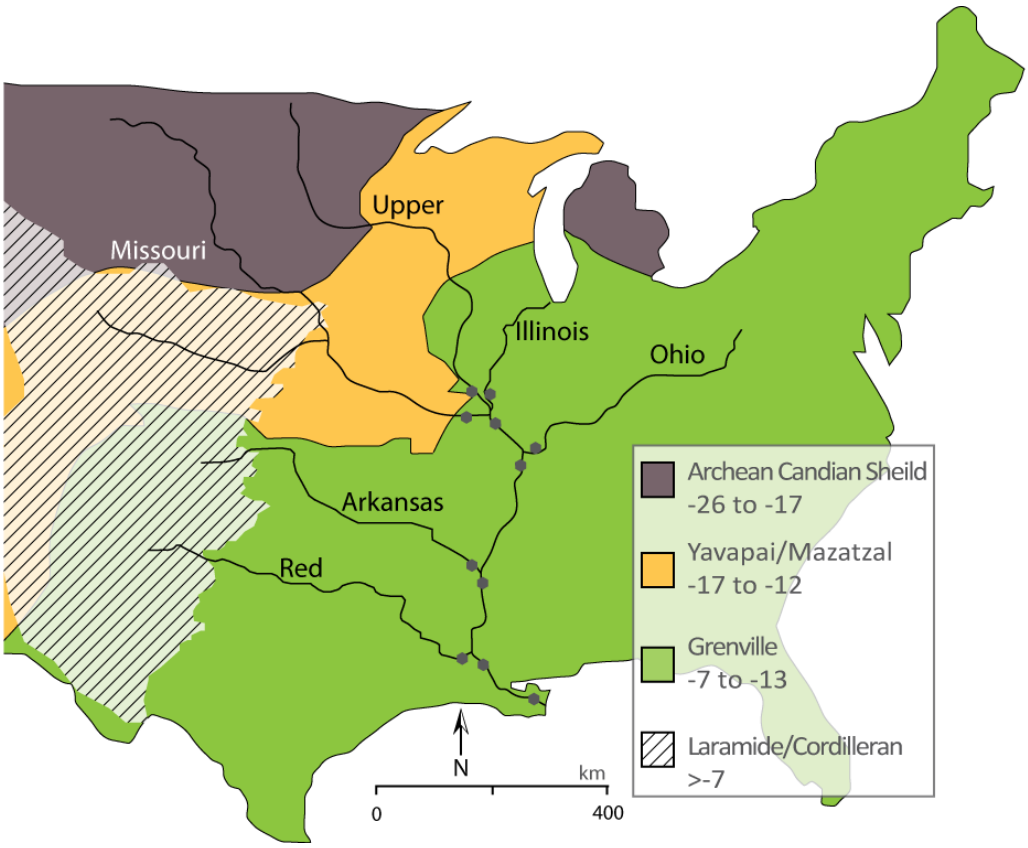

Figure 4. 1 Map of North America showing the trace of the trunk Mississippi River and its major tributaries. Black hexagons show the location of samples used in this study. Shading indicates regional average Nd isotope composition from Patchett et al. (1999) that define the large scale heterogeneity of εNd in the source regions.

4.3.1 Historic and Modern Hydrology

Most of the sediment discharge in the Mississippi River has historically come from the Missouri River, while most of the water discharge is derived from the Ohio (Alexander et al., 2012; Meade & Moody, 2010). The Missouri River still provides much of the suspended sediment load, but this number has been checked by dams and water control structures built on the river in the 1960s (Mason et al., 2017; J.P.M. Syvitski, C., Kettner, & Green, 2005). This is

most evident when looking at historic measurements in which suspended sediment load plummeted from 500 Mt/yr to about 100 Mt/yr after the addition of the Ft. Randall and Big Bend dams on the Missouri River (Mason et al., 2017). Locks and dams have perhaps been responsible for the greatest change in hydrology and sediment supply in the basin. While wicker lock structures were built on the Ohio River as early as the mid-1800s, it was not until the 1940s-1960s that major changes to the Mississippi River and its tributaries were constructed (Alexander et al., 2012; Mason et al., 2017). While not a dam, the Old River Control Structure, used to control flooding in the lower reaches of the Mississippi, cut off flow from the Red River to the lower Mississippi River in 1963 and diverts 30% of the Mississippi discharge to the Atchafalaya Basin.

The construction of levees for flood control has also led to a decrease in sediment reaching the terrestrial delta. These structures effectively channelize the river and cut off sediment supply to the floodplain and delta plain. As early as 1718-1727, French colonists built 4 foot high levees along the banks of the river in New Orleans to try and counteract the floods that occurred almost yearly (Colten, 2006; D. Rogers, 2005; J. D. Rogers, 2008). These small structures, built in the style of European levees, were not very effective on the large-scale floods of the Mississippi. For the next 100 years, levees were intermittent at best, and covered only small sections of the river. It was not until the Swamp Act of 1849-1850 (following a series of bad flood years) that the government took on the issue of flood control along the Mississippi. In the late 1800s, a series of catastrophic floods led to a more comprehensive and higher levee complex. This cycle of flooding and levee raising continued until the historic flood of 1927, after which levees were raised to a height of almost 25 feet at Lake Pontchartrain to prevent storm surge (J. D. Rogers, 2008)(Fig. 4.2). After this flood, levee systems along the entire Mississippi

and its tributaries were raised, effectively channelizing the Mississippi and cutting off sediment supply to the floodplain.

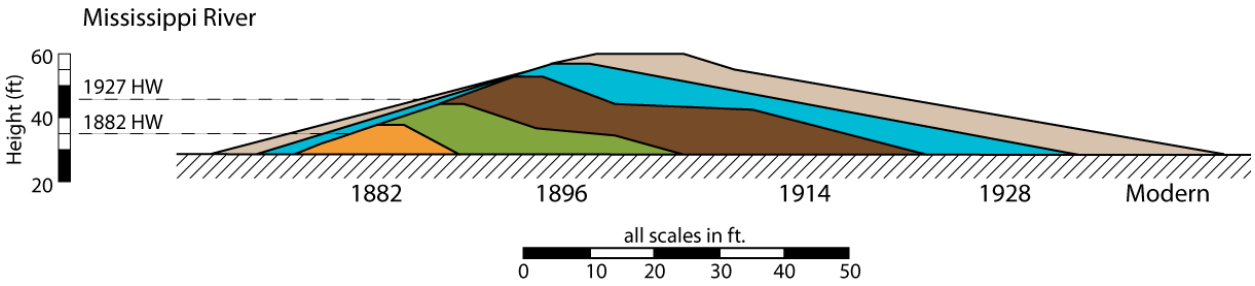

Figure 4. 2 Development of the Mississippi RIver levee elevations since the late 19th century. Redrawn from Moore (1972).

All of these manmade alterations to the modern regime within the last 60 years have culminated in a significant loss of sediment to the Mississippi River delta. Blum and Roberts (2009) have estimated a reduction of nearly 60% of sediment delivery to the delta and (Boesch et al. (1994) 25% of wetland loss in coastal Louisiana. This has exacerbated subsidence and loss of land and natural fishery areas along the entire coast of Louisiana, which had, up until recently, supported a thriving delta community.

4.3.2 Mississippi River Delta Complexes

Deltas around the world started forming around 7 ka in response to sea level rise stabilization following the end of the Pleistocene. In the 1950s, the classification of deltas and recognition of delta building sequences were extensively studied (McIntire, 1954), (Station & Kolb, 1958). Studies in the Mississippi River delta interpreted and defined 6 major delta progradation sequences (Coleman, Roberts, & Stone, 1998; D.E. Frazier, 1967; Harry H Roberts, 1997) (Fig. 4.3).

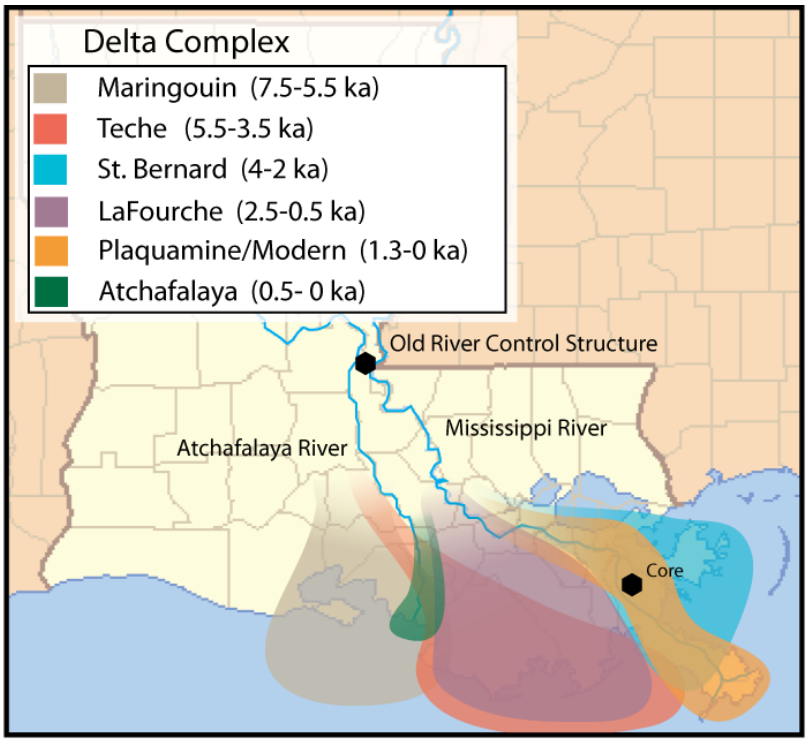

Figure 4. 3 Map of the Mississippi delta region showing the defined delta complexes spanning the time since 7.5 ka (Bentley, Blum, Maloney, Pond, & Paulsell, 2016). Black marker shows the location of the core analyzed in this study and the Old River Control Structure.

In general the delta plain is comprised of a series of delta complexes. A river transports sediment to a delta complex until there is no more accommodation space. When sediment transport becomes inefficient the river avulses to a new section of the delta plain thereby creating a new delta complex. For the Mississippi, the delta complexes are defined as the Maringouin dated to 7.5 to 5.5 ka, the Teche from 5.5-3.5 ka, the St. Bernard 4-2 ka, the LaFourche 2.5-0.5 ka, the Plaquemines/Modern 1.3 to present, and the Atchafalaya from .5 ka to present. These delta complexes have main points of progradation throughout their life; however, it is important to note that distributaries still remain active forming subdeltas in the other regions of the overall delta plain. This study specifically focuses on the Plaquemines and the St. Bernard subdeltas.

4.4 Methods

4.4.1 Sampling

Grab samples from the modern river within the modern levees were taken from each major tributary of the Mississippi and from the Mississippi trunk directly below major confluences. These were then separated until only the clay remained for Nd isotope analysis (Fig. 4.1, locations in Appendix C Supplemental Table 4.1). In addition, a 500cm core was extracted from within the Mississippi Delta (Fig. 4.4). This core was taken back to the lab, then cut and sampled for dating (OSL, radiocarbon, ^{210}Pb, and ^{137}Cs), grainsize, and isotope work as described below. Facies were interpreted using Coleman and Gagliano (1964).

4.4.2 Radiocarbon

An in situ shell, found within the core, was sent to the NOSAMS laboratory for analysis; then processed using the marine 13 curve in CALIB Radiocarbon Calibration program (Hughen et al., 2009)(Stuiver et al. 2019). Since the shell was collected in what is interpreted to be marine deposits in Breton Sound, a marine correction defined regionally in the Gulf of Mexico of 500 +/- 300 ^{14}C is used to account for the full variability within the reservoir (Törnqvist, Rosenheim, Hu, & Fernandez, 2015).

4.4.3 Optically Stimulated Luminescence Dating

Age control for Holocene deposits was determined using optically stimulated luminescence (OSL) dating of quartz in sediments. This technique dates the last time the sediment was exposed to sunlight, presumably during transport. It is widely applied to quartz-bearing sediment deposited in the past 200 ky (Rhodes, 2011). Depositional ages of sediment were determined by OSL dating of quartz sand following the single-aliquot regenerative dose

method (Murray & Wintle, 2000). While OSL dating can be challenging in fluvial environments, deposits from these settings can be accurately dated by selecting depositional facies most likely to have been reset by sunlight exposure (Fuchs & Owen, 2008; Rittenour, 2008; Wyshnytzky, Rittenour, Nelson, & Thackray, 2015). Samples were processed at the Utah State University Luminescence Laboratory. This study targeted horizontally bedded sand and silt beds from fluvial deposits to reduce the influence of incomplete resetting (partial bleaching) of the luminescence signal.

Three OSL samples were collected in a dark room and shipped to Utah State University (USU) Luminescence Laboratory for optically stimulated luminescence (OSL) dating of quartz sand (Huntley, 1985; Murray & Wintle, 2000). Samples were opened under dim amber light (~590 nm) and sediment from the inner portions of the sample tubes was sieved and treated with hydrochloric acid to dissolve carbonates. Then chlorine bleach was used to remove organic material. Heavy mineral separation (sodium polytungstate, 2.7 g/cm^3) and concentrated hydrofluoric and hydrochloric acids were used to remove feldspars, etched quartz grains, and prevented formation of fluorite precipitates (see (Rittenour, 2008)for details). The samples were re-sieved to remove the <63μm grain-size fraction of etched quartz and any partially dissolved feldspars (Wintle & Murray, 1997). Purity of the samples was checked using infrared (IR) stimulation on all aliquots.

Representative sediment around the samples was collected for dose rate analysis and submitted for ICP-MS and ICP-AES analyses of K, Rb, Th, and U content. In-situ gravimetric moisture content was measured for all samples. For those with <5.8% measured water content, we used an average value of 5.8±3.0% to represent the moisture content over burial history. Dose

rate calculations include cosmic dose rate contribution by using sample depth, elevation, and longitude/latitude following Prescott and Hutton (1994), influence of water attenuation, uncertainty in elemental measurements and dose rate conversion factors (Aitken, 1998; Guerin, Mercier, & Adamiec, 2011).

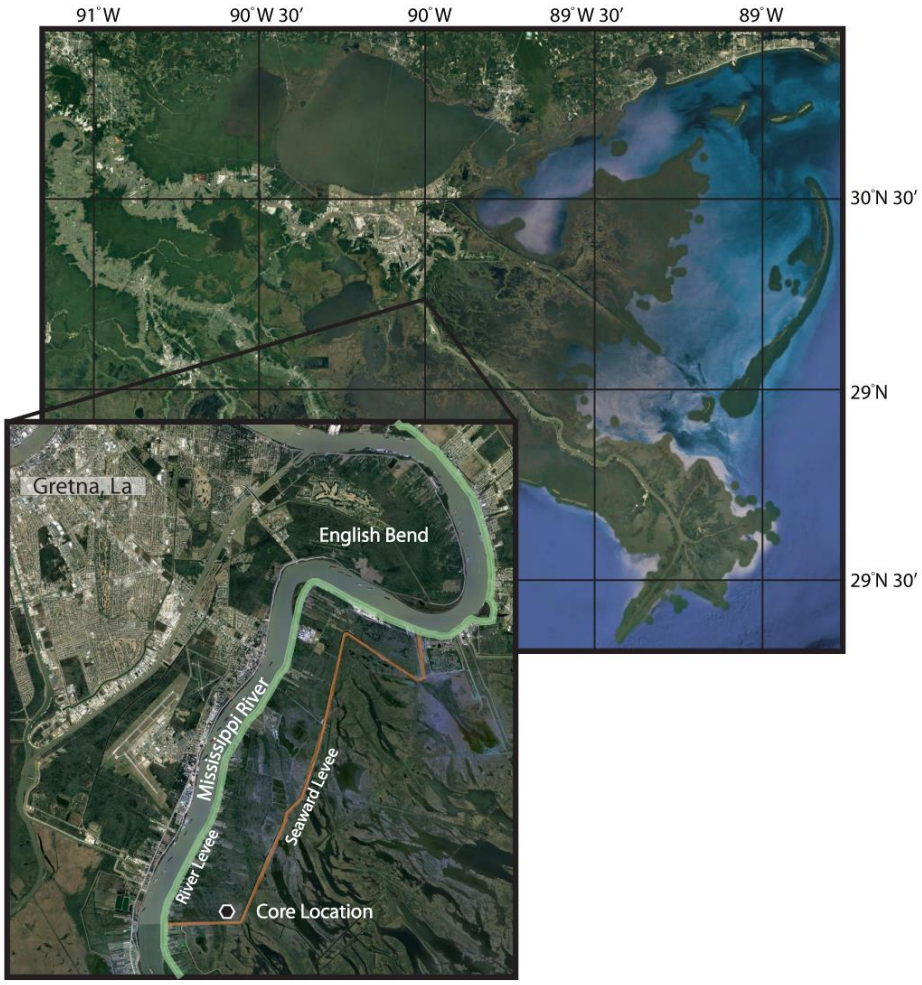

Figure 4. 4 Aerial photograph of the Mississippi delta. Inset photograph is a closeup of the region around the core location showing the relationship of the seaward levee and the Mississippi River channel (Hoffman, 1988; Ross & Villeneuve, 2003; Dahl, Holm, Gardner, Hubacher, & Foland, 1999).

4.4.4 Pb-210 and Cs-137

Cesium-137 and Lead-210 are commonly used for age control when investigating historic Quaternary sedimentary deposits (C. A. Nittrouer, Sternberg, Carpenter, & Bennett, 1979; Noller, 2000). 210Pb has a geologically short half-life that can date with high confidence modern sediment deposited within the last 150 years. This makes it more effective than radiocarbon dating for very recent deposits. Similarly, ^{137}Cs, with its short half-life and introduction into soil at a detectable level in 1954 from nuclear bomb testing, can help calibrate 210Pb and provide modern age control on sediment (Tylmann, W., Bonk, A., Goslar, T., Wulf, S., & Grosjean, M., 2016).

Samples for ^{137}Cs and ^{210}Pb detection were dried in an oven at 55° C , then weighed and pulverized using a mortar and pestle to homogenize the particle size. Samples were then packed to fill 12 mm diameter plastic well vials with an air tight seal. Samples were then run after three weeks (to allow sufficient time for secular equilibrium to be reached) on a Canberra SAGe gamma well detector that measures up to 2000 keV for 24 hours. Energies at respective photopeaks were measured as follows: ^{137}Cs at 661.7 keV, ^{210}Pb at 46.5 keV, ^{214} Pb at 295 keV and 351 keV, and ^{214}Bi at 609 keV. The units of measurement for the radioactivity used in this study are disintegrations per minute (dpm) or 1/60th of a Becquerel (Bq).

4.4.5 Nd and Sr isotopes

Care was taken to decarbonate samples (core and grab samples) prior to analysis with 20% acetic acid because Sr isotope compositions are strongly controlled by carbonate compositions and this study targets the siliciclastic sediment compositions only. Decarbonation lasted for six days until no further fizzing was observed when samples were exposed to unreacted acid. Samples were washed by deionized water and dried before being ground into

powders. Isotopic compositions of Nd and Sr were determined by Finnigan Neptune multi-collector inductively coupled plasma mass spectrometer (MC-ICP-MS) at the Woods Hole Oceanographic Institute. Nd and Sr isotope analyses were corrected against La Jolla Nd standard $^{143}Nd/^{144}Nd=0.511847$ and NBS987 standard $^{87}Sr/^{86}Sr=0.710240$. Procedural blanks were 20–25 pg for Sr and 50–70 pg for Nd. We calculate the parameter ϵ_{Nd} after (DePaolo and Wasserburg, 1976) using a $^{143}Nd/^{144}Nd$ value of 0.512638 for the Chondritic Uniform Reservoir (CHUR) (Hamilton, Onions, Bridgwater, & Nutman, 1983).

4.4.6 Grain Size

Grain size analysis followed the procedures of Hülse and Bentley (2012). A small amount of sample was placed into a cleaned 50 ml plastic centrifuge tube and 5–7 ml of sodium metaphosphate solution was added. The tube was capped and vortexed to deflocculate clay-sized sediment and separate organic particles. The sample was poured through an 850 µm sieve and funneled into a 15 ml glass test tube. After centrifuging and removing the clear supernatant, 2–3 ml of sodium metaphosphate and 5 ml of 30% H_2O_2 were added. Tubes were vortexed again and then put into a hot bath that was heated to 70˚C overnight. Reacted supernatant was then removed and 5 ml of sodium phosphate were added. Samples were then rinsed with deionized water, transferred into 50 ml plastic centrifuge tubes, and topped with sodium metaphosphate into a sample solution of up to 40 ml. Samples were vortexed again prior to grain size analysis on a Beckmann Coulter LS13 320 laser diffraction particle size analyzer at LSU. The obscuration of all running samples in the aqueous liquid module (ALM) was between 8–12 %.

4.5. Core Stratigraphy and Age Control

4.5.1 Core Stratigraphy

From 500 to 463 cm the core is a compact, massive, clay deposit marked with a sharp boundary on top. This transitions to silt interbedded with sand from 463 to 382. Silty deposits followed by a sandy bed with shell hash then moves to another dark, compact, massive clay deposit with shell hash beds (382 to 314 cm). A gradual transition is made into a thick series of coarsening upward interbedded sands and silts which span from 314 to 230 cm. A sharp boundary marks the transition to a fining upwards sand layer which is found from 230 to 175 cm. From 175 to 66 cm sands interbedded with silt and sand fine upwards towards more silt and clay-rich deposits. The core stratigraphy changes abruptly above 66 cm where the presence of organic material within the clay and silt becomes predominate to the surface.

4.5.2 Bay/Estuary

Dark, reduced, compact massive clay deposits were interpreted as bay/estuary deposits (Fig. 4.5). Sandy storm deposits can be found within the clay together with whole shells mixed with shell hash. The bay/estuary deposits are found at the base of the core from 463 to 500 cm and further up the core from 314 to 382 cm, indicating two separate intervals of marine dominated sedimentation in this location. An in situ oyster shell at a depth of 480 cm was dated by radiocarbon methods, constraining the age of the lowest bay deposits to 3.98 +/- 0.4 ka.

4.5.3 Prodelta/Delta Front

Prodelta/delta front sequences are represented in this core by coarsening upward deposits of interbedded silt and sand with intermittent clay beds.

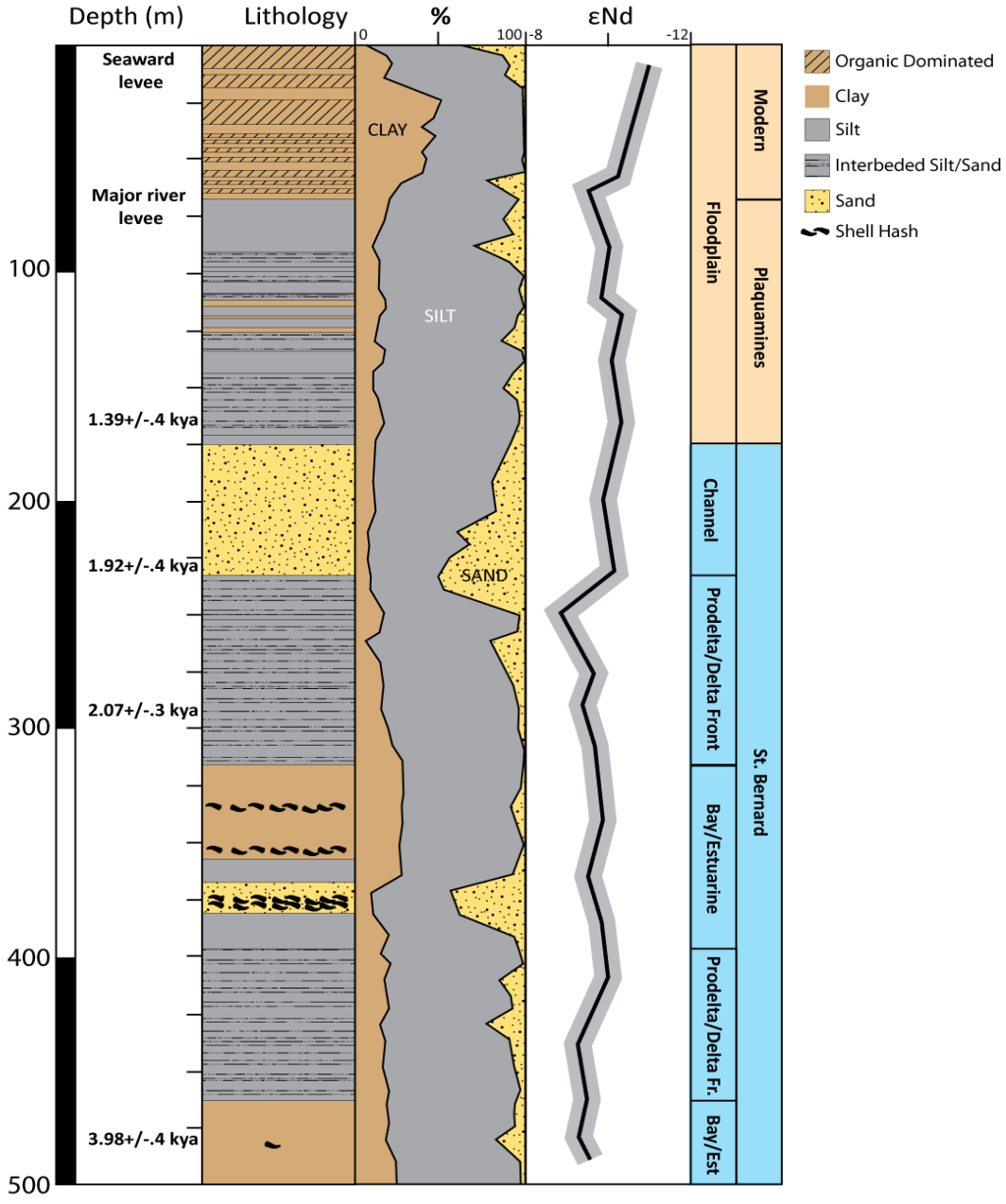

Figure 4. 5 Lithology log of the section cored in the Mississippi delta showing major % of sand, silt, and clay together with εNd values. Age control shown on left (methods described in text). Interpreted sedimentary environments and correlated delta complexes/ depositional events on the right.

These deposits are found within the core from 382 to 463 cm and from 230 to 314 cm. This facies is interpreted to represent as a prograding delta followed by a transgression of delta lobe which avulsed away from the core location, leading to a marine environment. The delta lobe then moved back towards the core location leading to reactivation of the prodelta/delta front. The upper prodelta/delta front sequence, from 230 to 314 cm is dated by OSL to 2.07+/-0.3 ka at 290 cm of depth. A very sandy deposit atop the prodelta/delta front sequence (230-175 cm) is interpreted as a channel deposit. This channel deposit yielded OSL ages of 1.92+/-0.4 ka.

4.5.4 Floodplain

The top 175 cm of the core are interpreted to represent fluvial floodplain environments. The interbedded sand and silt from 66 to 175 cm are indicative of levee overbank flood deposits in a terrestrial delta. An OSL date at 150 cm yielded an age of 1.39+/-.04 ka. Dating the sediment at the top of the core showed a ^{137}Cs peak at 10 cm depth, but this is absent by a depth of 20 cm, thus 15 cm is interpreted here as 1954 (Fig 4.5) (Supplemental Figure 4.1; Appendix C). Pb^{210} dating indicated an accumulation rate of 1.73 cm/yr for the top 70 cm of the core.

4.6. Nd Isotopes

Samples from modern tributaries of the Mississippi River show that those draining the western parts of the basin are more εNd positive than rivers derived from the north and east. We also note a general trend to more positive εNd values in the trunk river, moving downstream (Fig. 4.6). The greatest change in the Mississippi occurs downstream of the Missouri confluence after which the main trunk of the Mississippi does not show much variation (εNd = ~10.5 to 11.5).

Nd isotopic values do not vary greatly throughout the core within a range of εNd = -10.98 (10 cm) to -8.88 (250 cm). In general, the isotopic values from 250 to 500 cm are more positive than the εNd values above 250 cm. There is a significant shift to more negative εNd values in the top 66 cm of the core (εNd = ~ 10.2 to 11.0), which coincides with a change in sedimentation to more organic-rich clay material (Fig. 4.5 and 6).

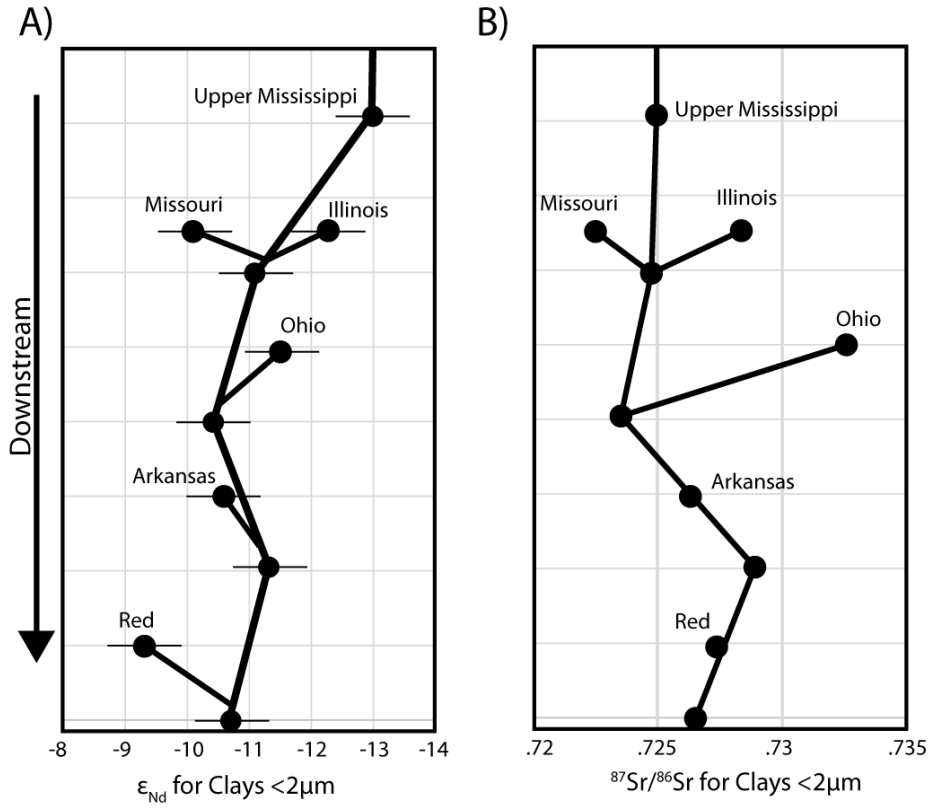

Figure 4. 6 Present day downstream evolution in A) Nd and B) Sr isotope compositions for clay separates from the trunk and major tributaries of the Mississippi. Note the gradual drift to more positive εNd values from source to the river mouth.

4.7. Discussion

4.7.1 Sedimentology

Based on OSL and radiocarbon ages provided by this study and the delta evolution models (Frazier 1967; Roberts 1997), this core captures two prodelta/delta front sequences of the

St. Bernard delta complex separated by a bay/estuarine environment, found between 500 and 175 cm depth (Fig. 4.5). The prodelta/delta front sequneces loosely correlate with two phases of St. Bernard delta building, found in Frazier (1967), which we date to just after 3.8+/-0.4 ka (radiocarbon) and between 2.07+/-0.3 ka and 1.92+/-0.4 ka. The St. Bernard delta complex is followed upsection by sediment that most likely represents occupation of the Plaquemines delta-building sequence, evident here by the OSL date of 1.39 +/- 0.4 ka at a depth of 150 cm. This change is represented by overbank levee/floodplain deposits that, as described earlier, change abruptly upsection. The sedimentation in the top 66 cm of the core is very fine grained and organic rich. We acknowledge here that these facies are likely anthropogenically influenced by the construction of both fluvial and seaward levees near the core site. USGS maps of the core site show the construction of a seaward levee between 1956 and 1966. This results in a reduction of sedimentation rates in the top of the core shown by the ^{210}Pb and ^{137}Cs results. As mentioned previously the ^{137}Cs dating methods indicated ~15cm of depth corresponds to 1954, which implies that 63 years of sedimentation are represented in approximately the top 15 cm of the core. This corresponds to a sedimentation rate of 0.23 cm/yr. The ^{210}Pb derived sedimentation rate over longer timescales (last 150 yr) is 1.73 cm/yr. We interpret the lower sedimentation rate within the upper 15 cm to be a result of the construction of the seaward levee in the 1960s, cutting off sediment supply during storm events (Fig. 4.4).

Extrapolating the ^{210}Pb date sedimentation rate of 1.73 cm/yr rate from 15 cm to 66 cm depth, where there is an abrupt change in lithology (to more organic rich sediment), indicates ~30 years of sedimentation in that depth interval (Fig. 4.5). This implies that the date at 66 cm depth is 1924, 30 years earlier, thus it is interesting the change in lithology observed closely correlates with a large increase in levee height around 1915 (D. Rogers, 2005)(Fig. 4.2). It is at

then corroborated though core lithology and age dating that at this point in time significant fluvial deposition was cut off from the site and any deposition after this date occurred when the seaward side of the levee was potentially breached by large hurricanes (eg. Besty:1965 or Katrina:2005).

4.7.2 Nd Interpretation

Nd isotope values for the Mississippi River sediment grab samples show that the Upper Mississippi, Illinois and Ohio River plot towards more negative εNd values (-11.5 to -13), while the Missouri, Arkansas and Red Rivers plot more positive (-10.5 to -9.5) (Fig. 4.6A). The western tributaries seem to have εNd signatures that are strongly influenced by erosion from the Grenville and possibly the Laramide/Cordilleran orogenic belts, while the eastern and northern tributaries source more εNd negative Grenville and Archean bedrock (Fig. 4.1 and 6). $^{87}Sr/^{86}Sr$ values of the tributaries also show regional variability, with the Ohio being marked by relatively higher values and the Missouri with lower values (Fig. 4.6B). However this study determined many of the tributaries have similar $^{87}Sr/^{86}Sr$ values to each other and consequently making Sr isotopes a poor provenance indicator in this system.

When examining the downstream evolution in εNd values, the Missouri makes the single largest contribution to the main trunk of the Mississippi River when it joins with the Upper Mississippi (Fig. 4.6). This tributary effectively pulls the mixed Mississippi sediment ~2 εNd points more positive after mixing with the main stream. In contrast, the Illinois is relatively negative compared to the downstream mixed sediment, indicating the weak influence this stream has on the mixed sediment. This is not surprising, given the modest relative discharge of the Illinois compared to the Missouri River (5.9 Mt/yr vs. 56.9 Mt/yr respectively). Moving

downstream, the other tributaries affect the overall εNd values of the sediment in the Mississippi very little. Overall though, variation between the eastern/northern and western tributaries can be seen and quantified, and therefore used as a provenance tool in mixed sediment from the Mississippi River.

To compare to previous Nd and Sr isotopic sediment measurements, our data are plotted with that from Goldstein and Jacobsen (1988) that were taken from the main tributaries and trunk of the Mississippi River (Fig. 4.7). We see that the εNd values of the core sediments plot close to both our new and older analyses of Mississippi and Missouri River sediments, i.e., around εNd -10, which correlates with the range of εNd values associated with the Grenville province (-13 to -7)(Fig. 4.7; Bream et al., 2004; James D Gleason et al., 1994; J.D. Gleason et al., 1995). εNd values from core sediment mainly cluster around the samples taken from the modern Missouri, Red and Arkansas Rivers (Fig. 4.7A). These values are associated with erosion from the more εNd positive Laramide/Cordilleran and Grenville sources that dominate the western parts of the basin.

If a closer look is taken at the Sr-Nd data from the core samples, a general up-core trend can be distinguished (Figs.4. 3 and 7). Samples from what is interpreted as St. Bernard delta deposits plot towards more positive εNd values and lower $^{87}Sr/^{86}Sr$, while those from the Plaquemines and the Modern deltas plot with more negative εNd and greater $^{87}Sr/^{86}Sr$ values (Fig. 4.7B). This can also be seen when the core is compared against the average εNd values for western and eastern/northern tributary sediments (Fig. 4.8). On average, samples from the St. Bernard delta have an εNd value of -9.6, while those from the Plaquemines have a value of -10.0

(Fig. 4.5). The most significant shift in the data are the εNd values in the top 66 cm of the core which have an average of εNd value of -10.6.

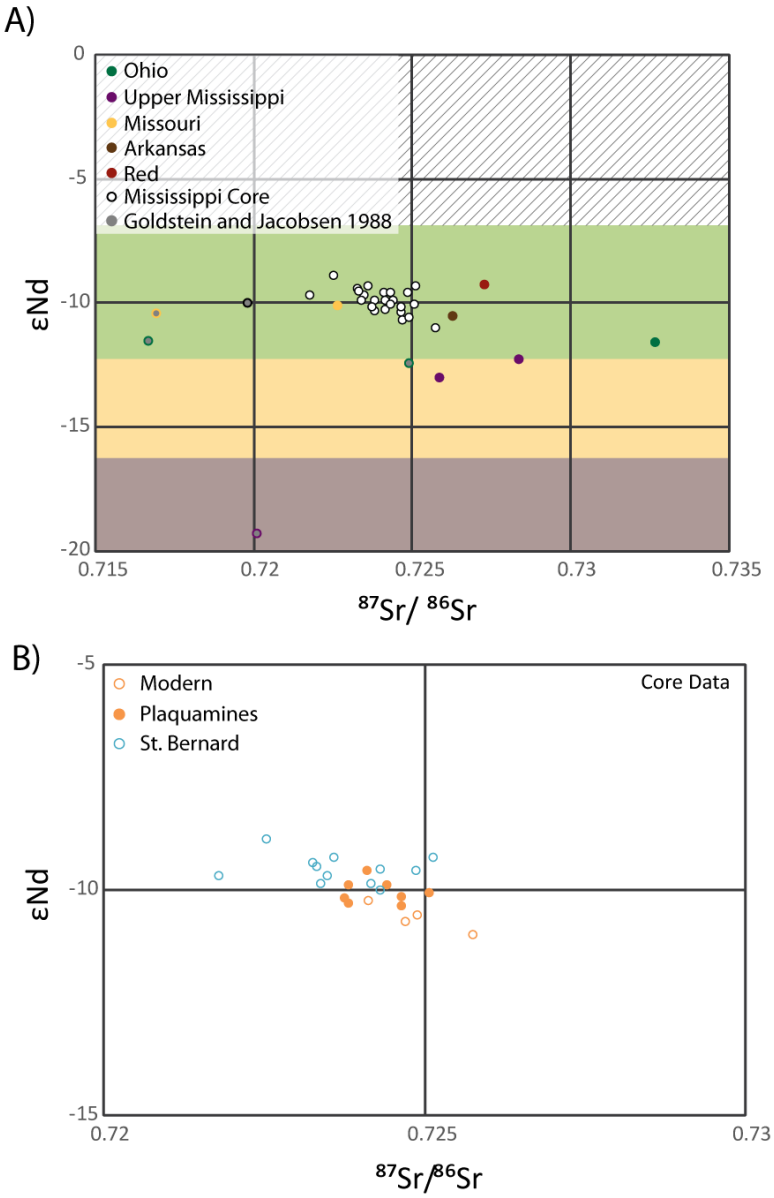

Figure 4. 7 A) Cross plot of Nd and Sr isotope values for both the cored samples and the modern Mississippi River samples compared with earlier measurements by Goldstein & Jacobsen (1988). Colored bands show the major Nd isotopic divisions of continental North America as shown in Figure 4.1. B) Cross plot of Nd and Sr isotope values of only the core samples and their interpreted correlation with the defined delta complexes of the Mississippi (see Fig. 4.3).

Slightly warmer and drier climate during the time of the St. Bernard delta building (2–4 ka) is hypothesized to have reduced the occurrence of mega floods (Knox, 1993), however this drying could have resulted in reduced vegetation cover in the western parts of the Mississippi catchment. A drier climate would lead to floodplain destabilization and therefore a greater sediment supply from the western drainages. The climate regime in the last 1 ky is both cooler and wetter (Aharon & Dhungana, 2017; Knox, 1993), which would lead to greater vegetation cover and a reduced supply of sediment from the west, thereby potentially explaining the shift towards more negative εNd values at the start of the Plaquemine/Modern delta sedimentation.

While the general trend towards more negative εNd values in the Plaquemines/Modern compared to the St. Bernard samples may reasonably be within uncertainty, the top 66 cm and modern sediment cannot be accounted for in this way. While the more negative shift in εNd in the top 66 cm could be associated with increased erosion within the northern and eastern tributaries of the Mississippi River, modern river samples do not suggest this to be the case (Fig 4.6A). Analysis of εNd from within the Upper Mississippi and Ohio Rivers presently shoe that they contribute very little to the main stream sediment flux (Fig. 4.6A). Conversely, reduced sediment flux from the western tributaries since the 1920s could produce a similar trend in isotope composition. While damming of these streams might have caused the up-core variation in isotope values, historical data shows that sediment flux did not reduce significantly until the 1950s and 1960s (Mason et al., 2017), when large-scale damming of these tributaries and the installation of the Old River Control structure in Louisiana occurred.

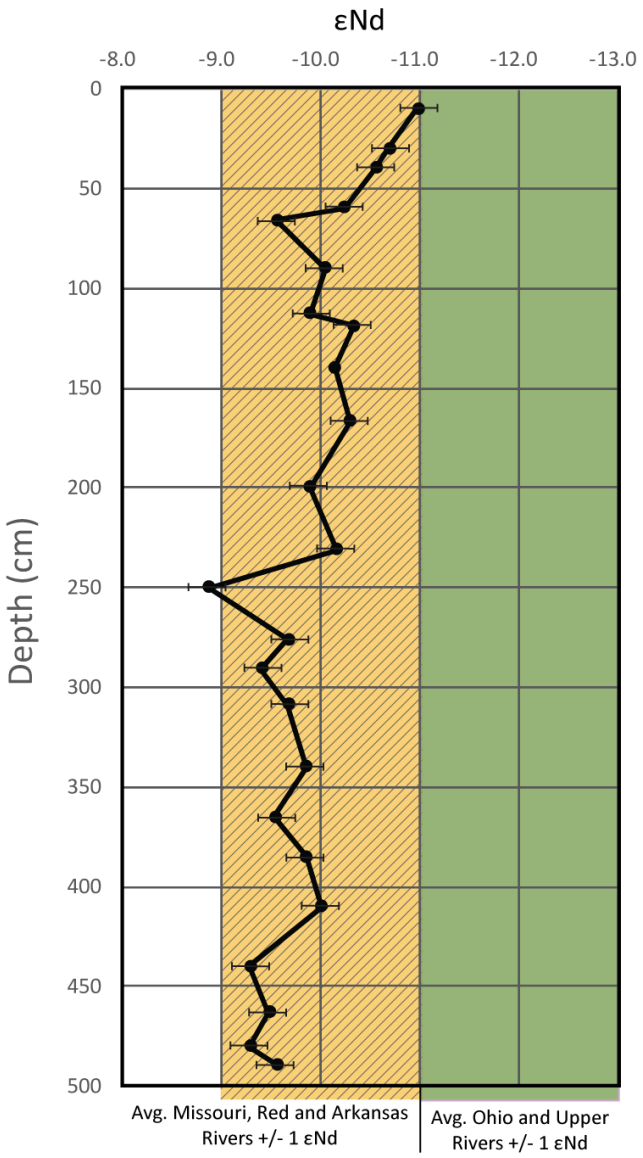

Figure 4. 8 Variations in the εNd values in the core plotted against depth and compared with the average values from the modern western and northern/eastern tributaries.

We argue the εNd shift towards more negative values in the top of the core can best be explained by the enhancement of levees along the Mississippi River, which cut off deposition of fluvial sediment to the core site in the 1920s (Fig. 4.4 and 5). After this, the only sediment the core site received after the construction of the higher levees would be from storm deposits or

longshore drift suspended sediments sourced from east of the Mississippi River delta (eg. Pearl and Mobile Rivers) until the construction of the seaward levee in the 1960s. Since eastern rivers are supplied by sediment from more negative εNd source terranes (Fig. 4.1) this could help explain the sharp negative trend in εNd found at the top of the core. However εNd data from these rivers does not exist and warrants further investigation.

4.8. Conclusions

We show that the western and eastern/northern drainages of the Mississippi River have distinctive Nd and Sr isotopic signatures. The western tributaries have more positive εNd values, while the eastern and northern tributaries have more negative εNd values. Most of the detrital grab samples from the modern river show a trend towards western (Missouri) εNd values, with little input from the northern and eastern tributaries. While most of these samples derive their provenance from Grenville sources (Fig. 4.1, 7), there seems to be a general trend towards less negative values as you move from the west to southeast when looking at the εNd values derived from the modern tributaries. In general, however, on a continental scale, the more positive εNd values that characterize the youngest Laramide/Cordilleran orogenic events have not significantly impacted the overall Grenville-dominated Nd isotopic signatures of the modern Mississippi sediment.

Two phases of St Bernard delta building (2–4 ka) are captured and dated to 1.92 +/- 0.4 to 3.98 +/- .4 in this core, as well as the beginning stages of the Plaquemines/Modern subdelta complex (<1.3 ka). In this study, overbank natural levee and floodplain aggradation are seen to be significantly curtailed by human influence, effectively slowing the accumulation rate going from 1.73 cm/yr before levee construction to approximately 0.23 cm/yr in the top 66 cm of core.

With significant changes such as these, it is evident why the Mississippi Delta is presently facing such problems with subsidence and floodplain nourishment.

Isotope compositions of sediment from the Mississippi over the last 3 ka have remained consistent. With an average value of -9.9 εNd, this is slightly less negative than other values recorded from the modern system at -10 εNd (S. J. Goldstein & Jacobsen, 1988). This can most likely be explained by the more positive εNd values associated with the St. Bernard delta sequence derived from western sources. The sharp trend towards more negative values in the top 66 cm of the core is interpreted to be anthropogenically driven. With the construction of more robust levees along the Mississippi River in the 1920's the floodplain was cut off from overbank fluvial deposits, likely only receiving sediment from major storms which resuspended sediment from sources to the east of the Mississippi River with a more negative εNd isotopic signature.

4.9 References Cited

Aharon, P., & Dhungana, R. (2017). Ocean-atmosphere interactions as drivers of mid-to-late Holocene rapid climate changes: Evidence from high-resolution stalagmite records at DeSoto Caverns, Southeast USA. *Quaternary Science Reviews, 170*, 69-81. doi:https://doi.org/10.1016/j.quascirev.2017.06.023

Aitken, M. J. (1998). *An introduction to optical dating*. Oxford: Oxford University Press.

Alexander, J. S., Wilson, R. C., & Green, W. R. (2012). *A brief history and summary of the effects of river engineering and dams on the Mississippi River system and delta*: US Department of the Interior, US Geological Survey.

Allen, P. A. (2008a). From landscapes into geological history. *Nature, 451*, 274. doi:doi:10.1038/nature06586

Allen, P. A. (2008b). Time scales of tectonic landscapes and their sediment routing systems. In K. Gallagher, S. J. Jones, & J. Wainwright (Eds.), *Landscape Evolution: Denudation, Climate and Tectonics over Different Time and Space Scales* (Vol. 296, pp. 7-28). London: Geological Society.

Amidon, W. H., Burbank, D. W., & Gehrels, G. E. (2005). Construction of detrital mineral populations: insights from mixing of U-Pb zircon ages in Himalayan rivers. *Basin Research, 17*(4), 463-485.

Belousova, E., Griffin, W., O'Reilly, S. Y., & Fisher, N. (2002). Apatite as an indicator mineral for mineral exploration: trace-element compositions and their relationship to host rock type. *Journal of Geochemical Exploration, 76*(1), 45-69.

Bhatia, M. R., & Crook, K. A. (1986). Trace element characteristics of graywackes and tectonic setting discrimination of sedimentary basins. *Contributions to Mineralogy and Petrology, 92*(2), 181-193.

Bickford, M., & Van Schmus, W. (1985). Discovery of two Proterozoic granite-rhyolite terranes in the buried midcontinent basement: The case for shallow drill holes *Observation of the Continental Crust through Drilling I* (pp. 355-364): Springer.

Black, L. P., Kamo, S. L., Allen, C. M., Aleinikoff, J. N., Davis, D. W., Korsch, R. J., & Foudoulis, C. (2003). TEMORA 1: a new zircon standard for Phanerozoic U-Pb geochronology. *Chemical Geology, 200*, 155–170.

Blum, M., & Pecha, M. (2014). Mid-Cretaceous to Paleocene North American drainage reorganization from detrital zircons. *Geology*. doi:10.1130/g35513.1

Blum, M. D., & Roberts, H. H. (2009). Drowning of the Mississippi Delta due to insufficient sediment supply and global sea-level rise. *Nature Geoscience, 2*(7), 488-491. doi:10.1038/ngeo553

Boesch, D. F., Josselyn, M. N., Mehta, A. J., Morris, J. T., Nuttle, W. K., Simenstad, C. A., & Swift, D. J. (1994). Scientific assessment of coastal wetland loss, restoration and management in Louisiana. *Journal of Coastal Research*, i-103.

Bouch, J. E., Hole, M. J., Trewin, N. H., Chenery, S., & Morton, A. C. (2002). Authigenic apatite in a fluvial sandstone sequence; evidence for rare-earth element mobility during diagenesis and a tool for diagenetic correlation. *Journal of Sedimentary Research, 72*(1), 59-67.

Bouquillon, A., France-Lanord, C., Michard, A., & Tiercelin, J. (1990). Sedimentology and isotopic chemistry of the Bengal Fan sediments: the denudation of the Himalaya. In J. R. Cochran, D. A. V. Stow, & C. Auroux (Eds.), *Proceedings of the Ocean Drilling Program, Scientific Results* (Vol. 116, pp. 43-58). College Station, TX: Ocean Drilling Program.

Bowring, S. A., & Karlstrom, K. E. (1990). Growth, stabilization, and reactivation of Proterozoic lithosphere in the southwestern United States. *Geology, 18*(12), 1203-1206.

Bream, B. R., Hatcher, R. D., Miller, C. F., Fullagar, P. D., Tollo, R., McLelland, J., . . . Bartholomew, M. (2004). Detrital zircon ages and Nd isotopic data from the southern Appalachian crystalline core, Georgia, South Carolina, North Carolina, and Tennessee: New provenance constraints for part of the Laurentian margin. *MEMOIRS-GEOLOGICAL SOCIETY OF AMERICA*, 459-476.

Budzinski, H., & Tischendorf, G. (1989). Distribution of REE among minerals in the Hercynian postkinematic granites of Westerzgebirge-Vogtland, GDR. *Zeitschrift fur Geologische Wissenschaften, 17*(11), 1019-1031.

Burbank, D. W., & Anderson, R. S. (2001). *Tectonic Geomorphology*. Oxford: Blackwell.

Castelltort, S., & Van Den Driessche, J. (2003). How plausible are high-frequency sediment supply-driven cycles in the stratigraphic record? *Sedimentary Geology, 157*, 3–13.

Chang, L., Howie, R., & Zussman, J. (1996). Rock-Forming Minerals, Volume 5B, Non-Silicates (pp. 383): Longman Group Harlow, UK.

Chauvel, C., Bureau, S., & Poggi, C. (2010). Comprehensive Chemical and Isotopic Analyses of Basalt and Sediment Reference Materials. *Geostandards and Geoanalytical Research, 35*(1), 125-143. doi:doi: 10.1111/j.1751-908X.2010.00086.x

Chew, D. M., Sylvester, P. J., & Tubrett, M. N. (2011). U–Pb and Th–Pb dating of apatite by LA-ICPMS. *Chemical Geology, 280*(1-2), 200-216.

Clift, P. D., & Giosan, L. (2012). Sediment Source-to-Sink Processes in the Indus River since the Last Glacial Maximum. *Geophysical Research Abstracts, 14*, EGU2012-1657.

Coleman, J. M., Roberts, H. H., & Stone, G. W. (1998). Mississippi River delta: an overview. *Journal of Coastal Research, 14*(3), 698-716.

Colten, C. E. (2006). *An unnatural metropolis: Wresting New Orleans from nature*: LSU Press.

Corfu, F., Krogh, T., Kwok, Y., & Jensen, L. (1989). U–Pb zircon geochronology in the southwestern Abitibi greenstone belt, Superior Province. *Canadian Journal of Earth Sciences, 26*(9), 1747-1763.

Corrigan, D., & Hanmer, S. (1997). Anorthosites and related granitoids in the Grenville orogen: A product of convective thinning of the lithosphere? *Geology*, *25*(1), 61-64.

Craddock, W. H., & Kylander-Clark, A. R. C. (2013). U-Pb ages of detrital zircons from the Tertiary Mississippi River Delta in central Louisiana: Insights into sediment provenance. *Geosphere, 9*(6), 1832-1851. doi:10.1130/GES00917.1

Dahl, P. S., Holm, D. K., Gardner, E. T., Hubacher, F. A., & Foland, K. A. (1999). New constraints on the timing of Early Proterozoic tectonism in the Black Hills (South

Dakota), with implications for docking of the Wyoming province with Laurentia. *Geological Society of America Bulletin, 111*(9), 1335-1349.

Dalziel, I. W. (1991). Pacific margins of Laurentia and East Antarctica-Australia as a conjugate rift pair: Evidence and implications for an Eocambrian supercontinent. *Geology, 19*(6), 598-601.

Davidson, A. (1995). A review of the Grenville orogen in its North American type area. *AGSO Journal of Australian Geology and Geophysics, 16*(1), 3-24.

DePaolo, D. J. (1981). Neodymium isotopes in the Colorado Front Range and crust–mantle evolution in the Proterozoic. *Nature, 291*(5812), 193.

DePaolo, D. J., & Wasserburg, G. J. (1976). Nd isotopic variations and petrogenetic models. *Geophysical Research Letters, 3*(5), 249-252.

Dickinson, W. R. (2008). Impact of differential zircon fertility of granitoid basement rocks in North America on age populations of detrital zircons and implications for granite petrogenesis. *Earth and Planetary Science Letters, 275*(1-2), 80-92. doi:doi:10.1016/j.epsl.2008.08.003

Drake Jr, A. A., Sinha, A., Laird, J., & Guy, R. (1989). The taconic orogen. *The Appalachian-Ouachita orogen in the United States: Boulder, Colorado, Geological Society of America, Geology of North America, 2*, 101-177.

Dunlea, A. G., Murray, R. W., Sauvage, J., Spivack, A. J., Harris, R. N., & D'Hondt, S. (2015). Dust, volcanic ash, and the evolution of the South Pacific Gyre through the Cenozoic. *Paleoceanography, 30*(8), 1078-1099. doi:doi:10.1002/2015PA002829

Fan, M., DeCelles, P. G., Gehrels, G. E., Dettman, D. L., Quade, J., & Peyton, S. L. (2011). Sedimentology, detrital zircon geochronology, and stable isotope geochemistry of the lower Eocene strata in the Wind River Basin, central Wyoming. *Bulletin, 123*(5-6), 979-996.

Fildani, A., Hessler, A. M., Mason, C. C., McKay, M. P., & Stockli, D. F. (2018). Late Pleistocene glacial transitions in North America altered major river drainages, as revealed by deep-sea sediment. *Scientific Reports, 8*(1), 13839.

Fildani, A., McKay, M. P., Stockli, D., Clark, J., Dykstra, M. L., Stockli, L., & Hessler, A. M. (2016). The ancestral Mississippi drainage archived in the late Wisconsin Mississippi deep-sea fan. *Geology*. doi:10.1130/g37657.1

Fleischer, M., & Altschuler, Z. (1986). The lanthanides and yttrium in minerals of the apatite group-an analysis of the available data. *Neues Jahrbuch für Mineralogie, Monatshefte*, 467-480.

France-Lanord, C., Derry, L., & Michard, A. (1993). Evolution of the Himalaya since Miocene time: Isotopic and sedimentologic evidence from the Bengal Fan In P. J. Treloar & M. P. Searle (Eds.), *Himalayan Tectonics* (Vol. 74, pp. 603–621). London: Geological Society.

Frazier, D. E. (1967). Recent deltaic deposits of the Mississippi River: their development and chronology. *Gulf Coast Association of Geological Societies Transactions, 17*, 287-315.

Frazier, D. E. (1967). Recent deltaic deposits of the Mississippi River: their development and chronology. *Gulf Coast Association Geological Society Transactions, 17*, 287–315.

Fuchs, M., & Owen, L. A. (2008). Luminescence dating of glacial and associated sediments: review, recommendations and future directions. *Boreas, 37*, 636-659.

Fuentes, F., DeCelles, P. G., Constenius, K. N., & Gehrels, G. E. (2011). Evolution of the Cordilleran foreland basin system in northwestern Montana, USA. *GSA Bulletin, 123*(3-4), 507-533.

Coleman, J. M., & Gagliano, S. M. (1964). Cyclic sedimentation in the Mississippi River deltaic plain.

Garzanti, E., Andó, S., France-Lanord, C., Censi, P., Vignola, P., Galy, V., & Lupker, M. (2011). Mineralogical and chemical variability of fluvial sediments 2. Suspended-load silt (Ganga–Brahmaputra, Bangladesh). *Earth and Planetary Science Letters, 302*, 107–120. doi:doi:10.1016/j.epsl.2010.11.043

Gehrels, G. E. (2014). Detrital Zircon U-Pb Geochronology Applied to Tectonics. *Annual Review of Earth and Planetary Sciences, 42*, 127-149. doi:DOI: 10.1146/annurev-earth-050212-124012

Gerdes, A., & Zeh, A. (2006). Combined U-Pb and Hf isotope LA-(MC-)ICP-MS analyses of detrital zircons: Comparison with SHRIMP and new constraints for the provenance and age of an Armorican metasediment in Central Germany. *Earth and Planetary Science Letters, 249*(1-2), 47-61.

Gleason, J. D., Patchett, P. J., Dickinson, W. R., & Ruiz, J. (1994). Nd isotopes link Ouachita turbidites to Appalachian sources. *Geology, 22*(4), 347-350.

Gleason, J. D., Patchett, P. J., Dickinson, W. R., & Ruiz, J. (1995). Nd isotopic constraints on sediment sources of the Ouachita-Marathon fold belt. *Geological Society of America Bulletin, 107*(10), 1192–1210. doi:doi: 10.1130/0016-7606(1995)107<1192:NICOSS>2.3.CO;2

Goldstein, S. J., & Jacobsen, S. B. (1988). Nd and Sr isotopic systematics of river water suspended material; Implications for crustal evolution. *Earth and Planetary Science Letters, 87*(3), 249-265.

Goldstein, S. L., & Hemming, S. R. (2003). Long-lived isotopic tracers in oceanography, paleoceanography, and ice-sheet dynamics. *Treatise on geochemistry, 6*, 625.

Goldstein, S. L., O'Nions, R. K., & Hamilton, P. J. (1984). A Sm-Nd isotopic study of atmospheric dusts and particulates from major river systems. *Earth and Planetary Science Letters, 70*(2), 221-236.

Granet, M., Chabaux, F., Stille, P., France-Lanord, C., & Pelt, E. (2007). Time-scales of sedimentary transfer and weathering processes from U-series nuclides: Clues from the Himalayan rivers. *Earth and Planetary Science Letters, 261*(3-4), 389-406.

Gregory, B., Herrmann, A. D., Ireland, T., & Clift, P. D. (2018). Zircon U-Pb Dating Comparisons in a Highly Altered River System, Mississippi River, USA. *Basin Research, in review*.

Guerin, G., Mercier, N., & Adamiec, G. (2011). Dose rate conversion factors: update. *Ancient Thermo Luminesence, 29*(1), 5-8.

Hamilton, P. J., Onions, R. K., Bridgwater, D., & Nutman, A. (1983). Sm-Nd Studies of Archean Metasediments and Metavolcanics from West Greenland and Their Implications for the Earths Early History. *Earth and Planetary Science Letters, 62*(2), 263-272.

Hanson, R. E., Puckett Jr, R. E., Keller, G. R., Brueseke, M. E., Bulen, C. L., Mertzman, S. A., . . . McCleery, D. A. (2013). Intraplate magmatism related to opening of the southern Iapetus Ocean: Cambrian Wichita igneous province in the Southern Oklahoma rift zone. *Lithos, 174*, 57-70.

Heimann, D. C., Sprague, L. A., & Blevins, D. W. (2011). *Trends in suspended-sediment loads and concentrations in the Mississippi River Basin, 1950-2009*: US Department of the Interior, US Geological Survey.

Heslop, D., Shaw, J., Bloemendal, J., Chen, F., Wang, J., & Parker, E. (1999). Sub-millennial scale variations in East Asian monsoon systems recorded by dust deposits from the north-western Chinese Loess Plateau. *Physics and Chemistry of the Earth, Part A: Solid Earth and Geodesy, 24*(9), 785-792. doi:doi:10.1016/S1464-1895(99)00115-5

Hoffman, P. F. (1988). United plates of America, the birth of a craton: Early Proterozoic assembly and growth of Laurentia. *Annual Review of Earth and Planetary Sciences, 16*(1), 543-603.

Hoffman, P. F. (1989). Precambrian geology and tectonic history of North America. In A. W. Bally & A. R. Palmer (Eds.), *The Geology of North America-An Overview* (pp. 447-511). Boulder, CO: Geological Society of America

.

Horton, J. W., Drake, A. A., & Rankin, D. W. (1989). Tectonostratigraphic terranes and their Paleozoic boundaries in the central and southern Appalachians. *Geological Society of America Special Papers, 230*, 213-246.

Hu, D., Clift, P. D., Böning, P., Hannigan, R., Hillier, S., Blusztajn, J., . . . Fuller, D. Q. (2013). Holocene evolution in weathering and erosion patterns in the Pearl River delta. *Geochemistry Geophysics Geosystems, 14*. doi:doi:10.1002/ggge.20166

Hughen, K. A., Baillie, M. G. L., Bard, E., Bayliss, A., Beck, J. W., Bertrand, C., . . . Weyhenmeyer, C. W. (2009). Marine 04 radiocarbon calibration curves 0-50,000 years cal BP. *Radiocarbon, 46*, 1059-1086.

Hülse, P., & Bentley, S. J. (2012). A 210Pb sediment budget and granulometric record of sediment fluxes in a subarctic deltaic system: the Great Whale River, Canada. *Estuarine and Coastal Shelf Science, 109*, 41–52. doi:doi:10.1016/j.ecss.2012.05.019

Huntley, D. (1985). On the zeroing of the thermoluminescence of sediments. *Physics and Chemistry of Minerals, 12*(2), 122-127.

Iizuka, T., Hirata, T., Komiya, T., Rino, S., Katayama, I., Motoki, A., & Maruyama, S. (2005). U-Pb and Lu-Hf isotope systematics of zircons from the Mississippi River sand: Implications for reworking and growth of continental crust. *Geology, 33*(6), 485-488.

Jonell, T. N., Li, Y., Blusztajn, J., Giosan, L., & Clift, P. D. (2018). Signal or noise? Isolating grain size effects on Nd and Sr isotope variability in Indus delta sediment provenance. *Chemical Geology*. doi:doi:10.1016/j.chemgeo.2018.03.036

Karlstrom, K., Bowring, S. A., & Reed, J. (1993). Proterozoic orogenic history of Arizona. *Precambrian: Conterminous US: Boulder, Colorado, Geological Society of America, Geology of North America, 2*, 188-211.

Karlstrom, K. E., Åhäll, K.-I., Harlan, S. S., Williams, M. L., McLelland, J., & Geissman, J. W. (2001). Long-lived (1.8–1.0 Ga) convergent orogen in southern Laurentia, its extensions to Australia and Baltica, and implications for refining Rodinia. *Precambrian Research, 111*(1-4), 5-30.

Karlstrom, K. E., & Humphreys, E. D. (1998). Persistent influence of Proterozoic accretionary boundaries in the tectonic evolution of southwestern North America: Interaction of cratonic grain and mantle modification events. *Rocky Mountain Geology, 33*(2), 161-179.

Knox, J. C. (1993). Large increases in flood magnitude in response to modest changes in climate. *Nature, 361*(6411), 430.

Lawrence, R. L., Cox, R., Mapes, R. W., & Coleman, D. S. (2011). Hydrodynamic fractionation of zircon age populations. *Geological Society of America Bulletin, 123*, 295–305.

Liu, C., Clift, P. D., Murray, R. W., Blusztajn, J., Ireland, T., Wan, S., & Ding, W. (2017). Geochemical Evidence for Initiation of the Modern Mekong Delta in the southwestern South China Sea after 8 Ma. *Chemical Geology, 451*, 38–54. doi:doi:10.1016/j.chemgeo.2017.01.008

Ludwig, W., & Probst, J. L. (1998). River sediment discharge to the oceans: present-day controls and global budgets. *American Journal of Science, 298*, 265–295.

Malusa, M. G., Resentini, A., & Garzanti, E. (2016). Hydraulic sorting and mineral fertility bias in detrital geochronology. *Gondwana Research, 31*, 1-19. doi:doi:10.1016/j.gr.2015.09.002

Mason, C. C., Fildani, A., Gerber, T., Blum, M. D., Clark, J. D., & Dykstra, M. (2017). Climatic and anthropogenic influences on sediment mixing in the Mississippi source-to-sink system using detrital zircons: Late Pleistocene to recent. *Earth and Planetary Science Letters, 466*, 70-79. doi:http://dx.doi.org/10.1016/j.epsl.2017.03.001

May, S. R., Gray, G. G., Summa, L. L., Stewart, N. R., Gehrels, G. E., & Pecha, M. E. (2013). Detrital zircon geochronology from the Bighorn Basin, Wyoming, USA: Implications for tectonostratigraphic evolution and paleogeography. *Bulletin, 125*(9-10), 1403-1422.

McDonough, W. F., & Sun, S.-S. (1995). The composition of the Earth. *Chemical Geology, 120*(3-4), 223-253.

McIntire, W. G. (1954). *Correlation of prehistoric settlements and delta development*: Louisiana State University.

McLelland, J., Daly, J. S., & McLelland, J. M. (1996). The Grenville orogenic cycle (ca. 1350-1000 Ma); an Adirondack perspective. *Tectonophysics, 265*(1-2), 1-28.

McLennan, S., Hemming, S., McDaniel, D., & Hanson, G. (1993). Geochemical approaches to sedimentation, provenance, and tectonics. *Special Papers-Geological Society of America*, 21-21.

Meade, R. H., & Moody, J. A. (2010). Causes for the decline of suspended-sediment discharge in the Mississippi River system, 1940–2007. *Hydrological Processes: An International Journal, 24*(1), 35-49.

Moecher, D. P., & Samson, S. D. (2006). Differential zircon fertility of source terranes and natural bias in the detrital record: implications for sedimentary provenance analysis. *Earth and Planetary Science Letters, 247*((3-4), 252–266.

Moecher, D. P., & Samson, S. D. (2006). Differential zircon fertility of source terranes and natural bias in the detrital zircon record: Implications for sedimentary provenance analysis. *Earth and Planetary Science Letters, 247*(3), 252-266. doi:doi:10.1016/j.epsl.2006.04.035

Montgomery, D. R. (2007). *Dirt: The erosion of civilizations*. Berkeley: University of California Press.

Moores, E. (1991). Southwest US-East Antarctic (SWEAT) connection: a hypothesis. *Geology, 19*(5), 425-428.

Morton, A., & Yaxley, G. (2007). Detrital apatite geochemistry and its application in provenance studies. *Special Papers-Geological Society of America, 420*, 319.

Morton, A. C. (1991). Geochemical studies of detrital heavy minerals and their application to provenance research. In A. C. Morton, S. P. Todd, & P. D. W. Haughton (Eds.), *Developmentsin Sedimentary Provenance Studies* (Vol. 57, pp. 31-45). London: Geological Society.

Muehlberger, W. R., Denison, R. E., & Lidiak, E. G. (1967). Basement rocks in continental interior of United States. *AAPG Bulletin, 51*(12), 2351-2380.

Mueller, P. A., Heatherington, A. L., Wooden, J. L., Shuster, R. D., Nutman, A. P., & Williams, I. S. (1994). Precambrian zircons from the Florida basement: A Gondwanan connection. *Geology, 22*(2), 119-122.

Murray, A. S., & Wintle, A. G. (2000). Luminescence dating of quartz using an improved single-aliquot regenerative-dose protocol. *Radiation Measurements, 32*, 57-72.

Naeser, N. D., Naeser, C. W., & McCulloh, T. H. (1989). The application of fission-track dating to the depositional and thermal history of rocks in sedimentary basins *Thermal history of sedimentary basins* (pp. 157-180): Springer.

Nash, W. P. (1984). Phosphate minerals in terrestrial igneous and metamorphic rocks *Phosphate minerals* (pp. 215-241): Springer.

Nelson, B. K., & DePaolo, D. J. (1985). Rapid production of continental crust 1.7 to 1.9 b.y. ago: Nd isotopic evidence from the basement of the North American mid-continent. *Geological Society of America Bulletin, 96*(6), 746-754. doi:doi: 10.1130/0016-7606(1985)96

Nittrouer, C. A., Sternberg, R. W., Carpenter, R., & Bennett, J. T. (1979). The use of 210Pb geochronology as a sedimentological tool: Application to the Washington continental shelf. *Marine Geology, 31*, 297-316.

Nittrouer, J. A., & Viparelli, E. (2014). Sand as a stable and sustainable resource for nourishing the Mississippi River delta. *Nature Geoscience, 7*(5), 350.

Noller, J. S. (2000). Lead-210 geochronology. *Quaternary Geochronology*, 115-120.

Otvos, E. G. (1975). Southern limits of Pleistocene loess, Mississippi valley. *Southeastern Geology, 17*, 27-38.

Otvos, E. G. (2015). The last interglacial stage: Definitions and marine highstand, North America and Eurasia. *Quaternary International, 383*, 158-173.

Paola, C., Heller, P. L., & Angevine, C. L. (1992). The large-scale dynamics of grain-size variation in alluvial basins, 1: Theory. *Basin Research, 4*(2), 73–90. doi:DOI: 10.1111/j.1365-2117.1992.tb00145.x

Park, H., Barbeau Jr, D. L., Rickenbaker, A., Bachmann-Krug, D., & Gehrels, G. (2010). Application of foreland basin detrital-zircon geochronology to the reconstruction of the southern and central Appalachian orogen. *The Journal of Geology, 118*(1), 23-44.

Patchett, P. J., Ross, G. M., & Gleason, J. D. (1999). Continental drainage in North America during the Phanerozoic from Nd isotopes. *Science, 283*(5402), 671-673.

Pearce, N. J. G., Perkins, W. T., Westgate, J. A., Gorton, M. P., Jackson, S. E., Neal, C. R., & Chenery, S. P. (1997). A compilation of new and published major and trace element data for NIST SRM 610 and NIST SRM 612 glass reference materials. *Geostandards Newsletter-the Journal of Geostandards and Geoanalysis, 21*(1), 115-144.

Prescott, J. R., & Hutton, J. T. (1994). Cosmic ray contributions to dose rates for luminescence and ESR dating: large depths and long-term time variations. *Radiation Measurements, 23*, 497-500.

Rhodes, E. J. (2011). Optically Stimulated Luminescence Dating of Sediments over the Past 200,000 Years. *Annual Review of Earth and Planetary Sciences, 39*, 461-488. doi:doi: 10.1146/annurev-earth-040610-133425

Rittenour, T. M. (2008). Luminescence dating of fluvial deposits: applications to geomorphic, palaeoseismic and archaeological research. *Boreas, 37*, 613-635.

Roberts, H., Coleman, J., Bentley, S., & Walker, N. (2003). An embryonic major delta lobe: A new generation of delta studies in the Atchafalaya-Wax Lake Delta system.

Roberts, H. H. (1997). Dynamic changes of the Holocene Mississippi River delta plain: the delta cycle. *Journal of Coastal Research*, 605-627.

Roberts, H. H. (1997). Dynamic changes of the Holocene Mississippi River delta plain: The delta cycle. *Journal of Coastal Research, 13*(3), 605-627.

Rogers, D. (2005). History of the New Orleans flood protection system. *Investigation of the performance of the New Orleans flood protection systems in Hurricane Katrina on August 29*.

Rogers, J. D. (2008). Development of the New Orleans flood protection system prior to Hurricane Katrina. *Journal of geotechnical and geoenvironmental engineering, 134*(5), 602-617.

Romans, B. W., Castelltort, S., Covault, J. A., Fildani, A., & Walsh, J. P. (2016). Environmental signal propagation in sedimentary systems across timescales. *Earth-Science Reviews, 153*, 7–29. doi:doi:10.1016/j.earscirev.2015.07.012

Ross, G. M., Patchett, P. J., Hamilton, M., Heaman, L., DeCelles, P. G., Rosenberg, E., & Giovanni, M. K. (2005). Evolution of the Cordilleran Orogen (southwestern Alberta, Canada) inferred from detrital mineral geochronology, geochemistry, and Nd isotopes in the foreland basin. *Geological Society of America Bulletin, 117*(5-6), 747-763.

Ruddiman, W. F. (2003). The Anthropogenic Greenhouse Era Began Thousands of Years Ago. *Climatic Change, 61*(3), 261-293. doi:DOI: 10.1023/B:CLIM.0000004577.17928.fa

Sevastjanova, I., Clements, B., Hall, R., Belousova, E. A., Griffin, W. L., & Pearson, N. (2011). Granitic magmatism, basement ages, and provenance indicators in the Malay Peninsula: insights from detrital zircon U–Pb and Hf-isotope data. *Gondwana Research, 19*(4), 1024-1039.

Shaw, C. A., & Karlstrom, K. E. (1999). The Yavapai-Mazatzal crustal boundary in the southern Rocky Mountains. *Rocky Mountain Geology, 34*(1), 37-52.

Singh, S. C., Carton, H., Tapponnier, P., Hananto, N. D., Chauhan, A. P. S., Hartoyo, D., . . . Martin, J. (2008). Seismic evidence for broken oceanic crust in the 2004 Sumatra earthquake epicentral region. *Nature Geoscience, 1*, 777-781. doi:doi:10.1038/ngeo336

Sláma, J., Košler, J., Condon, D. J., Crowley, J. L., Gerdes, A., Hanchar, J. M., . . . Whitehouse, M. J. (2008). Plezovice zircon A new natural reference material for U–Pb and Hf isotopic microanalysis. *Chemical Geology, 249*, 1-35. doi:doi:10.1016/j.chemgeo.2007.11.005

Station, W. E., & Kolb, C. R. (1958). *Geology of the Mississippi River deltaic plain, southeastern Louisiana*.

Sundell, K., & Saylor, J. E. (2017). Unmixing detrital geochronology age distributions. *Geochemistry Geophysics Geosystems, 18*, 2872–2886.

Syvitski, J. P. M., C., V., Kettner, A. J., & Green, P. (2005). Impact of humans on the flux of terrestrial sediment to the global coastal ocean. *Science, 308*, 376-380.

Syvitski, J. P. M., & Kettner, A. J. (2011). Sediment flux and the Anthropocene. *Philosophical Transactions of the Royal Society of London, Series A: Mathematical and Physical Sciences, 369*, 957–975. doi:doi:10.1098/rsta.2010.0329

Syvitski, J. P. M., & Milliman, J. D. (2007). Geology, geography and humans battle for dominance over the delivery of sediment to the coastal ocean. *Journal of Geology, 115*, 1-19.

Syvitski, J. P. M., & Saito, Y. (2007). Morphodynamics of deltas under the influence of humans. *Global and Planetary Change, 57*, 261–282.

Törnqvist, T. E., Rosenheim, B. E., Hu, P., & Fernandez, A. B. (2015). Radiocarbon dating and calibration. *Handbook of Sea-Level Research, edited by: Shennan, I., Long, AJ, and Horton, BP*, 349-360.

Tylmann, W., Bonk, A., Goslar, T., Wulf, S., & Grosjean, M. (2016). Calibrating 210Pb dating results with varve chronology and independent chronostratigraphic markers: problems and implications. *Quaternary Geochronology, 32*, 1-10.

Van Schmus, W. (1976). A Discussion on global tectonics in Proterozoic times-Early and Middle Proterozoic history of the Great Lakes area, North America. *Phil. Trans. R. Soc. Lond. A, 280*(1298), 605-628.

Vermeesch, P. (2004). How many grains are needed for a provenance study? *Earth and Planetary Science Letters, 224*, 351–441.

Vermeesch, P., Resentini, A., & Garzanti, E. (2016). An R package for statistical provenance analysis. *Sedimentary Geology, 336*, 14-25. doi:doi:10.1016/j.sedgeo.2016.01.009

Wayne, W. J. (1952). Pleistocene evolution of the Ohio and Wabash valleys. *The Journal of Geology, 60*(6), 575-585.

Whitmeyer, S. J., & Karlstrom, K. E. (2007). Tectonic model for the Proterozoic growth of North America. *Geosphere, 3*, 220–259.

Wiedenbeck, M., Allé, P., Corfu, F., Griffin, W. L., Meier, M., Oberli, F., . . . Spiegel, W. (1995). Three natural zircon standards for U-Th-Pb, Lu-Hf tarce element and REE analyses. *Geostandards Newsletter, 19*(1), 1-23. doi:doi:10.1111/j.1751-908X.1995.tb00147.x

Wilson, S. A. (1997). Data compilation for USGS reference material BHVO-2, Hawaiian Basalt. *U.S. Geological Survey Open-File Report*.

Wintle, A., & Murray, A. (1997). The relationship between quartz thermoluminescence, photo-transferred thermoluminescence, and optically stimulated luminescence. *Radiation Measurements, 27*(4), 611.

Wyshnytzky, C. E., Rittenour, T. M., Nelson, M. S., & Thackray, G. (2015). Luminescence dating of late Pleistocene proximal glacial sediments in the Olympic Mountains,

Washington. *Quaternary International, 362*, 116–123. doi:doi:10.1016/j.quaint.2014.08.024

Yang, S., Zhang, F., & Wang, Z. (2012). Grain size distribution and age population of detrital zircons from the Changjiang (Yangtze) River system, China. *Chemical Geology, 296-297*, 26-38.

Zalasiewicz, J., Williams, M., Steffen, W., & Crutzen, P. (2010). The New World of the Anthropocene. *Environmental Science and Technology, 44*(7), 2228–2231. doi:DOI: 10.1021/es903118j

CHAPTER 5. CONCLUSIONS

In general, this dissertation seeks to understand the provenance relationships within the Mississippi River catchment. Chapter 1 enforces the importance of western North America, specifically the Missouri River, in regards to sand flux to the Mississippi. Despite the fact the source rock containing younger ages zircon only represent a small area within the Mississippi and associated drainages, young mountain building followed by later glaciation events have created a sediment rich, unconsolidated source accessed by the modern rivers in western North America. When compared to other zircon studies, instability in sediment flux is seen throughout the river which is interpreted here as anthropogenic influence to the system.

Using apatite REE and trace element data as a provenance indicator demonstrated the limitations of traditional methods for interpreting large-scale detrital populations. This study found element ternary plots a useful tool for categorizing geochemical data of single grain populations. The benefits of using categorical data are important for the application of statistical unmixing models for provenance interpretations. Overall, regional sediment contributions compared favorably with zircon from the same sample, which reinforces the use of this mineral as a provenance tool. This method could be further improved through a more rigorous categorization process using hierarchical clustering and additional analysis with the microprobe to classify grains by OH, Cl, and F.

Finally, the Nd and Sr isotopes used to interpret provenance in the Mississippi delta over the last 3 ky show similar findings to both zircon and apatite. Results display that older εNd signatures of Grenville origin largely control the signature of the Mississippi River. Within the core, delta deposits have more positive εNd values at the base that generally trend towards more

negative in the most recent sediment. The most extensive shift is seen within the last ~100 years which coincides with large-scale engineering projects along the Mississippi and within the delta. This shows that, within the delta, modern anthropogenic affects have had a significant effect on sedimentation within the delta.

When viewed holistically these studies highlight the importance of human controls on the modern Mississippi River, and suggest that these recent alterations have fundamentally changed the way in which sediment is transported from source to sink. Fluvial system are complicated by nature, making provenance interpretation difficult even without accounting for modern alteration of the drainage. Traditional geologic practices of using modern rivers as analogues for their ancestral fluvial complexes must therefore carefully consider alteration to the catchment before direct comparison can be made. Unfortunately, the way in which rivers around the world have been altered in the last 100 years has affects that are far more serious than just geological interpretation of the past. These changes are currently endangering coastal and wetland environments which sustain a variety of wildlife and local communities. Studies involving the changes in these fluvial systems are direly important for the future of coastal sustainability and preservation as a whole.

APPENDIX A. SUPPLEMENTARY DATA FOR CHAPTER 2

Table A.1 Supplementary of Zircon ICPMS Results

$^{207}Pb/^{206}Pb$	2σ	$^{207}Pb/^{235}U$	2σ	$^{206}Pb/^{238}U$	2σ	Age (Ma) $^{207}Pb/^{206}Pb$	2σ	Age (Ma) $^{207}Pb/^{235}U$	2σ	Age (Ma) $^{206}Pb/^{238}U$	2σ	Con%	Best Age
Miss S. of Red lat 37.12 lon -91.66													
0.0579	0.003	0.0278	0.0016	0.00497	0.00018	460	100	27.8	1.6	31.9	1.1	85.3	31.9
0.0578	0.0081	0.039	0.019	0.00587	0.00086	350	240	32	30	37.7	5.4	82.2	37.7
0.0691	0.0048	0.0351	0.0027	0.00381	0.00016	780	130	35	2.6	24.5	1	70.0	24.5
0.0561	0.0048	0.0397	0.004	0.00501	0.00027	350	170	39.4	3.9	32.2	1.8	81.7	32.2
0.0616	0.0059	0.0424	0.0047	0.00489	0.00031	490	170	41.9	4.5	31.4	2	74.9	31.4
0.0488	0.0038	0.0549	0.0046	0.0081	0.00034	120	140	54.1	4.4	52	2.2	96.1	52
0.0586	0.0036	0.0628	0.0049	0.00771	0.00043	470	130	61.6	4.6	49.5	2.8	80.4	49.5
0.0679	0.0059	0.0655	0.0075	0.00706	0.00067	710	140	63.9	6.8	45.3	4.2	70.9	45.3
0.0483	0.0016	0.0747	0.0035	0.01152	0.00081	117	67	73	3.3	73.8	5.1	98.9	73
0.0516	0.0022	0.0747	0.0043	0.01072	0.00065	238	82	73	4	68.7	4.1	94.1	73
0.052	0.0028	0.0814	0.0047	0.01139	0.00042	240	100	79.3	4.4	73	2.7	92.1	73
0.0655	0.0036	0.0872	0.0085	0.00945	0.00063	710	110	84.2	7.6	60.6	4	72.0	60.6
0.053	0.0042	0.0902	0.0082	0.0122	0.00064	250	150	87.1	7.5	78.1	4.1	89.7	78.1
0.057	0.014	0.103	0.026	0.0125	0.001	310	490	89	33	80.2	6.4	90.1	80.2
0.0575	0.0031	0.095	0.0065	0.01221	0.00058	450	100	91.8	5.9	78.2	3.7	85.2	78.2
0.063	0.0038	0.1054	0.0081	0.01197	0.00068	620	110	101.2	7.2	76.7	4.3	75.8	76.7
0.0536	0.0022	0.1096	0.0055	0.01537	0.00056	320	77	105.3	4.9	98.3	3.6	93.4	98.3
0.0549	0.0049	0.114	0.016	0.0147	0.0011	290	140	107	13	93.9	7	87.8	93.9
0.0502	0.0017	0.1176	0.0071	0.017	0.0016	196	68	112.5	6.2	108.7	9.7	96.6	112.5
0.075	0.0091	0.137	0.022	0.01242	0.00056	850	150	127	17	79.5	3.6	62.6	79.5
0.0525	0.0016	0.1338	0.0055	0.01808	0.0007	284	64	127.3	4.9	115.5	4.4	90.7	115.5
0.0803	0.0098	0.146	0.032	0.01251	0.00087	970	160	132	21	80.1	5.5	60.7	80.1

$^{207}Pb/^{206}Pb$	2σ	$^{207}Pb/^{235}U$	2σ	$^{206}Pb/^{238}U$	2σ	Age (Ma) $^{207}Pb/^{206}Pb$	2σ	Age (Ma) $^{207}Pb/^{235}U$	2σ	Age (Ma) $^{206}Pb/^{238}U$	2σ	Con%	Best Age
0.0519	0.0021	0.1875	0.0093	0.0264	0.001	260	85	173.8	7.9	167.7	6.6	96.5	167.7
0.05	0.0015	0.1891	0.0071	0.0282	0.0011	185	63	175.5	6.1	179.5	7	97.7	175.5
0.0515	0.0016	0.2089	0.0086	0.0302	0.0019	246	66	192.1	7.1	192	11	100.0	192.1
0.0593	0.0034	0.22	0.016	0.02673	0.00086	500	100	200	13	170	5.4	85.0	170
0.054	0.0016	0.2228	0.0093	0.0292	0.0011	350	63	203.6	7.6	185.5	6.7	91.1	185.5
0.0529	0.0045	0.252	0.022	0.0342	0.0017	250	160	225	18	217	10	96.4	217
0.0668	0.005	0.5	0.21	0.048	0.014	700	140	342	59	289	69	84.5	289
0.0557	0.0012	0.559	0.021	0.0745	0.0031	424	48	449	14	463	18	96.9	449
0.0713	0.0014	0.696	0.022	0.2111	0.0075	956	39	534	13	1232	39	71.1	534
0.0627	0.0017	1.002	0.043	0.1174	0.0054	676	55	700	21	714	31	98.00	700
0.0665	0.0074	1.09	0.16	0.123	0.014	710	88	712	46	735	75	96.77	712
0.0647	0.0014	1.103	0.041	0.1281	0.0051	751	46	751	19	775	29	96.80	751
0.0975	0.0036	1.67	0.32	0.125	0.031	1534	77	870	100	720	130	82.76	870
0.0866	0.0017	1.546	0.085	0.1475	0.0088	1341	38	934	38	883	50	94.54	934
0.0841	0.003	1.65	0.087	0.1434	0.0084	1259	68	976	33	859	47	88.01	976
0.0748	0.0021	1.716	0.075	0.1662	0.0083	1041	54	1005	28	987	46	98.21	987
0.0737	0.0017	1.762	0.057	0.1783	0.0069	1016	48	1027	21	1055	37	96.16	1055
0.0741	0.0017	1.81	0.14	0.178	0.016	1028	46	1027	40	1042	78	98.64	1027
0.0729	0.002	1.831	0.08	0.1854	0.0079	989	57	1048	28	1094	42	89.4	1094
0.0786	0.0027	1.85	0.1	0.171	0.011	1131	63	1050	35	1012	59	89.5	1012
0.0745	0.0021	1.833	0.071	0.1834	0.0079	1029	60	1051	25	1083	42	94.8	1083
0.0754	0.0016	1.845	0.062	0.1833	0.0067	1068	42	1056	22	1083	36	98.6	1083
0.0748	0.0021	1.856	0.08	0.1818	0.0077	1041	57	1057	28	1074	42	96.8	1074
0.0868	0.0026	2.13	0.58	0.176	0.034	1329	64	1065	61	1000	140	75.2	1329
0.0775	0.002	1.908	0.096	0.1849	0.0094	1116	52	1071	35	1089	51	97.6	1089
0.0757	0.0013	1.916	0.066	0.1868	0.0073	1079	35	1081	23	1101	39	97.96	1079
0.0765	0.0021	1.927	0.074	0.178	0.0064	1088	50	1084	25	1054	35	96.88	1054

$^{207}Pb/^{206}Pb$	2σ	$^{207}Pb/^{235}U$	2σ	$^{206}Pb/^{238}U$	2σ	Age (Ma) $^{207}Pb/^{206}Pb$	2σ	Age (Ma) $^{207}Pb/^{235}U$	2σ	Age (Ma) $^{206}Pb/^{238}U$	2σ	Con%	Best Age
0.0778	0.0024	1.99	0.13	0.187	0.016	1115	61	1094	38	1093	77	98.03	1115
0.0778	0.0025	2.01	0.13	0.191	0.018	1112	63	1099	39	1112	87	100.00	1112
0.098	0.0019	1.982	0.095	0.335	0.025	1576	38	1100	27	1840	100	83.3	1576
0.0772	0.0017	1.989	0.073	0.1847	0.008	1114	42	1105	25	1089	43	97.76	1114
0.0769	0.0024	2.016	0.073	0.1958	0.0078	1089	64	1115	25	1150	42	94.4	1150
0.0787	0.0017	2.033	0.064	0.1868	0.0073	1152	43	1122	21	1101	39	95.57	1101
0.0793	0.0019	2.057	0.071	0.1938	0.0086	1164	44	1129	23	1138	46	97.8	1164
0.0793	0.0027	2.08	0.1	0.188	0.011	1150	64	1131	33	1104	57	96.00	1104
0.0814	0.003	2.078	0.086	0.1907	0.0071	1191	76	1132	30	1123	38	94.29	1123
0.0806	0.0031	2.12	0.13	0.191	0.012	1171	71	1139	39	1120	62	95.64	1120
0.0797	0.0022	2.109	0.077	0.1961	0.0078	1168	52	1145	25	1151	42	98.54	1151
0.09	0.0045	2.35	0.16	0.1924	0.0085	1364	90	1206	43	1131	45	82.9	1131
0.0812	0.0019	2.37	0.14	0.214	0.015	1210	47	1219	35	1237	76	97.77	1210
0.0842	0.0022	2.56	0.23	0.227	0.029	1276	52	1258	47	1290	120	98.90	1276
0.0844	0.0017	2.589	0.092	0.2282	0.0091	1289	41	1290	25	1321	48	97.52	1289
0.0841	0.0015	2.616	0.084	0.2303	0.0089	1286	36	1299	23	1332	46	96.42	1286
0.0979	0.003	2.69	0.13	0.1955	0.0095	1559	58	1311	35	1146	51	73.51	1146
0.0885	0.0023	2.88	0.11	0.244	0.01	1376	48	1367	28	1402	53	98.1	1376
0.0886	0.0019	2.873	0.098	0.2416	0.0099	1383	40	1368	26	1391	51	99.4	1383
0.0878	0.0022	3	0.25	0.25	0.026	1359	49	1377	45	1410	110	96.3	1359
0.0886	0.0014	2.91	0.087	0.2332	0.008	1387	32	1379	21	1348	41	97.19	1387
0.0934	0.0023	2.96	0.11	0.2344	0.0089	1480	44	1390	27	1354	45	91.49	1480
0.089	0.0026	3.08	0.12	0.247	0.011	1384	55	1418	30	1419	55	97.5	1384
0.0929	0.0036	3.28	0.19	0.251	0.013	1448	70	1455	43	1437	67	99.24	1437
0.0965	0.0024	3.28	0.18	0.249	0.02	1540	48	1455	41	1415	93	91.88	1540
0.0921	0.0023	3.23	0.11	0.251	0.011	1452	47	1456	26	1439	54	99.10	1452
0.0925	0.0024	3.36	0.14	0.26	0.014	1460	47	1482	35	1480	69	98.6	1460

$^{207}Pb/^{206}Pb$	2σ	$^{207}Pb/^{235}U$	2σ	$^{206}Pb/^{238}U$	2σ	Age (Ma) $^{207}Pb/^{206}Pb$	2σ	Age (Ma) $^{207}Pb/^{235}U$	2σ	Age (Ma) $^{206}Pb/^{238}U$	2σ	Con%	Best Age
0.0976	0.0046	3.47	0.21	0.257	0.0082	1541	66	1502	37	1471	42	95.46	1471
0.0915	0.003	4.7	1	0.355	0.071	1426	55	1560	100	1800	240	73.8	1426
0.1071	0.0017	4.01	0.17	0.279	0.013	1745	29	1622	36	1578	65	90.43	1745
0.1026	0.0024	4.14	0.25	0.295	0.025	1657	43	1639	43	1640	110	98.97	1657
0.1035	0.0019	4.1	0.18	0.284	0.014	1679	34	1641	35	1601	70	95.35	1679
0.1061	0.0025	4.41	0.56	0.305	0.043	1719	42	1656	60	1660	160	96.57	1719
0.1046	0.0025	4.4	0.33	0.309	0.028	1688	53	1681	48	1700	120	99.3	1688
0.1028	0.0019	4.38	0.16	0.317	0.014	1667	34	1700	29	1768	67	93.9	1667
0.1047	0.002	4.39	0.15	0.298	0.012	1700	36	1702	28	1676	57	98.6	1700
0.1074	0.0018	4.46	0.14	0.299	0.011	1749	30	1717	25	1681	55	96.1	1749
0.1049	0.0025	4.67	0.39	0.333	0.043	1694	48	1725	50	1800	160	93.7	1694
0.1057	0.0026	4.78	0.25	0.323	0.019	1711	46	1761	43	1789	90	95.4	1711
0.1071	0.0022	4.79	0.22	0.321	0.022	1739	41	1769	34	1777	95	97.8	1739
0.1151	0.0029	5.13	0.17	0.332	0.013	1867	45	1833	28	1842	62	98.66	1867
0.1118	0.0017	5.39	0.18	0.342	0.015	1823	28	1875	27	1886	66	96.5	1823
0.118	0.002	5.52	0.18	0.35	0.014	1919	31	1895	28	1929	65	99.5	1919
0.116	0.0019	5.52	0.17	0.352	0.014	1888	30	1896	26	1935	66	97.5	1888
0.1703	0.0054	9.37	0.49	0.413	0.021	2539	52	2352	47	2214	92	87.20	2539
0.1884	0.0047	9.72	0.59	0.386	0.041	2712	47	2382	45	2050	150	75.59	2712
0.1602	0.0024	10.24	0.29	0.464	0.015	2453	25	2450	25	2451	68	99.92	2453
0.1804	0.0035	12.28	0.45	0.509	0.021	2648	33	2613	33	2638	88	99.62	2648
0.1849	0.0041	13.11	0.46	0.518	0.02	2687	36	2676	33	2677	86	99.63	2687
0.1893	0.0035	13.63	0.5	0.525	0.023	2729	31	2711	34	2702	98	99.01	2729
0.1866	0.005	14.15	0.59	0.539	0.024	2699	42	2743	39	2763	99	97.63	2699
Red lat 31.21 lon -92.09													
0.0517	0.0039	0.0746	0.0063	0.01036	0.0003	210	120	72.7	5.8	66.4	1.9	91.33	66.4

$^{207}Pb/^{206}Pb$	2σ	$^{207}Pb/^{235}U$	2σ	$^{206}Pb/^{238}U$	2σ	Age (Ma) $^{207}Pb/^{206}Pb$	2σ	Age (Ma) $^{207}Pb/^{235}U$	2σ	Age (Ma) $^{206}Pb/^{238}U$	2σ	Con%	Best Age
0.0508	0.0015	0.1078	0.0039	0.01534	0.00048	218	60	103.8	3.5	98.1	3	94.51	98.1
0.0712	0.0094	0.113	0.023	0.01107	0.00053	660	220	105	18	70.9	3.4	67.52	70.9
0.0529	0.002	0.1173	0.007	0.01597	0.00065	294	73	112.2	6.1	102.1	4.1	91.00	102.1
0.0517	0.0014	0.1717	0.0077	0.0241	0.0011	256	59	160.4	6.6	153.4	6.9	95.64	160.4
0.053	0.0014	0.1879	0.0056	0.02542	0.00086	317	60	174.7	4.8	161.8	5.4	92.62	174.7
0.0587	0.0039	0.201	0.016	0.02452	0.00064	470	110	184	12	156.1	4	84.84	156.1
0.0527	0.0035	0.213	0.018	0.02891	0.00089	257	89	194	13	183.7	5.6	94.69	183.7
0.0529	0.0031	0.229	0.019	0.03088	0.00091	270	93	207	14	196	5.7	94.69	196
0.0523	0.0016	0.2388	0.008	0.033	0.0012	283	64	217.2	6.5	209.4	7.5	96.41	217.2
0.0682	0.0047	0.291	0.022	0.03054	0.00082	760	120	256	17	193.9	5.1	75.74	193.9
0.0526	0.0017	0.292	0.011	0.03998	0.00083	287	67	259.6	8.5	252.7	5.1	97.34	252.7
0.0525	0.0013	0.293	0.01	0.0402	0.0011	290	56	260.2	8.1	254	6.9	97.62	254
0.0526	0.0018	0.295	0.011	0.04044	0.00093	285	70	261.4	8.2	255.5	5.8	97.74	255.5
0.0553	0.0032	0.299	0.016	0.0393	0.0011	360	100	264	12	248.4	7.1	94.09	248.4
0.0581	0.0023	0.308	0.016	0.0383	0.0013	490	81	271	12	242.1	8.1	89.34	242.1
0.0623	0.0026	0.484	0.028	0.0557	0.0019	632	84	397	18	349	11	87.91	349
0.0587	0.0017	0.534	0.016	0.0659	0.0019	530	61	433	11	411	12	94.92	433
0.0572	0.0023	0.539	0.022	0.0696	0.0035	470	88	436	14	433	21	99.31	436
0.056	0.0013	0.543	0.018	0.0698	0.002	436	51	439	12	434	12	98.86	434
0.0604	0.0037	0.552	0.038	0.0657	0.0021	544	95	440	22	410	13	93.18	410
0.0575	0.0019	0.553	0.022	0.0694	0.002	480	69	445	14	432	12	97.08	432
0.0578	0.0017	0.56	0.022	0.0704	0.0028	494	61	449	14	438	17	97.55	449
0.0635	0.0018	0.583	0.019	0.0666	0.0022	700	59	465	12	415	14	89.25	465
0.0579	0.0012	0.598	0.017	0.0745	0.002	510	45	475	11	463	12	97.47	475
0.0617	0.0019	0.612	0.023	0.0717	0.0022	636	63	483	14	446	13	92.34	446
0.06	0.0018	0.62	0.026	0.0742	0.0021	578	64	487	16	461	13	94.66	461
0.0596	0.0017	0.626	0.024	0.0757	0.0025	567	60	491	15	470	15	95.72	470

$^{207}Pb/^{206}Pb$	2σ	$^{207}Pb/^{235}U$	2σ	$^{206}Pb/^{238}U$	2σ	Age (Ma) $^{207}Pb/^{206}Pb$	2σ	Age (Ma) $^{207}Pb/^{235}U$	2σ	Age (Ma) $^{206}Pb/^{238}U$	2σ	Con%	Best Age
0.0629	0.0015	0.636	0.019	0.0731	0.0021	686	52	499	12	455	12	91.18	455
0.0595	0.0018	0.685	0.027	0.0839	0.0032	565	65	528	16	519	19	98.30	528
0.0629	0.004	0.743	0.05	0.0856	0.0031	633	88	557	24	529	19	94.97	529
0.0637	0.0058	0.766	0.08	0.0861	0.0022	630	100	565	30	532	13	94.16	532
0.0625	0.0022	0.843	0.032	0.0972	0.0021	654	71	617	17	598	13	96.92	598
0.0656	0.0019	0.861	0.041	0.0946	0.0035	770	57	626	20	582	21	92.97	626
0.063	0.0025	0.901	0.051	0.1037	0.0048	665	79	645	25	635	28	98.45	645
0.0652	0.0011	0.926	0.024	0.1024	0.0026	771	37	664	13	628	15	94.58	664
0.0641	0.0021	1.004	0.05	0.1116	0.004	723	70	702	24	681	23	97.01	681
0.0706	0.0021	1.021	0.054	0.1033	0.0035	920	60	707	26	633	20	89.53	633
0.068	0.0017	1.192	0.042	0.1271	0.0048	848	54	793	19	770	28	97.10	793
0.069	0.0021	1.42	0.11	0.154	0.018	875	67	888	35	912	85	97.30	888
0.0723	0.0016	1.587	0.048	0.1588	0.0052	979	45	961	19	949	29	98.75	961
0.0733	0.0021	1.677	0.054	0.1648	0.0039	1003	53	996	19	983	21	98.69	996
0.0755	0.0034	1.73	0.11	0.1646	0.0085	1048	82	1011	37	980	47	96.93	980
0.0739	0.0022	1.746	0.071	0.1698	0.0049	1011	62	1018	26	1010	27	99.21	1010
0.0739	0.0022	1.754	0.083	0.1711	0.0068	1016	54	1019	28	1016	37	99.71	1016
0.0744	0.0015	1.776	0.063	0.1738	0.0078	1041	39	1031	23	1030	42	98.94	1041
0.0728	0.0014	1.782	0.067	0.1777	0.0081	997	42	1033	22	1051	42	98.26	1051
0.0745	0.0019	1.793	0.06	0.1746	0.0064	1037	49	1038	22	1035	35	99.71	1035
0.0757	0.0019	1.802	0.075	0.1718	0.0068	1070	47	1038	27	1020	37	98.27	1020
0.0735	0.0014	1.792	0.049	0.1765	0.0059	1017	39	1039	18	1046	32	99.33	1046
0.0756	0.0018	1.805	0.065	0.1721	0.0057	1069	48	1041	24	1022	31	98.17	1022
0.0745	0.0017	1.809	0.056	0.1753	0.0052	1040	45	1044	20	1040	28	99.62	1040
0.0728	0.0019	1.812	0.069	0.1794	0.0081	996	54	1046	24	1061	44	98.57	1061
0.075	0.0017	1.826	0.06	0.1756	0.0055	1053	45	1050	21	1042	30	99.24	1042
0.0746	0.0017	1.829	0.056	0.1782	0.0067	1042	46	1051	20	1055	36	99.62	1055

$^{207}Pb/^{206}Pb$	2σ	$^{207}Pb/^{235}U$	2σ	$^{206}Pb/^{238}U$	2σ	Age (Ma) $^{207}Pb/^{206}Pb$	2σ	Age (Ma) $^{207}Pb/^{235}U$	2σ	Age (Ma) $^{206}Pb/^{238}U$	2σ	Con%	Best Age
0.0753	0.0015	1.85	0.061	0.1776	0.0061	1065	39	1059	21	1052	33	99.34	1052
0.0774	0.0036	1.88	0.11	0.1751	0.0062	1072	95	1059	35	1038	34	98.02	1038
0.0758	0.002	1.862	0.058	0.1759	0.0042	1074	51	1064	20	1044	23	98.12	1044
0.0779	0.0023	1.863	0.059	0.1734	0.0053	1123	52	1064	20	1029	29	96.71	1029
0.0777	0.0018	1.894	0.069	0.1759	0.006	1122	48	1072	25	1043	33	97.29	1043
0.0792	0.0014	1.899	0.048	0.1736	0.0054	1168	35	1078	16	1030	29	88.18	1168
0.0821	0.0048	1.99	0.18	0.1729	0.0067	1170	100	1087	45	1026	36	94.39	1026
0.078	0.0024	1.96	0.091	0.1807	0.0065	1121	61	1092	30	1068	35	97.80	1068
0.092	0.023	2.3	0.78	0.1729	0.006	1210	130	1105	66	1026	33	92.85	1026
0.0806	0.004	2.05	0.13	0.1831	0.0067	1149	91	1114	38	1082	36	97.13	1082
0.0769	0.0014	2.016	0.054	0.1916	0.0057	1114	37	1119	18	1129	31	99.11	1129
0.0781	0.0022	2.053	0.083	0.1893	0.0062	1132	50	1126	26	1116	34	99.11	1116
0.0849	0.0039	2.09	0.12	0.1766	0.0056	1262	84	1131	38	1047	31	92.57	1047
0.0844	0.0017	2.081	0.066	0.1779	0.0054	1291	39	1137	22	1054	29	92.70	1054
0.0779	0.0017	2.082	0.063	0.1938	0.0071	1131	44	1138	21	1140	38	99.82	1140
0.0789	0.0017	2.106	0.078	0.1928	0.0074	1157	43	1144	25	1134	39	99.13	1134
0.0801	0.0016	2.125	0.067	0.1913	0.0058	1187	41	1152	22	1126	31	97.74	1126
0.0776	0.0014	2.124	0.057	0.1981	0.0064	1126	38	1153	18	1163	34	99.13	1163
0.0782	0.0016	2.15	0.064	0.1987	0.0064	1141	40	1161	20	1166	34	99.57	1166
0.0826	0.0031	2.18	0.11	0.191	0.0079	1221	74	1162	33	1123	42	96.64	1123
0.0815	0.003	2.166	0.086	0.1914	0.0042	1204	63	1163	25	1128	23	96.99	1128
0.079	0.0016	2.18	0.059	0.1992	0.0054	1159	41	1171	18	1170	29	99.91	1170
0.0791	0.0014	2.199	0.068	0.2008	0.0071	1167	34	1176	22	1177	38	99.14	1167
0.0808	0.0021	2.235	0.08	0.1999	0.0069	1200	48	1186	25	1172	37	98.82	1172
0.0801	0.0021	2.236	0.096	0.1987	0.0099	1190	52	1188	29	1166	53	98.15	1166
0.081	0.0015	2.247	0.063	0.2002	0.006	1212	37	1192	20	1175	32	98.57	1175
0.0806	0.0015	2.261	0.073	0.2037	0.0082	1202	37	1195	22	1192	43	99.75	1202

$^{207}Pb/^{206}Pb$	2σ	$^{207}Pb/^{235}U$	2σ	$^{206}Pb/^{238}U$	2σ	Age (Ma) $^{207}Pb/^{206}Pb$	2σ	Age (Ma) $^{207}Pb/^{235}U$	2σ	Age (Ma) $^{206}Pb/^{238}U$	2σ	Con%	Best Age
0.0811	0.0018	2.285	0.065	0.2038	0.0063	1210	43	1203	20	1194	34	99.25	1194
0.0833	0.0026	2.35	0.11	0.2041	0.0085	1253	57	1218	31	1194	45	98.03	1194
0.0916	0.0016	2.373	0.069	0.1871	0.006	1451	33	1230	20	1104	32	89.76	1104
0.0826	0.0015	2.442	0.062	0.2139	0.0065	1251	35	1251	18	1248	34	99.76	1248
0.0845	0.002	2.46	0.1	0.2101	0.0072	1290	43	1253	27	1227	38	97.92	1227
0.0867	0.0021	2.673	0.094	0.2234	0.0086	1340	46	1314	26	1297	45	98.71	1297
0.0872	0.0021	2.714	0.088	0.226	0.0087	1350	45	1325	25	1310	46	97.04	1350
0.0868	0.0023	2.8	0.12	0.232	0.012	1343	52	1348	31	1342	60	99.93	1343
0.0886	0.0018	2.88	0.1	0.2347	0.009	1384	40	1368	26	1356	46	97.98	1384
0.0895	0.0025	2.96	0.11	0.2388	0.008	1394	55	1389	28	1377	41	99.14	1377
0.0889	0.0018	2.962	0.094	0.2402	0.0072	1391	40	1392	23	1385	37	99.50	1385
0.0899	0.002	2.98	0.1	0.2394	0.0083	1411	42	1395	24	1381	42	99.00	1381
0.0888	0.0015	2.973	0.068	0.2422	0.0066	1390	36	1397	17	1396	34	99.93	1396
0.092	0.0028	3.08	0.12	0.2417	0.0067	1445	53	1420	27	1393	35	98.10	1393
0.0901	0.0014	3.161	0.074	0.2532	0.0065	1422	30	1444	18	1453	33	97.82	1422
0.0956	0.002	3.26	0.1	0.2475	0.0093	1529	38	1465	25	1422	48	93.00	1529
0.1018	0.0034	3.4	0.13	0.2423	0.0086	1630	62	1495	29	1395	44	93.31	1395
0.095	0.0027	3.43	0.14	0.2581	0.0076	1515	48	1505	29	1478	39	98.21	1478
0.101	0.0018	3.51	0.1	0.2503	0.0065	1635	33	1524	22	1438	33	94.36	1438
0.1007	0.0017	3.61	0.12	0.2592	0.0091	1629	32	1545	25	1482	46	90.98	1629
0.1064	0.0019	3.83	0.12	0.2605	0.0098	1732	32	1591	26	1488	50	85.91	1732
0.0993	0.0018	3.88	0.1	0.2822	0.0086	1602	34	1604	21	1599	43	99.81	1602
0.1054	0.0024	3.95	0.17	0.273	0.014	1714	40	1616	33	1550	70	90.43	1714
0.1041	0.0026	3.96	0.13	0.279	0.011	1690	46	1622	27	1584	55	93.73	1690
0.1127	0.003	4.01	0.13	0.255	0.011	1835	47	1632	26	1460	54	79.56	1835
0.1006	0.0021	4.09	0.12	0.2942	0.0093	1625	38	1647	24	1659	46	97.91	1625
0.1019	0.0023	4.16	0.16	0.298	0.012	1652	41	1660	32	1675	61	98.61	1652

$^{207}Pb/^{206}Pb$	2σ	$^{207}Pb/^{235}U$	2σ	$^{206}Pb/^{238}U$	2σ	Age (Ma) $^{207}Pb/^{206}Pb$	2σ	Age (Ma) $^{207}Pb/^{235}U$	2σ	Age (Ma) $^{206}Pb/^{238}U$	2σ	Con%	Best Age
0.107	0.0024	4.53	0.18	0.306	0.012	1738	38	1725	32	1714	60	98.62	1738
0.1105	0.0023	4.73	0.15	0.31	0.011	1797	37	1765	26	1734	52	96.49	1797
0.1213	0.003	5.61	0.24	0.332	0.014	1963	46	1907	37	1840	65	93.73	1963
0.1307	0.0017	6.28	0.15	0.3465	0.0087	2103	23	2011	21	1915	41	91.06	2103
0.17	0.0024	10.96	0.3	0.464	0.013	2553	24	2512	26	2453	58	96.08	2553
Miss. S. of Arkansas lat 35.51 lon-91.16													
0.0573	0.0032	0.0285	0.0018	0.0036	0.00014	440	110	28.5	1.8	23.16	0.92	81.26	23.16
0.0481	0.0014	0.0326	0.0016	0.00489	0.0002	108	58	32.5	1.5	31.5	1.3	96.92	31.5
0.0473	0.0023	0.0341	0.0019	0.0052	0.00016	69	92	34	1.9	33.4	1	98.24	33.4
0.0516	0.0022	0.0348	0.0018	0.00491	0.00022	244	86	34.7	1.7	31.6	1.4	91.07	31.6
0.0599	0.0033	0.0411	0.0025	0.00504	0.00036	530	120	40.8	2.4	32.4	2.3	79.41	32.4
0.0556	0.0045	0.0418	0.0035	0.00546	0.00022	340	150	41.5	3.4	35.1	1.4	84.58	35.1
0.065	0.0055	0.042	0.0036	0.00476	0.00022	630	160	41.6	3.5	30.6	1.4	73.56	30.6
0.0522	0.0023	0.0527	0.0026	0.00733	0.00025	263	87	52.1	2.5	47.1	1.6	90.40	47.1
0.0625	0.0031	0.0529	0.0032	0.00617	0.0003	630	100	52.2	3	39.7	1.9	76.05	39.7
0.0511	0.0017	0.0654	0.0032	0.00923	0.00037	230	71	64.2	3.1	59.2	2.4	92.21	59.2
0.0488	0.0015	0.0663	0.0027	0.00985	0.00036	137	62	65.1	2.5	63.2	2.3	97.08	63.2
0.0485	0.0014	0.0677	0.0049	0.0103	0.001	121	57	66.3	4.4	65.9	6.3	99.40	66.3
0.0496	0.0015	0.0696	0.0027	0.01025	0.00046	170	62	68.2	2.5	65.7	2.9	96.33	68.2
0.0505	0.0028	0.0701	0.0041	0.01013	0.00036	190	110	68.6	3.8	65	2.3	94.75	65
0.0599	0.0029	0.0745	0.004	0.00906	0.00037	540	100	72.8	3.8	58.1	2.4	79.81	58.1
0.0498	0.0018	0.0789	0.0043	0.01142	0.00046	173	75	77	4	73.2	2.9	95.06	73.2
0.0503	0.0019	0.0799	0.0042	0.01153	0.00052	195	75	77.8	3.9	73.9	3.3	94.99	73.9
0.0663	0.0039	0.0807	0.0058	0.00886	0.00048	720	120	78.5	5.4	56.8	3	72.36	56.8
0.0516	0.0021	0.0825	0.0038	0.01158	0.00039	243	83	80.4	3.5	74.2	2.5	92.29	74.2
0.0678	0.0024	0.0836	0.004	0.00902	0.00052	823	73	81.3	3.7	57.8	3.3	71.09	57.8

$^{207}Pb/^{206}Pb$	2σ	$^{207}Pb/^{235}U$	2σ	$^{206}Pb/^{238}U$	2σ	Age (Ma) $^{207}Pb/^{206}Pb$	2σ	Age (Ma) $^{207}Pb/^{235}U$	2σ	Age (Ma) $^{206}Pb/^{238}U$	2σ	Con%	Best Age
0.057	0.0038	0.0867	0.0064	0.01104	0.00047	410	130	84.1	6	70.7	3	84.07	70.7
0.0488	0.0013	0.1059	0.004	0.01573	0.00056	136	57	102.1	3.7	100.6	3.6	98.53	100.6
0.0489	0.0015	0.1078	0.0045	0.01597	0.0006	140	64	103.7	4.1	102.1	3.8	98.46	102.1
0.0522	0.0025	0.1082	0.0065	0.01496	0.00057	262	95	103.9	5.9	95.7	3.6	92.11	95.7
0.0566	0.003	0.1089	0.0071	0.01404	0.00069	410	110	104.5	6.4	89.9	4.4	86.03	89.9
0.0504	0.0019	0.1095	0.0047	0.01599	0.00077	198	77	105.3	4.3	102.2	4.9	97.06	105.3
0.0522	0.0025	0.1126	0.0056	0.01578	0.00065	266	96	108.1	5.1	100.9	4.1	93.34	100.9
0.0516	0.0014	0.1212	0.0077	0.017	0.0012	255	57	115.7	6.5	108.8	7.3	94.04	115.7
0.0595	0.0028	0.1273	0.0069	0.01553	0.00058	529	96	121.2	6.2	99.3	3.7	81.93	99.3
0.0539	0.0014	0.1324	0.0056	0.01789	0.00083	349	58	125.9	5.1	114.2	5.2	90.71	125.9
0.127	0.0091	0.247	0.024	0.01377	0.00066	1940	120	220	19	88.2	4.2	40.09	88.2
0.0541	0.0015	0.373	0.014	0.0501	0.002	356	59	321	11	315	12	98.13	321
0.0599	0.0017	0.485	0.019	0.0592	0.003	576	60	400	12	370	18	92.50	400
0.0579	0.0015	0.531	0.017	0.0667	0.0025	506	56	431	11	416	15	96.52	431
0.0576	0.0015	0.552	0.017	0.0695	0.0021	493	57	445	11	433	13	97.30	445
0.0587	0.0018	0.582	0.019	0.0721	0.0023	526	66	464	12	448	14	96.55	464
0.0601	0.0017	0.583	0.021	0.0707	0.0029	581	61	464	14	440	17	94.83	464
0.0595	0.0014	0.597	0.018	0.0724	0.002	568	51	474	12	451	12	95.15	451
0.0726	0.0028	0.624	0.058	0.0611	0.0048	958	80	479	35	381	29	79.54	381
0.0618	0.0021	0.641	0.029	0.0749	0.0024	631	76	500	17	465	14	93.00	465
0.0599	0.0015	0.732	0.024	0.089	0.0035	579	55	556	14	549	20	98.74	556
0.0981	0.0076	1.33	0.12	0.115	0.012	1470	120	824	56	695	73	84.34	824
0.0729	0.0013	1.662	0.048	0.165	0.0054	1001	38	990	18	983	29	99.29	990
0.0737	0.0016	1.744	0.052	0.172	0.0064	1021	42	1021	20	1021	35	100.00	1021
0.0758	0.002	1.763	0.08	0.1699	0.0087	1070	54	1023	28	1008	47	94.21	1008
0.0748	0.0013	1.785	0.055	0.1727	0.0055	1053	36	1036	18	1025	30	97.34	1025
0.0744	0.0014	1.799	0.064	0.1752	0.0067	1042	37	1039	23	1038	37	99.62	1038

$^{207}Pb/^{206}Pb$	2σ	$^{207}Pb/^{235}U$	2σ	$^{206}Pb/^{238}U$	2σ	Age (Ma) $^{207}Pb/^{206}Pb$	2σ	Age (Ma) $^{207}Pb/^{235}U$	2σ	Age (Ma) $^{206}Pb/^{238}U$	2σ	Con%	Best Age
0.075	0.0012	1.808	0.039	0.1743	0.0044	1062	32	1046	14	1035	24	97.46	1035
0.0752	0.0014	1.861	0.059	0.1792	0.0061	1063	38	1063	20	1061	33	99.81	1061
0.0805	0.0023	1.911	0.089	0.1727	0.0086	1189	54	1075	31	1023	47	86.04	1023
0.0768	0.0023	1.93	0.068	0.1825	0.0064	1095	50	1086	23	1078	35	98.45	1078
0.0892	0.0028	2.022	0.074	0.1651	0.0063	1382	58	1116	25	983	35	71.13	983
0.0782	0.0022	2.038	0.078	0.1892	0.0072	1130	58	1121	26	1115	39	98.67	1115
0.0878	0.0046	2.053	0.097	0.171	0.0059	1311	98	1122	32	1016	32	77.50	1016
0.0843	0.0023	2.058	0.075	0.177	0.006	1280	49	1129	24	1049	33	81.95	1049
0.0793	0.0015	2.073	0.068	0.1893	0.0065	1168	38	1135	22	1116	35	95.55	1116
0.0806	0.0016	2.091	0.079	0.1881	0.0076	1200	39	1138	26	1108	41	92.33	1200
0.0792	0.0019	2.117	0.071	0.1939	0.0068	1161	47	1149	23	1140	37	98.19	1140
0.0843	0.0029	2.146	0.098	0.185	0.0074	1268	65	1154	30	1091	40	86.04	1091
0.0775	0.0017	2.144	0.077	0.2013	0.0086	1120	44	1156	25	1178	46	94.82	1120
0.0783	0.0014	2.153	0.072	0.1989	0.0067	1146	35	1160	23	1167	36	98.17	1146
0.0823	0.0035	2.19	0.12	0.1951	0.0098	1202	85	1165	35	1144	52	95.17	1144
0.0795	0.0019	2.171	0.067	0.1977	0.0056	1167	49	1167	21	1161	30	99.49	1161
0.0818	0.0029	2.213	0.095	0.198	0.0093	1207	69	1175	30	1160	50	96.11	1160
0.0884	0.0033	2.24	0.1	0.1835	0.0064	1354	72	1184	32	1084	34	80.06	1084
0.0798	0.0016	2.235	0.069	0.2033	0.0071	1180	41	1187	22	1190	38	99.15	1190
0.0805	0.0016	2.278	0.076	0.2054	0.0075	1198	39	1200	23	1201	40	99.75	1198
0.0826	0.002	2.306	0.077	0.2026	0.007	1242	49	1208	23	1187	37	95.57	1187
0.0844	0.0018	2.55	0.091	0.2197	0.0096	1290	40	1279	26	1276	50	98.91	1290
0.0849	0.0018	2.578	0.081	0.22	0.007	1300	43	1289	23	1279	37	98.38	1279
0.0934	0.0024	2.69	0.12	0.2091	0.0094	1479	49	1314	32	1220	50	82.49	1479
0.0868	0.002	2.826	0.09	0.2362	0.008	1342	45	1357	24	1364	42	98.36	1364
0.09	0.0024	2.867	0.086	0.2312	0.0071	1408	49	1368	23	1338	37	95.03	1338
0.0886	0.0015	2.887	0.079	0.2357	0.0072	1388	32	1374	20	1362	37	98.13	1338

$^{207}Pb/^{206}Pb$	2σ	$^{207}Pb/^{235}U$	2σ	$^{206}Pb/^{238}U$	2σ	Age (Ma) $^{207}Pb/^{206}Pb$	2σ	Age (Ma) $^{207}Pb/^{235}U$	2σ	Age (Ma) $^{206}Pb/^{238}U$	2σ	Con%	Best Age
0.0899	0.0022	3.1	0.13	0.25	0.011	1406	47	1420	32	1434	56	98.01	1406
0.0916	0.0019	3.123	0.088	0.248	0.0089	1447	40	1433	21	1424	46	98.41	1447
0.0907	0.0018	3.16	0.11	0.253	0.01	1430	38	1439	26	1449	51	98.67	1430
0.0908	0.0017	3.21	0.13	0.258	0.016	1432	37	1450	27	1470	70	97.35	1432
0.0943	0.0016	3.42	0.1	0.2631	0.0095	1506	33	1503	24	1502	48	99.73	1506
0.0996	0.0017	3.565	0.099	0.2587	0.0077	1610	32	1536	22	1481	39	91.99	1610
0.1022	0.0016	3.71	0.1	0.2622	0.0074	1657	29	1568	22	1498	38	90.40	1657
0.1066	0.0022	3.85	0.22	0.264	0.019	1730	41	1583	41	1496	87	86.47	1730
0.1033	0.002	3.93	0.14	0.277	0.012	1675	35	1612	28	1570	59	93.73	1675
0.1008	0.0017	3.93	0.12	0.2824	0.0097	1632	33	1614	25	1599	48	97.98	1632
0.1018	0.0023	3.96	0.14	0.2813	0.0093	1646	40	1617	27	1594	47	96.84	1646
0.1031	0.0019	4.08	0.16	0.287	0.013	1671	34	1639	32	1621	65	97.01	1671
0.1053	0.0019	4.28	0.13	0.294	0.01	1712	34	1682	25	1659	51	96.90	1712
0.1056	0.0023	4.36	0.16	0.3	0.013	1713	39	1694	30	1684	63	98.31	1713
0.1063	0.0019	4.35	0.13	0.298	0.012	1728	34	1697	25	1674	57	96.88	1728
0.1054	0.0019	4.39	0.13	0.3009	0.009	1713	32	1703	24	1692	45	98.77	1713
0.1058	0.0022	4.4	0.16	0.302	0.012	1717	38	1703	30	1695	59	98.72	1717
0.1062	0.002	4.56	0.17	0.313	0.017	1727	35	1732	28	1746	74	98.90	1727
0.1112	0.0023	4.82	0.15	0.3137	0.0095	1809	38	1782	25	1755	46	97.01	1809
0.1109	0.0021	4.95	0.16	0.324	0.012	1804	38	1803	27	1803	59	99.94	1804
0.1389	0.0082	5.63	0.43	0.291	0.013	2142	95	1875	63	1638	65	76.47	1638
0.1265	0.0024	5.65	0.29	0.328	0.026	2041	35	1909	34	1810	100	88.68	2041
0.1456	0.0074	6.11	0.41	0.301	0.011	2243	80	1959	54	1692	54	75.43	1692
0.1494	0.0032	6.47	0.24	0.317	0.016	2329	37	2030	33	1764	75	75.74	2329
0.1782	0.0034	8.16	0.29	0.332	0.013	2628	32	2237	32	1841	64	70.05	2628
0.2063	0.0044	10.2	0.36	0.359	0.014	2867	34	2442	32	1971	67	68.75	2867
0.1776	0.0031	10.34	0.35	0.421	0.014	2624	29	2455	31	2256	65	85.98	2624

$^{207}Pb/^{206}Pb$	2σ	$^{207}Pb/^{235}U$	2σ	$^{206}Pb/^{238}U$	2σ	Age (Ma) $^{207}Pb/^{206}Pb$	2σ	Age (Ma) $^{207}Pb/^{235}U$	2σ	Age (Ma) $^{206}Pb/^{238}U$	2σ	Con%	Best Age
0.1847	0.0034	12.81	0.39	0.503	0.018	2689	31	2657	29	2618	77	97.36	2689
Arkansas lat 33.91 lon -91.25													
0.059	0.0032	0.0346	0.0025	0.00429	0.00025	500	110	34.5	2.4	27.6	1.6	80.00	27.6
0.0577	0.0053	0.0446	0.005	0.00555	0.00029	390	150	44.1	4.7	35.7	1.8	80.95	35.7
0.0551	0.0034	0.0776	0.0062	0.01031	0.00054	350	120	75.5	5.7	66.1	3.5	87.55	66.1
0.0545	0.0093	0.098	0.031	0.01176	0.0008	200	250	88	23	75.3	5.1	85.57	75.3
0.0498	0.0017	0.1129	0.0068	0.017	0.0018	179	68	108.2	5.9	108	11	99.82	108.2
0.0555	0.0076	0.123	0.016	0.0164	0.0012	270	120	116	12	105	7.6	90.52	105
0.0514	0.0023	0.171	0.011	0.0242	0.0012	234	89	159.4	9.4	154.2	7.8	96.74	154.2
0.049	0.002	0.179	0.013	0.0278	0.0021	148	80	166	12	176	13	93.98	166
0.053	0.0021	0.2	0.011	0.0278	0.0018	297	80	184.3	9.2	177	11	96.04	184.3
0.0506	0.0014	0.21	0.016	0.0308	0.0032	214	60	192	12	195	19	98.44	192
0.0549	0.0028	0.241	0.017	0.0331	0.0024	370	100	217	15	209	15	96.31	209
0.052	0.0018	0.248	0.011	0.0351	0.0018	263	74	223.9	8.7	222	11	99.15	223.9
0.0731	0.0049	0.291	0.026	0.0296	0.0036	890	130	255	19	187	21	73.33	255
0.0533	0.0025	0.303	0.02	0.0417	0.0032	304	95	266	15	263	20	98.87	266
0.0545	0.0015	0.437	0.024	0.0589	0.0037	370	58	366	15	368	22	99.45	366
0.072	0.0019	0.455	0.022	0.0466	0.003	964	56	378	15	293	18	77.51	378
0.0618	0.0023	0.498	0.028	0.0587	0.003	630	73	407	18	367	18	90.17	367
0.0603	0.0021	0.528	0.026	0.0645	0.0035	577	75	428	17	402	21	93.93	428
0.0652	0.0033	0.598	0.04	0.0674	0.0037	716	90	469	23	419	22	89.34	419
0.0614	0.002	0.594	0.027	0.0707	0.0034	621	72	470	17	440	21	93.62	470
0.0618	0.0017	0.64	0.045	0.077	0.0084	644	62	495	24	474	46	95.76	495
0.0716	0.0048	0.672	0.046	0.0682	0.0021	870	120	514	26	425	13	82.68	425
0.0615	0.0021	0.67	0.031	0.0794	0.0032	623	75	517	18	492	19	95.16	517
0.067	0.0039	0.871	0.074	0.0938	0.0056	750	110	621	35	576	33	92.75	576

$^{207}Pb/^{206}Pb$	2σ	$^{207}Pb/^{235}U$	2σ	$^{206}Pb/^{238}U$	2σ	Age (Ma) $^{207}Pb/^{206}Pb$	2σ	Age (Ma) $^{207}Pb/^{235}U$	2σ	Age (Ma) $^{206}Pb/^{238}U$	2σ	Con%	Best Age
0.2159	0.0062	0.97	0.17	0.0339	0.0068	2933	46	651	46	212	38	32.57	212
0.0651	0.0018	0.935	0.043	0.1052	0.0056	754	57	665	22	643	33	96.69	665
0.1095	0.0026	0.987	0.052	0.0665	0.0044	1775	44	690	26	414	26	60.00	414
0.0924	0.003	1.28	0.2	0.102	0.014	1443	84	784	57	613	74	78.19	784
0.0823	0.0019	1.59	0.13	0.143	0.014	1238	45	941	46	851	73	90.44	941
0.0773	0.0028	1.793	0.099	0.171	0.01	1091	76	1030	35	1012	54	92.76	1012
0.0761	0.0016	1.822	0.072	0.1743	0.008	1085	41	1046	26	1032	44	95.12	1085
0.0812	0.0024	1.98	0.29	0.18	0.031	1203	55	1055	58	1030	130	85.62	1203
0.0749	0.0016	1.854	0.069	0.1802	0.0071	1052	44	1058	24	1066	38	98.67	1066
0.0758	0.0018	1.896	0.069	0.1831	0.0082	1074	48	1073	25	1080	44	99.44	1080
0.0787	0.0021	1.98	0.22	0.187	0.024	1145	52	1075	47	1080	110	94.32	1145
0.078	0.0024	1.93	0.11	0.18	0.012	1120	61	1075	37	1058	62	94.46	1120
0.0772	0.0022	1.94	0.11	0.181	0.011	1104	56	1079	36	1068	59	96.74	1104
0.0757	0.0019	1.921	0.079	0.1857	0.0091	1071	50	1080	27	1094	49	97.85	1094
0.0765	0.0022	1.928	0.09	0.186	0.011	1087	56	1080	32	1095	61	99.26	1087
0.0761	0.0016	1.942	0.088	0.187	0.01	1086	40	1086	29	1100	54	98.71	1086
0.0767	0.0023	1.939	0.081	0.1848	0.0087	1089	61	1086	28	1089	47	100.00	1089
0.0785	0.0023	1.939	0.076	0.1807	0.0077	1135	59	1088	25	1068	42	94.10	1068
0.0755	0.0016	1.948	0.079	0.1885	0.009	1070	41	1090	26	1109	48	96.36	1070
0.0766	0.0018	1.959	0.08	0.188	0.0096	1093	48	1093	27	1106	52	98.81	1093
0.0775	0.0018	1.959	0.085	0.185	0.011	1119	46	1093	28	1091	55	97.50	1119
0.0785	0.0024	1.969	0.096	0.1833	0.0097	1133	61	1094	32	1081	52	95.41	1081
0.0775	0.0022	1.979	0.093	0.1866	0.0094	1111	56	1097	32	1098	51	98.83	1098
0.0786	0.0023	1.994	0.091	0.1867	0.0097	1137	58	1104	30	1099	52	96.66	1099
0.0791	0.0023	2.07	0.13	0.189	0.013	1148	58	1117	41	1109	68	96.60	1148
0.0819	0.0021	2.047	0.093	0.1821	0.009	1224	50	1121	30	1074	48	87.75	1074
0.0907	0.0059	2.12	0.19	0.1676	0.0095	1360	95	1123	52	994	52	73.09	994

$^{207}Pb/^{206}Pb$	2σ	$^{207}Pb/^{235}U$	2σ	$^{206}Pb/^{238}U$	2σ	Age (Ma) $^{207}Pb/^{206}Pb$	2σ	Age (Ma) $^{207}Pb/^{235}U$	2σ	Age (Ma) $^{206}Pb/^{238}U$	2σ	Con%	Best Age
0.0794	0.0023	2.12	0.1	0.196	0.011	1158	57	1144	33	1146	58	98.96	1146
0.0785	0.0025	2.18	0.15	0.206	0.021	1128	68	1151	44	1190	97	94.50	1128
0.0837	0.0034	2.19	0.13	0.193	0.014	1239	76	1159	39	1125	71	90.80	1125
0.0802	0.0018	2.284	0.083	0.209	0.01	1184	50	1200	25	1218	52	97.13	1184
0.0815	0.0017	2.302	0.084	0.2063	0.0095	1220	46	1205	26	1205	50	98.77	1220
0.0922	0.003	2.46	0.15	0.201	0.023	1438	73	1239	43	1160	100	80.67	1438
0.0868	0.0022	2.476	0.092	0.211	0.011	1337	51	1257	27	1226	56	91.70	1337
0.0847	0.0028	2.52	0.12	0.218	0.011	1281	62	1266	33	1264	59	98.67	1264
0.0901	0.0029	2.6	0.13	0.21	0.012	1400	61	1284	36	1219	64	87.07	1400
0.09	0.0021	2.75	0.12	0.224	0.013	1413	43	1331	31	1296	66	91.72	1413
0.0877	0.0021	2.84	0.12	0.235	0.011	1361	45	1355	30	1357	55	99.71	1361
0.0895	0.0025	2.91	0.13	0.239	0.012	1395	52	1373	34	1373	64	98.42	1395
0.0907	0.0023	3.2	0.49	0.263	0.044	1422	50	1387	64	1440	170	98.73	1422
0.0926	0.0022	3.07	0.18	0.241	0.019	1462	48	1403	42	1376	87	94.12	1462
0.0924	0.0024	3.05	0.14	0.242	0.014	1458	49	1407	36	1387	69	95.13	1458
0.0901	0.0021	3.04	0.11	0.248	0.013	1413	44	1410	27	1421	66	99.43	1413
0.0901	0.0026	3.08	0.16	0.249	0.015	1404	55	1411	38	1423	77	98.65	1404
0.0923	0.0025	3.1	0.13	0.247	0.013	1455	51	1421	32	1413	66	97.11	1455
0.0904	0.002	3.11	0.12	0.25	0.01	1420	43	1425	31	1432	52	99.15	1420
0.0896	0.0023	3.35	0.44	0.288	0.053	1397	52	1429	63	1550	190	89.05	1397
0.0909	0.0023	3.28	0.41	0.261	0.027	1427	48	1433	51	1470	110	96.99	1427
0.1076	0.0025	3.17	0.12	0.215	0.01	1746	42	1440	30	1251	54	71.65	1746
0.0935	0.0021	3.27	0.13	0.255	0.012	1484	42	1463	30	1460	60	98.38	1484
0.091	0.0027	3.46	0.39	0.276	0.029	1422	55	1468	57	1540	120	91.70	1422
0.0954	0.0025	3.47	0.17	0.267	0.015	1518	48	1503	40	1515	77	99.80	1518
0.1104	0.0029	3.49	0.17	0.23	0.013	1789	47	1510	36	1328	67	74.23	1789
0.0984	0.0022	3.78	0.15	0.281	0.014	1582	42	1578	32	1590	67	99.49	1582

$^{207}Pb/^{206}Pb$	2σ	$^{207}Pb/^{235}U$	2σ	$^{206}Pb/^{238}U$	2σ	Age (Ma) $^{207}Pb/^{206}Pb$	2σ	Age (Ma) $^{207}Pb/^{235}U$	2σ	Age (Ma) $^{206}Pb/^{238}U$	2σ	Con%	Best Age
0.0986	0.0028	3.98	0.39	0.3	0.034	1574	54	1585	54	1650	140	95.17	1574
0.1016	0.0026	4.1	0.28	0.301	0.033	1636	49	1626	46	1660	130	98.53	1636
0.1008	0.0028	4.08	0.2	0.295	0.015	1618	53	1634	39	1657	72	97.59	1618
0.1026	0.0027	4.16	0.18	0.297	0.015	1655	48	1652	35	1665	73	99.40	1655
0.101	0.0024	4.42	0.59	0.328	0.053	1627	45	1655	61	1750	180	92.44	1627
0.1032	0.0027	4.25	0.2	0.299	0.018	1666	47	1666	38	1673	85	99.58	1666
0.1015	0.003	4.37	0.34	0.33	0.04	1627	57	1669	54	1780	160	90.60	1627
0.1036	0.0029	4.27	0.19	0.303	0.016	1671	51	1674	36	1697	78	98.44	1671
0.1046	0.0029	4.3	0.2	0.299	0.016	1687	50	1678	37	1674	79	99.23	1687
0.1064	0.0031	4.31	0.19	0.296	0.015	1719	52	1681	37	1663	74	96.74	1719
0.1038	0.0024	4.33	0.18	0.305	0.015	1681	42	1686	35	1708	74	98.39	1681
0.1032	0.0024	4.33	0.18	0.308	0.017	1669	42	1686	34	1722	81	96.82	1669
0.1052	0.0029	4.33	0.18	0.302	0.016	1699	50	1686	34	1691	77	99.53	1699
0.1056	0.0021	4.33	0.18	0.301	0.016	1715	37	1687	33	1685	76	98.25	1715
0.105	0.0031	4.39	0.25	0.306	0.021	1688	61	1687	43	1700	100	99.29	1685
0.1052	0.0026	4.41	0.2	0.304	0.017	1700	46	1699	36	1698	79	99.88	1700
0.1029	0.0019	4.43	0.16	0.315	0.014	1668	34	1709	29	1755	68	94.78	1668
0.106	0.0028	4.51	0.26	0.312	0.02	1714	48	1709	45	1733	94	98.89	1714
0.1044	0.003	4.61	0.27	0.325	0.028	1682	52	1728	42	1790	120	93.58	1682
Miss. S. of Ohio lat 36.95 lon -89.11													
0.0496	0.0026	0.0319	0.0018	0.00474	0.00021	160	100	31.9	1.8	30.5	1.3	95.61	30.5
0.0489	0.0039	0.0326	0.0036	0.0045	0.00036	100	120	32.4	3.4	28.9	2.3	89.20	28.9
0.0554	0.0039	0.0353	0.0028	0.00446	0.00019	350	130	35.1	2.7	28.7	1.2	81.77	28.7
0.0575	0.004	0.0361	0.0029	0.00451	0.00019	420	130	35.9	2.8	29	1.2	80.78	29
0.0597	0.0082	0.0397	0.0066	0.00462	0.00022	380	190	39.1	6.1	29.7	1.4	75.96	29.7
0.0543	0.0026	0.0406	0.0027	0.00549	0.00034	341	98	40.4	2.6	35.3	2.2	87.38	35.3

$^{207}Pb/^{206}Pb$	2σ	$^{207}Pb/^{235}U$	2σ	$^{206}Pb/^{238}U$	2σ	Age (Ma) $^{207}Pb/^{206}Pb$	2σ	Age (Ma) $^{207}Pb/^{235}U$	2σ	Age (Ma) $^{206}Pb/^{238}U$	2σ	Con%	Best Age
0.0515	0.0018	0.0434	0.0031	0.00613	0.00065	244	72	43	3	39.4	4.1	91.63	43
0.0567	0.0025	0.0454	0.0022	0.00599	0.00029	429	93	45	2.1	38.5	1.8	85.56	38.5
0.122	0.011	0.0468	0.0047	0.00278	0.00023	1780	170	46.2	4.5	17.9	1.5	38.74	17.9
0.0567	0.0037	0.0496	0.0046	0.00645	0.00034	400	120	48.9	4.3	41.4	2.2	84.66	41.4
0.0479	0.0013	0.0609	0.0024	0.00922	0.00037	100	56	60	2.3	59.1	2.3	98.50	59.1
0.0495	0.003	0.0636	0.0051	0.00953	0.00085	140	110	62.3	4.8	61.1	5.4	98.07	62.3
0.0516	0.0023	0.0666	0.0039	0.00953	0.00039	242	88	65.3	3.6	61.1	2.5	93.57	61.1
0.0515	0.0024	0.0682	0.0041	0.00968	0.00057	234	91	66.8	3.8	62.1	3.6	92.96	62.1
0.0634	0.0037	0.0689	0.0057	0.00757	0.00034	640	120	67.3	5.3	48.6	2.2	72.21	48.6
0.0638	0.0069	0.0705	0.0087	0.00804	0.00035	530	190	68.4	8	51.6	2.2	75.44	51.6
0.0491	0.0013	0.0723	0.0026	0.01041	0.00042	146	54	70.8	2.4	66.8	2.7	94.35	70.8
0.0524	0.0017	0.0759	0.0029	0.01051	0.00029	281	69	74.2	2.7	67.4	1.9	90.84	67.4
0.0535	0.0042	0.0778	0.0072	0.01049	0.00067	270	150	75.5	6.6	67.2	4.3	89.01	67.2
0.0481	0.0039	0.0806	0.0093	0.01185	0.00071	70	140	77.8	8.9	75.9	4.5	97.56	75.9
0.0483	0.0016	0.0871	0.0035	0.01283	0.00057	111	64	84.7	3.3	82.2	3.6	97.05	84.7
0.0576	0.0024	0.0901	0.0051	0.01162	0.00059	464	85	87.4	4.7	74.5	3.8	85.24	74.5
0.0517	0.0021	0.0932	0.0044	0.01326	0.00051	245	82	90.3	4.1	84.9	3.2	94.02	84.9
0.059	0.0026	0.0941	0.005	0.01153	0.00042	518	93	91	4.6	73.9	2.7	81.21	73.9
0.0503	0.0014	0.1006	0.0042	0.01396	0.00049	198	59	97.1	3.9	89.3	3.1	91.97	89.3
0.055	0.0033	0.1014	0.0071	0.01367	0.00061	350	110	97.6	6.4	87.5	3.9	89.65	87.5
0.0536	0.0025	0.1018	0.0064	0.0137	0.00057	315	96	98.1	5.9	87.7	3.6	89.40	87.7
0.0539	0.0018	0.103	0.0053	0.01399	0.00071	340	72	99.2	4.9	89.5	4.5	90.22	89.5
0.0498	0.0016	0.1034	0.0048	0.01472	0.00064	175	66	99.7	4.4	94.2	4.1	94.48	94.2
0.0621	0.0027	0.1036	0.006	0.01188	0.00053	628	94	99.8	5.5	76.1	3.4	76.25	76.1
0.0473	0.0019	0.1047	0.0058	0.01597	0.00094	71	77	100.8	5.3	102.1	6	98.71	100.8
0.0492	0.0015	0.1047	0.0043	0.01554	0.00057	153	62	100.9	3.9	99.4	3.6	98.51	99.4
0.0486	0.0012	0.1054	0.0041	0.01584	0.00064	123	52	101.6	3.8	101.3	4.1	99.70	101.6

$^{207}Pb/^{206}Pb$	2σ	$^{207}Pb/^{235}U$	2σ	$^{206}Pb/^{238}U$	2σ	Age (Ma) $^{207}Pb/^{206}Pb$	2σ	Age (Ma) $^{207}Pb/^{235}U$	2σ	Age (Ma) $^{206}Pb/^{238}U$	2σ	Con%	Best Age
0.0503	0.0015	0.1056	0.0046	0.01505	0.00067	199	63	101.8	4.2	96.2	4.2	94.50	96.2
0.0555	0.0032	0.125	0.021	0.0149	0.0014	370	110	117	15	95.2	8.5	81.37	95.2
0.0484	0.0012	0.1278	0.0057	0.01866	0.0009	121	53	121.8	5.1	119.1	5.7	97.78	121.8
0.0594	0.0019	0.144	0.0089	0.01745	0.00099	552	69	135.9	7.7	111.4	6.2	81.97	111.4
0.0489	0.0026	0.179	0.017	0.0274	0.0031	125	89	165	14	174	19	94.55	165
0.05022	0.0009	0.1802	0.0055	0.02554	0.00096	198	41	168	4.7	162.5	6	96.73	168
0.0506	0.0014	0.1808	0.0076	0.0251	0.001	214	58	168.3	6.5	159.6	6.4	94.83	159.6
0.0493	0.0013	0.1828	0.0082	0.0263	0.0012	158	55	169.9	6.9	167	7.4	98.29	169.9
0.0507	0.0014	0.1865	0.0067	0.0271	0.0011	214	58	173.3	5.7	172.2	7.1	99.37	173.3
0.053	0.002	0.194	0.011	0.0271	0.0012	304	77	179.4	8.9	172.2	7.5	95.99	172.2
0.06	0.0021	0.2139	0.0098	0.0263	0.0011	566	74	196.1	8.1	167.2	6.6	85.26	167.2
0.0528	0.0031	0.22	0.016	0.0301	0.0013	271	95	200	12	190.8	7.9	95.40	190.8
0.0477	0.0014	0.222	0.014	0.0321	0.0031	88	59	203	10	203	19	100.00	203
0.0609	0.0027	0.232	0.012	0.0275	0.0014	580	91	211	10	174.7	8.6	82.80	174.7
0.0519	0.0014	0.262	0.01	0.0369	0.0015	268	59	235.5	8.3	233.1	9.4	98.98	235.5
0.0705	0.0051	0.294	0.025	0.02908	0.00097	820	120	258	18	184.7	6.1	71.59	184.7
0.0533	0.0013	0.395	0.025	0.0549	0.0043	325	49	334	16	344	25	97.01	334
0.0569	0.0018	0.555	0.021	0.0718	0.0031	463	69	446	14	447	18	99.78	446
0.0766	0.0044	0.969	0.07	0.0842	0.0074	1020	110	674	34	518	40	76.85	674
0.0919	0.002	1.406	0.042	0.1088	0.0039	1452	41	888	18	665	23	74.89	888
0.0703	0.0022	1.61	0.1	0.155	0.01	908	63	961	32	925	53	96.25	961
0.0749	0.0027	1.84	0.097	0.1775	0.0084	1032	68	1047	34	1050	46	98.26	1050
0.0732	0.0018	1.864	0.078	0.178	0.011	1001	49	1061	25	1050	55	95.10	1001
0.0708	0.0016	1.896	0.082	0.1738	0.009	933	48	1071	26	1029	46	89.71	1029
0.0773	0.0074	1.97	0.22	0.18	0.015	1037	84	1072	44	1056	73	98.17	1056
0.0785	0.0017	1.927	0.091	0.179	0.012	1145	44	1081	28	1057	60	92.31	1145
0.0772	0.0022	1.99	0.14	0.184	0.013	1103	56	1095	34	1083	62	98.19	1103

$^{207}Pb/^{206}Pb$	2σ	$^{207}Pb/^{235}U$	2σ	$^{206}Pb/^{238}U$	2σ	Age (Ma) $^{207}Pb/^{206}Pb$	2σ	Age (Ma) $^{207}Pb/^{235}U$	2σ	Age (Ma) $^{206}Pb/^{238}U$	2σ	Con%	Best Age
0.0782	0.0021	2.022	0.092	0.1903	0.0091	1132	54	1113	31	1119	49	98.85	1119
0.076	0.002	2.022	0.068	0.1805	0.0057	1074	55	1117	22	1068	31	99.44	1068
0.0789	0.0022	2.071	0.099	0.1862	0.0083	1148	54	1129	32	1097	45	95.56	1097
0.0758	0.0017	2.24	0.12	0.197	0.019	1073	49	1181	29	1142	83	93.57	1073
0.0811	0.0019	2.361	0.092	0.2163	0.0095	1209	45	1223	28	1258	50	95.95	1209
0.078	0.0016	2.386	0.09	0.211	0.014	1134	44	1231	23	1228	63	91.71	1134
0.0903	0.0015	2.684	0.091	0.2154	0.0082	1425	32	1318	25	1254	43	88.00	1425
0.0863	0.0018	2.81	0.11	0.23	0.01	1332	42	1348	28	1331	53	99.92	1332
0.0857	0.0023	2.82	0.14	0.229	0.014	1311	50	1348	33	1318	66	99.47	1311
0.0866	0.002	2.82	0.14	0.235	0.016	1337	43	1349	32	1349	73	99.10	1337
0.0874	0.0013	2.903	0.081	0.2318	0.007	1290	29	1378	21	1341	36	98.31	1364
0.0845	0.002	2.98	0.17	0.23	0.016	2900	45	1384	38	1326	77	97.21	1290
0.0892	0.002	3	0.15	0.238	0.013	1301	43	1394	35	1369	66	98.21	1394
0.0848	0.0016	3.01	0.13	0.242	0.011	1378	39	1401	28	1389	55	93.24	1301
0.0883	0.0018	3.03	0.12	0.244	0.012	1407	39	1407	30	1402	60	98.26	1378
0.0896	0.0018	3.06	0.11	0.249	0.01	1275	39	1415	27	1429	51	98.44	1407
0.0841	0.0022	3.11	0.22	0.244	0.023	1463	52	1415	37	1390	96	90.98	1275
0.0947	0.0048	3.19	0.24	0.261	0.026	1858	88	1420	55	1470	120	99.52	1463
0.0968	0.0024	3.35	0.14	0.256	0.014	1664	46	1479	34	1462	70	94.51	1547
0.1026	0.0019	3.37	0.14	0.231	0.012	1708	34	1487	32	1335	60	80.23	1664
0.1055	0.0024	3.42	0.15	0.235	0.014	1588	43	1496	33	1351	69	79.10	1708
0.0993	0.0031	3.54	0.18	0.257	0.015	1614	53	1521	35	1465	67	92.25	1588
0.1	0.002	3.57	0.11	0.2524	0.0084	1483	37	1537	26	1448	43	89.71	1614
0.0935	0.0021	3.63	0.17	0.271	0.022	1655	46	1544	30	1530	88	96.83	1483
0.1024	0.0023	3.94	0.16	0.274	0.013	1569	42	1610	33	1553	65	93.84	1655
0.0976	0.0018	3.97	0.16	0.278	0.014	1630	35	1619	27	1573	62	99.75	1569
0.1014	0.0027	4.2	0.18	0.292	0.012	1674	50	1660	37	1645	59	99.08	1630

$^{207}Pb/^{206}Pb$	2σ	$^{207}Pb/^{235}U$	2σ	$^{206}Pb/^{238}U$	2σ	Age (Ma) $^{207}Pb/^{206}Pb$	2σ	Age (Ma) $^{207}Pb/^{235}U$	2σ	Age (Ma) $^{206}Pb/^{238}U$	2σ	Con%	Best Age
0.1036	0.0026	4.26	0.15	0.305	0.014	1688	44	1676	29	1711	66	97.79	1674
0.1039	0.0017	4.25	0.11	0.298	0.0093	1702	30	1678	22	1678	46	99.41	1688
0.1049	0.0022	4.34	0.15	0.307	0.013	1683	38	1692	29	1719	64	99.00	1702
0.1037	0.0019	4.42	0.21	0.306	0.02	2140	34	1704	31	1706	85	98.63	1683
0.0987	0.0018	4.46	0.22	0.295	0.015	1702	33	1712	30	1657	64	95.85	1591
0.1046	0.0015	4.426	0.099	0.3078	0.0082	1741	27	1713	18	1727	40	98.53	1702
0.107	0.0019	4.59	0.3	0.315	0.021	1664	32	1728	37	1749	86	99.54	1741
0.1031	0.0026	4.99	0.19	0.313	0.012	2110	47	1807	31	1748	59	94.95	1664
0.1384	0.009	5.32	0.46	0.277	0.012	2521	110	1815	71	1569	62	74.36	1569
0.1671	0.003	9.11	0.53	0.404	0.033	2442	33	2323	46	2160	120	85.68	2521
0.1608	0.0051	9.87	0.44	0.45	0.019	2573	54	2405	40	2385	83	97.67	2442
0.1726	0.0039	11.68	0.44	0.506	0.026	2660	36	2566	34	2620	110	98.17	2573
0.1828	0.0054	12.78	0.65	0.518	0.026	2652	47	2638	48	2670	110	99.62	2660
0.1806	0.0032	12.55	0.34	0.501	0.017	2657	29	2639	25	2610	70	98.42	2652
0.1816	0.0037	13.19	0.93	0.547	0.062	2747	37	2661	46	2730	180	97.25	2657
0.1916	0.0037	13.42	0.46	0.477	0.024	2917	34	2700	28	2497	92	90.90	2747
0.2139	0.0063	15.92	0.96	0.548	0.033		48	2838	55	2790	130	95.65	2917
Upper Miss. lat 39.72 lon -91.35													
0.0505	0.0022	0.0709	0.0043	0.0105	0.0013	197	86	69.3	4	66.9	8	33.96	69.3
0.0502	0.0021	0.089	0.02	0.0118	0.0015	178	77	83	15	75.3	9.2	42.30	75.3
0.0549	0.0042	0.087	0.012	0.01116	0.00088	310	130	83.3	9.9	71.5	5.5	23.06	71.5
0.0513	0.003	0.0919	0.0078	0.0131	0.0012	210	110	88.7	7	83.7	7.6	39.86	88.7
0.0587	0.0037	0.34	0.027	0.0425	0.0033	460	120	292	19	268	20	58.26	292
0.0563	0.0025	0.497	0.03	0.0631	0.0038	418	91	405	20	393	23	94.02	405
0.069	0.02	0.597	0.08	0.0739	0.0057	500	240	431	69	457	34	91.40	457
0.0659	0.0029	0.547	0.043	0.0625	0.0068	757	97	434	28	388	39	51.25	434

$^{207}Pb/^{206}Pb$	2σ	$^{207}Pb/^{235}U$	2σ	$^{206}Pb/^{238}U$	2σ	Age (Ma) $^{207}Pb/^{206}Pb$	2σ	Age (Ma) $^{207}Pb/^{235}U$	2σ	Age (Ma) $^{206}Pb/^{238}U$	2σ	Con%	Best Age
0.0622	0.0033	0.59	0.04	0.0685	0.0044	612	92	464	24	426	26	69.61	464
0.056	0.0017	0.597	0.05	0.077	0.0077	430	67	466	27	474	43	89.77	466
0.0751	0.0073	0.82	0.1	0.0772	0.0031	870	180	580	45	479	18	55.06	479
0.0618	0.0033	0.801	0.059	0.0927	0.0056	601	93	587	29	569	33	94.68	587
0.0706	0.0034	0.91	0.075	0.091	0.0056	880	92	643	33	559	32	63.52	559
0.365	0.016	1.19	0.12	0.025	0.0046	3726	75	767	48	158	27	4.24	767
0.0711	0.0018	1.421	0.087	0.145	0.014	941	53	887	28	862	66	91.60	887
0.0806	0.002	1.503	0.073	0.1355	0.0081	1191	49	921	30	815	46	68.43	921
0.0738	0.0027	1.693	0.08	0.1639	0.0086	998	73	996	29	975	45	97.70	996
0.0739	0.0021	1.702	0.067	0.1639	0.006	1014	56	1002	26	977	33	96.35	977
0.0758	0.0024	1.741	0.079	0.1652	0.0082	1063	59	1014	29	982	45	92.38	982
0.0729	0.0019	1.76	0.099	0.176	0.016	988	57	1019	30	1033	77	95.45	988
0.0759	0.0021	1.757	0.079	0.168	0.013	1068	58	1021	26	992	64	92.88	1068
0.0776	0.0024	1.776	0.09	0.1622	0.0081	1108	62	1025	32	966	44	87.18	966
0.075	0.0024	1.794	0.091	0.179	0.019	1037	70	1031	31	1044	88	99.32	1044
0.0761	0.0026	1.806	0.094	0.172	0.011	1062	70	1035	32	1015	57	95.57	1015
0.0774	0.0022	1.83	0.1	0.169	0.011	1106	57	1044	30	998	56	90.24	998
0.0769	0.0026	1.824	0.078	0.1698	0.0087	1085	65	1046	27	1007	46	92.81	1007
0.0744	0.0018	1.88	0.16	0.185	0.021	1034	49	1049	41	1075	98	96.03	1034
0.0753	0.0021	1.85	0.11	0.179	0.015	1051	61	1052	31	1053	73	99.81	1051
0.0745	0.0017	1.91	0.14	0.184	0.019	1038	46	1066	36	1076	86	96.34	1038
0.072	0.02	1.83	0.21	0.182	0.012	640	500	1068	64	1069	65	32.97	1069
0.0798	0.0044	1.95	0.17	0.177	0.016	1129	86	1071	45	1039	76	92.03	1039
0.0742	0.0029	1.94	0.11	0.189	0.011	1009	95	1074	46	1106	60	90.39	1106
0.0768	0.0017	1.945	0.083	0.182	0.012	1101	44	1089	24	1071	56	97.28	1101
0.0823	0.0053	2.01	0.16	0.175	0.012	1160	110	1091	48	1032	61	88.97	1032
0.0787	0.002	2.01	0.12	0.184	0.016	1146	52	1107	32	1080	71	94.24	1146

$^{207}Pb/^{206}Pb$	2σ	$^{207}Pb/^{235}U$	2σ	$^{206}Pb/^{238}U$	2σ	Age (Ma) $^{207}Pb/^{206}Pb$	2σ	Age (Ma) $^{207}Pb/^{235}U$	2σ	Age (Ma) $^{206}Pb/^{238}U$	2σ	Con%	Best Age
0.0837	0.0047	2.11	0.15	0.18	0.01	1220	110	1113	69	1063	54	87.13	1063
0.0764	0.0021	2.09	0.13	0.201	0.021	1081	58	1130	36	1162	95	92.51	1081
0.0793	0.0019	2.12	0.11	0.193	0.016	1162	51	1141	34	1127	78	96.99	1162
0.0793	0.0018	2.12	0.12	0.191	0.015	1163	45	1141	34	1119	71	96.22	1163
0.0807	0.0039	2.15	0.13	0.1891	0.0094	1148	95	1146	42	1112	50	96.86	1112
0.0794	0.0019	2.18	0.13	0.198	0.017	1165	47	1162	31	1151	76	98.80	1165
0.0823	0.0024	2.34	0.2	0.206	0.025	1229	56	1198	44	1190	100	96.83	1229
0.0815	0.0022	2.3	0.11	0.204	0.015	1211	55	1200	32	1185	70	97.85	1211
0.0805	0.002	2.47	0.16	0.224	0.023	1191	51	1244	39	1280	100	92.53	1191
0.0842	0.0023	2.45	0.11	0.2059	0.0087	1278	50	1247	31	1203	45	94.13	1203
0.0848	0.0024	2.46	0.1	0.207	0.011	1289	54	1249	30	1209	57	93.79	1289
0.0814	0.0021	2.56	0.18	0.229	0.027	1208	56	1268	40	1300	110	92.38	1208
0.0881	0.0018	2.57	0.18	0.21	0.017	1371	41	1272	38	1218	80	88.84	1371
0.0886	0.0025	2.57	0.17	0.211	0.023	1371	58	1274	36	1214	95	88.55	1371
0.0865	0.0026	2.57	0.12	0.2114	0.0094	1325	56	1281	32	1232	49	92.98	1232
0.0859	0.0021	2.67	0.2	0.226	0.024	1319	49	1296	41	1290	100	97.80	1319
0.0868	0.0022	2.7	0.25	0.231	0.034	1336	57	1300	44	1300	130	97.31	1336
0.091	0.0023	2.75	0.13	0.216	0.012	1428	49	1329	34	1254	65	87.82	1428
0.0863	0.0018	2.83	0.15	0.234	0.016	1331	41	1351	31	1346	75	98.87	1331
0.0827	0.002	2.88	0.18	0.246	0.015	1246	44	1352	46	1406	76	87.16	1246
0.0923	0.0025	2.82	0.11	0.2178	0.0085	1454	50	1353	27	1267	44	87.14	1267
0.0836	0.0024	2.88	0.12	0.2431	0.0085	1257	64	1364	34	1399	44	88.70	1339
0.0888	0.0027	2.93	0.13	0.2329	0.009	1373	59	1378	33	1346	47	98.03	1346
0.0901	0.0016	2.93	0.15	0.233	0.016	1419	35	1379	30	1340	73	94.43	1419
0.1195	0.0025	3.06	0.15	0.183	0.011	1938	37	1408	34	1079	57	76.63	1938
0.0936	0.0024	3.05	0.13	0.234	0.013	1483	49	1409	31	1350	64	91.03	1483
0.0882	0.0022	3.14	0.15	0.256	0.016	1371	47	1426	37	1455	80	93.87	1371

$^{207}Pb/^{206}Pb$	2σ	$^{207}Pb/^{235}U$	2σ	$^{206}Pb/^{238}U$	2σ	Age (Ma) $^{207}Pb/^{206}Pb$	2σ	Age (Ma) $^{207}Pb/^{235}U$	2σ	Age (Ma) $^{206}Pb/^{238}U$	2σ	Con%	Best Age
0.0916	0.002	3.19	0.16	0.246	0.013	1446	42	1437	37	1410	66	97.51	1446
0.0944	0.0019	3.23	0.12	0.244	0.011	1504	39	1456	27	1402	55	93.22	1504
0.1267	0.0038	3.37	0.2	0.193	0.014	2028	56	1472	46	1126	75	55.52	2028
0.0894	0.0021	3.47	0.17	0.275	0.015	1399	45	1503	40	1558	76	88.63	1399
0.1002	0.0024	3.85	0.35	0.282	0.039	1612	46	1571	46	1560	140	96.77	1612
0.1051	0.0021	3.97	0.14	0.269	0.01	1705	38	1620	27	1533	50	89.91	1705
0.1014	0.0025	4.02	0.19	0.282	0.015	1634	44	1622	37	1591	75	97.37	1634
0.1002	0.002	4.04	0.21	0.291	0.025	1616	40	1627	34	1627	99	99.32	1616
0.1038	0.0027	4.08	0.24	0.282	0.02	1674	49	1628	42	1582	93	94.50	1674
0.1052	0.002	4.47	0.26	0.306	0.023	1708	35	1704	41	1702	99	99.65	1708
0.1113	0.0025	4.72	0.19	0.301	0.013	1808	41	1759	30	1688	61	93.36	1808
0.1132	0.0023	5.14	0.3	0.327	0.028	1840	40	1821	40	1800	110	97.83	1840
0.1002	0.0021	5.37	0.33	0.385	0.037	1615	42	1854	45	2060	130	72.45	1615
0.1102	0.0048	5.67	0.62	0.375	0.047	1750	150	1895	54	1990	170	86.29	1750
0.144	0.0037	8.2	0.39	0.399	0.016	2260	43	2233	42	2153	75	95.27	2260
0.1893	0.0038	9.44	0.5	0.354	0.02	2728	33	2356	46	1937	93	71.00	2728
0.1672	0.0038	9.61	0.44	0.41	0.02	2519	37	2377	43	2199	91	87.30	2519
0.1654	0.0036	10.4	0.33	0.45	0.018	2501	37	2461	29	2382	78	95.24	2501
0.1799	0.0039	12.45	0.47	0.492	0.021	2642	36	2625	35	2566	90	97.12	2642
0.186	0.0032	12.63	0.39	0.483	0.017	2701	28	2643	28	2529	72	93.63	2701
0.1843	0.0047	13.6	1.1	0.541	0.067	2678	42	2681	55	2700	200	99.18	2678
0.1838	0.0036	13.45	0.82	0.533	0.051	2678	34	2684	44	2690	170	99.55	2678
0.1887	0.0079	13.41	0.56	0.517	0.029	2700	56	2687	43	2650	120	98.15	2700
0.1913	0.0044	13.99	0.88	0.531	0.056	2741	40	2721	46	2680	170	97.77	2741
0.1941	0.0038	14.09	0.59	0.516	0.027	2769	32	2739	37	2660	110	96.06	2769
0.1919	0.0051	14.54	0.87	0.548	0.046	2743	43	2757	47	2770	160	99.02	2743
0.2006	0.0039	15.26	0.68	0.543	0.031	2823	31	2810	43	2760	130	97.77	2823

$^{207}Pb/^{206}Pb$	2σ	$^{207}Pb/^{235}U$	2σ	$^{206}Pb/^{238}U$	2σ	Age (Ma) $^{207}Pb/^{206}Pb$	2σ	Age (Ma) $^{207}Pb/^{235}U$	2σ	Age (Ma) $^{206}Pb/^{238}U$	2σ	Con%	Best Age
0.3454	0.0076	34.6	2.2	0.726	0.068	3677	35	3600	45	3440	180	93.55	3677
Missouri lat 38.69 lon -90.66													
0.0495	0.0042	0.028	0.013	0.0058	0.0012	140	150	25	17	37.1	7.7	51.60	37.1
0.0588	0.0039	0.0347	0.0025	0.00431	0.00018	470	140	34.6	2.5	27.7	1.1	80.06	27.7
0.0604	0.0048	0.0347	0.0029	0.00417	0.00018	490	150	34.6	2.9	26.8	1.1	77.46	26.8
0.0596	0.0073	0.0359	0.0071	0.00433	0.00066	390	170	35.3	6.4	27.8	4.2	78.75	27.8
0.0618	0.0063	0.0387	0.0063	0.00436	0.00034	510	130	38.1	5.7	28	2.2	73.49	28
0.0508	0.0023	0.0386	0.0019	0.00563	0.00034	207	88	38.4	1.9	36.2	2.2	94.27	38.4
0.0595	0.0067	0.0403	0.0063	0.0048	0.00027	400	170	39.7	5.8	30.9	1.7	77.83	30.9
0.062	0.0077	0.0413	0.0096	0.00521	0.00073	470	190	40.1	8.9	33.5	4.6	83.54	33.5
0.0569	0.0038	0.0404	0.0027	0.00518	0.0002	410	130	40.2	2.6	33.3	1.3	82.84	33.3
0.0577	0.0043	0.045	0.0057	0.00561	0.00049	420	140	44.3	5.3	36	3.1	81.26	36
0.06	0.013	0.051	0.012	0.00597	0.0003	330	180	49	10	38.4	1.9	78.37	38.4
0.0658	0.0072	0.0504	0.006	0.00552	0.00028	560	200	49.6	5.7	35.5	1.8	71.57	35.5
0.0658	0.0074	0.0551	0.0075	0.0059	0.00019	590	170	53.9	6.9	37.9	1.2	70.32	37.9
0.0559	0.0042	0.0591	0.0049	0.00764	0.00029	370	150	58.1	4.7	49.1	1.9	84.51	49.1
0.0523	0.0027	0.0602	0.0032	0.00845	0.00036	260	100	59.3	3.1	54.2	2.3	91.40	54.2
0.0537	0.0035	0.0658	0.0055	0.0088	0.00047	300	120	64.4	5.2	56.4	3	87.58	56.4
0.04739	0.001	0.0698	0.0026	0.01064	0.00039	75	43	68.4	2.5	68.2	2.5	99.71	68.2
0.0482	0.0019	0.0702	0.0035	0.01055	0.00037	105	78	68.8	3.3	67.6	2.4	98.26	67.6
0.0561	0.0038	0.0718	0.0097	0.00916	0.00094	370	120	69.5	8.4	58.7	5.9	84.46	58.7
0.0493	0.0021	0.0714	0.0038	0.0105	0.00042	150	85	69.8	3.6	67.3	2.7	96.42	67.3
0.056	0.0025	0.0762	0.009	0.00981	0.0008	408	91	73.9	7.6	62.9	5.1	85.12	62.9
0.0544	0.0033	0.0764	0.0052	0.01017	0.00048	330	120	74.5	4.9	65.2	3	87.52	65.2
0.0506	0.0021	0.0765	0.0032	0.01103	0.00042	204	81	74.8	3	70.7	2.7	94.52	70.7
0.0578	0.0058	0.08	0.0093	0.00992	0.00049	370	170	77.3	8.3	63.6	3.1	82.28	63.6

$^{207}Pb/^{206}Pb$	2σ	$^{207}Pb/^{235}U$	2σ	$^{206}Pb/^{238}U$	2σ	Age (Ma) $^{207}Pb/^{206}Pb$	2σ	Age (Ma) $^{207}Pb/^{235}U$	2σ	Age (Ma) $^{206}Pb/^{238}U$	2σ	Con%	Best Age
0.0481	0.003	0.0801	0.0047	0.01229	0.0005	90	110	78.1	4.4	78.8	3.2	99.10	78.8
0.0501	0.0026	0.0811	0.0044	0.01181	0.00043	180	100	79	4.1	75.7	2.8	95.82	75.7
0.0493	0.0014	0.0841	0.0029	0.01242	0.00046	158	60	81.9	2.7	79.5	2.9	97.07	81.9
0.0521	0.002	0.0862	0.0042	0.01197	0.00046	265	77	83.8	3.9	76.7	2.9	91.53	76.7
0.0508	0.0014	0.0893	0.0029	0.01273	0.00039	222	57	86.8	2.7	81.6	2.5	94.01	81.6
0.0523	0.0016	0.0939	0.0046	0.013	0.00056	282	67	91	4.3	83.2	3.6	91.43	83.2
0.0638	0.0062	0.095	0.013	0.011	0.0018	570	150	91	11	70	11	76.92	70
0.0513	0.0022	0.0988	0.0082	0.0141	0.0014	227	81	95.1	7.1	89.9	9	94.53	95.1
0.0495	0.0016	0.1004	0.0036	0.01473	0.00048	169	66	97	3.3	94.2	3.1	97.11	94.2
0.0509	0.0018	0.1033	0.0044	0.01475	0.00051	219	74	99.7	4	94.3	3.2	94.58	94.3
0.0497	0.0021	0.1046	0.0057	0.01542	0.00081	165	83	100.7	5.2	98.6	5.2	97.91	98.6
0.052	0.0023	0.111	0.006	0.0155	0.00058	257	88	106.5	5.4	99.1	3.7	93.05	99.1
0.0611	0.0065	0.113	0.015	0.0133	0.0011	460	160	107	13	85	6.9	79.44	85
0.063	0.01	0.119	0.036	0.01224	0.00059	430	180	107	23	78.4	3.7	73.27	78.4
0.0657	0.0059	0.114	0.015	0.01224	0.00093	650	140	108	12	78.4	5.8	72.59	78.4
0.0548	0.005	0.114	0.014	0.0146	0.0006	290	130	108	12	93.4	3.8	86.48	93.4
0.0603	0.0068	0.121	0.029	0.0132	0.0016	410	180	110	21	84.6	9.8	76.91	84.6
0.0479	0.0026	0.1212	0.0065	0.0185	0.00066	90	100	115.8	5.8	118.2	4.2	97.93	118.2
0.0569	0.0031	0.1245	0.0076	0.0159	0.00062	430	110	118.6	6.8	101.6	3.9	85.67	101.6
0.0675	0.0098	0.134	0.033	0.0135	0.0018	560	170	121	23	86	11	71.07	86
0.0622	0.0051	0.133	0.012	0.01547	0.00057	560	150	126	11	99	3.6	78.57	99
0.0657	0.0029	0.1329	0.0082	0.0146	0.0006	743	86	126.2	7.2	93.4	3.8	74.01	93.4
0.0626	0.0043	0.149	0.017	0.0175	0.0022	600	120	138	14	111	13	80.43	111
0.0561	0.0021	0.1478	0.0075	0.01899	0.00067	421	77	139.5	6.5	121.3	4.2	86.95	121.3
0.0507	0.001	0.1517	0.0045	0.02162	0.00056	218	43	143.3	3.9	137.8	3.5	96.16	137.8
0.0601	0.0051	0.271	0.038	0.0314	0.0023	480	140	235	25	199	14	84.68	199
0.0583	0.0039	0.502	0.041	0.0622	0.0035	450	130	405	27	388	21	95.80	388

$^{207}Pb/^{206}Pb$	2σ	$^{207}Pb/^{235}U$	2σ	$^{206}Pb/^{238}U$	2σ	Age (Ma) $^{207}Pb/^{206}Pb$	2σ	Age (Ma) $^{207}Pb/^{235}U$	2σ	Age (Ma) $^{206}Pb/^{238}U$	2σ	Con%	Best Age
0.0594	0.0022	0.599	0.03	0.0728	0.0027	546	69	473	18	453	16	95.77	453
0.0603	0.0016	0.605	0.021	0.0728	0.0025	590	58	479	13	453	15	94.57	479
0.0569	0.0019	0.632	0.026	0.0806	0.0031	460	71	495	17	499	18	99.19	495
0.0609	0.0017	0.724	0.029	0.0852	0.003	611	61	549	17	526	18	95.81	549
0.063	0.0017	0.84	0.033	0.096	0.0038	684	54	615	18	590	22	95.93	615
0.0638	0.0027	0.918	0.067	0.1026	0.0052	684	83	650	31	628	30	96.62	628
0.0643	0.0012	1.01	0.034	0.1137	0.004	741	40	706	17	693	23	98.16	706
0.1274	0.0031	1.418	0.06	0.081	0.0038	2049	41	890	24	501	22	56.29	501
0.1024	0.004	1.6	0.14	0.114	0.01	1634	66	933	58	689	58	73.85	689
0.0736	0.0017	1.624	0.074	0.16	0.0098	1013	48	971	26	952	50	98.04	971
0.0745	0.0018	1.828	0.055	0.1781	0.0057	1038	49	1051	20	1055	31	99.62	1055
0.0759	0.0016	1.867	0.057	0.1786	0.0061	1079	41	1065	20	1057	33	99.25	1057
0.074	0.0016	1.875	0.066	0.1844	0.0087	1029	41	1067	21	1087	45	98.13	1029
0.0785	0.0024	1.9	0.073	0.1757	0.0064	1133	62	1074	26	1041	35	96.93	1041
0.076	0.0016	1.939	0.079	0.1844	0.0071	1080	45	1087	26	1088	38	99.91	1088
0.0782	0.0025	2.008	0.081	0.1875	0.0082	1125	63	1111	27	1105	44	99.46	1105
0.089	0.0032	2.17	0.11	0.1748	0.0076	1370	64	1158	33	1036	41	89.46	1036
0.0805	0.0023	2.16	0.1	0.1937	0.0095	1185	55	1158	33	1137	50	98.19	1137
0.0812	0.0019	2.261	0.074	0.2023	0.0075	1210	45	1194	23	1185	40	99.25	1185
0.0826	0.0026	2.31	0.11	0.204	0.0099	1230	66	1203	33	1192	52	99.09	1192
0.0886	0.0021	2.32	0.13	0.189	0.012	1380	45	1204	32	1107	60	91.94	1380
0.0805	0.0016	2.467	0.072	0.222	0.0071	1199	38	1258	21	1290	37	97.46	1290
0.0914	0.0021	2.55	0.16	0.203	0.014	1438	48	1259	49	1184	73	94.04	1438
0.0836	0.0032	2.54	0.15	0.221	0.012	1253	60	1269	34	1281	57	99.05	1281
0.0852	0.0019	2.9	0.097	0.2468	0.009	1308	41	1375	25	1418	46	96.87	1308
0.0922	0.0022	2.97	0.17	0.235	0.019	1454	47	1383	35	1348	85	97.47	1454
0.0876	0.0017	3	0.14	0.252	0.017	1361	40	1395	31	1435	79	97.13	1361

$^{207}Pb/^{206}Pb$	2σ	$^{207}Pb/^{235}U$	2σ	$^{206}Pb/^{238}U$	2σ	Age (Ma) $^{207}Pb/^{206}Pb$	2σ	Age (Ma) $^{207}Pb/^{235}U$	2σ	Age (Ma) $^{206}Pb/^{238}U$	2σ	Con%	Best Age
0.0887	0.0021	3.02	0.11	0.2461	0.0088	1384	44	1404	29	1415	45	99.22	1384
0.0913	0.0024	3.1	0.2	0.253	0.032	1431	56	1416	35	1420	120	99.72	1431
0.0899	0.0022	3.12	0.18	0.255	0.023	1405	49	1421	37	1443	97	98.45	1405
0.0911	0.002	3.18	0.11	0.255	0.01	1436	42	1446	27	1457	53	99.24	1436
0.0919	0.0024	3.21	0.14	0.254	0.012	1447	50	1448	34	1454	60	99.59	1447
0.0917	0.0024	3.3	0.15	0.259	0.012	1438	61	1466	34	1477	59	99.25	1477
0.0945	0.0021	3.62	0.12	0.28	0.014	1503	46	1545	26	1583	67	97.54	1503
0.1021	0.0027	3.89	0.19	0.273	0.012	1644	50	1595	36	1550	62	97.18	1644
0.1029	0.0019	4.24	0.19	0.296	0.016	1669	33	1668	32	1661	71	99.58	1669
0.1035	0.0026	4.41	0.17	0.308	0.011	1673	45	1703	30	1727	53	98.59	1673
0.1038	0.0026	4.47	0.21	0.314	0.018	1676	48	1709	39	1750	83	97.60	1676
0.11	0.0024	4.62	0.12	0.3039	0.008	1788	40	1747	20	1708	39	97.77	1708
0.1061	0.0019	4.65	0.16	0.318	0.013	1726	32	1749	27	1773	60	98.63	1726
0.1116	0.0022	4.74	0.17	0.307	0.011	1816	36	1764	29	1722	55	97.62	1816
0.112	0.0023	5.02	0.22	0.323	0.018	1821	38	1810	33	1794	77	99.12	1821
0.1876	0.0034	9.58	0.38	0.371	0.016	2714	30	2379	38	2022	77	84.99	2714
0.1797	0.0028	10.61	0.34	0.427	0.015	2645	26	2480	29	2286	67	92.18	2645
Miss. S. of Missouri, Illinois, and Upper lat 38.54 lon -90.25													
0.042	0.012	0.012	0.047	0.00602	0.00086	-140	470	35.6	5.7	38.7	5.5	91.29	38.7
0.0578	0.0033	0.0398	0.0024	0.00502	0.00024	460	110	39.6	2.4	32.3	1.5	81.57	32.3
0.0616	0.0053	0.0417	0.0056	0.00475	0.00018	510	140	41.1	5.2	30.5	1.2	74.21	30.5
0.0512	0.0034	0.0421	0.0044	0.00613	0.00074	200	110	41.6	4.1	39.3	4.7	94.47	41.6
0.0582	0.005	0.0426	0.0046	0.00527	0.00026	400	140	42.1	4.4	33.9	1.7	80.52	42.1
0.0597	0.0037	0.0434	0.0033	0.00528	0.00023	510	120	43	3.2	33.9	1.5	78.84	33.9
0.0589	0.0046	0.0482	0.0044	0.00586	0.00018	450	120	47.6	4.1	37.7	1.1	79.20	37.7
0.0614	0.0059	0.0512	0.0068	0.00585	0.00037	480	170	50.2	6.4	37.6	2.4	74.90	37.6

$^{207}Pb/^{206}Pb$	2σ	$^{207}Pb/^{235}U$	2σ	$^{206}Pb/^{238}U$	2σ	Age (Ma) $^{207}Pb/^{206}Pb$	2σ	Age (Ma) $^{207}Pb/^{235}U$	2σ	Age (Ma) $^{206}Pb/^{238}U$	2σ	Con%	Best Age
0.0602	0.003	0.0592	0.0038	0.00714	0.00034	550	100	58.2	3.6	45.9	2.2	78.87	45.9
0.0564	0.006	0.065	0.012	0.00771	0.00047	320	160	62	10	49.5	3	79.84	49.5
0.0558	0.003	0.0718	0.0046	0.00938	0.00044	389	98	70.2	4.3	60.1	2.8	85.61	60.1
0.0574	0.0029	0.0719	0.0041	0.00903	0.0003	450	100	70.4	3.9	58	1.9	82.39	58
0.0496	0.0015	0.0766	0.0029	0.01117	0.00034	170	63	74.9	2.8	71.6	2.2	95.59	71.6
0.0547	0.0027	0.079	0.005	0.01035	0.00029	348	95	77	4.6	66.4	1.8	86.23	66.4
0.066	0.043	0.13	0.2	0.011	0.0048	80	480	80	48	69	28	86.25	69
0.0536	0.0023	0.083	0.011	0.0114	0.0016	315	86	80.2	9.5	73	10	91.02	80.2
0.0539	0.0016	0.0827	0.0032	0.0111	0.00032	342	64	80.6	3	71.2	2.1	88.34	71.2
0.0521	0.0022	0.0843	0.0051	0.01166	0.00046	260	83	82	4.6	74.7	2.9	91.10	74.7
0.0531	0.0039	0.0847	0.0085	0.01144	0.00037	269	91	82	7	73.3	2.4	89.39	73.3
0.0485	0.0022	0.089	0.015	0.0131	0.0014	112	85	85	11	83.5	8.5	98.24	83.5
0.0551	0.0028	0.0901	0.0078	0.0122	0.0015	360	100	87.1	7	78	9.1	89.55	87.1
0.0572	0.0056	0.093	0.016	0.01153	0.00071	370	140	89	13	73.8	4.5	82.92	73.8
0.0575	0.0039	0.097	0.018	0.012	0.0013	441	90	91	13	76.8	8.1	84.40	76.8
0.0603	0.0071	0.099	0.015	0.01163	0.00048	420	160	94	13	74.5	3.1	79.26	74.5
0.04	0.028	0.078	0.06	0.0115	0.0016	-300	1100	94	20	74	10	78.72	74
0.052	0.0049	0.103	0.017	0.0141	0.0014	201	96	98	13	90.3	8.5	92.14	90.3
0.0503	0.0014	0.1024	0.004	0.01477	0.00057	198	59	98.8	3.7	94.5	3.6	95.65	94.5
0.0509	0.0026	0.1074	0.0067	0.016	0.0017	207	97	103.1	6	102	10	98.93	103.1
0.0539	0.0021	0.1121	0.0063	0.01502	0.00067	329	75	107.6	5.7	96.1	4.2	89.31	96.1
0.037	0.025	0.124	0.045	0.0144	0.0019	-330	970	108	25	92	12	85.19	92
0.0572	0.0042	0.114	0.012	0.01427	0.00056	400	110	108.8	9.7	91.3	3.6	83.92	91.3
0.0491	0.0018	0.114	0.008	0.0168	0.0014	150	73	109	7.1	107.5	8.8	98.62	109
0.0536	0.0017	0.1155	0.0064	0.01574	0.00091	331	66	110.6	5.8	100.6	5.8	90.96	100.6
0.0587	0.0041	0.12	0.013	0.01459	0.00068	460	120	114	11	93.4	4.3	81.93	93.4
0.067	0.0032	0.1227	0.007	0.01337	0.00061	770	100	117.1	6.3	85.6	3.9	73.10	85.6

$^{207}Pb/^{206}Pb$	2σ	$^{207}Pb/^{235}U$	2σ	$^{206}Pb/^{238}U$	2σ	Age (Ma) $^{207}Pb/^{206}Pb$	2σ	Age (Ma) $^{207}Pb/^{235}U$	2σ	Age (Ma) $^{206}Pb/^{238}U$	2σ	Con%	Best Age
0.0581	0.0024	0.1247	0.007	0.01548	0.00065	490	83	118.9	6.2	99	4.1	83.26	99
0.0589	0.0052	0.139	0.041	0.0158	0.002	450	110	123	23	101	12	82.11	101
0.056	0.033	0.06	0.14	0.0152	0.0034	-180	980	124	38	96	21	77.42	96
0.0641	0.0053	0.14	0.013	0.01591	0.0008	600	150	131	11	101.7	5.1	77.63	101.7
0.0635	0.006	0.144	0.019	0.0166	0.0016	570	130	134	14	106.3	9.9	79.33	106.3
0.0541	0.0022	0.1834	0.0094	0.02443	0.0008	340	84	170.3	7.9	155.5	5.1	91.31	155.5
0.052	0.0016	0.184	0.012	0.0258	0.0022	268	64	170.7	9.9	164	13	96.07	170.7
0.0526	0.0016	0.189	0.0083	0.0261	0.0011	291	63	175.3	7	166.1	7	94.75	166.1
0.0513	0.0027	0.181	0.036	0.0295	0.0051	240	110	180	14	186	30	96.67	180
0.0592	0.0022	0.212	0.01	0.02585	0.00089	534	74	194.5	8.6	164.5	5.6	84.58	164.5
0.0517	0.0011	0.2359	0.0074	0.0331	0.0011	259	46	214.7	6.1	209.8	7.1	97.72	214.7
0.0523	0.0025	0.278	0.02	0.038	0.002	260	84	246	15	240	12	97.56	240
0.057	0.0013	0.446	0.014	0.0568	0.002	473	50	373	10	356	12	95.44	373
0.061	0.0019	0.485	0.02	0.0576	0.0022	612	64	399	13	361	13	90.48	361
0.0551	0.0017	0.507	0.039	0.0683	0.0084	392	67	410	22	422	45	97.07	410
0.0613	0.0022	0.591	0.043	0.0713	0.0082	611	74	464	24	440	44	94.83	464
0.0614	0.0017	0.756	0.028	0.0894	0.0034	628	58	569	16	551	20	96.84	569
0.0635	0.0025	0.833	0.055	0.0957	0.0066	678	82	605	29	587	38	97.02	587
0.0721	0.0017	1.53	0.067	0.1526	0.0071	971	47	935	26	913	39	97.65	935
0.0749	0.0021	1.711	0.096	0.168	0.014	1038	63	999	33	993	70	99.40	999
0.0743	0.0021	1.732	0.065	0.17	0.0075	1028	56	1014	24	1009	41	99.51	1009
0.0771	0.0022	1.875	0.073	0.176	0.0066	1102	58	1065	26	1043	36	97.93	1043
0.076	0.0015	1.892	0.052	0.1805	0.0058	1083	40	1075	18	1068	31	99.35	1068
0.0759	0.0021	1.935	0.069	0.185	0.0068	1071	55	1087	23	1092	37	99.54	1092
0.0835	0.0034	1.99	0.11	0.1725	0.0063	1234	81	1100	34	1024	35	93.09	1024
0.0805	0.0024	2.01	0.13	0.186	0.018	1181	64	1102	35	1082	86	98.19	1181
0.0825	0.0025	2.128	0.076	0.1873	0.0067	1234	56	1152	24	1105	36	95.92	1105

$^{207}Pb/^{206}Pb$	2σ	$^{207}Pb/^{235}U$	2σ	$^{206}Pb/^{238}U$	2σ	Age (Ma) $^{207}Pb/^{206}Pb$	2σ	Age (Ma) $^{207}Pb/^{235}U$	2σ	Age (Ma) $^{206}Pb/^{238}U$	2σ	Con%	Best Age
0.082	0.0021	2.48	0.15	0.222	0.02	1224	54	1249	38	1275	89	97.92	1224
0.0839	0.002	2.565	0.098	0.223	0.01	1275	46	1282	28	1291	53	99.30	1275
0.0896	0.0023	2.83	0.22	0.233	0.024	1398	50	1333	47	1320	110	99.02	1398
0.0882	0.0019	2.81	0.082	0.2301	0.0063	1375	42	1353	22	1333	33	98.52	1333
0.0942	0.0029	2.93	0.21	0.226	0.019	1488	56	1365	42	1297	86	95.02	1488
0.0902	0.0018	3.01	0.11	0.243	0.01	1419	38	1403	28	1396	53	99.50	1419
0.09	0.0014	3.037	0.066	0.2436	0.0055	1419	30	1414	17	1404	29	99.29	1404
0.0933	0.0025	3.09	0.14	0.239	0.012	1474	52	1416	34	1374	60	97.03	1474
0.0906	0.0019	3.07	0.11	0.247	0.011	1426	40	1419	26	1419	55	100.00	1426
0.0913	0.0016	3.099	0.082	0.2453	0.0069	1444	34	1428	20	1412	35	98.88	1444
0.091	0.0026	3.13	0.1	0.251	0.011	1425	55	1433	25	1441	54	99.44	1441
0.0915	0.0016	3.17	0.12	0.251	0.011	1450	33	1441	28	1440	56	99.93	1450
0.0905	0.0013	3.157	0.073	0.2523	0.0068	1430	28	1443	18	1448	35	99.65	1430
0.0901	0.0023	3.21	0.14	0.258	0.013	1410	48	1447	33	1469	66	98.48	1410
0.0906	0.0025	3.45	0.2	0.279	0.021	1413	59	1494	42	1569	98	94.98	1413
0.1032	0.0037	3.58	0.15	0.2519	0.0086	1649	67	1533	32	1445	45	94.26	1445
0.0963	0.0016	3.64	0.11	0.274	0.0099	1546	31	1552	25	1557	50	99.68	1546
0.0994	0.0031	3.75	0.22	0.278	0.024	1585	62	1561	42	1560	100	99.94	1585
0.1011	0.0024	4.13	0.29	0.297	0.025	1629	43	1634	44	1650	110	99.02	1629
0.1052	0.0034	4.13	0.22	0.288	0.019	1692	58	1640	41	1614	91	98.41	1692
0.1005	0.0019	4.1	0.13	0.295	0.011	1625	34	1646	27	1663	53	98.97	1625
0.1025	0.0026	4.18	0.16	0.294	0.013	1654	46	1659	31	1656	64	99.82	1654
0.1056	0.0017	4.28	0.13	0.294	0.011	1719	29	1682	25	1655	53	98.39	1719
0.1055	0.0028	4.43	0.19	0.306	0.017	1703	50	1703	35	1708	80	99.71	1703
0.1021	0.0026	4.47	0.19	0.318	0.015	1648	46	1711	36	1769	71	96.61	1648
0.1044	0.0017	4.48	0.12	0.3098	0.009	1697	31	1721	22	1736	44	99.13	1697
0.1044	0.0017	4.54	0.19	0.317	0.018	1696	32	1729	27	1763	77	98.03	1696

$^{207}Pb/^{206}Pb$	2σ	$^{207}Pb/^{235}U$	2σ	$^{206}Pb/^{238}U$	2σ	Age (Ma) $^{207}Pb/^{206}Pb$	2σ	Age (Ma) $^{207}Pb/^{235}U$	2σ	Age (Ma) $^{206}Pb/^{238}U$	2σ	Con%	Best Age
0.108	0.0018	4.63	0.13	0.3105	0.0098	1759	31	1749	23	1739	48	99.43	1759
0.1088	0.0019	4.7	0.16	0.313	0.012	1772	32	1758	28	1748	57	99.43	1772
0.1082	0.0021	4.77	0.18	0.319	0.012	1760	36	1770	30	1779	59	99.49	1760
0.1118	0.0027	4.98	0.23	0.321	0.016	1813	44	1798	39	1783	76	99.17	1813
0.1165	0.004	5.05	0.27	0.314	0.017	1874	60	1806	45	1748	82	96.79	1874
0.1162	0.0025	5.07	0.2	0.315	0.012	1888	38	1819	33	1760	60	96.76	1888
0.16	0.0036	10.44	0.38	0.473	0.018	2445	39	2462	33	2486	80	99.03	2445
0.1871	0.005	13.37	0.8	0.527	0.049	2700	46	2677	48	2670	160	99.74	2700
0.1844	0.0031	13.29	0.36	0.521	0.016	2687	28	2693	25	2695	65	99.93	2687
0.1874	0.0046	13.48	0.6	0.522	0.029	2706	39	2694	41	2680	120	99.48	2706
Illinois lat 39.15 lon -90.62													
0.0547	0.008	0.0478	0.0095	0.00627	0.00055	290	290	46.3	9.7	40.2	3.5	86.83	40.2
0.0553	0.0025	0.245	0.02	0.0326	0.0033	390	96	219	16	206	20	94.06	219
0.055	0.002	0.458	0.026	0.0587	0.0028	382	75	379	17	367	17	96.83	367
0.0569	0.0017	0.502	0.048	0.0636	0.007	458	66	404	26	394	39	97.52	404
0.0638	0.0019	0.517	0.03	0.0592	0.0062	705	65	419	18	368	35	87.83	419
0.0597	0.0015	0.565	0.036	0.0682	0.0076	573	53	450	19	422	41	93.78	450
0.0602	0.003	0.581	0.041	0.073	0.0075	560	110	455	33	451	41	99.12	455
0.0602	0.0057	0.67	0.18	0.0722	0.0092	515	87	470	51	444	49	94.47	444
0.0624	0.0047	0.611	0.059	0.0723	0.0076	580	120	471	31	446	43	94.69	471
0.0831	0.004	0.599	0.036	0.0563	0.0071	1210	100	471	21	350	41	74.31	471
0.0583	0.002	0.611	0.032	0.075	0.0051	509	76	479	19	465	30	97.08	479
0.0761	0.0026	0.627	0.036	0.0612	0.0067	1060	73	488	21	380	38	77.87	488
0.0608	0.0018	0.658	0.043	0.081	0.012	608	65	507	23	494	60	97.44	507
0.0606	0.0018	0.678	0.049	0.0798	0.006	595	66	517	24	493	34	95.36	517
0.0769	0.0039	0.694	0.053	0.0651	0.0058	1052	91	526	27	404	33	76.81	526

$^{207}Pb/^{206}Pb$	2σ	$^{207}Pb/^{235}U$	2σ	$^{206}Pb/^{238}U$	2σ	Age (Ma) $^{207}Pb/^{206}Pb$	2σ	Age (Ma) $^{207}Pb/^{235}U$	2σ	Age (Ma) $^{206}Pb/^{238}U$	2σ	Con%	Best Age
0.0622	0.0021	0.869	0.06	0.102	0.011	646	75	625	28	621	58	99.36	625
0.0616	0.0018	0.887	0.065	0.104	0.01	630	65	635	27	630	53	99.21	635
0.0611	0.0019	0.903	0.077	0.106	0.01	617	63	640	30	646	56	99.06	640
0.0856	0.0026	0.923	0.087	0.081	0.013	1301	61	645	37	492	67	76.28	645
0.0713	0.0023	1.51	0.12	0.154	0.017	940	79	913	43	909	82	99.56	913
0.0773	0.0037	1.57	0.11	0.144	0.0092	1076	97	933	47	862	51	92.39	933
0.0737	0.0019	1.557	0.068	0.1507	0.0089	1010	55	945	26	901	47	95.34	945
0.0738	0.002	1.639	0.073	0.1571	0.0072	1014	56	977	27	938	40	96.01	977
0.0824	0.0031	1.687	0.083	0.1473	0.007	1215	94	986	42	883	39	89.55	883
0.0747	0.0021	1.699	0.084	0.162	0.01	1037	57	997	30	964	54	96.69	997
0.0743	0.0021	1.733	0.095	0.166	0.012	1026	57	1010	29	984	58	95.91	1026
0.0742	0.0018	1.75	0.11	0.169	0.015	1028	52	1011	35	997	75	96.98	1028
0.0793	0.0028	1.738	0.078	0.1543	0.0052	1146	65	1014	27	923	29	80.54	923
0.0761	0.0022	1.8	0.1	0.17	0.014	1074	56	1032	34	1004	67	93.48	1074
0.075	0.0018	1.83	0.15	0.176	0.017	1048	50	1035	41	1029	85	98.19	1048
0.0737	0.0021	1.84	0.12	0.177	0.013	1008	58	1042	37	1043	65	96.53	1008
0.0746	0.002	1.86	0.16	0.184	0.025	1036	56	1043	40	1060	110	97.68	1036
0.0747	0.0019	1.838	0.085	0.176	0.015	1042	54	1050	27	1038	68	99.62	1042
0.0753	0.0027	1.851	0.093	0.177	0.012	1034	77	1051	33	1044	63	99.03	1044
0.0743	0.0019	1.854	0.096	0.178	0.013	1031	51	1053	31	1049	63	98.25	1031
0.0779	0.0033	1.88	0.12	0.1702	0.0093	1091	86	1055	39	1009	50	92.48	1009
0.0746	0.0021	1.93	0.12	0.184	0.012	1033	60	1077	31	1080	61	95.45	1033
0.0773	0.0034	1.95	0.14	0.185	0.02	1093	66	1081	35	1076	91	98.44	1093
0.0867	0.0028	1.95	0.12	0.165	0.017	1322	67	1082	35	972	83	73.52	1322
0.0766	0.0023	1.94	0.11	0.182	0.014	1081	66	1083	33	1069	68	98.89	1081
0.0769	0.0019	1.956	0.095	0.1797	0.0092	1099	51	1088	33	1061	49	96.54	1061
0.0811	0.0021	1.99	0.13	0.179	0.018	1200	56	1093	39	1044	88	87.00	1200

$^{207}Pb/^{206}Pb$	2σ	$^{207}Pb/^{235}U$	2σ	$^{206}Pb/^{238}U$	2σ	Age (Ma) $^{207}Pb/^{206}Pb$	2σ	Age (Ma) $^{207}Pb/^{235}U$	2σ	Age (Ma) $^{206}Pb/^{238}U$	2σ	Con%	Best Age
0.0769	0.002	1.99	0.13	0.182	0.011	1096	54	1093	36	1071	55	97.72	1096
0.0851	0.002	1.971	0.091	0.1653	0.0088	1298	58	1094	30	982	48	75.65	982
0.0765	0.0016	1.968	0.086	0.183	0.01	1095	42	1096	27	1077	52	98.36	1095
0.0819	0.0029	1.978	0.096	0.172	0.01	1207	68	1097	31	1019	52	84.42	1019
0.0785	0.0026	2.001	0.091	0.185	0.015	1127	65	1106	29	1083	70	96.10	1127
0.087	0.0037	2.05	0.16	0.167	0.014	1312	78	1109	40	989	66	75.38	989
0.0803	0.003	2.048	0.092	0.1815	0.0084	1165	72	1121	31	1072	46	92.02	1072
0.0768	0.002	2.11	0.15	0.199	0.02	1094	53	1128	42	1153	97	94.61	1094
0.0857	0.0033	2.12	0.16	0.18	0.024	1290	72	1135	38	1048	98	81.24	1290
0.0805	0.0024	2.12	0.1	0.189	0.013	1183	61	1144	32	1108	63	93.66	1183
0.0873	0.0026	2.144	0.092	0.176	0.01	1338	63	1153	30	1041	54	77.80	1041
0.086	0.0025	2.16	0.11	0.182	0.013	1314	55	1154	32	1066	68	81.13	1314
0.0792	0.0023	2.2	0.12	0.2	0.015	1153	58	1168	33	1162	73	99.22	1153
0.0793	0.002	2.28	0.15	0.207	0.019	1160	52	1186	40	1198	91	96.72	1160
0.0808	0.002	2.25	0.1	0.199	0.013	1196	51	1187	29	1162	63	97.16	1196
0.0837	0.0022	2.31	0.11	0.198	0.012	1263	56	1202	32	1156	63	91.53	1263
0.0813	0.0016	2.33	0.14	0.205	0.019	1215	41	1208	30	1186	80	97.61	1215
0.0786	0.0024	2.338	0.092	0.2118	0.0087	1136	75	1211	35	1234	45	91.37	1234
0.0845	0.0026	2.47	0.12	0.209	0.012	1274	62	1250	35	1216	62	95.45	1216
0.086	0.002	2.54	0.14	0.211	0.015	1323	45	1271	33	1226	72	92.67	1323
0.0832	0.0021	2.56	0.1	0.218	0.01	1257	47	1280	29	1267	52	99.20	1257
0.0853	0.002	2.63	0.16	0.216	0.013	1305	45	1283	45	1252	67	95.94	1305
0.0847	0.002	2.65	0.23	0.224	0.025	1292	47	1288	41	1280	100	99.07	1292
0.0874	0.002	2.64	0.17	0.215	0.017	1354	44	1293	37	1244	80	91.88	1354
0.0817	0.0023	2.73	0.27	0.247	0.041	1214	56	1305	45	1370	140	87.15	1214
0.0859	0.0028	2.92	0.44	0.245	0.039	1304	63	1323	61	1360	150	95.71	1304
0.0856	0.002	2.75	0.15	0.232	0.019	1311	51	1328	33	1331	89	98.47	1311

$^{207}Pb/^{206}Pb$	2σ	$^{207}Pb/^{235}U$	2σ	$^{206}Pb/^{238}U$	2σ	Age (Ma) $^{207}Pb/^{206}Pb$	2σ	Age (Ma) $^{207}Pb/^{235}U$	2σ	Age (Ma) $^{206}Pb/^{238}U$	2σ	Con%	Best Age
0.0807	0.0018	2.735	0.088	0.24	0.01	1197	50	1331	23	1383	51	84.46	1197
0.0894	0.0019	2.79	0.12	0.225	0.018	1396	48	1345	27	1294	79	92.69	1396
0.0885	0.0029	2.83	0.15	0.229	0.014	1364	61	1346	38	1321	73	96.85	1364
0.0884	0.002	3	0.19	0.245	0.024	1376	44	1389	36	1390	100	98.98	1376
0.0894	0.0024	3.05	0.16	0.248	0.024	1390	55	1407	32	1410	100	98.56	1390
0.0911	0.0026	3.11	0.14	0.245	0.014	1424	62	1424	31	1401	70	98.38	1424
0.0937	0.0029	3.25	0.15	0.25	0.017	1473	61	1454	35	1428	81	96.95	1473
0.0959	0.0024	3.37	0.17	0.254	0.022	1525	54	1483	34	1438	94	94.30	1525
0.0923	0.0022	3.39	0.16	0.261	0.015	1456	45	1488	33	1487	71	97.87	1456
0.094	0.0021	3.54	0.15	0.268	0.015	1493	45	1524	33	1519	73	98.26	1493
0.1077	0.0032	3.94	0.3	0.263	0.024	1739	49	1586	52	1480	110	85.11	1739
0.1077	0.003	3.87	0.18	0.254	0.012	1743	48	1593	34	1451	58	83.25	1743
0.1367	0.0043	4.26	0.41	0.228	0.031	2147	96	1632	65	1290	130	60.08	2147
0.1032	0.0025	4.23	0.29	0.299	0.036	1664	49	1658	41	1650	130	99.16	1664
0.1015	0.0037	4.31	0.28	0.305	0.022	1623	56	1667	46	1690	100	95.87	1623
0.1018	0.003	4.32	0.31	0.308	0.032	1632	57	1668	46	1700	130	95.83	1632
0.1051	0.0024	4.29	0.19	0.293	0.023	1700	46	1678	31	1639	95	96.41	1700
0.1027	0.0023	4.39	0.24	0.304	0.018	1657	45	1688	41	1695	87	97.71	1657
0.1096	0.0019	4.7	0.21	0.303	0.016	1785	33	1754	32	1698	74	95.13	1785
0.1349	0.0037	5.61	0.33	0.301	0.026	2144	48	1895	42	1670	110	77.89	2144
0.1193	0.0038	5.71	0.29	0.345	0.023	1919	57	1912	41	1890	100	98.49	1919
0.1115	0.0027	6	0.28	0.383	0.02	1802	58	1959	36	2075	89	84.85	1802
0.1916	0.0039	11.54	0.7	0.436	0.043	2746	35	2542	44	2280	150	83.03	2746
0.1868	0.0045	12.89	0.6	0.491	0.027	2700	41	2647	46	2550	110	94.44	2700
0.1926	0.0048	13.56	0.81	0.505	0.045	2750	43	2691	47	2590	150	94.18	2750
0.1888	0.0047	13.96	0.94	0.533	0.051	2718	41	2713	51	2700	160	99.34	2718
0.191	0.0045	14.08	0.66	0.522	0.027	2738	40	2731	46	2680	110	97.88	2738

$^{207}Pb/^{206}Pb$	2σ	$^{207}Pb/^{235}U$	2σ	$^{206}Pb/^{238}U$	2σ	Age (Ma) $^{207}Pb/^{206}Pb$	2σ	Age (Ma) $^{207}Pb/^{235}U$	2σ	Age (Ma) $^{206}Pb/^{238}U$	2σ	Con%	Best Age
0.1847	0.0041	14.07	0.75	0.546	0.044	2684	37	2731	42	2760	140	97.17	2684
0.1879	0.0039	14.08	0.57	0.528	0.023	2714	35	2738	39	2718	95	99.85	2714
0.1844	0.0035	14.52	0.59	0.557	0.026	2684	32	2768	37	2830	100	94.56	2684
0.1908	0.0037	15.74	0.73	0.585	0.032	2740	32	2839	42	2940	120	92.70	2740
Ohio lat 37.12 lon -88.13													
0.0729	0.0031	0.532	0.032	0.0541	0.0052	961	81	428	19	338	31	78.97	428
0.0553	0.0015	0.558	0.04	0.0729	0.0061	405	60	443	23	451	34	98.19	443
0.0603	0.0029	0.573	0.041	0.0696	0.0063	564	75	454	22	431	37	94.93	454
0.0576	0.0018	0.638	0.036	0.082	0.0078	490	66	496	20	504	46	98.39	496
0.0884	0.0085	0.684	0.052	0.0612	0.0065	1160	160	519	29	380	39	73.22	519
0.0697	0.0033	0.687	0.046	0.0747	0.0081	870	94	522	28	460	47	88.12	522
0.093	0.022	0.76	0.21	0.0601	0.0058	1200	160	528	49	374	35	70.83	374
0.0732	0.0025	0.7	0.036	0.0704	0.0062	986	68	534	19	436	37	81.65	534
0.0657	0.0022	0.897	0.065	0.098	0.0088	763	66	639	29	598	51	93.58	639
0.0904	0.0084	1.03	0.21	0.0775	0.0075	1280	120	667	51	477	44	71.51	477
0.111	0.022	1.42	0.59	0.0695	0.0073	1330	210	670	110	430	43	64.18	430
0.079	0.0052	1.59	0.14	0.151	0.017	1070	120	938	48	887	92	94.56	938
0.0915	0.0026	1.58	0.1	0.129	0.015	1435	53	944	36	767	81	81.25	944
0.0709	0.0017	1.57	0.1	0.159	0.012	937	48	945	33	946	61	99.89	945
0.0828	0.0019	1.61	0.12	0.142	0.015	1248	47	961	32	846	70	88.03	961
0.0766	0.0035	1.68	0.11	0.164	0.016	1060	110	968	69	967	85	99.90	968
0.0766	0.0028	1.632	0.095	0.152	0.0078	1078	62	970	32	909	42	93.71	970
0.0727	0.0018	1.626	0.081	0.162	0.011	985	50	971	27	961	57	98.97	971
0.0758	0.0033	1.66	0.11	0.158	0.012	1051	65	977	35	941	60	96.32	977
0.0784	0.0017	1.66	0.057	0.157	0.016	1143	45	988	21	924	84	93.52	988
0.0721	0.0021	1.679	0.097	0.167	0.011	966	53	988	31	990	54	99.80	988

$^{207}Pb/^{206}Pb$	2σ	$^{207}Pb/^{235}U$	2σ	$^{206}Pb/^{238}U$	2σ	Age (Ma) $^{207}Pb/^{206}Pb$	2σ	Age (Ma) $^{207}Pb/^{235}U$	2σ	Age (Ma) $^{206}Pb/^{238}U$	2σ	Con%	Best Age
0.0726	0.0017	1.668	0.072	0.1659	0.0093	983	50	988	27	985	50	99.70	988
0.0723	0.0023	1.69	0.1	0.172	0.016	961	67	990	34	1008	85	98.18	990
0.073	0.0016	1.704	0.082	0.1672	0.009	1001	43	1001	27	993	48	99.20	1001
0.0723	0.0022	1.77	0.15	0.176	0.018	971	75	1005	49	1030	94	97.51	971
0.0743	0.0022	1.737	0.085	0.169	0.012	1024	57	1012	28	1002	59	97.85	1024
0.0748	0.0021	1.756	0.082	0.171	0.016	1039	57	1020	28	1005	84	96.73	1039
0.0732	0.002	1.81	0.14	0.181	0.019	993	58	1027	40	1058	90	96.98	993
0.0746	0.0017	1.79	0.11	0.172	0.012	1043	46	1028	31	1017	61	97.51	1043
0.0755	0.0031	1.81	0.14	0.173	0.016	1046	63	1029	37	1014	83	96.94	1046
0.0756	0.0023	1.79	0.097	0.175	0.017	1057	61	1029	33	1023	88	96.78	1057
0.0741	0.0017	1.79	0.1	0.176	0.015	1028	47	1030	31	1030	82	99.81	1028
0.0791	0.0026	1.82	0.1	0.172	0.018	1147	80	1031	44	1004	94	87.53	1147
0.0744	0.0024	1.84	0.15	0.18	0.018	1021	64	1033	44	1054	87	96.77	1021
0.0794	0.004	1.81	0.095	0.17	0.017	1134	75	1035	34	995	91	87.74	1134
0.0749	0.0016	1.808	0.087	0.178	0.017	1051	44	1038	30	1040	90	98.95	1051
0.0745	0.0025	1.816	0.071	0.182	0.017	1025	67	1044	25	1062	88	96.39	1025
0.0747	0.0028	1.837	0.083	0.18	0.018	1025	88	1045	35	1048	94	97.76	1025
0.0814	0.0023	1.837	0.099	0.162	0.014	1203	69	1046	31	959	76	79.72	1203
0.0734	0.0015	2.02	0.38	0.197	0.035	1011	44	1056	57	1110	140	90.21	1011
0.0777	0.0017	1.878	0.088	0.177	0.017	1124	46	1064	27	1038	87	92.35	1124
0.0804	0.002	1.89	0.11	0.174	0.017	1189	47	1065	33	1018	90	85.62	1189
0.0837	0.004	1.94	0.16	0.169	0.018	1229	87	1069	46	989	94	80.47	1229
0.0786	0.0031	1.9	0.1	0.18	0.017	1117	79	1069	32	1054	91	94.36	1117
0.0728	0.002	1.93	0.16	0.19	0.019	988	65	1071	36	1104	94	96.92	988
0.0769	0.0017	1.894	0.077	0.182	0.016	1104	42	1071	25	1063	84	96.29	1104
0.0767	0.0019	1.893	0.072	0.18	0.014	1096	46	1072	24	1057	77	96.44	1096
0.08	0.002	1.901	0.074	0.172	0.016	1176	53	1073	27	1009	85	85.80	1176

$^{207}Pb/^{206}Pb$	2σ	$^{207}Pb/^{235}U$	2σ	$^{206}Pb/^{238}U$	2σ	Age (Ma) $^{207}Pb/^{206}Pb$	2σ	Age (Ma) $^{207}Pb/^{235}U$	2σ	Age (Ma) $^{206}Pb/^{238}U$	2σ	Con%	Best Age
0.0791	0.0035	1.95	0.12	0.181	0.017	1129	75	1080	37	1060	87	93.89	1129
0.0781	0.0019	1.95	0.13	0.185	0.022	1130	55	1081	37	1076	99	95.22	1130
0.0785	0.0035	1.97	0.15	0.183	0.018	1116	70	1084	39	1065	92	95.43	1116
0.0779	0.0023	1.952	0.089	0.184	0.016	1117	58	1089	29	1077	85	96.42	1117
0.0755	0.0029	2	0.13	0.203	0.023	1040	97	1089	52	1170	110	87.50	1040
0.0788	0.0022	1.97	0.1	0.182	0.017	1145	53	1090	35	1062	92	92.75	1145
0.0774	0.0017	1.97	0.11	0.186	0.018	1116	46	1092	30	1084	94	97.13	1116
0.076	0.0014	1.964	0.093	0.185	0.01	1086	36	1093	28	1091	54	99.54	1086
0.0775	0.0019	1.97	0.1	0.187	0.018	1115	50	1094	33	1087	95	97.49	1115
0.0786	0.0017	1.99	0.12	0.181	0.011	1147	43	1099	32	1066	56	92.94	1147
0.0787	0.0019	1.979	0.073	0.185	0.016	1148	45	1101	25	1080	85	94.08	1148
0.0767	0.0021	2.07	0.16	0.2	0.022	1089	59	1118	39	1150	100	94.40	1089
0.089	0.012	2.12	0.24	0.176	0.016	1250	110	1119	49	1033	85	82.64	1033
0.0786	0.0021	2.06	0.12	0.189	0.013	1143	49	1119	34	1106	66	96.76	1143
0.0772	0.0016	2.06	0.12	0.196	0.019	1112	42	1121	33	1138	98	97.66	1112
0.0774	0.0018	2.09	0.16	0.189	0.018	1115	47	1126	38	1100	92	98.65	1115
0.0832	0.0024	2.18	0.21	0.194	0.024	1246	59	1138	51	1110	110	89.09	1246
0.0836	0.0024	2.21	0.26	0.202	0.035	1256	62	1139	55	1140	150	90.76	1256
0.095	0.017	2.19	0.21	0.181	0.02	1330	110	1145	49	1050	100	78.95	1050
0.0814	0.003	2.134	0.098	0.1881	0.008	1198	62	1148	31	1108	44	92.49	1108
0.0885	0.0026	2.16	0.14	0.181	0.021	1365	67	1150	37	1055	94	77.29	1365
0.0793	0.0021	2.15	0.13	0.198	0.018	1159	50	1152	33	1149	94	99.14	1159
0.0805	0.0019	2.156	0.068	0.196	0.017	1195	44	1162	21	1136	91	95.06	1195
0.0797	0.002	2.22	0.16	0.205	0.021	1170	51	1163	42	1180	110	99.15	1170
0.0862	0.0071	2.21	0.13	0.193	0.019	1251	88	1166	36	1117	97	89.29	1251
0.0835	0.0048	2.23	0.15	0.198	0.017	1226	77	1173	39	1148	91	93.64	1226
0.0812	0.0014	2.189	0.065	0.194	0.016	1214	39	1173	20	1130	83	93.08	1214

$^{207}Pb/^{206}Pb$	2σ	$^{207}Pb/^{235}U$	2σ	$^{206}Pb/^{238}U$	2σ	Age (Ma) $^{207}Pb/^{206}Pb$	2σ	Age (Ma) $^{207}Pb/^{235}U$	2σ	Age (Ma) $^{206}Pb/^{238}U$	2σ	Con%	Best Age
0.0809	0.0026	2.26	0.15	0.204	0.018	1193	57	1183	34	1178	91	98.74	1193
0.0833	0.0037	2.29	0.15	0.204	0.021	1230	80	1191	38	1180	100	95.93	1230
0.0812	0.0028	2.3	0.16	0.202	0.018	1197	59	1192	38	1170	93	97.74	1197
0.0817	0.0023	2.42	0.34	0.204	0.023	1215	60	1193	55	1170	110	96.30	1215
0.0874	0.0047	2.33	0.17	0.196	0.018	1308	83	1199	42	1138	95	87.00	1308
0.0823	0.0019	2.4	0.18	0.208	0.016	1238	43	1220	39	1207	77	97.50	1238
0.0816	0.0018	2.46	0.16	0.221	0.021	1218	50	1242	36	1265	96	96.14	1218
0.0901	0.0041	2.49	0.16	0.204	0.019	1386	69	1249	38	1178	99	84.99	1386
0.0862	0.0027	2.49	0.13	0.207	0.013	1322	50	1255	32	1207	63	91.30	1322
0.0835	0.0024	2.61	0.24	0.227	0.026	1257	55	1265	53	1290	130	97.37	1257
0.0848	0.0027	2.64	0.24	0.224	0.024	1282	63	1281	46	1280	120	99.84	1282
0.0853	0.0022	2.59	0.14	0.217	0.013	1306	48	1283	37	1260	64	96.48	1306
0.0896	0.0021	2.73	0.18	0.221	0.021	1400	46	1317	39	1260	100	90.00	1400
0.0872	0.0026	2.73	0.12	0.232	0.022	1341	55	1325	32	1320	110	98.43	1341
0.0917	0.002	2.78	0.16	0.22	0.017	1447	44	1331	39	1270	83	87.77	1447
0.0848	0.002	2.85	0.21	0.246	0.023	1293	53	1344	40	1390	100	92.50	1293
0.089	0.002	2.82	0.14	0.232	0.02	1389	44	1349	32	1330	100	95.75	1389
0.085	0.0023	2.91	0.27	0.252	0.033	1291	56	1351	47	1410	130	90.78	1291
0.0887	0.0038	3.06	0.28	0.25	0.025	1365	58	1385	51	1410	110	96.70	1365
0.0898	0.0023	2.97	0.15	0.238	0.019	1405	45	1387	32	1358	94	96.65	1405
0.0949	0.0037	3.14	0.26	0.239	0.024	1493	62	1415	44	1350	120	90.42	1493
0.0913	0.0018	3.15	0.13	0.25	0.022	1442	38	1435	30	1420	110	98.47	1442
0.0904	0.0018	3.3	0.22	0.263	0.024	1422	41	1460	40	1480	120	95.92	1422
0.1069	0.0034	3.36	0.32	0.222	0.022	1722	53	1463	44	1270	110	73.75	1722
0.0925	0.0031	3.31	0.2	0.262	0.026	1442	75	1463	39	1470	130	98.06	1442
0.0927	0.0021	3.41	0.3	0.267	0.03	1465	48	1477	45	1490	140	98.29	1465
0.0959	0.0025	3.38	0.2	0.263	0.028	1528	49	1481	39	1470	130	96.20	1528

$^{207}Pb/^{206}Pb$	2σ	$^{207}Pb/^{235}U$	2σ	$^{206}Pb/^{238}U$	2σ	Age (Ma) $^{207}Pb/^{206}Pb$	2σ	Age (Ma) $^{207}Pb/^{235}U$	2σ	Age (Ma) $^{206}Pb/^{238}U$	2σ	Con%	Best Age
0.0947	0.0032	3.38	0.19	0.263	0.025	1501	46	1483	37	1480	120	98.60	1501
0.0917	0.002	3.4	0.19	0.274	0.028	1447	45	1484	39	1530	130	94.26	1447
0.1119	0.0028	5.1	0.32	0.33	0.026	1816	42	1814	40	1810	110	99.67	1816
0.1263	0.0043	5.89	0.39	0.352	0.04	2023	54	1928	52	1890	170	93.43	2023
0.1483	0.0052	6.98	0.47	0.352	0.038	2295	63	2067	60	1890	170	82.35	2295
0.1586	0.0028	9.37	0.56	0.432	0.04	2433	31	2353	40	2260	170	92.89	2433

APPENDIX B. SUPPLEMENTARY DATA FOR CHAPTER 3

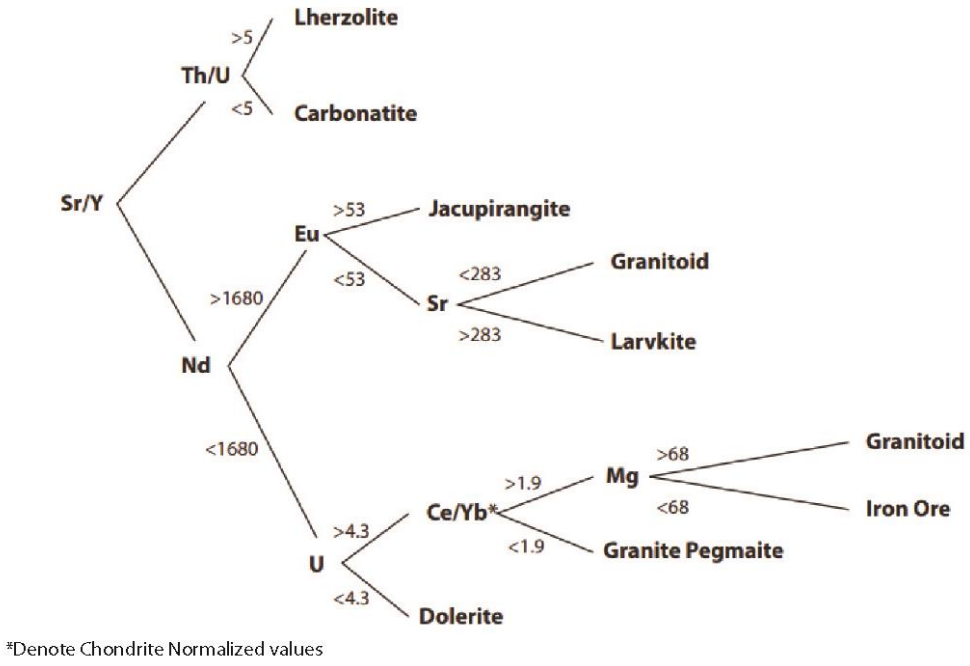

Supplementary Figure B. 1 A reference version of the cladogram found in Belousova et al. (2002) used to discriminate apatite source rock.

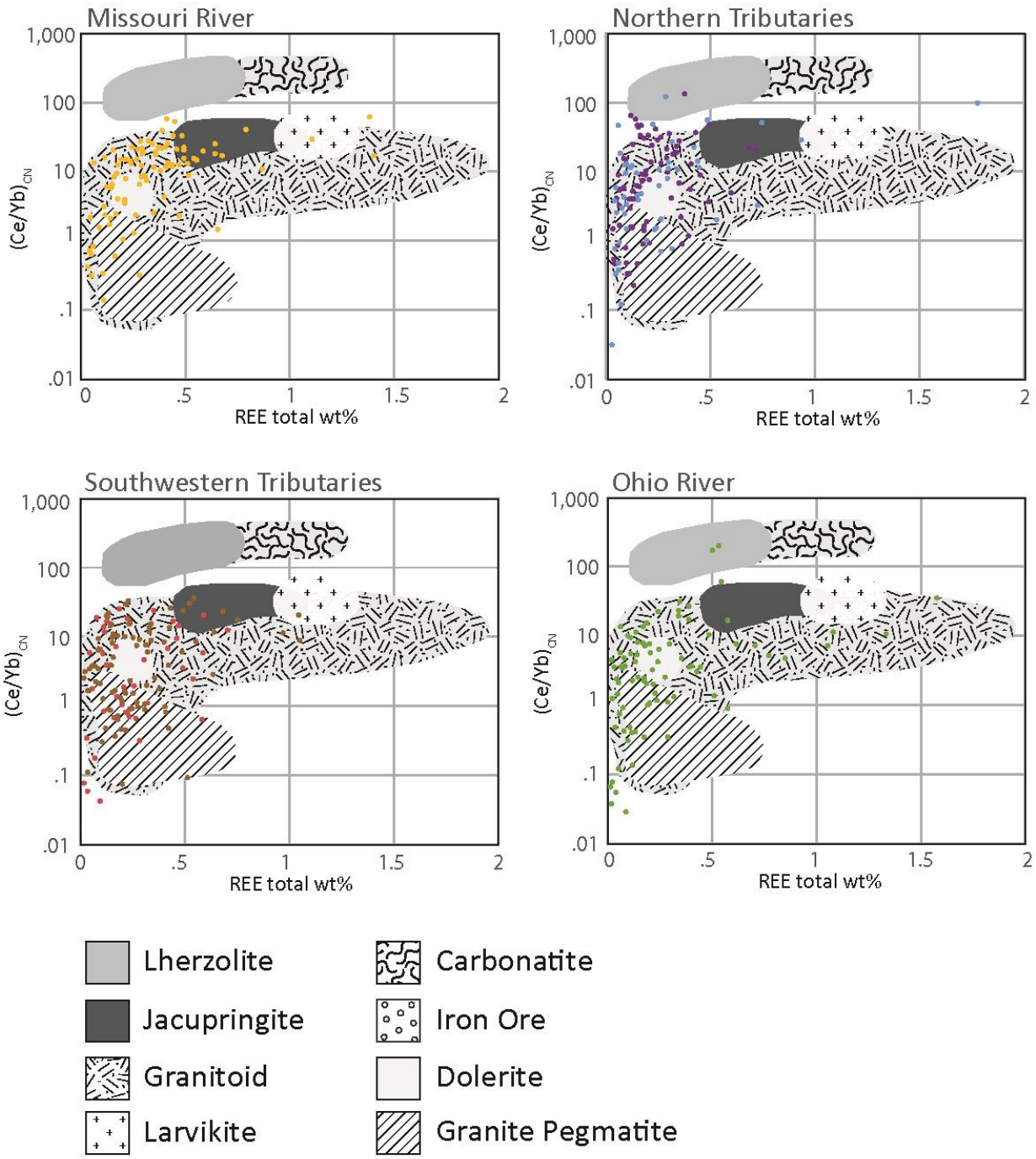

Supplementary Figure B. 2 Cross plots of chondrite normal Ce/Yb against total weight % REEs with fields showing the predicted source rock type from Morton and Yaxley (2007) and Belousova et al. (2002). (A) Missouri, (B) Northern Tributaries, (C) Southwest Tributaries, and (D) Ohio.

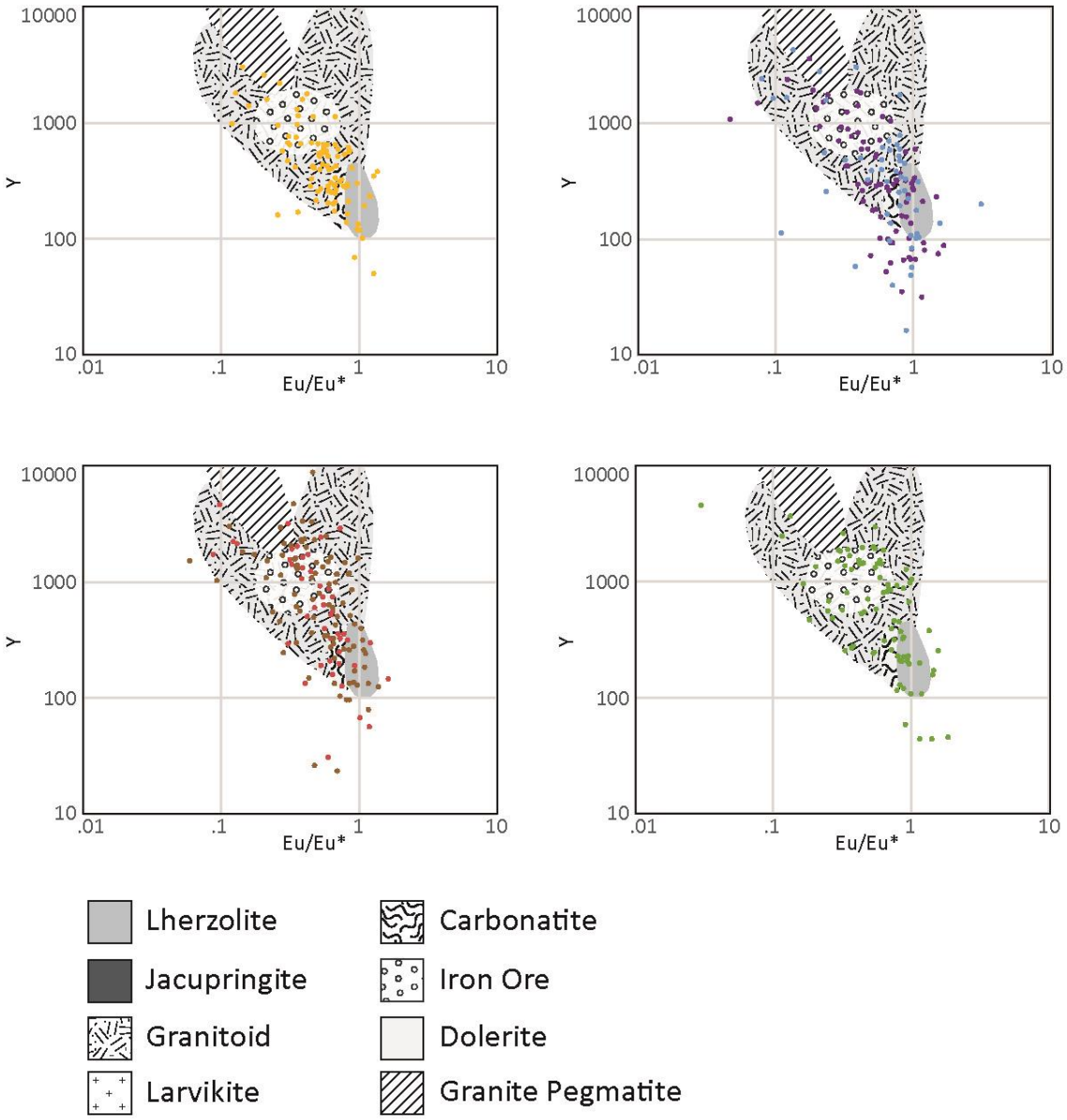

Supplementary Figure B. 3 Cross plots of Eu/Eu* against Y concentrations for single apatite grains with fields showing the predicted source rock types from (A. Morton & Yaxley, 2007) and (Belousova et al., 2002), divided by tributary. (A) Missouri, (B) Northern Tributaries, (C) Southwest Tributaries, and (D) Ohio.

Supplementary Table B. 1 Laser Setting

Spot Size	Shot Frequency	Laser Energy	Burst Count	Gas Flow
25um	10 Hz	30%	700-800	700 l/min

Supplementary Table B. 2 Table showing Statistics and Reproducibility of Apatite Standards

	^{55}Mn	^{57}Fe	^{88}Sr	^{89}Y	^{232}Th	^{238}U
Blue Trace Elements						
max	218.0	191.0	273.0	196.9	882.0	67.5
min	189.9	158.7	244.2	153.9	766.0	2.8
std	7.5	7.4	7.5	14.5	26.5	29.0
avg	199.3	180.7	257.2	168.4	843.8	24.2
Durango						
max	97.6	282.6	502.0	717.0	153.7	8.3
min	86.2	251.4	454.0	630.0	138.9	0.4
std	3.9	10.9	13.3	28.5	4.5	3.6
avg	92.0	269.7	472.9	672.9	145.0	3.1

	La*	Ce*	Pr*	Nd*	Sm*	Eu*	Gd*	Tb*	Dy*	Ho*	Er*	Tm*	Yb*	Lu*
Blue REEs														
max	403.0	886.0	104.8	360.0	62.9	9.8	53.8	6.9	36.3	6.8	18.2	2.2	13.1	1.6
min	324.0	730.0	89.0	311.2	52.2	8.4	42.4	5.6	28.7	5.3	14.5	1.8	10.3	1.3
std	19.1	43.2	4.6	14.5	3.0	0.3	2.8	0.4	2.1	0.4	1.1	0.1	0.8	0.1
avg	363.7	812.4	94.5	330.8	55.2	8.8	45.6	5.9	31.0	5.8	15.6	1.9	11.1	1.4
Durango														
max	3500.0	5740.0	468.0	1550.0	207.0	20.3	204.0	22.9	116.0	23.3	65.2	7.8	45.5	6.0

min	2970.0	4680.0	436.0	1394.0	185.3	18.4	181.0	20.7	104.6	21.1	58.2	7.0	40.8	5.4
std	178.2	295.5	10.4	40.4	6.7	0.6	7.2	0.7	3.4	0.7	1.9	0.2	1.4	0.2
avg	3155.1	5020.0	449.1	1464.7	198.3	19.3	189.7	21.5	109.7	22.2	61.1	7.3	42.8	5.6

Supplementary Table B. 3 Apatite Trace Element Data ppm

Sample ID	**^{55}Mn**	**^{57}Fe**	**^{88}Sr**	**^{89}Y**	**La**	**Ce**	**Pr**	**Nd**	**Sm**	**Eu**	**Gd**	**Tb**	**Dy**	**Ho**	**Er**	**Tm**	**Yb**
Mississippi S. of Red																	
X2501_1	648	223.2	492	119	94	277	35.8	158.9	28.9	8.38	29.1	3.62	19.03	4.02	11.25	1.467	9.82
X2501_2	1127	468	791	460	706	2530	289	1151	201	26.6	158.7	19.4	94.9	17.63	43.5	5.14	29.6
X2501_3	428	208	444	242	83.3	290	44.9	218.4	53.4	11.54	54	7.18	38.7	7.83	21.4	2.82	17.71
X2501_4	330	196	1910	1392	28	92	14.6	82	35.2	12.49	79.3	19.2	169.7	46.3	139.5	17.64	97.5
X2501_6	445	887	1530	353	725	1976	215.9	841	137	19.36	126.1	15.23	74.3	13.17	31.7	3.67	20.98
X2501_7	281	167	539	45.3	26.3	97.6	14.67	71.7	13.31	4.93	13.41	1.61	8.29	1.63	4.1	0.494	2.99
X2501_8	522	203	277	2150	43.3	287	71.4	507	222	40.7	326	59.4	386	78.4	207	26.5	155.3
X2501_9	901	622	1193	147.2	417	1402	180.1	716	98.9	22.54	76.8	7.69	32.5	5.29	12.83	1.388	8.21
X2501_10	330	205	945	238	39.4	191	39.7	267	98.3	30.1	104.3	12.1	53.7	8.61	19	2.17	13.5
X2501_11	379	210	598	117.5	332	888	84.5	286	34.8	10.05	34	3.69	18.98	3.9	10.82	1.423	10.28
X2501_12	1143	496	872	198	559	1750	210	815	122.8	26.3	99.1	10.64	46.6	7.42	17.1	1.801	10.63
X2501_13	196.8	174	504	222	192	595	73.8	321	50.9	20	50.6	6.01	32.7	6.91	20.2	2.6	17.8
X2501_14	1142	471	2018	460	1623	3880	379	1318	183.6	43.9	159.7	17.99	90.5	16.98	43.6	4.94	30
X2501_15	701	609	860	458	1610	3780	341	1183	181	29.9	143	17.5	88	16.2	40.5	4.82	29.2
X2501_16	292	180.3	1465	98.5	8.34	47.4	12.67	99.9	48.5	15.87	45.2	5.25	22.4	3.51	7.51	0.812	4.91
X2501_17	368	223	250.3	1308	29.6	142.2	34.1	255	154.5	21.59	202.5	38.5	243.5	50.3	131.7	15.55	92.8
X2501_18	109	191	232.9	689	73.8	259	44.6	249	126	16.2	135	21.7	127	24.9	65.5	8.2	52.6
X2501_19	616	972	929	464	1033	3000	350	1400	262	28	183.3	20.8	98	17.17	41.2	4.36	25.6
X2501_20	474	433	1103	270	266	808	108.6	504	116.5	33.9	93.5	11.4	58.7	10.63	24.44	2.57	14.55
X2501_21	333	193	355	70.6	88	311	44.4	186	38.3	10.08	24.5	2.6	12.11	2.31	6.16	0.761	4.92
X2501_22	416	205	416	1004	113.3	448	104.1	753	308	47.4	263	36.1	195.7	38.2	98.9	11.75	69.2
X2501_23	512	216	90.3	3190	325	1422	233	1177	414	59	414	66.9	416	93.8	276	37.2	254
X2501_24	462	215	364	445	64	345	69.7	377	124.8	24.3	99.1	13.62	75.2	15	41	5.44	36.5
X2501_25	567	266	1327	225.6	323	1122	168	733	160	35.3	99.1	11.06	51	8.63	20.8	2.22	13.45
X2501_26	890	356	654	242.9	442	1255	170.1	730	174.5	21.42	116	12.61	55.3	9.39	22.4	2.37	13.61
X2501_27	730	310	399	1369	1214	5770	827	3440	808	84.1	528	64.1	302	53	127.4	13.82	75.1

Sample ID	^{55}Mn	^{57}Fe	^{88}Sr	^{89}Y	La	Ce	Pr	Nd	Sm	Eu	Gd	Tb	Dy	Ho	Er	Tm	Yb
X2501_28	461	229	1003	254	456	987	104.3	380	78.3	14.78	62.4	8.05	44.4	9.13	25.6	3.41	22.1
X2501_29	177.2	185.9	2282	145	588	1750	213	838	126.9	27.4	79.6	6.9	26.7	4.63	11.87	1.32	8.53
X2501_30	827	220	279	197.1	734	1202	111.8	379	64.7	10.7	53.4	6.16	32.2	6.62	19.2	2.6	17.8
X2501_31	929	452	2151	433	1074	2690	300	1217	225.4	48	165.1	18.6	87.4	15.82	40.3	4.71	27
X2501_32	1048	325	662	893	548	1887	265.5	1270	323	29.4	266.8	35.6	184	33.3	81.8	9.47	52.1
X2501_33	277.9	511	249.4	872	139.5	633	120.9	646	285	12.55	329	51.2	245	34.8	58.8	3.91	14.03
X2501_34	558	1055	1311	452	678	1646	213.4	939	191.5	27.02	151.5	18.19	89.7	16.49	40.3	4.6	25.9
X2501_35	165	310	959	127.2	219	814	111.2	469	76.1	22	57.1	5.49	23.6	4.31	11.23	1.362	8.81
X2501_36	267	186	1012	347	628	1830	214.9	888	158.2	30.6	130.8	14.1	66.6	12.46	33.5	4.17	27.3
X2501_37	1660	854	815	212	533	1420	183	710	110.4	20.1	89.7	9.5	43.1	7.61	19.1	2.11	13.2
X2501_38	261	183	385	354	252	963	145.7	717	148.1	35.3	148.3	16.22	75.9	13.78	32.1	3.16	17.14
X2501_39	530	214	410	88	142	377	43.2	179	28.4	7.2	29.4	2.92	14.4	2.92	8	0.9	6.5
X2501_40	447	206	62	2450	222.8	783	139.5	751	291	18.61	419	79.9	520	100.7	260	32.7	202.3
X2501_1	621	218	296	1292	783	2220	311	1500	425	70	435	52.7	261	48.4	125.6	15.3	90.2
X2501_2	501	766	877	478	557	1410	185	770	155	24.4	150	18.5	95.3	17.4	42.6	4.62	25.8
X2501_3	1387	469	738	367	154.5	481	82.6	411	122.5	32.7	122.5	16.07	79.8	14.18	34.7	4.05	23.2
X2501_4	1568	455	991	397	1650	3280	344	1179	157	26	139.2	14.99	74.5	14.3	39.3	4.65	27.2
X2501_5	79.5	311	5360	260	123.6	376	69.9	392	168.4	44.1	229	26.4	90.4	10	14.75	1.066	4.65
X2501_6	343	266	142.4	3740	749	1980	322	1760	638	13	855	139.7	764	142	318	32.3	158.2
X2501_7	1035	301	113.3	2410	139.4	525	101.7	597	263	42.2	436	85.1	543	99.5	232	25.3	131.5
X2501_8	5220	656	61.2	2230	211	776	129	569	258	7.4	317	67.7	421	77.2	206	29.3	183
X2501_9	401	946	333	604	350	941	139.9	641	140.3	36.8	161	22.2	119.3	21.9	55.2	6.41	36.2
X2501_10	265	177	323	766	328	1290	232	1220	293	9.6	267	34.4	178	31.3	74.3	8.43	44.9
X2501_12	281	240	168.5	1019	12.54	93.4	28.2	222	130.6	10.92	198	33.8	200	39.2	100.2	11.35	59.6
X2501_13	1318	652	995	212	762	1750	195	690	101.5	18.2	89.3	9.57	45.1	8.13	20.4	2.25	12.8
X2501_14	1175	292	548	471	1042	2600	316	1272	198	46	169	19.5	94.3	17.9	44.8	5.13	29.6
X2501_16	1467	416	1033	201.1	744	1408	139.5	449	62	14.84	58.8	6.29	33.2	6.71	19.5	2.63	17.1
X2501_17	1173	196	717	129.4	442	920	85.9	259	33.1	12.3	35.2	3.62	17.3	3.67	11	1.44	10.5
X2501_18	362	213	252	866	6.63	76.8	30.8	279	142	44.1	193	29.5	164	32.8	82	9.62	54.7
X2501_19	34.5	159	685	357	32.1	309	74.5	545	253	81.7	296	35.4	138.8	16.7	24.5	1.5	5.28
X2501_20	415	172	356	311	252	625	74.7	291	58.6	18.9	66.3	8.29	44.4	9.99	30.5	4.15	28.6
X2501_21	58.1	199	8880	365	1238	3610	524	2100	345	85.2	252	24.4	97.6	14.8	33.1	3.13	16.1
X2501_22	344	198	445	240	574	1267	133.6	490	75.2	22	75.7	8.63	45.5	9	24.7	3.15	21.6
X2501_23	1356	393	1759	404	763	2040	254	944	156	33	126.4	14.24	66.8	12.9	35.4	4.47	28.5

Sample ID	^{55}Mn	^{57}Fe	^{88}Sr	^{89}Y	La	Ce	Pr	Nd	Sm	Eu	Gd	Tb	Dy	Ho	Er	Tm	Yb
X2501_24	1111	539	718	198	522	1510	199	776	127	19.2	96.9	10.16	43.9	7.42	17.9	1.96	10.63
X2501_25	403	218	577	743	707	2040	257	1056	207	28.8	198	25.1	131.7	26	72	9.39	61.7
X2501_26	1129	497	735	188	532	1560	202	784	127.2	19.1	98.8	10.11	43.5	7.33	18.1	1.92	10.41
X2501_27	1374	241	203.4	1438	39.7	357	94.8	591	236	30.1	273	47.5	283	57.5	152	19	107.5
X2501_28	778	329	720	90.5	807	1372	126.8	446	61.4	13.5	54.7	4.96	20.2	3.61	8.88	0.974	5.84
X2501_29	221	196	681	48.9	94	264	32.8	127.9	16.7	5.83	16.5	1.79	8.17	1.67	4.72	0.603	4.26
X2501_30	947	423	499	236	1237	2630	277	905	128.2	19.8	109	10.74	48.5	8.54	21.5	2.32	12.9
X2501_31	1052	680	945	126.7	431	1202	155	615	93.2	19.1	75	7.65	29.9	4.9	11.4	1.15	5.96
X2501_32	323	200	193	613	8.22	42.4	11.17	95.6	58.8	12.1	108	19.6	116	23.7	60.1	7.04	43.1
X2501_33	708	294	734	573	434	1379	205	951	218	35.6	195	24	112.4	19.9	47.6	5.1	27.1
X2501_34	684	823	636	405	857	2030	257	1026	174	16.6	146	17.5	83.4	15.4	38.5	4.44	25.1
X2501_35	56.3	173	7700	152	197	678	104.6	455	83.9	21.8	68.3	6.84	30.1	5.14	12.06	1.278	7.4
X2501_36	293	308	458	603	518	1590	224	931	197	18.7	200	25.6	133.4	23.4	56.4	6.38	34.9
X2501_37	1318	489	991	227	278	859	109.4	438	75.4	18.5	72.5	8.94	45	8.9	23.5	2.87	16.8
X2501_38	581	213	408	296	44.3	275	60.1	329	79.3	15.9	74.8	10.69	57	11.28	30.5	3.86	23.7
X2501_39	1213	313	238	2250	170.5	765	138	729	292	48.6	387	74.5	468	96.4	258	30.8	157
X2501_40	809	240	395	72.5	339	436	36.5	122.7	19.1	5.02	20.5	2.32	13.1	2.81	7.68	0.968	6.27
X2501_41	499	617	722	622	684	1850	254	1087	223	21	220	26.8	135.8	25.4	62	6.75	36
X2501_42	1154	771	858	187	544	1580	203	805	125	19.9	98	10.01	41.3	7.03	16.3	1.68	9.75
X2501_43	920	375	489	610	133.1	616	118.6	628	223	47.2	218	30.6	146	23.6	57	6.52	36.7
X2501_44	220	190	320	111	122.4	369	44.7	173	30.5	7.2	30.9	3.63	18.9	3.89	10.8	1.37	8.59
X2501_45	474	208	537	386	700	1389	143	510	75.8	22.6	83.7	10.14	56.9	13.1	39.9	5.29	37.9
X2501_46	489	286	165.2	527	369	1345	218	1040	232	31.6	193	23.3	105.3	19.7	51.3	6.05	36.5
X2501_47	376	208	364	1708	452	1406	212	903	252	26.5	282	51.7	324	66.1	171	21.2	113.5
X2501_48	514	246	727	273	374	999	122.3	470	75.5	14.1	74	8.53	44.7	9.42	26.9	3.39	22.2
X2501_49	1724	298	148.2	2190	148	585	101.9	510	189	3.86	256	52.7	373	82.2	235	31.2	196
X2501_50	114.7	180	3790	88.4	40.6	192	35.1	189	44.2	12.8	40.5	4.76	21.1	3.34	6.98	0.637	3.17
X2501_51	235	213	1024	169	352	1068	124.5	446	65	8.52	57.6	6.01	28.5	5.49	14.8	1.69	10.35
X2501_52	743	229	263	2540	14.74	56.3	9.68	52.2	24.8	8.36	61.9	19.4	227	83.3	366	61.8	418
X2501_53	527	235	481	411	334	826	108.4	442	75.7	15.1	77.3	10.16	59.4	13.4	40.7	5.77	40.2
X2501_54	405	226	107.8	1137	86.6	320	63.5	410	175	36.1	236	37.7	221	44.9	113	13.3	74.4
X2501_55	954	336	644	284	799	1750	181	640	94.1	16.4	94	10.87	54	11.2	30.7	3.78	23.8
X2501_56	266	370	1746	160.7	1.06	2.74	0.79	7.33	7.99	3.96	21.3	3.85	24.8	5.44	15.3	2.01	11.74
X2501_57	213	222	1534	94.9	243	757	100.5	416	59.6	16.5	46.9	4.33	18.3	3.4	9.76	1.071	7.21

Sample ID	^{55}Mn	^{57}Fe	^{88}Sr	^{89}Y	La	Ce	Pr	Nd	Sm	Eu	Gd	Tb	Dy	Ho	Er	Tm	Yb
X2501_59	539	316	2770	336	737	1670	198	789	139	34.6	126	15	71.9	13.1	33.1	3.74	21
X2501_60	238	207	1286	172	1147	2850	292	1034	137.4	31.4	105.4	9.49	36.2	6.47	16.5	1.92	12.2
X2501_61	1188	264	352	206	1054	1710	147	477	62.7	9.86	61.3	6.75	33.8	7.42	20.8	2.76	18.7
X2501_62	857	351	685	211	538	1373	159.6	614	101.2	17.7	82	8.73	39.6	6.96	18.6	2.13	13
Red River (Southwest)																	
X2502_1	2740	388	177.4	1051	177.6	580	87.5	389	121.8	14.45	133.1	27.69	184.9	37.2	105.5	14.49	91.9
X2502_2	2666	408	231.8	1400	102.9	436	83.1	467	220.7	23.73	285	60.8	356	60.6	143.4	16.4	90.4
X2502_3	463	209	57.4	2410	269	1070	191	954	291	47.3	309	50.6	314	69.6	212	29.7	206
X2502_4	971	199	145.7	354	209	689	93.9	379	69.3	13.95	60.6	7.55	42	9.38	31.2	4.77	38.1
X2502_5	947	284	77.5	1722	139.5	607	111.9	605	323	9.61	448	89.9	455	59.3	113.3	12.21	66.2
X2502_6	2080	493	581	498	1301	3380	417	1510	253	28.7	190.3	21.97	105.6	18.94	50.1	5.86	34.7
X2502_7	1120	315	935	124	180	558	81.3	361	62.9	12.9	48.7	5.54	27.5	4.93	12.6	1.42	8.29
X2502_9	7910	699	61.7	2151	223.8	671	104.2	469	173.8	7.61	231	53.8	378	71.3	192	25.5	154
X2502_1	605	252	196	3170	111.1	431	86.6	569	271	29.4	395	74.9	512	107	308	43.1	296
X2502_2	1266	414	80.9	4650	393	1460	278	1470	585	18.2	699	123.6	817	176	529	82.7	494
X2502_4	701	266	242	592	587	1620	199	707	115	16.3	115	15	87.2	19.1	62.4	9.5	74.1
X2502_5	618	286	211	872	142	786	165	875	204	36.2	193	26.4	152	32.5	91.3	12.5	89.3
X2502_7	1117	458	851	393	1278	2340	243	816	129	21.2	122	14.5	72.1	15.2	41.3	4.89	29.7
X2502_8	56.2	234	610	29.8	0.092	0.575	0.148	1.19	0.78	0.247	2.26	0.435	3.18	0.879	2.78	0.309	1.6
X2502_9	310	345	432	919	767	1940	288	1310	285	44.3	282	36.7	195	36.3	91.7	10.54	59.2
X2502_10	2210	453	147.5	1555	108.6	444	86.9	463	207	22.9	300	64.8	400	72.7	171	21.5	118
X2502_11	497	295	279	1710	105.2	460	92.4	570	260	37.6	343	57	352	68.2	174	21.8	124
X2502_12	310	255	447	245	22.4	144	32.7	178	50.6	11.1	52.6	7.44	43.3	9.09	24.3	3.04	17.1
X2502_13	361	249	153.1	870	59	260	54	305	112	22.5	143	21.3	127	26.8	83	10.8	66
X2502_14	677	247	367	318	1.75	8.58	2.14	20.4	17.4	4.94	40.2	7.52	52.8	12.3	36.1	4.91	32.1
X2502_15	377	278	440	295	206	547	75.7	316	62.5	22.6	62.8	7.9	44.6	10.9	33.2	4.38	29.9
X2502_16	333	263	1925	186	99.7	393	69.5	331	68.5	18.1	60.9	7.33	37.4	7.31	18.8	2.18	12.5
X2502_17	583	251	137	2230	116.4	534	113	726	301	12.5	403	69.2	415	89.2	252	29.8	172
X2502_18	307	258	122.8	2010	149	544	109.3	647	237	28.6	314	50	308	67.4	195	26.3	167
X2502_19	607	259	148.3	625	2300	3740	321	1016	141	23.8	151	18	95	21.1	62.8	9.1	63.2
X2502_20	433	250	208.4	188	56.4	184	30.8	155	51.2	8.79	63.3	8.28	39	7.35	17.6	1.78	10.2
X2502_21	200.7	354	248	205	209	489	58.9	245	46.6	8.63	47.1	6.74	36.1	7.54	20.5	2.65	18.1
X2502_22	1698	387	231	1313	92.3	340	70.1	392	171	23.6	247	49.4	300	54.7	138	18	112

Sample ID	^{55}Mn	^{57}Fe	^{88}Sr	^{89}Y	La	Ce	Pr	Nd	Sm	Eu	Gd	Tb	Dy	Ho	Er	Tm	Yb
X2502_23	438	260	1044	54.2	121.2	391	55.9	225	31.4	10.14	24.1	2.29	9.41	1.76	4.83	0.609	4.32
X2502_24	985	586	1320	741	929	2300	316	1410	268	50.6	252	31.7	156	29.7	75.7	9.03	50.4
X2502_25	472	233	429	288	0.154	0.661	0.207	1.64	2.62	0.76	16.7	4.71	41.2	11.9	41	6.08	40.6
X2502_26	976	270	347	1222	67.7	269	56.7	333	170	27.4	256	49.1	293	52.9	122.8	14.2	84
X2502_27	257	279	186.4	318	3.03	12.6	2.45	15.9	9.1	3.25	23.5	6.1	53.5	12.5	27.1	2.25	7.88
X2502_28	953	238	77.1	2890	753	2310	358	1500	363	85	426	61.3	349	84	239	30.7	201
X2502_29	439	377	1336	308	808	1900	221	868	153	35.4	131	15.7	71.3	11.8	28	2.93	16.5
X2502_30	563	223	281	1930	5.73	29.1	6.61	49.1	39.7	6.64	112	26.1	204	48.9	153	21.9	148
X2502_31	2300	395	460	1620	879	2710	422	1960	459	52.9	451	65.2	355	68.1	169	18	97.1
X2502_32	416	285	563	1603	1001	2260	292	1289	261	27.8	282	42	244	56.7	164	22.4	136
X2502_33	1265	446	1203	350	260	741	116	558	133	29.9	123	15.6	74.5	13	31.4	3.79	21.6
X2502_34	263	233	587	157	227	480	72.5	437	118	21.8	107	10.5	41.7	6.64	13.2	1.22	5.94
X2502_35	263	210	610	130.8	352	1011	143	541	79.5	8.89	64.3	6.33	28.2	5.15	12.4	1.39	8.34
X2502_36	1003	659	1513	511	1063	2420	342	1350	238	42.6	217	25.4	128	22.9	55.2	6.04	35
X2502_37	251.1	237	430	554	3.59	31.7	15	168	98.8	21.9	134	18	100.5	20.9	53.7	6.51	38.4
X2502_38	236	332	396	741	548	1470	210	1024	225	37	233	30.2	157	29.7	70.8	7.37	40.3
X2502_39	455	231	695	143	275	553	57.8	225	32.9	17.1	37.7	4.21	22	4.61	13.3	1.65	9.9
X2502_40	182.2	212	1748	65.5	31.1	142	24.8	133	22.5	6.52	19.5	2.28	10.72	2.17	6.15	0.737	5.15
X2502_41	287	627	1830	195	527	1130	155	564	104	21.5	93	10.2	46.8	9.1	22.7	2.42	13.1
Miss. S. of Arkansas (not used in study)																	
X2601a_1	363	200	437	189	154	559	75.7	304	54.4	16.2	50.7	5.12	24.8	4.86	14.2	2.01	14.4
X2601a_2	1006	451	1600	532	1620	4310	409	1510	239	47.7	212	22.2	107.7	18.6	47.1	5.55	31.4
X2601a_3	135.7	296	171	550	825	3050	384	1500	482	6.18	501	58.8	197	18.6	21.9	1.006	4.33
X2601a_4	501	667	3380	144	296	791	92.1	349	64.4	16.7	58.9	5.96	28	4.96	12.45	1.38	7.88
X2601a_5	50	262	557	301	571	1201	128.7	496	88.3	17	85.6	10	53.6	9.97	26.2	3.3	18.3
X2601a_6	1098	275	189	2750	229	955	145.5	694	301	11.47	380	67.7	435	87.1	243	34.3	208
X2601a_7	2980	352	380	1060	120	517	86.9	453	192	15.7	220	36.7	219	37.2	88.4	10.84	59.9
X2601a_8	535	800	1308	272	297	942	120.9	526	112.3	36.4	104.4	11.6	56.7	9.74	22.3	2.37	12.33
X2601a_9	641	377	979	580	722	2040	218	853	174	29.1	167	20.4	109.7	21.2	55	6.7	37.8
X2601a_10	449	252	213	300	317	1174	142	581	120.9	25	111.6	11.26	54.2	9.89	25.1	2.88	18.2
X2601a_11	478	221	335	159.3	24.8	123.8	23.1	122.6	38.4	8.21	40.6	5.1	27.4	5.5	14.52	1.81	10.69
X2601a_12	1467	602	948	391	964	3210	329	1198	190	26.1	163	16.4	77.9	13.4	32	3.67	20.5
X2601a_13	479	208	335	141.2	37.3	126.2	17.2	76.2	23	11.1	28.4	3.75	20.6	4.24	11.73	1.573	11.16

Sample ID	^{55}Mn	^{57}Fe	^{88}Sr	^{89}Y	La	Ce	Pr	Nd	Sm	Eu	Gd	Tb	Dy	Ho	Er	Tm	Yb
X2601a_14	211	204	253	992	381	1700	221	976	253	6.06	277	38.8	198	33.9	78.4	8.86	45
X2601a_15	636	218	247	952	1169	3510	382	1430	261	15.2	245	31.3	168	33.2	84.3	10.56	58.1
X2601a_16	405	278	158.3	2150	64.7	236	38.1	185	86.5	34.6	156.5	32.3	266	68.2	212	32.4	210
X2601a_17	457	202	317	307	643	1850	198	663	111.4	12.3	98.6	10.95	55	10.77	28.6	3.51	20.8
X2601a_19	403	355	352	332	48.7	165	26.3	140	69.7	16.7	132	23.1	105.2	11.57	15.4	1.197	5.04
X2601a_20	171	184	525	36.5	48.8	157	19.8	80.6	16	6.97	13.9	1.31	5.57	1.081	2.86	0.329	2.28
X2601a_21	814	207	982	256	1103	2170	188	579	93	23.2	86.3	9.05	42.6	8.69	23.5	3.01	19.7
X2601_1	768	254	1028	287	1260	2420	201	757	108	26.8	95	10.3	49.5	10.4	28.7	3.67	24.7
X2601_3	2490	254	243	2390	231	1065	177	887	324	23.2	365	63.1	365	73.4	200	26.7	171
X2601_5	156	259	514	214	60.4	329	62	320	79	15.8	64.5	8.6	38.5	7.98	22.9	2.67	16.7
X2601_6	809	487	1860	460	1142	3060	345	1320	212	42.5	188	20.4	96.6	18	44.5	4.95	29.3
X2601_7	526	212	60.6	1910	223	940	149	748	215	78.8	283	42.7	240	55.2	160	21.3	158
X2601_8	84.5	247	148	237	1210	2130	157	430	49.1	6.9	54	5.97	30.8	7.15	22.4	2.89	20.5
X2601_9	274	230	463	371	90	380	57.3	311	76	12.5	91	12	63.5	13.7	36.5	4.2	26.8
X2601_10	825	303	1720	263	611	1570	150	535	81.7	18.6	74.8	8.16	38.8	8.23	23.6	2.97	19.9
X2601_11	268	292	408	169	1200	3080	289	981	130	14.9	97	8.57	33.7	5.86	15.5	1.65	9.35
X2601_12	1590	732	807	237	556	1670	201	790	135	25	115	12.5	52.3	9.3	23	2.46	14.2
X2601_13	447	724	674	642	920	2570	316	1190	241	27.7	228	28	134	24.5	58.7	6.39	34.8
X2601_14	511	208	381	497	419	1330	204	860	159	37.8	156	16.8	82	17	46.7	5.84	37.8
X2601_15	2250	459	1680	536	2270	5570	551	1830	230	39.9	194	19	86.1	17.1	48.2	5.97	38.7
X2601_16	470	218	355	915	2740	6390	594	2290	345	118	335	33.9	156	31.7	87.9	10.8	73.5
X2601_17	1357	323	441	2530	807	3930	586	2760	633	78.8	583	78.7	427	81.1	214	25.8	156
X2601_19	672	222	160	1410	466	1770	271	1270	317	19.2	303	46	248	49.1	133	16.2	102.2
X2601_20	930	674	798	337	1400	3830	386	1340	196	26.8	153	15.2	67.2	12.4	33.5	3.87	24.9
X2601_22	1132	258	168	1700	148	595	101.4	488	186	23.6	239	45	281	58.7	170	18.6	106
X2601_23	1151	647	931	138	463	1380	169	688	119	21.7	92.4	8.88	34.7	5.14	11.7	1.15	6.48
X2601_24	875	603	742	344	730	2150	255	962	160	22.2	132.4	14.9	73.8	13.4	35.9	4.19	24.6
X2601_25	277	194	270	50.7	93.6	241	23.8	93.8	13.2	6.38	13.4	1.42	7.19	1.61	4.96	0.674	4.85
X2601_26	1124	345	684	234	1050	2500	240	936	149	17.6	123	12.31	55.1	9.7	23.8	2.57	15
X2601_27	1269	568	915	348	906	2670	305	1202	186	23.9	147	16	71.4	12.5	32.1	3.51	19.8
X2601_28	240	179	611	342	281	1160	156	630	116	26.3	97	10.7	54.4	11.2	31.7	4.49	30.6
X2601_29	2620	428	81.5	4160	460	2020	321	1660	695	19.2	853	132	742	149	428	57.4	352
X2601_30	172	182	2300	203	168	604	75.9	273	49.9	7.38	42.4	6.02	34.2	6.67	18.8	2.46	15.1
X2601_31	1580	391	111.3	2630	333	1390	218	1070	376	26.6	415	75	449	85.8	226	29.5	187

Sample ID	^{55}Mn	^{57}Fe	^{88}Sr	^{89}Y	La	Ce	Pr	Nd	Sm	Eu	Gd	Tb	Dy	Ho	Er	Tm	Yb
X2601_32	6920	1840	505	950	644	1830	229	888	227	49.2	220	32.7	185	35	98	13.8	87.5
X2601_33	1225	403	736	190	1221	2290	182	581	76.4	16.1	71.8	7.04	33.4	6.46	18	2.07	13.22
X2601_34	339	1470	279	599	87	276	36.8	156	65.3	9.4	121.6	23.8	145.9	26.6	61.5	6.33	32.6
X2601_35	1239	516	733	207	461	1370	187	722	131.9	21	105.6	10.89	47.3	7.71	17.9	1.92	10.79
X2601_36	593	203	615	247	176	645	88.3	398	64.8	16.5	66	7.45	39.7	8.47	24	3.05	21
X2601_37	617	638	1281	557	628	1850	214	944	181	31.1	169	21	106.4	20.3	53.2	5.78	33
X2601_38	1245	719	729	224	457	1410	181	709	119.5	18.5	95.3	9.83	46.5	8.02	21.1	2.28	13.1
X2601_39	516	214	300	650	950	2730	297	1024	184	33.5	160	19.4	102.2	21.3	63.7	9.07	65.2
X2601_40	406	221	821	1047	53.6	378	108.1	731	273	77.3	263	37.2	193	37.8	103.5	14	91.6
X2601_41	321	196	284	396	21	69	15	103	57.6	10.6	89.8	13.9	76.6	15.5	39.9	4.5	23.8
X2601_42	388	240	579	65.4	415	720	71.7	232	28.4	10.69	26.6	2.37	10.82	2.23	5.94	0.703	4.33
X2601_43	212	258	104.1	163	159	279	30.3	123	27.2	7.08	32.7	4.82	29.3	6.31	17.8	2.23	13.2
X2601_45	551	260	425	146.3	540	1011	100	329	46.4	10.55	42.6	4.76	25.2	5.07	15	1.98	12.9
Arkansas River (Southwest)																	
X2602_1	291.7	202.6	1039	129.5	94.8	392	69.8	358	62.7	14.54	49.4	5.1	22.83	4.34	11.65	1.338	8.59
X2602_2	1688	392	180.1	1520	729	2142	296	1394	433	7.55	444	63.7	334	61.4	143.3	15.15	75.1
X2602_3	481	223.5	161.7	2306	220.3	895	183.9	1152	539	83.9	661	103.8	546	93.5	194.1	19.56	107.5
X2602_4	423	196.5	224.8	953	869	3100	424	1780	330	54.2	248	29.7	152	31.3	89	11.69	74.6
X2602_5	384	219.8	387.6	215	473	683	62.3	219.7	39.1	7.69	38.2	4.9	28.2	6.45	19.04	2.7	17.8
X2602_6	613	212.6	251.6	1136	225.2	751	124.3	652	204.6	16.25	198.5	29.3	174.2	38.5	114	15.54	98.4
X2602_7	874	221.6	291.4	1731	92	358	80.2	577	316	16.6	334	54.8	323	64.1	178.8	26.8	171.3
X2602_8	528	202.9	192.4	1066	66.4	311	66.6	407	162	10.21	162.6	27.4	167.6	35.2	97.1	13.08	74.9
X2602_9	835	231.4	190	240.1	1375	2316	204.4	693	112.3	8.38	81.3	8.4	39	8.04	22.6	2.92	18.28
X2602_10	504	211	118.9	2460	147.4	608	131.2	860	452	78.9	463	79.4	473	92.3	237	28.8	147
X2602_11	299.3	197.3	258.8	358	303	694	89.9	379	92.4	11.55	74.4	10.12	56.7	12.12	34.7	4.77	28.9
X2602_12	812	660	365	490	204.8	550	81.7	424	144.6	18.9	122.5	18.08	100.8	19.27	47.9	5.88	30.3
X2602_13	602	205.2	94.5	1500	363	1280	195	947	310	51.3	254	37.7	217	46.7	134.1	21	135
X2602_15	1601	561	1078	339	761	1844	218.4	866	179.4	25.1	107.3	12.63	63.3	11.87	31.8	4.28	25.1
X2602_16	503	226	361	166.8	96.7	278	37.5	162.3	39.6	10.1	31.7	4.11	23.8	5.06	15.44	2.35	15.51
X2602_17	815	217.1	130.9	8940	76.7	301	65.8	500	421	73.3	695	165.1	1211	278	811	121.9	711
X2602_20	368.1	210.3	438	780	570	1482	214.5	1018	242.8	23.31	209.2	28.23	148.6	28.6	71.2	8.98	51.1
X2602_21	843	628	995	790	758	2003	267.9	1202	232.6	34.9	225.3	30.3	157	29.8	75	8.42	50.2
X2602_22	357	188.6	523	22.6	4.21	17.2	3.3	19.1	4.8	1.12	6.22	0.75	3.92	0.772	1.99	0.216	1.42

Sample ID	^{55}Mn	^{57}Fe	^{88}Sr	^{89}Y	La	Ce	Pr	Nd	Sm	Eu	Gd	Tb	Dy	Ho	Er	Tm	Yb
X2602_24	399	269	1442	587	1387	4020	483	1930	258	47.8	231	26.2	127.1	23.1	58.1	6.02	36.7
X2602_25	960	231	133.2	1296	99.5	424	80	426	138.3	17.27	197.3	44.4	288	51.3	105.4	9.28	53.2
X2602_26	421	195	194.9	1084	77.1	394	81.8	432	140.5	21.4	180.9	36	226	42.6	98.7	9.94	53.3
X2602_27	2030	384	293	692	1820	4470	440	1550	188	26.7	201	23.2	119.1	23.5	64.7	7.69	53.6
X2602_28	277	186	848	130.8	297	795	89.3	353	39.3	13.89	40.2	4.32	20.8	4.23	12.01	1.43	10.85
X2602_29	2170	304	158.8	2330	244	1048	179	863	214	27.8	258	47.3	343	79.8	249	32	209
X2602_30	954	237	231.5	1608	556	1573	184.1	777	167	58	237	37.7	243.7	53.2	154	18.95	130.5
X2602_31	1511	255	153.4	2000	137.8	650	129.2	726	261	38.9	390	71.9	443	81.2	194	21.3	122.8
X2602_32	1408	535	1036	290	1259	3290	337	1223	139.3	26.2	124.2	13.13	60.6	10.79	27.5	2.98	18.7
X2602_33	1442	263	14.64	1169	2179	5930	712	3020	461	115.4	448	52.1	251	44	103.1	10.28	60.5
X2602_34	509	267	1122	508	582	1738	224.1	1008	167.2	44.2	179	21.16	109	19.83	49	5.11	31.1
X2602_35	1189	332	682	321	1296	3110	306	1092	132.2	24.6	116.6	12.16	56.9	10.55	27.9	3.23	21.6
X2602_37	592	283	568	1341	2206	5290	609	2474	405	65	395	51.1	280	52.7	136.9	15.83	97.6
X2602_38	476	257	615	93.2	258	648	78.4	295	41.7	9.56	36.5	3.65	17.03	3.18	8.35	1.002	6.86
X2602_40	794	218.2	256.5	1674	100.5	486	120.3	864	313	28.8	396	59.6	356	70.7	177.6	19.9	113.8
X2602_41	222.6	176.5	3010	126.5	406	1246	166.4	669	83.9	22.1	63.8	5.63	24.1	4.34	11.38	1.3	8.94
X2602_42	671	191	125.5	3000	6.39	63.6	21.3	198	160	8.05	344	75.5	535	112	283	33.5	185
X2602_43	172.4	182	229.1	94.5	17.45	70.1	14.46	83.8	23.4	5.9	22.6	3.02	15.38	3.13	8.76	1.214	8.99
X2602_44	440	208	103.6	1630	88	318.7	62.7	392	181.8	42	287.3	47.2	293.8	59.3	150.4	16.73	93
X2602_45	744	201.7	248.6	1574	207.6	803	144.2	758	265.2	27.7	283	45.2	273	54.9	146.5	18.56	111.6
X2602_46	1106	206	125.8	1830	23	207	49.4	303	163	9	283	53.3	352	67.9	175	21	120.6
X2602_47	645	365	191.6	1512	102.6	501	100	592	283	20.6	386	64.7	339	54.5	115.5	12.17	70.1
X2602_48	305	262	188.9	1330	571	2130	292	1220	254	26.2	250	36.6	221	46	135	18.2	116.3
X2602_49	649	217	184.6	1383	21.8	134.8	33.5	236	131.5	16.8	201	40.8	257	47.4	109.3	12.02	60.9
X2602_50	808	206	397	145.1	501	1320	139.6	526	81.1	9.51	63.7	6.08	25.4	4.44	11.62	1.296	8.41
X2602_51	290	187	315	120.4	214	382	35.4	124.2	21.2	8.91	21.6	2.73	16.5	3.71	11.96	1.72	12.54
X2602_52	304	486	917	179	268	700	87.7	383	74.1	23.6	66.9	7.84	38.1	6.91	16.06	1.81	10.09
X2602_1	443	299	271.1	602	728	1545	171.5	697	134.8	14.27	141.5	19.35	104.7	20.68	55.3	6.77	41.8
X2602_2	1049	252	190.9	849	0.357	1.65	0.595	10.12	21.5	11.34	74.6	16.79	125.2	29.6	90.3	13.26	89.9
X2602_3	487	316	335	270	243	921	135.1	610	106.4	18.32	86.4	9.98	49.8	9.23	24.8	2.95	18.47
X2602_4	840	1250	1177	2940	817	2260	365	1840	598	51.3	695	115.1	672	129.4	303	32	168
X2602_5	1469	903	1167	340	1396	2610	293	1163	181.4	29.2	140.6	14.9	67	12.31	31.9	3.74	22.8
X2602_6	1586	399	244.4	3360	202.2	960	199.1	1181	497	61.1	565	103.9	631	119	311	37.9	213
X2602_7	467	1064	1022	255.1	296.4	706	101.8	502	100.9	31.6	93.1	11.11	53.8	9.55	22.4	2.4	13.48

Sample ID	^{55}Mn	^{57}Fe	^{88}Sr	^{89}Y	La	Ce	Pr	Nd	Sm	Eu	Gd	Tb	Dy	Ho	Er	Tm	Yb
X2602_8	411.3	1017	327.4	1016	1511	3252	417	1812	344	8.91	297.3	38.1	196.3	36.2	91.9	10.34	58.5
X2602_9	2315	337	269.7	982	47.2	248.1	58.5	400	174.2	37.9	207.9	36.3	209.3	37.6	92.2	10.79	59
X2602_10	1297	317	49.7	2281	1502	5390	819	4140	856	91.1	742	94.1	468	85.8	206.1	22.37	126
X2602_11	1158	326	379.2	491	493	1468	220.6	1006	168.1	31.5	128.2	14.42	71.8	14.55	41.2	5.19	34
X2602_12	510	310	1591	130.1	232.8	659	93.2	435	67.7	12.55	56.8	5.56	24.3	4.41	11.05	1.18	7.16
X2602_13	322	1153	954	649	440	1193	179.4	938	210.3	46.6	197	25.4	131.9	24	56	6.03	33.9
X2602_14	1122	297	355.7	551	906	1737	184.2	712	113	12.39	110	14.41	79.9	17.12	49.9	6.36	40.6
X2602_15	384	265	412	625	79.6	358	66.5	370	83.6	15.35	87	12.15	73.5	17.33	56.1	8.1	60.6
X2602_16	353	288	78.9	2220	101.1	338	64.9	415	175	24.8	276	49.2	323	72.8	210	26.4	158.2
X2602_17	980	277	315.6	1464	81.7	309	66.4	476	205.4	55.3	283	44	261	54.1	145.7	17.65	101.7
X2602_19	476	241	465	1450	127.6	509	104.4	669	233.7	36.4	275.4	44	258.4	50.7	129.7	15.63	91.7
X2602_20	524	1356	1259	388	404	979	139.8	704	145.2	43.5	135.2	16.49	81.8	14.35	34.8	3.66	20.39
X2602_21	1276	330	730	420	116.9	321	51.1	270	76.1	15.92	82.8	11.89	67.5	13.57	37.1	4.86	32.5
X2602_22	655	307	424.3	236.4	123.1	346	51.2	253.5	51	17.05	50.5	6.31	35.6	7.77	22.94	3.05	21.7
X2602_23	900	354	149.2	2065	182.5	765	151.6	863	304.2	28.95	303	53	335	67.5	198.4	27.8	167.6
X2602_24	283	203	466	100.4	40	142.3	23.7	126.7	22.7	5.01	23.1	2.63	14.2	3.32	9.27	1.2	8.72
X2602_25	342.1	237	495	260	76.2	239.2	38.8	211.8	52	12.54	56.4	7.14	38.8	8.15	23.7	3.16	22.4
X2602_26	420.7	289	228	1165	167.9	592	109.8	632	179.4	47.3	200.5	29.5	172.8	37.8	108.8	14.15	95.7
X2602_27	379	763	810	274.3	280.6	660	95.2	469	96.3	25.8	90.6	11.21	55.6	9.9	23.4	2.54	14.08
X2602_28	418.6	392	240.9	541	755	1699	202.2	850	157.8	11.02	156.5	19.42	101	19.03	47.2	4.99	26.6
X2602_29	346.1	221	296.1	293	2.01	11.72	3.86	40.7	30.4	3.88	47.5	7.65	47.2	9.74	26.7	3.66	23.2
X2602_30	424	494	1798	428	398	1233	190.5	915	184.9	47.2	150	18.45	92.7	16.51	40.2	4.49	26.8
X2602_31	500	255	437	311	622	1165	120.3	494	83.8	26.6	83.9	9.31	46.3	9.22	24	2.62	15.88
X2602_32	426	247	284.4	1165	191.6	872	176.1	1019	254	51.8	252	33.6	183.5	37.9	107.2	12.98	80.1
X2602_33	531	303	150.2	4740	164.3	663	137.5	929	459	54.9	691	129.9	811	164.9	438	52.7	298
X2602_34	782	226	193.4	1164	108.6	333	62.8	367	137	32.2	180.2	28.1	166.2	36.3	101.6	12.91	83
X2602_35	1186	412	376.9	451	1348	2093	223	869	144.3	11.13	134.3	16.18	82	16.14	43.3	5.33	32.7
X2602_36	1818	489	140.6	3310	241	908	176.4	1037	450	67.9	568	109.5	674	126.2	325	40.5	237
X2602_37	429	230	580	76.4	443	631	58.7	217	27.5	9.18	24.7	2.62	13.09	2.57	7.31	0.882	6
X2602_38	215.4	199	2724	253.9	349	1310	209.9	975	143.2	31.9	99.8	10.33	44.9	8.16	21.9	2.51	16.72
X2602_39	1452	345	148.8	2150	199.8	632	106.5	572	219	20.5	274	56.1	379	77	208	26.1	149
X2602_40	739	348	1019	1172	33.8	132.8	27.7	196	92	15.63	131	26.6	180	38.6	113.5	15.32	93.9
X2602_42	492	250	415	25.3	8.78	27.5	4.3	22.9	5.25	0.8	6.21	0.775	4.09	0.887	2.36	0.274	1.85
X2602_44	322	235	554	133	66.4	182	27.7	146	31.5	8.63	31.9	4.02	21.4	4.39	12.4	1.56	10.3

Sample ID	^{55}Mn	^{57}Fe	^{88}Sr	^{89}Y	La	Ce	Pr	Nd	Sm	Eu	Gd	Tb	Dy	Ho	Er	Tm	Yb
Miss. S. of Ohio (not used in study)																	
X2603_1	380	246	309	281	59.9	299	58.8	336	106.9	11.6	93.5	11.25	55.8	9.76	24	2.77	15.5
X2603_2	261	243	230	3410	183	692	124.6	741	305	6.55	460	87.2	577	120	317	36.3	182
X2603_3	1960	574	630	245	587	1620	181	633	97.4	17.5	84.7	9.58	44.7	8.4	21.7	2.65	15.85
X2603_4	1244	242	391	1630	120.6	614	125.2	726	264	45.2	280	44.9	272	52.1	143	18.8	119
X2603_5	1109	224	207	1610	115.7	530	97.8	547	236	24.3	295	54.6	313	53.6	125.5	15.4	93.6
X2603_6	1342	221	680	227	256	766	98.6	420	85.4	13.9	83.5	9.38	43.5	7.65	19.4	2.14	13.07
X2603_7	276	314	735	383	608	1710	197	860	164	35.1	147	17.3	84.2	14.5	33.7	3.55	19.1
X2603_8	909	465	861	203	626	1800	217	830	149.2	26.9	113.7	11.83	47.5	7.53	17.41	1.771	9.6
X2603_9	5600	540	426	1149	87	420	81.2	444	193	47	245	45.2	262	45.9	104.7	11.91	70.2
X2603_10	969	653	396	826	997	2730	288	1105	215	18.3	195	27.2	145.5	28.7	78.5	9.89	60.4
X2603_12	268	222	253	113.6	1.26	5.6	1.11	9	7.8	3.68	17.2	3.01	20.2	3.96	10.83	1.29	8.34
X2603_13	1138	249	351	271	1261	2220	214	830	134.6	11.94	121.2	12.33	56.8	9.65	24.3	2.53	14.6
X2603_14	1076	331	1021	550	231	738	120.7	575	172	34	177.8	23.1	115.4	19.6	44.4	4.62	25.1
X2603_15	140.8	236	252	1128	15.2	60.5	11.97	69.3	37.3	8.84	83.2	19.6	149.6	33.7	90.7	10.37	53
X2603_17	1121	876	1707	428	929	2610	313	1183	207	38.5	166	18.3	86.7	15.4	40	4.54	26
X2603_18	218	206	3920	107.8	113.1	493	83.2	394	73.9	18.6	56.2	5.4	21.1	3.55	8.36	0.918	5.94
X2603_19	1790	633	76	2560	193	839	143.5	721	276	24.5	349	66.5	427	82.2	204	24.4	141.7
X2603_20	209.4	229	2182	329	489	999	140.2	644	131.6	30.3	124.1	14.58	70.6	12.44	29.5	3.24	17.63
X2603_21	550	218	683	181	853	1314	96.7	311	44.6	12.31	46.5	5.23	27.1	5.77	17	2.31	15.73
X2603_22	1376	227	312	3180	378	1600	239	1116	344	24.5	363	66.1	424	90.5	267	39.2	255
X2603_23	412	261	327	423	261	798	107.8	479	115.1	59.5	112.7	14.2	76	14.39	39.5	4.98	31
X2603_24	418	209	421	45.4	75.1	255	30.6	123	19.1	4.23	16.9	1.85	8.66	1.75	5.12	0.694	4.88
X2603_25	766	233	394	353	497	1150	116	404	67.5	23.9	68.4	8.52	47.9	10.47	32.1	4.5	31.8
X2603_26	412	211	299	450	236	822	125	553	120	16.2	113	14.5	77.4	15.1	42.1	5.13	31.1
X2603_27	815	535	1740	186	1450	2900	247	870	122	24	100.2	9.18	37.1	6.58	16.8	1.89	12
X2603_28	294	203	329	457	86	426	85.5	464	134	20.1	119.2	15.4	78.9	15.11	40.7	5.08	31.7
X2603_29	1379	1239	485	847	572	2100	277	1244	346	14.08	314	40.5	187	30.2	64.2	6.51	34
X2603_30	1216	823	853	204	584	1980	227	852	133.7	19.7	101.8	10.2	42.9	7.13	17.4	1.88	10.88
X2603_31	681	387	460	380	791	2650	289	1042	185	22.5	153	17.4	84.2	14.7	36.5	3.98	21.9
X2603_32	583	1011	1163	461	714	2030	212	824	141	19.5	118.7	15.15	77.4	14.75	37.8	4.54	26.1
X2603_33	546	824	1000	334	526	1660	188	757	134	26.6	132	14.6	69.8	12.8	30.9	3.58	20

Sample ID	^{55}Mn	^{57}Fe	^{88}Sr	^{89}Y	La	Ce	Pr	Nd	Sm	Eu	Gd	Tb	Dy	Ho	Er	Tm	Yb
Upper Mississippi River (Northern)																	
X2701_1	419	226	885	347	78.7	566	127	755	175	36.4	136	15.6	70.3	12.5	30.9	3.59	21.7
X2701_2	737	570	312	4520	2300	7320	891	3580	743	69.5	703	110.5	671	145.1	429	57.5	354
X2701_3	149.5	236	202	795	550	2270	349	1740	404	25.1	331	38.3	180.4	31.1	73.6	7.62	40.5
X2701_4	412	250	315	755	124	559	113	680	220	42.2	215	27.3	145	26	67.7	7.89	45.1
X2701_5	445	227	642	168	188	660	96	408	71.6	18.7	56.7	6.29	29.6	5.36	14.3	1.94	13.5
X2701_6	696	212	206	699	1303	3940	469	1880	322	26.1	279	30.4	143.8	26.3	64.2	6.64	35.7
X2701_7	560	228	523	135.9	8.42	30.8	5.42	30.8	12.5	4.38	19.6	3.76	26.4	5.91	16.78	2.29	13.53
X2701_8	490	857	1083	533	472	1400	186	803	169	27.9	183	23.3	119.9	22.5	53.4	5.38	28.6
X2701_9	185	212	273	85.7	440	940	80.9	266	34.4	16.2	29.7	2.86	13.18	2.67	7.65	0.94	6.07
X2701_10	319	513	185.5	1079	751	2210	286	1218	271	3.82	291	40	212	39.5	94	9.86	49.3
X2701_11	143.5	193	1224	34.3	193.8	613	71.4	274	32.3	7.03	23.5	2.02	7.66	1.281	3.25	0.323	1.86
X2701_13	245	180	373	704	514	1710	248	1158	233	38.1	213	25.4	128.2	25.1	66.7	8.08	50
X2701_14	165.1	184.9	1139	565	78.5	296	61.9	401	139.5	38.1	156.1	18.91	94.5	18.23	48.4	5.99	38.4
X2701_15	313	194.4	450	282	762	1796	206.3	829	126.8	18.93	104.8	10.61	48.3	9.17	25.8	3	19
X2701_16	407.1	190	305	72.9	236.7	589	80.6	347	49	19.97	37.6	2.96	11.24	2.16	5.82	0.672	4.73
X2701_17	175.8	186.3	6250	318	90	560	131.9	841	207	42.5	167.1	17.13	73	12.1	29	3.14	18.2
X2701_18	638	225	288	316	227	821	99.8	415	86.5	25.5	82.7	10.27	49.9	10.25	28.4	3.53	22.3
X2701_19	1272	269	93.2	3590	222	931	155.6	759	334	19.48	433	86.6	553	109.4	289	36.1	211
X2701_20	230	205	610	154	62.2	289	54.8	275	63.8	15.8	53.3	5.82	28.5	5.42	14	1.6	9.86
X2701_21	294	194	752	30.7	6.05	22.2	3.95	22.8	6.38	2.23	6.66	0.72	4.01	0.887	2.73	0.434	2.98
X2701_22	80.3	172	2600	203	13.3	75	18.3	138	69.9	19.8	82.6	10.05	45.1	7.31	16.5	1.73	9.1
X2701_23	667	225	180	1800	333	1310	213	1070	358	45.6	392	51.3	272	53.9	148	18.2	121.3
X2701_24	312	200	684	64.9	98.6	353	54.1	220	31.5	8.65	22.5	2.25	9.61	1.94	5.33	0.653	4.5
X2701_25	385	236	1004	365	138	545	101.9	530	137	31.4	127.4	15	69.7	12.76	33	3.88	23.8
X2701_26	421	218	383	335	92.4	327	59.4	357	114.6	35.8	122	13.62	67.4	12.55	31	3.62	22
X2701_27	210	225	1250	229	417	1690	205	843	126	49.6	92.5	8.96	38.4	6.75	19.6	2.48	15.8
X2701_30	382	216	433	296	139.4	582	94.4	488	132.6	35.2	104.2	12.58	59.3	10.41	26.7	3.07	18.7
X2701_31	290	183	583	78.9	29.4	111.4	19.5	99.3	23.6	8.77	25.3	2.67	12.5	2.58	6.96	0.854	5.48
X2701_32	453	218	282	418	365	1910	301	1320	260	22.9	206	22.2	97.2	15.6	32.6	2.86	13.4
X2701_33	541	249	242	1140	133	483	88.3	470	151	30.8	204	32.8	194	39.2	106	12.5	69
X2701_34	208	173	203	889	29	135	26.6	174	71.8	9.05	119.6	21.4	142.3	31.7	88	10.76	57.5
X2701_35	732	212	363	294	563	1810	203	800	124	19.7	98.9	10.35	49.1	9.5	26.5	3.16	20.1
X2701_36	312	206	465	51.2	220	759	96	371	47.3	7.62	30.7	2.45	8.93	1.67	4.31	0.429	2.6

Sample ID	^{55}Mn	^{57}Fe	^{88}Sr	^{89}Y	La	Ce	Pr	Nd	Sm	Eu	Gd	Tb	Dy	Ho	Er	Tm	Yb
X2701_37	241	232	1097	91.3	211	855	124.9	503	74.6	13.8	53.6	5.05	19.8	3.29	7.88	0.841	4.98
X2701_38	219	215	419	70.1	219	822	101	417	60.5	7.71	41.3	3.7	14.42	2.34	6.28	0.63	3.68
X2701_39	685	832	939	587	729	2220	252	1023	193	25.9	175	21.7	112.1	21.2	53.6	6.1	34.9
X2701_40	489	220	357	299	257	926	120.5	540	97.5	13.12	92.8	10.41	50.7	10.03	26.5	3.02	18.23
X2701_41	375	198	384	764	12.3	80	24.4	239	132	15.5	166	24.9	139.7	27.5	71.8	8.68	50.3
X2701_42	464	220	257	912	166	581	92.8	459	147.8	14.4	180	27.1	158.4	30.3	83.8	11.03	71.2
X2701_43	258	216	188.5	591	88	382	71	378	112.4	34.8	113.4	16.6	97.5	19.56	54.9	7.46	49.3
X2701_44	567	299	480	207	418	1110	126	537	96.5	32.8	91.9	9.69	44.2	7.71	17.5	1.76	9.15
X2701_45	100.2	238	1370	263	279	1098	152	697	141.5	37.7	105.3	10.89	46.6	8.12	20.9	2.46	15.8
X2701_46	1282	532	772	172.5	472	1450	181	749	121.3	15.93	85.3	8.63	36.5	6.05	14.9	1.577	8.98
X2701_47	280	205	262	301	92.7	354	62.7	332	94.8	13.6	95.5	11.52	55.5	10.39	26.5	3	17.7
X2701_1	317	437	219.7	1243	688	1719	251	1248	277	28.5	317	40.9	215	43.2	108.8	11.34	61.2
X2701_2	1519	334	571	313	439	963	115.3	468	78.7	17.5	76.1	8.64	43.4	8.67	24.8	3.45	24.9
X2701_3	485	648	371	114	993	1492	130	414	50.6	10.84	46	4.67	22.4	4.17	10.7	1.301	8.24
X2701_4	406	326	569	98.3	648	1194	120.9	438	55.3	8.48	42.2	4.35	18.7	3.6	8.86	0.99	5.7
X2701_5	484	362	155.9	1035	42.1	177.3	35	208.5	78.4	16.13	79.7	19.39	158.4	35.5	100.3	14.9	107.1
X2701_6	320	303	171.3	1324	114.1	324	53.9	342	159.8	11.87	264	42	250	51.7	128.3	13.76	72.4
X2701_7	748	302	346	176	1133	2380	257	900	109.7	15.57	81.4	7.35	29.2	5.33	15.3	1.81	12.85
X2701_8	325.1	237	427	930	14.34	78.7	22	185.7	107.4	7.78	153.3	28.2	173.2	33.7	84	9.29	47.7
X2701_9	207.9	242	794	98.5	54.4	202.2	34.5	193.4	41.9	10.81	35.2	3.81	17.95	3.37	9.14	1.131	7.35
X2701_10	248.4	286	509	67.6	55.7	170.4	27.4	139.7	31.7	8.04	24.9	2.71	12.22	2.15	5.52	0.638	3.83
X2701_11	413	266	304	294	680	1754	227	1015	169	18.4	136.2	15.21	68	11.67	27.9	2.78	14.9
X2701_12	469	805	433	680	1855	3820	445	1729	271	32.4	221	26.3	126.6	22.7	57.4	6.5	37.1
X2701_14	187.6	270	1357	64.6	347	821	103	421	55.8	12.7	41.5	3.7	13.83	2.21	5.3	0.522	3.5
X2701_15	353	313	463	292	230	783	127.5	613	116.2	23.3	97.4	11.27	57	10.89	28.4	3.32	20.6
X2701_16	335	275	320	208.1	303	789	109.6	522	88.9	10.56	72.3	8.19	39.3	7.6	20.8	2.59	16.8
X2701_17	753	402	321	234	24.4	79.4	13.3	87.1	27.4	8.71	38.8	5.98	38.6	8.72	25.6	3.17	19.2
X2701_19	499	297	272	260	183.9	508	70.2	334	73.1	9.18	71.5	8.05	41.8	8.43	23.5	2.91	19.2
X2701_20	593	310	123.2	1750	178	516	85.3	438	154	12.6	215	38.9	254	54.1	150.6	18.9	112.1
X2701_21	677	380	307	277	500	1363	178	709	112.1	19.8	88.4	9.25	43	8.13	23	2.91	20.2
X2701_22	602	486	274.4	1520	9.52	64.3	18.57	165	132.3	11.5	239	48.8	304	54.9	121.8	12.2	58.5
X2701_25	254.9	263	462	587	55.7	252	59.9	411	150	19.6	165	21.4	101.6	18.3	45.6	5.27	32.5
X2701_27	396	266	627	79.5	122.2	364	54.6	273	49.9	13.2	39.3	3.57	14.09	2.52	6.44	0.734	4.92
X2701_28	447	268	261	508	45	151.7	30.6	226	91.2	16.2	118.8	15.8	86.9	17.7	47.8	5.96	38.6

Sample ID	^{55}Mn	^{57}Fe	^{88}Sr	^{89}Y	La	Ce	Pr	Nd	Sm	Eu	Gd	Tb	Dy	Ho	Er	Tm	Yb
X2701_29	327	261	1279	64.9	245	743	112.9	544	80.2	19.1	47	3.8	12.88	1.98	4.92	0.532	3.19
X2701_30	297.3	303	603	155.6	27.38	142.2	33.4	222.4	56.4	13.12	48.8	5.94	29	5.32	13.04	1.502	8.86
X2701_31	353	269	530	90.3	4.47	17.9	4.97	47.3	18.3	4.17	23.6	3.01	16.5	3.3	9.11	1.14	6.66
X2701_32	435	1709	230.8	1880	805	1988	282.7	1443	370	44.5	413	61.3	337	64.9	162.5	18.77	108.3
X2701_34	269	301	512	98.1	51.6	183.2	34.1	196	44.5	8.13	38.2	3.88	17.5	3.12	8.44	1.005	6.77
X2701_36	345	275	242.8	91	463	1056	114	407	45.5	15.1	38	3.34	14.2	2.75	7.65	0.887	6.3
X2701_37	322	224	324	420	116.1	798	215	1181	222	18.7	139.1	15.71	67.7	11.46	28.5	3.07	17.6
X2701_38	762	820	218	1920	632	2690	470	2590	585	31.1	533	70.6	365	67.5	168	19.2	109.4
X2701_39	343	306	152.5	820	204	665	107	592	161.4	19.8	178.2	24.6	135.5	26.7	74.1	9.88	69.6
X2701_40	517	750	228	1410	55.4	216	44.9	296	136	19.7	212	38.3	237	49.2	130	15.7	93.5
X2701_41	893	1158	951	153.2	483	1231	172.3	805	129	19.6	89.6	8.64	35.2	5.8	13.75	1.445	8.47
X2701_42	170.4	262	260	295	180.7	528	80.7	397	79.3	13.2	77	9.64	52.7	10.48	30	3.96	26.6
X2701_43	431	265	560	313	154.3	481	77.1	380	86.9	22.2	82.3	10.19	53.4	10.34	28.7	3.8	24.4
X2701_44	107	251	3620	271	1085	2660	337	1430	242	64.1	180	20.1	81.7	12.02	25	2.27	11.01
X2701_45	251.7	276	1066	61.3	934	2140	231	867	94.6	16.4	58.4	4.57	15.1	2.36	6.01	0.523	3.17
X2701_46	228	277	1624	257	385	1465	257	1326	222	38.2	148.1	14.18	56.2	9.41	24.2	2.82	18.2
X2701_47	1209	317	202.5	2360	289	1012	199	1208	508	20.2	639	87.1	451	79.5	206	27.8	176
X2701_48	297	514	124.3	1480	142.9	626	140.7	920	487	12.67	718	113.2	473	54	84.6	6.8	30
Missouri River (Missouri)																	
X2703a_1	366.3	195.5	430	189.6	362	841	101	378	54.9	17.6	52.2	5.76	28.2	5.99	17.44	2.18	14.23
X2703a_2	1200	304	1185	575	1189	2109	245.1	959	167.9	28.8	163.1	20.75	102.3	20.59	55.7	6.51	37.6
X2703a_3	460	220	442	284	1042	1924	194.8	648	95.3	16.77	92.3	10.42	50.3	9.88	27.2	3.19	18.45
X2703_1	679	717	1577	285	332	746	102.3	460	91.8	20.3	81.4	10.45	55.3	10.66	27.8	3.28	17.2
X2703_2	453	205	324	1300	61	315	79.9	534	300	34.3	361	55	308	53.6	124	13.1	65.7
X2703_3	675	419	3900	517	780	1626	218	922	196	39.3	174	20.8	107.1	19.6	49.8	5.62	30.4
X2703_4	506	748	905	656	1064	2390	301	1216	226	24.4	201	24.8	135.5	25	65.4	7.6	40.3
X2703_5	398	740	2023	305	626	1275	158.7	628	124.9	22.1	108.7	12.71	66.8	11.79	29.6	3.33	18.1
X2703_6	1254	603	951	606	1673	3410	382	1478	234	35.8	190	22.5	121.8	22.2	58.7	7.03	40.1
X2703_7	1426	592	472	752	1551	3540	473	1915	322	31.7	272.4	32	167	28.8	73.2	8.3	44.7
X2703_8	1614	643	934	418	1208	2570	316	1236	214	34.3	165	18.2	93.4	16	41.5	4.71	26.8
X2703_9	733	384	3250	564	843	2110	250	1045	219	52.1	187	22.4	119	20.6	50.7	5.9	33.3
X2703_10	497	227	341	644	243	880	145	671	162	27.2	146	18.7	111.5	21.6	60.4	8.24	53.6
X2703_11	1383	704	856	325	766	1870	252	984	173	21.3	134	14.4	72.7	12.4	31.7	3.68	20.5

Sample ID	^{55}Mn	^{57}Fe	^{88}Sr	^{89}Y	La	Ce	Pr	Nd	Sm	Eu	Gd	Tb	Dy	Ho	Er	Tm	Yb
X2703_12	1038	222	474	511	471	1410	176	684	132.6	22.7	117.9	14.9	92.4	18	52	7.02	46.2
X2703_13	295	238	126	1800	190	610	112.2	650	262	10.93	320	54.9	360	69.2	182	20.5	102.5
X2703_14	1500	630	765	510	1330	3770	397	1413	239	34	187	20.8	102.6	18.7	48.4	5.67	32
X2703_15	448	526	8910	117.7	201	484	60.5	257	54.2	15.72	48.3	5.53	26.3	4.5	10.88	1.162	6.37
X2703_16	234	255	831	48.7	98.6	210	22.8	80.2	14.4	5.72	15.7	1.6	8.01	1.69	4.38	0.541	3.36
X2703_17	454	219	178	1600	2350	8600	1037	3670	618	37.2	520	60.5	304	55.9	146	17.76	108
X2703_18	1540	920	1240	206	838	2280	236	820	110	20.3	87.3	9.15	42.9	7.81	19.7	2.29	12.3
X2703_19	1690	816	741	202	486	1590	204	776	123.1	19.4	89.6	9.5	42.1	7.29	18.5	2.08	12.15
X2703_20	984	206	470	421	101.1	357	56.1	306	91.5	19.6	101.9	13.8	78	15.9	43	5.21	32.5
X2703_21	724	218	1960	433	4330	7850	681	2100	288	43	232	19.5	83.4	15.3	40.8	4.5	27.4
X2703_22	512	207	391	535	193	700	106.7	519	139	20.9	130	16.7	86.3	17.4	48.2	5.99	37.4
X2703_23	1072	789	1107	421	927	2900	317	1198	197	24.8	154	18.1	84.3	15.7	41.3	4.8	28.1
X2703_24	931	628	1550	299	1022	2490	263	943	140	38.9	126	13.7	62.3	11.53	27.1	2.92	16.1
X2703_25	55.3	206	1151	344	3.77	18.7	4.33	35.3	25.9	15.8	63.9	11.84	70.7	12.52	28	2.7	12.77
X2703_26	1560	638	787	287	575	1590	183	641	106.1	19.9	92.7	10.84	55.5	10.31	26.4	3.21	18.6
X2703_27	511	320	404	614	99.1	426	75.1	435	126.3	33.9	149.6	21.4	112.6	22.8	59.5	7.19	44.3
X2703_28	667	310	332	974	205	1320	240	1340	361	12.97	361	47.5	217	37.1	78.7	7.62	38.1
X2703_29	714	857	1694	320	427	1180	151	618	112.7	24.2	99.7	12.81	60.7	11.01	27.4	3.04	17.7
X2703_30	1870	920	801	247	509	1450	181	728	117.8	20.7	95.1	11.01	48	8.26	20.6	2.33	14.81
X2703_31	1210	905	1273	265	1270	2770	257	839	111	21.4	93.8	10.4	48.6	9.02	23.5	2.83	18
X2703_32	350	240	424	379	490	1546	191.4	815	123.5	48.7	112.5	12.58	56.3	11.51	30.8	3.8	26.9
X2703_33	574	236	1597	528	6430	17500	2060	7410	864	173	536	51.9	171	22.8	49.4	3.65	19.1
X2703_34	636	228	271	170	1091	2720	243	818	82.1	14.9	63.9	6.01	25	4.63	12.84	1.48	10.76
X2703_35	593	203	372	259	248	743	94.4	395	68.1	11.76	62.8	8.25	41.6	8.13	22.1	2.79	19.3
X2703_36	932	288	181.2	2230	573	2000	264	1205	338	27.5	365	64.7	358	66.1	184	26.8	190
X2703_37	544	214	243	1590	21.2	77.1	15.8	106.6	62.3	10.72	135.7	32	209	44.2	123.2	16.82	123.6
X2703_38	1640	611	833	331	879	2350	251	1008	154	29.1	130.6	15.75	71	11.47	27.4	3.1	20
X2703_1	403	211.8	394	233	297	645	88.1	380	64.8	23.1	62.2	6.85	33.9	7.05	21.9	2.89	21.3
X2703_2	693	335	2680	588	1096	2020	280	1166	231	47.2	217	25.1	122.2	23	56.7	6.27	34.3
X2703_3	871	367	523	660	164.6	494	95.9	576	175.4	26.4	172.2	24.5	130.3	25	63.8	7.93	43.6
X2703_4	157	188	457	68.4	5.23	11.88	2.51	16.7	7.7	2.57	11.5	1.69	10.51	2.39	7.2	0.897	6.29
X2703_5	535	189.9	355	166	570	872	91.5	339	46.6	5.11	48.2	5.21	26.5	5.92	16.5	2.06	12.25
X2703_6	1090	485	737	243	206	470	70.9	331	70.6	14.03	68.8	9.06	46.1	8.91	24.3	2.92	16.9
X2703_7	566	563	1275	311	254	551	80.2	375	87.7	19.3	89.8	12.2	62.8	11.88	30.9	3.57	20.7

Sample ID	^{55}Mn	^{57}Fe	^{88}Sr	^{89}Y	La	Ce	Pr	Nd	Sm	Eu	Gd	Tb	Dy	Ho	Er	Tm	Yb
X2703_8	644	290	310	467	707	1437	185	738	132	11.68	121.8	15.7	83.2	17.3	48	5.83	35.4
X2703_9	397	238	5380	572	714	1195	156.7	713	154.4	40.7	160.8	21.5	110.9	21.4	54	6.05	30.5
X2703_10	335	173	189.5	284	18.7	76.1	19	141.6	53.2	13.8	60.9	7.37	40	8.4	23.6	3.09	19.8
X2703_11	340	180	180.2	207	9.64	45.2	10.98	92.4	37.3	10.21	46.7	5.81	30.6	6.26	18.6	2.34	15.5
X2703_12	310.3	197	198.6	160.5	12.74	35.6	10.05	74.3	29.2	7.63	34	4.36	22.61	4.8	13.11	1.697	10.98
X2703_13	882	264	499	670	285	760	122.4	591	170.1	24.4	191.9	26.3	137	26.4	67	7.66	41.5
X2703_14	919	201	200.5	413	1933	2930	301	1053	146.7	14.49	131	14.75	73.9	14.96	41.1	5.21	31.3
X2703_15	609	432	659	764	3160	5950	722	2660	382	32.3	297	32.8	147	26.6	68.5	7.9	43.8
X2703_16	792	602	299	1413	2190	4360	570	2230	389	17.6	347	47.2	250	48.2	127.7	15.5	86.7
X2703_17	202.5	225	328	674	65.2	289	68	465	179	17	200	27.2	140.1	25.2	60	6.83	36.8
X2703_18	457	173	344	293	144.6	416	64.5	299	62.6	14.98	58.4	8.02	43.8	9.49	28.5	4.08	28.8
X2703_19	602	191	417	99	21.9	64.6	11.5	70.6	21.8	7.57	26.9	3.43	17.6	3.61	9.68	1.092	6.45
X2703_20	357	575	1855	294	548	1108	139	605	113.9	22.4	109	12.6	66	12.5	29.8	3.33	18.4
X2703_21	327	169	178.7	949	21.1	120.8	32.3	249	110.4	9.41	142	23.1	149.1	31.6	96	13.4	79.2
X2703_22	1002	558	767	254	613	1429	213.9	935	168.9	23.2	130	13.78	59.3	10.22	23.2	2.5	13.9
X2703_23	501	301	3286	118.6	253.2	686	121.5	603	111	26.6	63.3	5.66	21.8	3.84	10.08	1.142	7.19
X2703_24	683	311	492	282	438	986	133.3	588	122.4	15.9	116.6	13.7	59.4	10.39	23.7	2.57	14
X2703_25	1185	459	716	555	1380	2820	331	1350	219	32.6	182	21.6	104	20.8	56.9	6.8	38.4
X2703_26	1164	380	651	651	1185	2670	337	1297	213	33.3	184	22.1	109.8	21	57	7.26	43.9
X2703_27	2576	287	387	1129	71.5	245	52.3	310	149	35.6	219	45.9	284	52.1	126	15.9	88.5
X2703_28	578	169.2	400	131.2	825	1890	239	875	96.4	24.5	61.7	4.8	16.1	3.26	11.4	1.95	16.1
X2703_29	855	255	483	1142	629	1608	250	1246	311	45.5	344	45.3	240	46.1	119	13.9	80.2
X2703_30	1190	349	804	388	1288	2310	281	1123	178.2	25.2	139.5	15.97	73.5	13.44	34.7	3.94	23.57
X2703_31	1359	606	715	266	651	1488	220	932	151.7	21.7	117.2	12.06	52.6	9.35	24.7	2.8	16.5
X2703_32	661	321	2524	653	832	1694	243	1159	251	49.2	229.8	27.01	134	25.3	61.8	6.65	35.5
X2703_33	1173	611	864	972	1200	2353	326.1	1444	297.9	31.19	284.3	36.42	191.4	37.2	94.2	10.53	57.7
X2703_34	700	177.6	176.5	568	378	894	123.4	538	113.3	9.68	122	16.16	89	19.36	54.8	7.1	49
X2703_35	706	355	481	649	1493	2770	335	1321	227	20.5	209	26	129.1	24.5	61.5	7.07	40.8
X2703_36	1107	308	723	255	1249	1987	223	791	106.7	18.4	90.4	9.14	43.2	8.51	23.4	2.94	18.8
X2703_37	1308	248.1	460.4	213.4	1635	1666	137	432	53.8	8.12	58.7	6.2	31.5	6.86	19.69	2.496	16.26
X2703_38	1552	368	586	1793	385	1104	196	1015	341	46.5	418	66.5	376	68.5	168	18.4	93.8
X2703_39	188.7	810	394	159.8	1187	2190	246	907	118.6	8.1	84.1	7.81	29.1	5.25	13.43	1.48	8.1
X2703_40	393	696	980	402	364	876	143	774	178	24.5	163	19.1	88.2	16.1	37.6	4.14	23.7
X2703_41	202.4	202	721	279	954	1760	209	874	145	32.9	128	13.7	59.8	11	29.6	3.5	21.5

Sample ID	^{55}Mn	^{57}Fe	^{88}Sr	^{89}Y	La	Ce	Pr	Nd	Sm	Eu	Gd	Tb	Dy	Ho	Er	Tm	Yb
X2703_42	680	191	342	3070	633	2160	398	2210	692	29.9	740	113	666	133	360	50.6	316
X2703_43	595	234	472	137	785	1119	117.7	415	57.1	13.6	55.3	5.55	27	5.33	14.2	1.71	10.7
X2703_44	1160	276	1280	402	79.2	198	34.5	179	56.4	17	75.1	11.59	69.3	14.2	39.4	4.7	27.7
X2703_45	922	469	1211	547	656	1354	199	931	180	29.5	159	20.7	106.9	20.1	53	5.83	33.9
X2703_46	635	410	1327	388	1940	4360	593	2360	330	51.1	212	22	87	14.29	35.5	3.98	22.7
X2703_47	531	178	388	2620	79.2	350	90.6	705	326	23.1	451	78.9	471	101.7	280	38.5	237
X2703_48	349.1	585	1529	543	1016	1916	250	1041	197.1	28.6	174.3	21.8	111.9	21.1	54.7	6.21	34.8
X2703_49	631	280	290	1163	298	785	134.1	704	228	28	306	46.4	289	60.9	148	15.3	70.7
X2703_50	738	335	767	198	871	1530	207	846	155	27.4	119	12.5	50.1	7.5	17.8	1.96	11.8
X2703_51	1443	361	837	401	1650	2390	234	878	123	22.6	112	13	67	14.3	42.4	5.34	33.3
Miss. S. of Illinois, Missouri, and Upper Miss. (not used in study)																	
X2704_1	1335	483	619	535	1191	3310	372	1443	265.2	35	199.1	23.42	112.2	20.03	49.8	5.78	34.3
X2704_2	375	462	11150	265	1723	3870	451	1773	275	61	181.3	17.04	67.5	10.36	24.3	2.37	12.31
X2704_3	608	190	442	404	557	1263	169.9	826	181.3	14.12	150.9	17.76	86.5	15.79	37.7	4.2	23.5
X2704_4	1874	488	749	1283	365	1178	186	915	309	29.5	310	47.4	271	51.3	127.1	14.41	72.6
X2704_5	183.6	177.7	1043	24.52	13.63	47	8.25	45.7	10.49	2.49	9.44	1.014	4.68	0.863	2.1	0.232	1.363
X2704_6	341.9	176.4	281.8	144	339	679	75	292	44.3	20.02	40.5	4	19.26	4.21	12.18	1.549	9.67
X2704_7	999	504	551	263.4	460	1443	209.5	937	182.7	20.34	120.3	12.97	56.6	9.55	23.4	2.71	15.55
X2704_8	1172	455	715	312	1277	2560	252	904	153.4	22.44	119.3	13.02	61.5	11.51	29.9	3.65	21.4
X2704_9	1176	216.5	276.8	632	32	135.4	28.83	194.3	113.5	29.4	157.4	29.3	169.5	29.5	69.3	8.68	48.2
X2704_10	842	243.7	585	321	559	1235	138.8	514	89.4	5.48	74.5	9.04	47.8	10.11	29.7	4.32	29.1
X2704_11	271.3	182.8	125.2	524	142.5	409	65.3	357	128.4	10.35	133.6	19.5	100.5	19.4	48	5.88	32.3
X2704_12	2794	605	202.8	1736	104.4	546	113.3	645	279	18.1	284	51.4	316	64	180.1	24.5	135.3
X2704_13	504	241.7	338.1	2490	193.3	762	139.8	768	332	23.1	407	72.5	440	90.2	246	31.3	167
X2704_14	1728	194	321.7	2235	187.1	786	153.4	851	374	30.2	444	83	477	82.7	201	25.8	150.2
X2704_15	1002	595	953	172.6	622	1488	184.9	761	123	18.34	87.1	9.01	37.7	6.21	14.97	1.657	9.73
X2704_16	1448	712	708	208.7	490	1242	162.9	666	109.8	18.9	92.5	10.01	45.7	7.82	19.14	2.087	12.73
X2704_17	383	306	348	93.8	446	761	74.6	274	39.4	8.4	38.4	4.32	21.1	3.84	9.57	1.008	6.5
X2704_18	320.4	611	661	568	504	1264	182.3	859	171.1	45.4	181.4	22.7	119.4	21.4	50.8	5.13	30.3
X2704_19	1329	395	546	1223	510	1753	266	1286	313	30.1	343	49.3	268	47.9	112.5	11.36	64.2
X2704_20	708	215.5	126.5	1536	228.5	746	123.8	650	219.6	22.96	332	51.3	301	59.4	149	15.68	99.3
X2704_21	995	501	672	365	1078	3100	359	1348	197	24	158.7	17.33	79.9	13.77	34.3	3.49	21.8
X2704_22	607	265	1314	164.5	616	1365	161.2	644	101.2	24.5	86.1	8.4	34.9	5.93	14.38	1.378	8.52

Sample ID	^{55}Mn	^{57}Fe	^{88}Sr	^{89}Y	La	Ce	Pr	Nd	Sm	Eu	Gd	Tb	Dy	Ho	Er	Tm	Yb
X2704_23	486	214	503	312	48.1	162.7	26.3	140.6	50.3	14.23	73.1	10.49	57.5	10.88	27.52	2.88	18.46
X2704_24	959	279	916	142.8	631	986	86.8	283	36.8	8.47	39	4.4	23.3	4.78	13.51	1.587	11.7
X2704_25	1459	319	725	364	576	1730	189	723	108.9	22	96.9	11.23	59.8	11.93	33.2	3.97	28.5
X2704_26	679	634	478	413	1073	2890	308	1145	157.5	18.4	145.2	16.91	83.6	15.63	40.5	4.27	28.6
X2704_27	230.9	186	394	100.9	132.3	418	56.3	233.7	32.1	9.33	29.8	3.45	17.41	3.57	10.15	1.121	8.04
X2704_28	473	213	402	109.8	161.7	498	62.1	249.1	37.6	7.02	35	3.84	19.35	3.9	10.45	1.186	8.31
X2704_29	583	836	912	313	204.6	629	89.4	408	92.6	24.4	102.8	13.18	68.4	12.62	30.7	3.02	18.3
X2704_30	345	194	426	46.5	153	333	36	138	17.9	12.9	16.7	1.84	8.49	1.6	4.25	0.441	3.39
X2704_31	1277	439	683	565	1073	3180	381	1358	225	37.2	186	22.5	108.8	20	50.9	5.72	37
X2704_32	792	865	1121	381	487	1390	172.1	714	138.7	29.6	132.5	16.76	82.6	15.01	35.4	3.75	22.8
X2704_33	597	254	186.9	865	247	999	168.4	789	192.3	8.26	182.3	26	143.5	29.2	82	11.01	78.3
X2704_34	1394	398	995	229.4	771	1501	140.3	465	65	16.24	60.5	6.94	35.9	7.46	22.2	2.84	20.7
X2704_35	527	259	380	72.2	16.7	61.5	10.55	52.4	13.55	3.33	14.4	2.13	11.47	2.45	6.63	0.829	5.38
X2704_36	289	193	298	216.1	115.5	505	87.2	458	98.1	8.26	79.5	9.58	45.3	8.21	20.21	2.27	12.37
X2704_37	1071	462	861	193.6	536	1535	187.1	737	129.4	25.01	95.8	10.23	43.7	7.18	16.54	1.855	10.68
X2704_38	354	186	433	381	357	1332	179.1	790	144.3	26.5	111.4	13.56	65.9	12.99	35.3	4.72	30.6
X2704_39	329	585	257	976	680	1869	263	1133	283	37	279	37.9	199.8	37.3	92.2	10.5	57.5
X2704_40	1003	230	73.7	3280	275	1130	175	862	368	6.32	492	92.2	563	111.6	288	34.2	178.5
Illinois River (Northern)																	
X2705_1	486	208	365	221	112.9	367	57.4	251	54.4	14	45.9	5.96	32.4	6.75	20.9	3.02	22.3
X2705_2	284	346	960	337	820	2390	272	1030	164	36.1	131	15.5	68.8	12.5	31.6	3.6	20.7
X2705_3	213.2	204	1224	617	5.03	16.4	4.24	31.9	28	9.83	94.9	21.8	148.8	25.6	54.6	5.74	27.8
X2705_4	104.1	202	2620	258	843	2690	364	1540	303	70.3	227	20.7	77.4	10.48	22.5	1.88	9.64
X2705_6	1400	252	267	1760	278	792	98.1	375	110.3	30.8	158.1	35.5	292	69.8	218	33.2	226
X2705_8	489	187	502	494	145.3	652	110.5	583	168.5	19.8	150.7	17.8	80.8	14.33	36.8	4.43	27.3
X2705_9	331	249	213	99	28.6	87	13.9	73.5	22.7	7.78	27.8	3.66	18.9	3.57	9.5	1.14	6.85
X2705_11	301	189	384	510	266	1940	132	569	111	25.3	102	12.5	63.7	12.9	34.7	4.46	28.5
X2705_12	270	175	1760	39.1	0.132	0.64	0.13	0.87	0.54	0.183	1.37	0.407	3.66	1.19	4.46	0.629	4.21
X2705_13	236	192	317	55.9	17.7	72.3	12.1	58.1	15	4.63	17.5	1.99	10.21	2.07	5.42	0.614	3.79
X2705_14	575	288	361	254	499	1890	161	629	119.4	7.91	107.3	12.07	53.2	9.14	21.6	2.34	14
X2705_15	416	210	689	698	1540	6020	728	2250	323	56.3	232	23.6	102	18.7	49.4	6.18	40.9
X2705_16	423	215	304	4310	388	2140	310	1460	422	18.1	504	81.4	521	106	288	35.7	212
X2705_18	688	234	271	134.4	115.3	411	43	158	32.4	15	31.8	3.74	19	3.88	10.78	1.329	8.55

Sample ID	^{55}Mn	^{57}Fe	^{88}Sr	^{89}Y	La	Ce	Pr	Nd	Sm	Eu	Gd	Tb	Dy	Ho	Er	Tm	Yb
X2705_20	306	201	256	134	4.66	30.5	7.32	49.6	24.8	5.67	32.6	4.84	25.1	4.66	12	1.37	7.88
X2705_21	163	212	1368	47.3	18.5	71.6	14.01	90.9	30.4	8.22	26.7	2.53	9.75	1.55	3.55	0.392	2.42
X2705_22	193.2	201.2	696	94.7	106	377	66.8	344	66.9	12.03	49.6	4.88	20.43	3.41	8.42	0.965	5.86
X2705_23	5090	648	172.5	1573	100.5	444	84	451	187	14.35	243	46	285	54.8	137.5	16.15	87.6
X2705_24	708	315	5160	3080	614	3080	550	2790	761	83.8	692	98.6	530	104.5	273	32.6	191
X2705_25	9.17	193.7	520.1	56.7	79.2	214.9	36.4	165	34.5	3.5	26.7	3.33	14.2	2.25	4.88	0.486	2.31
X2705_27	460	200.6	333	198.3	20.06	54.6	7.67	31	8.96	9.43	11.95	2.4	18.43	5.23	21.02	4.04	33.1
X2705_29	318.5	203.9	177.7	476	126.9	526	102.9	568	159.9	14.85	153.8	20.56	102.9	17.97	43.4	4.8	27.25
X2705_30	3352	242	59.08	2420	255.1	851	151.2	752	286.8	7.02	316	61.7	399	80.6	237	34.9	225
X2705_31	439	231	412	386	112.6	513	102.8	591	170	23.8	146	17.7	84	14.8	35.8	4.05	22.6
X2705_32	551	228	196.3	476	342	1192	187	787	191	31	156.6	17.51	79.9	14.79	40.2	5.36	37.8
X2705_33	586	221	590	107.8	203.4	507	58.2	230	33	10.51	33.2	3.36	16.57	3.52	10.01	1.234	8.81
X2705_34	312	220	321	309	40.8	218	44.4	258	91.5	17.5	91.7	12.66	64.4	11.74	29.1	3.26	17.5
X2705_35	342	220	752	172	63.6	254	44	222	64.4	19.8	61	7.19	34.3	6.32	16.1	1.93	12.03
X2705_36	410	253	476	309	12.27	54.6	11.71	79.7	39.4	15	57.7	9.28	55.2	11.19	29.2	3.76	23
X2705_37	268	466	1060	783	710	2560	230	805	180	41.2	164	22.3	117	21.2	53.8	6.26	36.4
X2705_38	11290	384	205	2820	171	1000	92.9	384	191	13.3	253	52.8	302	50.8	124.8	16.2	96.9
X2705_39	138	211	2200	390	5630	10500	880	1990	231	36.3	176	16.7	72	13	35.2	3.85	20.8
X2705_40	443	208	1238	380	251	1447	180	741	138.1	28.4	112.1	13.71	71.4	13.25	35.4	4.32	26.5
X2705_41	921	232	229	1660	173	741	117.2	546	205	7.47	220	41.6	259	49.6	135.5	17.3	102.9
X2705_42	302.3	219	213.9	105	301	529	52.2	195	27.6	8.27	31	3.47	16.6	3.6	9.64	1.25	8.7
X2705_44	491	196	291	100.1	131	338	43.2	188	37.5	12.1	35.9	3.85	18.2	3.52	9.36	0.961	5.41
X2705_45	387	238	257	326	13.83	64.6	14.33	94.6	37.7	10.67	45.9	7.18	48.2	11.01	35.9	5.18	35.1
X2705_47	720	548	6910	647	5490	12540	1420	4920	723	141	460	43.5	162	24.3	56.5	5.37	29.9
X2705_48	2440	563	114.3	1620	160	717	122.2	581	227	6.8	258	50.3	321	59.5	149.7	17.4	94
X2705_49	518	246	351.8	554	447	1636	280.4	1426	303	18.3	229	26.4	123.3	20.86	51.2	5.47	29.9
X2705_50	479	236	274	161.6	144	222	22.4	87.7	18.4	3.82	22.3	3.09	19.97	4.58	14.77	2.12	15.23
X2705_51	275	201	370	248	8.46	70.3	20.5	153	67.4	16.4	72.9	9.25	46.7	8.64	22.2	2.58	15.02
X2705_52	283.9	580	624	596	551	1270	184	867	192.6	44.8	180.5	22.9	120.1	21.37	52.4	5.94	31.9
X2705_53	127.8	349	264	110.6	393	1630	221	968	182	5.25	129.2	10.99	36.8	4.58	8.53	0.551	2.64
X2705_54	255	220	946	81.2	385	1330	144.4	461	51.5	13.6	40.3	3.2	13.57	2.44	7.25	0.826	5.55
X2705_55	330	251	366	441	68	231	36.8	194	88	24.3	106	13.6	75.3	15.4	42.1	5.25	31.6
X2705_56	202	260	512	321	1867	4290	509	1738	239	29.3	169.8	16.77	72	11.53	29.1	3.04	16.7
X2705_57	363	533	762	472	502	1430	195	834	172	39.9	162	20.2	104.6	18.3	44.4	4.79	26

Sample ID	^{55}Mn	^{57}Fe	^{88}Sr	^{89}Y	La	Ce	Pr	Nd	Sm	Eu	Gd	Tb	Dy	Ho	Er	Tm	Yb
X2705_58	582	415	2800	577	1044	2250	266	1021	190	36.6	170.7	21.02	114.5	21.13	57.1	6.9	39.6
X2705_59	319	310	287	190	192	696	90.8	378	73	16.6	64.4	6.95	35.5	6.85	19.4	2.3	14.6
X2705_60	269	218.1	1290	15.68	76.8	207	26.1	107.1	13.01	3.15	10.1	0.813	3.15	0.514	1.34	0.144	0.871
X2705_1	523	289	466	140	221	612	88.8	392	72	12.05	53.1	5.25	21.2	3.73	9.91	1.16	7.43
X2705_2	323.4	360	237.6	243	65.9	227	39.7	212	49.9	10.46	49.7	6.12	32.8	7.05	21.2	3.03	22.3
X2705_3	351	377	339.7	448	14.36	55.9	15.34	128.4	61.7	16.11	79.9	12.06	71.7	14.93	42.2	5.69	37.2
X2705_4	2022	980	100.1	2135	155.7	521	107.1	617	274	10.38	370	75.8	476	83.9	199.4	23.95	142.9
X2705_5	332.5	1290	625	405	309	774	116.5	614	135.9	33.5	131.9	16.86	85.2	14.82	34.7	3.63	19.84
X2705_6	430	372	188.9	849	2069	3690	365	1227	169.1	36.7	165.5	20.75	116.6	25.1	74.5	10.24	72.5
X2705_7	176.8	217	2201	1129	826	2940	473	2480	518	135.6	409	45.1	202.8	35.8	92.4	11.13	71.1
X2705_8	419	396	159.1	256.2	374	658	74.2	316	60.7	12.54	62	8.54	46	9.05	23.73	2.79	16.47
X2705_9	756	303	437	292.3	843	1621	174.7	676	104.6	13.46	91.7	10.86	53.1	10.2	27.2	3.33	20.3
X2705_11	242.4	310	205.4	50.6	58.9	112	13.4	55.4	10.8	16.1	12.8	1.48	7.35	1.52	4.32	0.528	3.55
X2705_12	319.6	1175	135	1938	1082	2533	341	1670	422	21.9	462	67.2	368	67.9	163.5	17.25	88.8
X2705_13	536	300	179.2	520	94	290	46.7	249	71.7	16.03	98.7	14.49	80.9	17.2	45.8	5.38	35
X2705_14	120.2	196	871	52.2	87.3	246	36.5	180	30	8.22	24.7	2.2	9.49	1.76	4.51	0.488	3.08
X2705_15	931	454	95.6	1350	89	340	62.7	346	149.8	8.8	194.1	38	238.3	46.2	121.1	15.03	85.1
X2705_16	288.6	229	398	333	190.2	539	88.5	507	128.9	24.9	115	13.76	63.6	11.37	27.8	2.95	15.63
X2705_17	2912	752	65.2	4700	1094	3410	542	2792	816	14.74	850	139.5	809	149.4	396	52.4	331
X2705_18	339.8	246	517	1425	668	2090	336	1693	441	8.3	395	56.2	290.5	52.1	130.3	15.01	84.8
X2705_19	320.6	1456	625	504	380	976	145.8	739	167.1	40.1	160.1	20.34	102.8	18.22	41.8	4.43	23.96
X2705_20	670	366	172.9	510	29.9	118.7	23.96	151.5	80.5	13.29	118.1	23.57	132.6	22.66	54.6	7.2	46.2
X2705_21	603	282	184.8	3370	118.7	507	113.4	788	343	34.5	473	98.9	677	133.2	297	25.59	111.2
X2705_22	932	586	218.9	274.3	641	1496	162.9	632	90.3	14.78	76.2	9.2	46.3	9.22	25.7	3.25	21.4
X2705_23	384	247	485	438	29.5	153.5	47.7	406	155	14.52	142.7	18.13	87.2	15.49	37.2	4.14	23.1
X2705_24	321.6	268	541	337	307	649	78.4	348	69.9	14.45	68	8.8	49.1	10.75	33.9	5	36.3
X2705_25	511	478	225.9	414	472	1363	185.1	801	137.4	37.8	107	13.31	65.9	12.87	37.3	5.32	39.2
X2705_26	1496	371	358.9	2291	895	3330	568	2980	562	134.6	538	69	358	69.9	184.7	22.74	145.9
Ohio River (Ohio)																	
X2801_1	325	225	2410	314	725	1950	223	771	119.6	24.1	95.2	11.74	59.3	11.13	29.2	3.51	20.7
X2801_2	784	272	235	572	510	1580	190	753	145	13.2	141	18.8	104.4	20.6	55.1	6.93	42.1
X2801_3	334	205	421	254	69.6	297	52.3	258	71.5	33.2	75.4	8.81	44.1	8.39	22	2.67	16.9
X2801_5	370	190	1191	307	1007	2240	207	631	82.7	14.7	75.1	8.28	43.9	9.27	27.8	3.9	26.1

Sample ID	^{55}Mn	^{57}Fe	^{88}Sr	^{89}Y	La	Ce	Pr	Nd	Sm	Eu	Gd	Tb	Dy	Ho	Er	Tm	Yb
X2801_6	463	278	318	394	22.1	104.7	20.8	127.8	51.6	12.53	72.2	11.19	68.3	14.4	39.3	4.86	29.1
X2801_7	390	180	276	462	72.5	380	84.8	494	137	28.9	124	16	82.8	16.2	44.1	5.58	34.9
X2801_8	1040	269	208	682	1085	3340	397	1460	255	17.5	220	26.6	137	25.3	64.2	7.18	41.1
X2801_9	757	238	157	1440	113.9	493	99.3	533	189	25.5	241	39.1	249	53	145	17.8	102.6
X2801_10	620	277	417	127.5	331	480	43.5	148.5	25.1	6.35	28.4	3.56	20.2	4.39	13.09	1.63	10.47
X2801_11	404	198	56	846	24.8	171	43.5	291	122	26.8	143	23.3	136	27.4	80.1	11.05	75.8
X2801_12	1880	283	321	1470	2850	5860	574	2040	368	48.3	373	45.7	240	49.4	138	17.2	107
X2801_14	306	207	525	209	38.1	223	50.5	296	81.1	18.4	69.5	8.45	41	7.48	18.4	2.17	13.4
X2801_15	727	295	738	156	26.7	179	48.1	309	88.7	33.6	69	7.23	32.8	5.7	14.1	1.61	10.1
X2801_16	253	177	307	45.2	97.4	266	32.5	128	19.7	10.3	18.3	1.65	7.32	1.47	4.16	0.552	3.99
X2801_17	738	260	53	1367	120	474	89	457	209	14.2	287	56.6	326	54	127.5	15.6	90.7
X2801_18	440	327	284	712	135	698	149	905	398	59.3	453	63.5	244	26.9	32.6	1.63	6.35
X2801_19	532	216	586	378	380	1330	160	632	103.9	40.5	103	12	63.9	13.1	38.4	5.35	42.1
X2801_20	2130	231	130.2	2020	426	1520	247	1201	443	70.1	480	83.2	470	83.9	196	20.5	101.5
X2801_21	859	438	255	1430	773	3130	462	2160	493	77.7	444	61	305	53.4	130	14.4	83.3
X2801_22	300	221	1027	57.6	3.77	21.3	4.79	35.9	16.7	4.65	19.1	2.36	11.7	2.15	5.1	0.585	3.51
X2801_23	3030	354	308	1690	141	584	97.2	533	245	28.8	331	63.8	364	63.2	152	18.4	105
X2801_24	155.8	205	17.02	106.8	550	549	42.5	133	19.3	5.65	20	2.56	14.5	3.32	10.29	1.43	10
X2801_25	514	201	93.2	1900	63.2	281	55.4	347	157	18.9	237	44.4	287	60.7	183	26.2	170
X2801_26	3480	278	186.2	1960	198	1141	196	914	303	48.6	309	56.7	345	65.8	181	26.5	180
X2801_27	618	205	852	222	250	1041	164	673	110.6	24.8	77.2	8.13	35.8	6.64	17.6	2.15	13.9
X2801_28	185.1	198	985	169.3	1.65	6.15	1.38	9.64	6.24	3.99	14.2	2.83	21	5.4	17.2	2.54	17
X2801_29	321	193	325	870	133.1	632	126.6	739	225	44.1	219	27	134.7	27.9	76.2	9.68	63.1
X2801_30	727	320	172.6	809	115.4	567	117.8	684	227	22.8	233	30.8	160.4	28.3	69	8.05	47.9
X2801_31	431	261	942	105.8	270	413	40.2	154	23	8.24	25	2.87	15.8	3.27	9.42	1.21	8.28
X2801_32	1006	245	289	934	253	951	133	606	125	30	140	19.1	125.9	30.5	98.1	14.01	97.4
X2801_33	192	530	1024	486	167	753	131.4	634	158	12.14	153	20.2	102.1	17.8	40.4	3.95	19.3
X2801_34	305	218	260	258	16.3	51.7	8.4	45.2	18.4	4.65	27.7	4.82	33.5	7.84	24.2	3.45	22.7
X2801_35	244	200	260	7.59	0.079	0.277	0.041	0.213	0.169	0.061	0.269	0.072	0.68	0.192	0.791	0.116	0.872
X2801_36	543	260	772	193	88.4	312	50.7	235	56.8	15.8	56.1	6.72	33.9	6.63	16.9	2.03	13.4
X2801_37	329	200	524	9	8.34	18	1.98	7.5	1.06	0.499	1.65	0.23	1.28	0.303	0.879	0.117	0.829
X2801_38	1236	283	421	1549	370	1850	322	1560	364	58.9	318	45.2	245	47.6	131	17.3	104.3
X2801_39	493	240	352	1880	400	1900	328	1730	445	78.2	414	59.8	320	62.4	164	19.2	111.6
X2801_40	279	201	809	227	20.7	130.6	28.1	184	58.3	16	58.7	7.78	40.4	7.64	18.7	2.23	12.8

Sample ID	^{55}Mn	^{57}Fe	^{88}Sr	^{89}Y	La	Ce	Pr	Nd	Sm	Eu	Gd	Tb	Dy	Ho	Er	Tm	Yb
X2801_41	790	281	515	245	770	2010	215	764	116.2	16.9	94.6	10.13	47.7	8.41	21.3	2.33	13
X2801_42	431	203	271	119.2	31.5	126.3	19.8	96.8	23.2	6.06	24.3	3.05	16.5	3.82	11.51	1.51	10.9
X2801_43	479	256	152.1	1550	186	713	125	622	206	27.3	253	40.3	244	52.2	140	17.2	100.8
X2801_44	727	245	189	196	359	950	96.6	313	47.1	15.4	43.9	4.92	26.3	5.5	17	2.2	14.1
X2801_45	188	231	187	242	969	2330	195	583	81.3	11.74	68.9	7.6	39.1	7.61	21.6	2.78	17.5
X2801_46	438	1140	399	963	740	2630	337	1378	300	13.7	274	35	183.5	33.4	84.2	9.46	52.1
X2801_1	324	687	671	330	144	489	94	560	135	32.5	117	12.9	61.3	11.7	30.4	3.67	23.9
X2801_2	328	418	476	270	864	1859	219	872	124.4	12.19	99.8	10.61	47	8.72	23.1	2.66	16.18
X2801_3	712	511	125.2	3740	362	1198	222	1300	563	25.1	788	149.1	908	165.3	362	37	185
X2801_4	365	423	180.5	1278	12.84	58.1	17.35	172.3	119.3	18.4	252	44.5	262	48.4	119.9	14.89	88.6
X2801_5	672	417	351	226.9	639	743	65	249	40.6	9.91	46.3	5.66	31.7	7.36	21.5	2.89	21.2
X2801_6	638	424	277	2990	80	437	116.7	871	360	61.9	431	75.5	467	99.6	295	41.2	267
X2801_7	216.5	334	388	114.9	58.1	225.4	40.1	221.2	41.5	8.74	33.8	4.02	19.65	3.72	10.03	1.291	8.06
X2801_8	1672	498	164.7	322	213	648	98	428	80.3	18.8	66.1	9.21	51.6	10.22	29.4	3.8	24.6
X2801_9	443	386	519	43.3	0.232	0.884	0.255	2.33	1.69	0.949	4.53	0.861	6	1.582	4.98	0.703	4.93
X2801_10	510	410	257	534	292	521	65.9	337	77.9	11.05	103	14.92	89.1	19.7	54.9	6.72	42.1
X2801_11	470	523	1182	1871	2136	4470	469	1675	274	23.1	262	39.5	241	54.6	174.1	26.8	191.2
X2801_12	653	367	275.8	1061	33.9	104.3	19.7	145.4	76.5	29.9	140.2	24.7	163.7	36.5	101.1	12.31	71.9
X2801_13	375	1520	667	452	345	865	131.1	648	145	34.1	141.5	18.9	94.4	16.7	39.3	4.14	22.7
X2801_14	273.2	344	2365	877	4220	8990	1097	4180	544	120.9	367	36.5	153.4	26.9	70.6	8.18	51.9
X2801_15	957	466	427	1279	23.9	148.2	42.3	342	159.1	49.4	224	38.6	234	44.2	110.4	13.33	74.5
X2801_16	335	437	375	1095	360	1595	290	1525	330	53.5	292	38.1	201	38.3	98.7	11.63	69.5
X2801_17	457	327	257.1	577	9.82	99.9	36.4	290	111	17.83	111.9	16.39	92.8	19.1	53.3	7.29	49.2
X2801_18	642	383	556	816	200.2	942	201.6	1196	285	52.7	250	31.2	158.2	28.6	70.1	8.04	46.4
X2801_19	588	425	1026	213	27.4	104.7	21.6	134.5	40.9	12.01	49.3	6.65	36.9	7.49	20.1	2.44	14.93
X2801_20	496	710	194.8	1521	1526	3530	470	2020	389	32	363	50.2	271	52.2	137.3	16.58	99.3
X2801_21	489	366	261	673	11.43	41	7.38	48.9	22.2	8.74	45.1	9.6	78.5	20.7	69.1	10.56	71.7
X2801_22	414	375	412	43.6	39.5	68.5	8.25	36.7	7.37	3.17	8.31	1.1	5.97	1.32	4.1	0.563	3.95
X2801_23	677	474	237.4	550	42.8	146.7	30.1	194	64.2	9.7	88	13.89	83.6	17.99	48	5.73	32.9
X2801_24	574	360	318	804	227	893	164	850	173	31.8	176	22.7	124.5	26	73.8	9.12	56.9
X2801_25	864	902	110.1	2530	1344	3370	479	2220	612	21.1	661	100.1	537	96.3	231	25	131.5
X2801_26	509	367	926	990	37.5	154	34.4	269	119.1	40.2	174	27.2	168	36.1	98.8	12.6	79.7
X2801_27	811	574	238.1	1832	158.4	668	149.1	1034	412	39.5	491	70.7	370	66.4	166	20.4	124.8
X2801_28	141.7	821	139.3	253	880	2710	448	2360	532	46.8	421	39.8	112.7	9.72	12.49	0.402	2.72

Sample ID	^{55}Mn	^{57}Fe	^{88}Sr	^{89}Y	La	Ce	Pr	Nd	Sm	Eu	Gd	Tb	Dy	Ho	Er	Tm	Yb
X2801_29	337	521	693	943	80.2	521	123.2	823	232	45.7	233	32.4	171	31.9	80.6	8.47	48.1
X2801_30	364	578	387	1341	410	1550	305	1739	427	66.5	404	54	281	50.6	125.8	14.71	90.1
X2801_31	557	431	156.8	2650	2180	5010	711	3280	669	62.7	672	92.1	502	96.7	246	26.9	141.9
X2801_32	388	337	258.8	202.7	290	457	43.5	153.1	28.9	7.61	33	5.06	30.5	6.8	19.5	2.63	16.87
X2801_33	1163	416	423	205.7	222.6	737	106.9	428	68.9	16.76	51.2	6.79	35.9	7.17	20.8	2.8	18.2
X2801_34	270	594	261	559	274	935	148	735	164	11.31	152	19.1	100.7	19.1	48.5	5.73	33.4
X2801_35	2827	1133	48.6	4640	411	1519	261	1347	560	5.26	710	144.9	913	177.3	476	60.2	355
X2801_36	567	275	177.3	1396	340	1021	179.1	964	247	24.2	263	40.7	237	47.7	124.4	14.53	81.8
X2801_37	229.7	565	357	277	1063	2580	363	1825	381	39.2	315	32.2	105.6	10.12	13.49	0.6	3.03
X2801_38	375	1183	110.8	471	757	2470	402	2180	735	36.4	638	59.6	181.1	18.01	27.2	1.64	8.28
X2801_39	298	302	361	370	4.56	16.52	3.24	20.1	9.73	3.17	17.8	4.18	39	12.51	50.2	8.51	63.5
X2801_40	366	280	252	1441	4.2	19.2	4.57	44.5	32.1	10	91.9	22.4	185	46.7	149	21.9	142.8
X2801_41	1225	420	2604	1977	3210	7090	910	3790	593	72.6	532	67.5	345	67	178.4	21.6	136.1

Supplementary Table 3. 3 Trace Element and REE continued

Sample ID	Lu	^{232}Th	^{238}U	La*	Ce*	Pr*	Nd*	Sm*	Eu*	Gd*	Tb*	Dy*	Ho*
Mississippi S. of Red													
X2501_1	1.806	8.53	25	293.75	307.78	275.38	278.77	137.62	113.24	93.87	70.98	63.43	54.32
X2501_2	3.74	10.89	4.86	2206.25	2811.11	2223.08	2019.30	957.14	359.46	511.94	380.39	316.33	238.24
X2501_3	2.71	3.76	9.99	260.31	322.22	345.38	383.16	254.29	155.95	174.19	140.78	129.00	105.81
X2501_4	10.74	3.1	0.225	87.50	102.22	112.31	143.86	167.62	168.78	255.81	376.47	565.67	625.68
X2501_6	2.69	19.71	10.86	2265.63	2195.56	1660.77	1475.44	652.38	261.62	406.77	298.63	247.67	177.97
X2501_7	0.478	5.09	7.18	82.19	108.44	112.85	125.79	63.38	66.62	43.26	31.57	27.63	22.03
X2501_8	18.19	2.74	11.17	135.31	318.89	549.23	889.47	1057.14	550.00	1051.61	1164.71	1286.67	1059.46
X2501_9	1.139	2.69	2.17	1303.13	1557.78	1385.38	1256.14	470.95	304.59	247.74	150.78	108.33	71.49
X2501_10	1.86	3.53	22.1	123.13	212.22	305.38	468.42	468.10	406.76	336.45	237.25	179.00	116.35
X2501_11	2.044	31.9	30.5	1037.50	986.67	650.00	501.75	165.71	135.81	109.68	72.35	63.27	52.70
X2501_12	1.36	7.25	4.38	1746.88	1944.44	1615.38	1429.82	584.76	355.41	319.68	208.63	155.33	100.27
X2501_13	2.97	36.1	11.63	600.00	661.11	567.69	563.16	242.38	270.27	163.23	117.84	109.00	93.38
X2501_14	3.82	50	5.93	5071.88	4311.11	2915.38	2312.28	874.29	593.24	515.16	352.75	301.67	229.46
X2501_15	3.67	9.28	10.66	5031.25	4200.00	2623.08	2075.44	861.90	404.05	461.29	343.14	293.33	218.92
X2501_16	0.661	0.819	9.57	26.06	52.67	97.46	175.26	230.95	214.46	145.81	102.94	74.67	47.43

Sample ID	Lu	^{232}Th	^{238}U	La*	Ce*	Pr*	Nd*	Sm*	Eu*	Gd*	Tb*	Dy*	Ho*
X2501_17	11.83	13.78	13.07	92.50	158.00	262.31	447.37	735.71	291.76	653.23	754.90	811.67	679.73
X2501_18	7.3	6.4	17.7	230.63	287.78	343.08	436.84	600.00	218.92	435.48	425.49	423.33	336.49
X2501_19	3.22	34.2	8.77	3228.13	3333.33	2692.31	2456.14	1247.62	378.38	591.29	407.84	326.67	232.03
X2501_20	1.805	3.9	1.527	831.25	897.78	835.38	884.21	554.76	458.11	301.61	223.53	195.67	143.65
X2501_21	0.775	3.97	3.75	275.00	345.56	341.54	326.32	182.38	136.22	79.03	50.98	40.37	31.22
X2501_22	9.1	12.45	25	354.06	497.78	800.77	1321.05	1466.67	640.54	848.39	707.84	652.33	516.22
X2501_23	42.4	64.4	31.5	1015.63	1580.00	1792.31	2064.91	1971.43	797.30	1335.48	1311.76	1386.67	1267.57
X2501_24	5.22	0.868	16.9	200.00	383.33	536.15	661.40	594.29	328.38	319.68	267.06	250.67	202.70
X2501_25	1.88	2.62	6.66	1009.38	1246.67	1292.31	1285.96	761.90	477.03	319.68	216.86	170.00	116.62
X2501_26	1.79	5.94	4.71	1381.25	1394.44	1308.46	1280.70	830.95	289.46	374.19	247.25	184.33	126.89
X2501_27	9.45	2.22	9.33	3793.75	6411.11	6361.54	6035.09	3847.62	1136.49	1703.23	1256.86	1006.67	716.22
X2501_28	3.24	114.6	67	1425.00	1096.67	802.31	666.67	372.86	199.73	201.29	157.84	148.00	123.38
X2501_29	1.45	35.1	18	1837.50	1944.44	1638.46	1470.18	604.29	370.27	256.77	135.29	89.00	62.57
X2501_30	3.03	13.47	7.27	2293.75	1335.56	860.00	664.91	308.10	144.59	172.26	120.78	107.33	89.46
X2501_31	3.51	13.16	2.33	3356.25	2988.89	2307.69	2135.09	1073.33	648.65	532.58	364.71	291.33	213.78
X2501_32	6.4	11.13	4.23	1712.50	2096.67	2042.31	2228.07	1538.10	397.30	860.65	698.04	613.33	450.00
X2501_33	1.606	0.038	67.8	435.94	703.33	930.00	1133.33	1357.14	169.59	1061.29	1003.92	816.67	470.27
X2501_34	3.45	24.1	8.6	2118.75	1828.89	1641.54	1647.37	911.90	365.14	488.71	356.67	299.00	222.84
X2501_35	1.393	36.7	44.8	684.38	904.44	855.38	822.81	362.38	297.30	184.19	107.65	78.67	58.24
X2501_36	4.33	41.1	16.35	1962.50	2033.33	1653.08	1557.89	753.33	413.51	421.94	276.47	222.00	168.38
X2501_37	1.88	5.99	4.85	1665.63	1577.78	1407.69	1245.61	525.71	271.62	289.35	186.27	143.67	102.84
X2501_38	2.66	58.8	19.7	787.50	1070.00	1120.77	1257.89	705.24	477.03	478.39	318.04	253.00	186.22
X2501_39	1.2	9.8	7.2	443.75	418.89	332.31	314.04	135.24	97.30	94.84	57.25	48.00	39.46
X2501_40	25.1	1.209	19.4	696.25	870.00	1073.08	1317.54	1385.71	251.49	1351.61	1566.67	1733.33	1360.81
X2501_1	12.97	122	62.3	2446.88	2466.67	2392.31	2631.58	2023.81	945.95	1403.23	1033.33	870.00	654.05
X2501_2	3.38	21.2	5.19	1740.63	1566.67	1423.08	1350.88	738.10	329.73	483.87	362.75	317.67	235.14
X2501_3	3.33	4.77	4.85	482.81	534.44	635.38	721.05	583.33	441.89	395.16	315.10	266.00	191.62
X2501_4	3.91	42.3	7.81	5156.25	3644.44	2646.15	2068.42	747.62	351.35	449.03	293.92	248.33	193.24
X2501_5	0.569	0.6	5.31	386.25	417.78	537.69	687.72	801.90	595.95	738.71	517.65	301.33	135.14
X2501_6	19.7	15.6	15.4	2340.63	2200.00	2476.92	3087.72	3038.10	175.68	2758.06	2739.22	2546.67	1918.92
X2501_7	15.1	5.04	17	435.63	583.33	782.31	1047.37	1252.38	570.27	1406.45	1668.63	1810.00	1344.59
X2501_8	21.7	1.58	22.9	659.38	862.22	992.31	998.25	1228.57	100.00	1022.58	1327.45	1403.33	1043.24
X2501_9	5.1	5.31	1.85	1093.75	1045.56	1076.15	1124.56	668.10	497.30	519.35	435.29	397.67	295.95
X2501_10	5.98	2.22	3.87	1025.00	1433.33	1784.62	2140.35	1395.24	129.73	861.29	674.51	593.33	422.97

Sample ID	Lu	^{232}Th	^{238}U	La*	Ce*	Pr*	Nd*	Sm*	Eu*	Gd*	Tb*	Dy*	Ho*
X2501_12	7.79	0.466	9.39	39.19	103.78	216.92	389.47	621.90	147.57	638.71	662.75	666.67	529.73
X2501_13	1.86	5.75	2.57	2381.25	1944.44	1500.00	1210.53	483.33	245.95	288.06	187.65	150.33	109.86
X2501_14	4.31	61.2	15.1	3256.25	2888.89	2430.77	2231.58	942.86	621.62	545.16	382.35	314.33	241.89
X2501_16	2.83	10.33	4.37	2325.00	1564.44	1073.08	787.72	295.24	200.54	189.68	123.33	110.67	90.68
X2501_17	2.19	2.92	1.21	1381.25	1022.22	660.77	454.39	157.62	166.22	113.55	70.98	57.67	49.59
X2501_18	7.98	0.175	10.9	20.72	85.33	236.92	489.47	676.19	595.95	622.58	578.43	546.67	443.24
X2501_19	0.562	42.3	0.029	100.31	343.33	573.08	956.14	1204.76	1104.05	954.84	694.12	462.67	225.68
X2501_20	6.06	15.3	16.9	787.50	694.44	574.62	510.53	279.05	255.41	213.87	162.55	148.00	135.00
X2501_21	1.9	54.3	3.6	3868.75	4011.11	4030.77	3684.21	1642.86	1151.35	812.90	478.43	325.33	200.00
X2501_22	3.68	51.5	39.5	1793.75	1407.78	1027.69	859.65	358.10	297.30	244.19	169.22	151.67	121.62
X2501_23	4.5	25.7	10.61	2384.38	2266.67	1953.85	1656.14	742.86	445.95	407.74	279.22	222.67	174.32
X2501_24	1.49	7.02	3.04	1631.25	1677.78	1530.77	1361.40	604.76	259.46	312.58	199.22	146.33	100.27
X2501_25	9.97	39.4	23.9	2209.38	2266.67	1976.92	1852.63	985.71	389.19	638.71	492.16	439.00	351.35
X2501_26	1.48	6.95	3.03	1662.50	1733.33	1553.85	1375.44	605.71	258.11	318.71	198.24	145.00	99.05
X2501_27	13.63	0.045	0.859	124.06	396.67	729.23	1036.84	1123.81	406.76	880.65	931.37	943.33	777.03
X2501_28	1.006	11.3	3.33	2521.88	1524.44	975.38	782.46	292.38	182.43	176.45	97.25	67.33	48.78
X2501_29	0.841	2.56	3.99	293.75	293.33	252.31	224.39	79.52	78.78	53.23	35.10	27.23	22.57
X2501_30	1.78	29.5	7.12	3865.63	2922.22	2130.77	1587.72	610.48	267.57	351.61	210.59	161.67	115.41
X2501_31	0.877	2.83	1.55	1346.88	1335.56	1192.31	1078.95	443.81	258.11	241.94	150.00	99.67	66.22
X2501_32	6.43	0.421	15.4	25.69	47.11	85.92	167.72	280.00	163.51	348.39	384.31	386.67	320.27
X2501_33	3.48	10.84	1.95	1356.25	1532.22	1576.92	1668.42	1038.10	481.08	629.03	470.59	374.67	268.92
X2501_34	3.67	22.6	7.09	2678.13	2255.56	1976.92	1800.00	828.57	224.32	470.97	343.14	278.00	208.11
X2501_35	1.09	4.98	2.56	615.63	753.33	804.62	798.25	399.52	294.59	220.32	134.12	100.33	69.46
X2501_36	4.71	69.4	17.4	1618.75	1766.67	1723.08	1633.33	938.10	252.70	645.16	501.96	444.67	316.22
X2501_37	2.38	3.61	3.19	868.75	954.44	841.54	768.42	359.05	250.00	233.87	175.29	150.00	120.27
X2501_38	3.88	9.38	14.1	138.44	305.56	462.31	577.19	377.62	214.86	241.29	209.61	190.00	152.43
X2501_39	18.2	5.28	23.3	532.81	850.00	1061.54	1278.95	1390.48	656.76	1248.39	1460.78	1560.00	1302.70
X2501_40	1.099	10.71	5.03	1059.38	484.44	280.77	215.26	90.95	67.84	66.13	45.49	43.67	37.97
X2501_41	4.72	10.31	1.95	2137.50	2055.56	1953.85	1907.02	1061.90	283.78	709.68	525.49	452.67	343.24
X2501_42	1.4	7.81	3.44	1700.00	1755.56	1561.54	1412.28	595.24	268.92	316.13	196.27	137.67	95.00
X2501_43	4.61	1.2	28.8	415.94	684.44	912.31	1101.75	1061.90	637.84	703.23	600.00	486.67	318.92
X2501_44	1.5	1.49	3.47	382.50	410.00	343.85	303.51	145.24	97.30	99.68	71.18	63.00	52.57
X2501_45	7.59	55.2	18.3	2187.50	1543.33	1100.00	894.74	360.95	305.41	270.00	198.82	189.67	177.03
X2501_46	5.46	1.29	0.83	1153.13	1494.44	1676.92	1824.56	1104.76	427.03	622.58	456.86	351.00	266.22

Sample ID	Lu	^{232}Th	^{238}U	La*	Ce*	Pr*	Nd*	Sm*	Eu*	Gd*	Tb*	Dy*	Ho*
X2501_47	14.4	1.77	3.37	1412.50	1562.22	1630.77	1584.21	1200.00	358.11	909.68	1013.73	1080.00	893.24
X2501_48	4.1	9.9	11.78	1168.75	1110.00	940.77	824.56	359.52	190.54	238.71	167.25	149.00	127.30
X2501_49	27.1	0.153	30.2	462.50	650.00	783.85	894.74	900.00	52.16	825.81	1033.33	1243.33	1110.81
X2501_50	0.364	0.751	0.513	126.88	213.33	270.00	331.58	210.48	172.97	130.65	93.33	70.33	45.14
X2501_51	1.79	42.8	11.27	1100.00	1186.67	957.69	782.46	309.52	115.14	185.81	117.84	95.00	74.19
X2501_52	59.3	11.2	22.4	46.06	62.56	74.46	91.58	118.10	112.97	199.68	380.39	756.67	1125.68
X2501_53	7.31	3.71	1.73	1043.75	917.78	833.85	775.44	360.48	204.05	249.35	199.22	198.00	181.08
X2501_54	10.28	6.19	24.6	270.63	355.56	488.46	719.30	833.33	487.84	761.29	739.22	736.67	606.76
X2501_55	3.76	17.5	7.02	2496.88	1944.44	1392.31	1122.81	448.10	221.62	303.23	213.14	180.00	151.35
X2501_56	1.59	0.034	0.032	3.31	3.04	6.08	12.86	38.05	53.51	68.71	75.49	82.67	73.51
X2501_57	1.25	12.5	4.4	759.38	841.11	773.08	729.82	283.81	222.97	151.29	84.90	61.00	45.95
X2501_59	2.7	11.9	3.27	2303.13	1855.56	1523.08	1384.21	661.90	467.57	406.45	294.12	239.67	177.03
X2501_60	2.03	45	7.17	3584.38	3166.67	2246.15	1814.04	654.29	424.32	340.00	186.08	120.67	87.43
X2501_61	3.53	36.3	7.37	3293.75	1900.00	1130.77	836.84	298.57	133.24	197.74	132.35	112.67	100.27
X2501_62	1.98	7.46	1.7	1681.25	1525.56	1227.69	1077.19	481.90	239.19	264.52	171.18	132.00	94.05
Red River (Southwest)													
X2502_1	12.22	1.853	37.1	555.00	644.44	673.08	682.46	580.00	195.27	429.35	542.94	616.33	502.70
X2502_2	10.5	0.32	25.6	321.56	484.44	639.23	819.30	1050.95	320.68	919.35	1192.16	1186.67	818.92
X2502_3	35.4	54	31.2	840.63	1188.89	1469.23	1673.68	1385.71	639.19	996.77	992.16	1046.67	940.54
X2502_4	7.89	12.93	7.58	653.13	765.56	722.31	664.91	330.00	188.51	195.48	148.04	140.00	126.76
X2502_5	7.29	2.54	16.05	435.94	674.44	860.77	1061.40	1538.10	129.86	1445.16	1762.75	1516.67	801.35
X2502_6	4.58	28.3	9.41	4065.63	3755.56	3207.69	2649.12	1204.76	387.84	613.87	430.78	352.00	255.95
X2502_7	1.15	1.64	1.97	562.50	620.00	625.38	633.33	299.52	174.32	157.10	108.63	91.67	66.62
X2502_9	18.1	1.273	44.5	699.38	745.56	801.54	822.81	827.62	102.84	745.16	1054.90	1260.00	963.51
X2502_1	45.8	16.8	17.9	347.19	478.89	666.15	998.25	1290.48	397.30	1274.19	1468.63	1706.67	1445.95
X2502_2	63.2	8.21	11.8	1228.13	1622.22	2138.46	2578.95	2785.71	245.95	2254.84	2423.53	2723.33	2378.38
X2502_4	14.6	25.9	10.8	1834.38	1800.00	1530.77	1240.35	547.62	220.27	370.97	294.12	290.67	258.11
X2502_5	13.9	8.69	90.8	443.75	873.33	1269.23	1535.09	971.43	489.19	622.58	517.65	506.67	439.19
X2502_7	4.77	25.7	4.69	3993.75	2600.00	1869.23	1431.58	614.29	286.49	393.55	284.31	240.33	205.41
X2502_8	0.201	0.011	8E-04	0.29	0.64	1.14	2.09	3.71	3.34	7.29	8.53	10.60	11.88
X2502_9	8.45	14.1	3.8	2396.88	2155.56	2215.38	2298.25	1357.14	598.65	909.68	719.61	650.00	490.54
X2502_10	14.4	1.07	35.1	339.38	493.33	668.46	812.28	985.71	309.46	967.74	1270.59	1333.33	982.43

Sample ID	Lu	^{232}Th	^{238}U	La*	Ce*	Pr*	Nd*	Sm*	Eu*	Gd*	Tb*	Dy*	Ho*
X2502_11	16.2	31.3	23.8	328.75	511.11	710.77	1000.00	1238.10	508.11	1106.45	1117.65	1173.33	921.62
X2502_12	2.71	0.084	3.83	70.00	160.00	251.54	312.28	240.95	150.00	169.68	145.88	144.33	122.84
X2502_13	11.3	7.5	4.44	184.38	288.89	415.38	535.09	533.33	304.05	461.29	417.65	423.33	362.16
X2502_14	5.05	0.175	8.08	5.47	9.53	16.46	35.79	82.86	66.76	129.68	147.45	176.00	166.22
X2502_15	4.97	7.1	6.7	643.75	607.78	582.31	554.39	297.62	305.41	202.58	154.90	148.67	147.30
X2502_16	1.89	0.031	1.33	311.56	436.67	534.62	580.70	326.19	244.59	196.45	143.73	124.67	98.78
X2502_17	23	1.91	13.7	363.75	593.33	869.23	1273.68	1433.33	168.92	1300.00	1356.86	1383.33	1205.41
X2502_18	27.3	8.57	16.1	465.63	604.44	840.77	1135.09	1128.57	386.49	1012.90	980.39	1026.67	910.81
X2502_19	10.4	25.6	3.88	7187.50	4155.56	2469.23	1782.46	671.43	321.62	487.10	352.94	316.67	285.14
X2502_20	1.57	3.35	2.45	176.25	204.44	236.92	271.93	243.81	118.78	204.19	162.35	130.00	99.32
X2502_21	3.25	20.1	18	653.13	543.33	453.08	429.82	221.90	116.62	151.94	132.16	120.33	101.89
X2502_22	14.1	0.97	54.2	288.44	377.78	539.23	687.72	814.29	318.92	796.77	968.63	1000.00	739.19
X2502_23	0.887	0.756	2.19	378.75	434.44	430.00	394.74	149.52	137.03	77.74	44.90	31.37	23.78
X2502_24	6.34	18	2.45	2903.13	2555.56	2430.77	2473.68	1276.19	683.78	812.90	621.57	520.00	401.35
X2502_25	6.47	4.78	24.2	0.48	0.73	1.59	2.88	12.48	10.27	53.87	92.35	137.33	160.81
X2502_26	9.86	0.351	14.7	211.56	298.89	436.15	584.21	809.52	370.27	825.81	962.75	976.67	714.86
X2502_27	0.842	0.062	1.21	9.47	14.00	18.85	27.89	43.33	43.92	75.81	119.61	178.33	168.92
X2502_28	38.1	94	70	2353.13	2566.67	2753.85	2631.58	1728.57	1148.65	1374.19	1201.96	1163.33	1135.14
X2502_29	2.16	31.7	12.7	2525.00	2111.11	1700.00	1522.81	728.57	478.38	422.58	307.84	237.67	159.46
X2502_30	22.5	4.04	3.11	17.91	32.33	50.85	86.14	189.05	89.73	361.29	511.76	680.00	660.81
X2502_31	12.5	18	2.68	2746.88	3011.11	3246.15	3438.60	2185.71	714.86	1454.84	1278.43	1183.33	920.27
X2502_32	19.8	99.1	15.4	3128.13	2511.11	2246.15	2261.40	1242.86	375.68	909.68	823.53	813.33	766.22
X2502_33	2.99	2.65	3.27	812.50	823.33	892.31	978.95	633.33	404.05	396.77	305.88	248.33	175.68
X2502_34	0.9	5.38	4.1	709.38	533.33	557.69	766.67	561.90	294.59	345.16	205.88	139.00	89.73
X2502_35	1.26	13.9	5.85	1100.00	1123.33	1100.00	949.12	378.57	120.14	207.42	124.12	94.00	69.59
X2502_36	4.85	16	2.78	3321.88	2688.89	2630.77	2368.42	1133.33	575.68	700.00	498.04	426.67	309.46
X2502_37	5.7	0.432	24.6	11.22	35.22	115.38	294.74	470.48	295.95	432.26	352.94	335.00	282.43
X2502_38	5.2	7.48	2.15	1712.50	1633.33	1615.38	1796.49	1071.43	500.00	751.61	592.16	523.33	401.35
X2502_39	1.92	23.9	25.6	859.38	614.44	444.62	394.74	156.67	231.08	121.61	82.55	73.33	62.30
X2502_40	0.995	4.4	3.8	97.19	157.78	190.77	233.33	107.14	88.11	62.90	44.71	35.73	29.32
X2502_41	1.87	40.6	10.3	1646.88	1255.56	1192.31	989.47	495.24	290.54	300.00	200.00	156.00	122.97
Miss. S. of Arkansas (not used in study)													
X2601a_1	2.61	21.7	23.4	481.25	621.11	582.31	533.33	259.05	218.92	163.55	100.39	82.67	65.68

Sample ID	Lu	^{232}Th	^{238}U	La*	Ce*	Pr*	Nd*	Sm*	Eu*	Gd*	Tb*	Dy*	Ho*
X2601a_2	4.24	49.1	4.54	5062.50	4788.89	3146.15	2649.12	1138.10	644.59	683.87	435.29	359.00	251.35
X2601a_3	0.582	35.3	72.5	2578.13	3388.89	2953.85	2631.58	2295.24	83.51	1616.13	1152.94	656.67	251.35
X2601a_4	1.004	10.15	2.04	925.00	878.89	708.46	612.28	306.67	225.68	190.00	116.86	93.33	67.03
X2601a_5	2.35	31.7	17.9	1784.38	1334.44	990.00	870.18	420.48	229.73	276.13	196.08	178.67	134.73
X2601a_6	26.8	17.1	30.9	715.63	1061.11	1119.23	1217.54	1433.33	155.00	1225.81	1327.45	1450.00	1177.03
X2601a_7	7.2	0.259	4.53	375.00	574.44	668.46	794.74	914.29	212.16	709.68	719.61	730.00	502.70
X2601a_8	1.67	5.07	2.23	928.13	1046.67	930.00	922.81	534.76	491.89	336.77	227.45	189.00	131.62
X2601a_9	5.2	19.2	5.56	2256.25	2266.67	1676.92	1496.49	828.57	393.24	538.71	400.00	365.67	286.49
X2601a_10	3.19	70.5	21.4	990.63	1304.44	1092.31	1019.30	575.71	337.84	360.00	220.78	180.67	133.65
X2601a_11	2.01	0.023	1.86	77.50	137.56	177.69	215.09	182.86	110.95	130.97	100.00	91.33	74.32
X2601a_12	2.88	11.91	4.17	3012.50	3566.67	2530.77	2101.75	904.76	352.70	525.81	321.57	259.67	181.08
X2601a_13	2.22	2.1	6.15	116.56	140.22	132.31	133.68	109.52	150.00	91.61	73.53	68.67	57.30
X2601a_14	5.5	4.08	21.5	1190.63	1888.89	1700.00	1712.28	1204.76	81.89	893.55	760.78	660.00	458.11
X2601a_15	7.44	5.88	1.21	3653.13	3900.00	2938.46	2508.77	1242.86	205.41	790.32	613.73	560.00	448.65
X2601a_16	32.1	26.5	14.6	202.19	262.22	293.08	324.56	411.90	467.57	504.84	633.33	886.67	921.62
X2601a_17	3.05	18.6	11.3	2009.38	2055.56	1523.08	1163.16	530.48	166.22	318.06	214.71	183.33	145.54
X2601a_19	0.626	0.83	9.13	152.19	183.33	202.31	245.61	331.90	225.68	425.81	452.94	350.67	156.35
X2601a_20	0.511	3.49	13.2	152.50	174.44	152.31	141.40	76.19	94.19	44.84	25.69	18.57	14.61
X2601a_21	3.37	87.4	22.6	3446.88	2411.11	1446.15	1015.79	442.86	313.51	278.39	177.45	142.00	117.43
X2601_1	4.16	128	33.4	3937.50	2688.89	1546.15	1328.07	514.29	362.16	306.45	201.96	165.00	140.54
X2601_3	22.1	8.55	16	721.88	1183.33	1361.54	1556.14	1542.86	313.51	1177.42	1237.25	1216.67	991.89
X2601_5	3.05	4.79	28.6	188.75	365.56	476.92	561.40	376.19	213.51	208.06	168.63	128.33	107.84
X2601_6	3.78	30.9	4.14	3568.75	3400.00	2653.85	2315.79	1009.52	574.32	606.45	400.00	322.00	243.24
X2601_7	30.9	60.7	118	696.88	1044.44	1146.15	1312.28	1023.81	1064.86	912.90	837.25	800.00	745.95
X2601_8	3.76	4.01	3.68	3781.25	2366.67	1207.69	754.39	233.81	93.24	174.19	117.06	102.67	96.62
X2601_9	4.79	17.8	2.63	281.25	422.22	440.77	545.61	361.90	168.92	293.55	235.29	211.67	185.14
X2601_10	3	29.1	9.68	1909.38	1744.44	1153.85	938.60	389.05	251.35	241.29	160.00	129.33	111.22
X2601_11	1.41	34.4	23.4	3750.00	3422.22	2223.08	1721.05	619.05	201.35	312.90	168.04	112.33	79.19
X2601_12	2.18	5.79	4.97	1737.50	1855.56	1546.15	1385.96	642.86	337.84	370.97	245.10	174.33	125.68
X2601_13	4.72	22.3	10	2875.00	2855.56	2430.77	2087.72	1147.62	374.32	735.48	549.02	446.67	331.08
X2601_14	6.76	85	65.8	1309.38	1477.78	1569.23	1508.77	757.14	510.81	503.23	329.41	273.33	229.73
X2601_15	5.81	56.5	8.1	7093.75	6188.89	4238.46	3210.53	1095.24	539.19	625.81	372.55	287.00	231.08
X2601_16	13.9	572	304	8562.50	7100.00	4569.23	4017.54	1642.86	1594.59	1080.65	664.71	520.00	428.38
X2601_17	21.2	50.6	46.6	2521.88	4366.67	4507.69	4842.11	3014.29	1064.86	1880.65	1543.14	1423.33	1095.95

Sample ID	Lu	^{232}Th	^{238}U	La*	Ce*	Pr*	Nd*	Sm*	Eu*	Gd*	Tb*	Dy*	Ho*
X2601_19	15.8	10.1	1.99	1456.25	1966.67	2084.62	2228.07	1509.52	259.46	977.42	901.96	826.67	663.51
X2601_20	3.54	50.1	18.4	4375.00	4255.56	2969.23	2350.88	933.33	362.16	493.55	298.04	224.00	167.57
X2601_22	13.6	7.3	17.1	462.50	661.11	780.00	856.14	885.71	318.92	770.97	882.35	936.67	793.24
X2601_23	0.891	3.95	2.91	1446.88	1533.33	1300.00	1207.02	566.67	293.24	298.06	174.12	115.67	69.46
X2601_24	3.63	11.5	5.07	2281.25	2388.89	1961.54	1687.72	761.90	300.00	427.10	292.16	246.00	181.08
X2601_25	1.1	13.3	11.7	292.50	267.78	183.08	164.56	62.86	86.22	43.23	27.84	23.97	21.76
X2601_26	2.08	19.4	5.73	3281.25	2777.78	1846.15	1642.11	709.52	237.84	396.77	241.37	183.67	131.08
X2601_27	2.67	11.24	3.88	2831.25	2966.67	2346.15	2108.77	885.71	322.97	474.19	313.73	238.00	168.92
X2601_28	5.48	56.9	86.2	878.13	1288.89	1200.00	1105.26	552.38	355.41	312.90	209.80	181.33	151.35
X2601_29	45.2	0.649	7.49	1437.50	2244.44	2469.23	2912.28	3309.52	259.46	2751.61	2588.24	2473.33	2013.51
X2601_30	2.14	6.93	2	525.00	671.11	583.85	478.95	237.62	99.73	136.77	118.04	114.00	90.14
X2601_31	23.6	9.9	13.1	1040.63	1544.44	1676.92	1877.19	1790.48	359.46	1338.71	1470.59	1496.67	1159.46
X2601_32	12.5	71.9	158	2012.50	2033.33	1761.54	1557.89	1080.95	664.86	709.68	641.18	616.67	472.97
X2601_33	2.18	19.2	6.93	3815.63	2544.44	1400.00	1019.30	363.81	217.57	231.61	138.04	111.33	87.30
X2601_34	3.55	13.3	1.94	271.88	306.67	283.08	273.68	310.95	127.03	392.26	466.67	486.33	359.46
X2601_35	1.51	5.07	3.95	1440.63	1522.22	1438.46	1266.67	628.10	283.78	340.65	213.53	157.67	104.19
X2601_36	3.83	12.2	6.6	550.00	716.67	679.23	698.25	308.57	222.97	212.90	146.08	132.33	114.46
X2601_37	4.35	15.9	3.21	1962.50	2055.56	1646.15	1656.14	861.90	420.27	545.16	411.76	354.67	274.32
X2601_38	1.91	5.46	3.46	1428.13	1566.67	1392.31	1243.86	569.05	250.00	307.42	192.75	155.00	108.38
X2601_39	11.59	120	62.9	2968.75	3033.33	2284.62	1796.49	876.19	452.70	516.13	380.39	340.67	287.84
X2601_40	13.4	3.85	70.7	167.50	420.00	831.54	1282.46	1300.00	1044.59	848.39	729.41	643.33	510.81
X2601_41	3.2	1.99	8.1	65.63	76.67	115.38	180.70	274.29	143.24	289.68	272.55	255.33	209.46
X2601_42	0.76	3.43	9.3	1296.88	800.00	551.54	407.02	135.24	144.46	85.81	46.47	36.07	30.14
X2601_43	2.02	23.7	31.6	496.88	310.00	233.08	215.79	129.52	95.68	105.48	94.51	97.67	85.27
X2601_45	2.11	46.7	30.9	1687.50	1123.33	769.23	577.19	220.95	142.57	137.42	93.33	84.00	68.51
Arkansas River (Southwest)													
X2602_1	1.506	12.79	16.03	296.25	435.56	536.92	628.07	298.57	196.49	159.35	100.00	76.10	58.65
X2602_2	9.23	3.36	7.26	2278.13	2380.00	2276.92	2445.61	2061.90	102.03	1432.26	1249.02	1113.33	829.73
X2602_3	15.66	34.2	43	688.44	994.44	1414.62	2021.05	2566.67	1133.78	2132.26	2035.29	1820.00	1263.51
X2602_4	12.88	247	78.2	2715.63	3444.44	3261.54	3122.81	1571.43	732.43	800.00	582.35	506.67	422.97
X2602_5	3.21	5.47	6.91	1478.13	758.89	479.23	385.44	186.19	103.92	123.23	96.08	94.00	87.16
X2602_6	16.35	14.04	32	703.75	834.44	956.15	1143.86	974.29	219.59	640.32	574.51	580.67	520.27
X2602_7	23.3	1.82	6.24	287.50	397.78	616.92	1012.28	1504.76	224.32	1077.42	1074.51	1076.67	866.22

Sample ID	Lu	^{232}Th	^{238}U	La*	Ce*	Pr*	Nd*	Sm*	Eu*	Gd*	Tb*	Dy*	Ho*
X2602_8	10.89	0.524	18.9	207.50	345.56	512.31	714.04	771.43	137.97	524.52	537.25	558.67	475.68
X2602_9	3.32	37.9	10.18	4296.88	2573.33	1572.31	1215.79	534.76	113.24	262.26	164.71	130.00	108.65
X2602_10	19.4	2.96	30.8	460.63	675.56	1009.23	1508.77	2152.38	1066.22	1493.55	1556.86	1576.67	1247.30
X2602_11	5.02	18.7	8.67	946.88	771.11	691.54	664.91	440.00	156.08	240.00	198.43	189.00	163.78
X2602_12	4.07	7.16	2.4	640.00	611.11	628.46	743.86	688.57	255.41	395.16	354.51	336.00	260.41
X2602_13	23.6	68.1	69.7	1134.38	1422.22	1500.00	1661.40	1476.19	693.24	819.35	739.22	723.33	631.08
X2602_15	3.81	7.76	2.36	2378.13	2048.89	1680.00	1519.30	854.29	339.19	346.13	247.65	211.00	160.41
X2602_16	2.91	6.56	6.76	302.19	308.89	288.46	284.74	188.57	136.49	102.26	80.59	79.33	68.38
X2602_17	96.2	28.5	26.7	239.69	334.44	506.15	877.19	2004.76	990.54	2241.94	3237.25	4036.67	3756.76
X2602_20	7.01	30.3	6.06	1781.25	1646.67	1650.00	1785.96	1156.19	315.00	674.84	553.53	495.33	386.49
X2602_21	6.75	8.45	2.19	2368.75	2225.56	2060.77	2108.77	1107.62	471.62	726.77	594.12	523.33	402.70
X2602_22	0.27	0.069	0.114	13.16	19.11	25.38	33.51	22.86	15.14	20.06	14.71	13.07	10.43
X2602_24	4.81	1.04	0.712	4334.38	4466.67	3715.38	3385.96	1228.57	645.95	745.16	513.73	423.67	312.16
X2602_25	6.36	0.553	8.67	310.94	471.11	615.38	747.37	658.57	233.38	636.45	870.59	960.00	693.24
X2602_26	5.52	0.068	3	240.94	437.78	629.23	757.89	669.05	289.19	583.55	705.88	753.33	575.68
X2602_27	7.7	44.3	15.4	5687.50	4966.67	3384.62	2719.30	895.24	360.81	648.39	454.90	397.00	317.57
X2602_28	1.95	1.11	5.03	928.13	883.33	686.92	619.30	187.14	187.70	129.68	84.71	69.33	57.16
X2602_29	25.9	4.17	5.99	762.50	1164.44	1376.92	1514.04	1019.05	375.68	832.26	927.45	1143.33	1078.38
X2602_30	20.03	30.6	30.9	1737.50	1747.78	1416.15	1363.16	795.24	783.78	764.52	739.22	812.33	718.92
X2602_31	13.69	2.04	31.1	430.63	722.22	993.85	1273.68	1242.86	525.68	1258.06	1409.80	1476.67	1097.30
X2602_32	2.56	9.39	4.7	3934.38	3655.56	2592.31	2145.61	663.33	354.05	400.65	257.45	202.00	145.81
X2602_33	7.65	19.8	5.5	6809.38	6588.89	5476.92	5298.25	2195.24	1559.46	1445.16	1021.57	836.67	594.59
X2602_34	4	8.95	4	1818.75	1931.11	1723.85	1768.42	796.19	597.30	577.42	414.90	363.33	267.97
X2602_35	3.1	53.5	15.78	4050.00	3455.56	2353.85	1915.79	629.52	332.43	376.13	238.43	189.67	142.57
X2602_37	12.72	37	9.24	6893.75	5877.78	4684.62	4340.35	1928.57	878.38	1274.19	1001.96	933.33	712.16
X2602_38	1.04	6.74	3.16	806.25	720.00	603.08	517.54	198.57	129.19	117.74	71.57	56.77	42.97
X2602_40	15.13	4.55	46.2	314.06	540.00	925.38	1515.79	1490.48	389.19	1277.42	1168.63	1186.67	955.41
X2602_41	1.51	14.9	3.96	1268.75	1384.44	1280.00	1173.68	399.52	298.65	205.81	110.39	80.33	58.65
X2602_42	21.7	0.784	4.09	19.97	70.67	163.85	347.37	761.90	108.78	1109.68	1480.39	1783.33	1513.51
X2602_43	1.627	1.92	6.95	54.53	77.89	111.23	147.02	111.43	79.73	72.90	59.22	51.27	42.30
X2602_44	12.9	2.37	10.65	275.00	354.11	482.31	687.72	865.71	567.57	926.77	925.49	979.33	801.35
X2602_45	14.27	11.77	56.7	648.75	892.22	1109.23	1329.82	1262.86	374.32	912.90	886.27	910.00	741.89
X2602_46	14.8	2.56	24.1	71.88	230.00	380.00	531.58	776.19	121.62	912.90	1045.10	1173.33	917.57
X2602_47	9.14	0.239	5.96	320.63	556.67	769.23	1038.60	1347.62	278.38	1245.16	1268.63	1130.00	736.49

Sample ID	Lu	^{232}Th	^{238}U	La*	Ce*	Pr*	Nd*	Sm*	Eu*	Gd*	Tb*	Dy*	Ho*
X2602_48	17.1	15	19.5	1784.38	2366.67	2246.15	2140.35	1209.52	354.05	806.45	717.65	736.67	621.62
X2602_49	7.23	0.298	3.3	68.13	149.78	257.69	414.04	626.19	227.03	648.39	800.00	856.67	640.54
X2602_50	1.475	8.78	5.52	1565.63	1466.67	1073.85	922.81	386.19	128.51	205.48	119.22	84.67	60.00
X2602_51	2.4	23.5	34.5	668.75	424.44	272.31	217.89	100.95	120.41	69.68	53.53	55.00	50.14
X2602_52	1.296	5.84	1.73	837.50	777.78	674.62	671.93	352.86	318.92	215.81	153.73	127.00	93.38
X2602_1	6.24	12.99	44.6	2275.00	1716.67	1319.23	1222.81	641.90	192.84	456.45	379.41	349.00	279.46
X2602_2	13.08	0.091	2.27	1.12	1.83	4.58	17.75	102.38	153.24	240.65	329.22	417.33	400.00
X2602_3	2.77	0.759	11.96	759.38	1023.33	1039.23	1070.18	506.67	247.57	278.71	195.69	166.00	124.73
X2602_4	21	27.7	67.2	2553.13	2511.11	2807.69	3228.07	2847.62	693.24	2241.94	2256.86	2240.00	1748.65
X2602_5	3.32	28.8	7.65	4362.50	2900.00	2253.85	2040.35	863.81	394.59	453.55	292.16	223.33	166.35
X2602_6	24.7	6.45	13.87	631.88	1066.67	1531.54	2071.93	2366.67	825.68	1822.58	2037.25	2103.33	1608.11
X2602_7	1.783	3.12	1.086	926.25	784.44	783.08	880.70	480.48	427.03	300.32	217.84	179.33	129.05
X2602_8	7.35	26.7	10.14	4721.88	3613.33	3207.69	3178.95	1638.10	120.41	959.03	747.06	654.33	489.19
X2602_9	6.79	0.057	2.77	147.50	275.67	450.00	701.75	829.52	512.16	670.65	711.76	697.67	508.11
X2602_10	16.76	23.43	14.34	4693.75	5988.89	6300.00	7263.16	4076.19	1231.08	2393.55	1845.10	1560.00	1159.46
X2602_11	5.8	12.89	5.99	1540.63	1631.11	1696.92	1764.91	800.48	425.68	413.55	282.75	239.33	196.62
X2602_12	1.232	7.48	3.66	727.50	732.22	716.92	763.16	322.38	169.59	183.23	109.02	81.00	59.59
X2602_13	4.37	3.27	0.857	1375.00	1325.56	1380.00	1645.61	1001.43	629.73	635.48	498.04	439.67	324.32
X2602_14	6.96	29.2	11.16	2831.25	1930.00	1416.92	1249.12	538.10	167.43	354.84	282.55	266.33	231.35
X2602_15	11.57	6.96	7.92	248.75	397.78	511.54	649.12	398.10	207.43	280.65	238.24	245.00	234.19
X2602_16	21.5	8.29	15.8	315.94	375.56	499.23	728.07	833.33	335.14	890.32	964.71	1076.67	983.78
X2602_17	14.74	3.22	30.3	255.31	343.33	510.77	835.09	978.10	747.30	912.90	862.75	870.00	731.08
X2602_19	12.47	7.51	20.22	398.75	565.56	803.08	1173.68	1112.86	491.89	888.39	862.75	861.33	685.14
X2602_20	2.68	2.94	0.665	1262.50	1087.78	1075.38	1235.09	691.43	587.84	436.13	323.33	272.67	193.92
X2602_21	5.21	2.41	4.07	365.31	356.67	393.08	473.68	362.38	215.14	267.10	233.14	225.00	183.38
X2602_22	4.02	0.654	3.9	384.69	384.44	393.85	444.74	242.86	230.41	162.90	123.73	118.67	105.00
X2602_23	20.6	4.44	7.69	570.31	850.00	1166.15	1514.04	1448.57	391.22	977.42	1039.22	1116.67	912.16
X2602_24	1.82	1.09	1.19	125.00	158.11	182.31	222.28	108.10	67.70	74.52	51.57	47.33	44.86
X2602_25	4.44	9.16	18	238.13	265.78	298.46	371.58	247.62	169.46	181.94	140.00	129.33	110.14
X2602_26	16.99	11.21	15.9	524.69	657.78	844.62	1108.77	854.29	639.19	646.77	578.43	576.00	510.81
X2602_27	1.94	5.13	1.64	876.88	733.33	732.31	822.81	458.57	348.65	292.26	219.80	185.33	133.78
X2602_28	3.63	11.99	17.14	2359.38	1887.78	1555.38	1491.23	751.43	148.92	504.84	380.78	336.67	257.16
X2602_29	3.46	0.31	2.4	6.28	13.02	29.69	71.40	144.76	52.43	153.23	150.00	157.33	131.62
X2602_30	3.76	21.4	8.85	1243.75	1370.00	1465.38	1605.26	880.48	637.84	483.87	361.76	309.00	223.11

Sample ID	Lu	^{232}Th	^{238}U	La*	Ce*	Pr*	Nd*	Sm*	Eu*	Gd*	Tb*	Dy*	Ho*
X2602_31	3.09	32.5	27.2	1943.75	1294.44	925.38	866.67	399.05	359.46	270.65	182.55	154.33	124.59
X2602_32	12.65	29.1	18.7	598.75	968.89	1354.62	1787.72	1209.52	700.00	812.90	658.82	611.67	512.16
X2602_33	38.8	35.2	67.7	513.44	736.67	1057.69	1629.82	2185.71	741.89	2229.03	2547.06	2703.33	2228.38
X2602_34	13.89	13.72	15.94	339.38	370.00	483.08	643.86	652.38	435.14	581.29	550.98	554.00	490.54
X2602_35	4.95	28	13.1	4212.50	2325.56	1715.38	1524.56	687.14	150.41	433.23	317.25	273.33	218.11
X2602_36	28.8	6.23	23.2	753.13	1008.89	1356.92	1819.30	2142.86	917.57	1832.26	2147.06	2246.67	1705.41
X2602_37	1.074	3.14	3.23	1384.38	701.11	451.54	380.70	130.95	124.05	79.68	51.37	43.63	34.73
X2602_38	2.97	22.1	13.54	1090.63	1455.56	1614.62	1710.53	681.90	431.08	321.94	202.55	149.67	110.27
X2602_39	17.3	1.28	6.13	624.38	702.22	819.23	1003.51	1042.86	277.03	883.87	1100.00	1263.33	1040.54
X2602_40	12.12	0.31	7.49	105.63	147.56	213.08	343.86	438.10	211.22	422.58	521.57	600.00	521.62
X2602_42	0.326	0.088	0.07	27.44	30.56	33.08	40.18	25.00	10.81	20.03	15.20	13.63	11.99
X2602_44	1.91	3.98	2.59	207.50	202.22	213.08	256.14	150.00	116.62	102.90	78.82	71.33	59.32
Miss. S. of Ohio (not used in study)													
X2603_1	2.1	0.225	8.69	187.19	332.22	452.31	589.47	509.05	156.76	301.61	220.59	186.00	131.89
X2603_2	22.8	0.156	18.5	571.88	768.89	958.46	1300.00	1452.38	88.51	1483.87	1709.80	1923.33	1621.62
X2603_3	2.31	7.39	4.09	1834.38	1800.00	1392.31	1110.53	463.81	236.49	273.23	187.84	149.00	113.51
X2603_4	16.2	0.747	15.5	376.88	682.22	963.08	1273.68	1257.14	610.81	903.23	880.39	906.67	704.05
X2603_5	11.48	9.76	12.69	361.56	588.89	752.31	959.65	1123.81	328.38	951.61	1070.59	1043.33	724.32
X2603_6	2.18	1.167	0.936	800.00	851.11	758.46	736.84	406.67	187.84	269.35	183.92	145.00	103.38
X2603_7	2.59	16.9	4.55	1900.00	1900.00	1515.38	1508.77	780.95	474.32	474.19	339.22	280.67	195.95
X2603_8	1.303	7.83	4.25	1956.25	2000.00	1669.23	1456.14	710.48	363.51	366.77	231.96	158.33	101.76
X2603_9	8.95	0.022	19.7	271.88	466.67	624.62	778.95	919.05	635.14	790.32	886.27	873.33	620.27
X2603_10	8.41	128.6	91.5	3115.63	3033.33	2215.38	1938.60	1023.81	247.30	629.03	533.33	485.00	387.84
X2603_12	1.12	0.09	0.37	3.94	6.22	8.54	15.79	37.14	49.73	55.48	59.02	67.33	53.51
X2603_13	2.18	19.4	7.61	3940.63	2466.67	1646.15	1456.14	640.95	161.35	390.97	241.76	189.33	130.41
X2603_14	3.18	6.38	4.54	721.88	820.00	928.46	1008.77	819.05	459.46	573.55	452.94	384.67	264.86
X2603_15	6.32	0.11	3.34	47.50	67.22	92.08	121.58	177.62	119.46	268.39	384.31	498.67	455.41
X2603_17	3.6	45.7	9.81	2903.13	2900.00	2407.69	2075.44	985.71	520.27	535.48	358.82	289.00	208.11
X2603_18	0.919	1.28	2.69	353.44	547.78	640.00	691.23	351.90	251.35	181.29	105.88	70.33	47.97
X2603_19	17.9	0.205	20	603.13	932.22	1103.85	1264.91	1314.29	331.08	1125.81	1303.92	1423.33	1110.81
X2603_20	2.42	44.1	7.53	1528.13	1110.00	1078.46	1129.82	626.67	409.46	400.32	285.88	235.33	168.11
X2603_21	2.88	28.7	8.3	2665.63	1460.00	743.85	545.61	212.38	166.35	150.00	102.55	90.33	77.97
X2603_22	35.5	6.2	3.84	1181.25	1777.78	1838.46	1957.89	1638.10	331.08	1170.97	1296.08	1413.33	1222.97

Sample ID	Lu	^{232}Th	^{238}U	La*	Ce*	Pr*	Nd*	Sm*	Eu*	Gd*	Tb*	Dy*	Ho*
X2603_23	4.65	19.1	19.7	815.63	886.67	829.23	840.35	548.10	804.05	363.55	278.43	253.33	194.46
X2603_24	0.94	8.22	6.8	234.69	283.33	235.38	215.79	90.95	57.16	54.52	36.27	28.87	23.65
X2603_25	5.82	88.3	37.2	1553.13	1277.78	892.31	708.77	321.43	322.97	220.65	167.06	159.67	141.49
X2603_26	4.53	10.9	3.8	737.50	913.33	961.54	970.18	571.43	218.92	364.52	284.31	258.00	204.05
X2603_27	1.79	21	5.32	4531.25	3222.22	1900.00	1526.32	580.95	324.32	323.23	180.00	123.67	88.92
X2603_28	4.77	28.8	13.49	268.75	473.33	657.69	814.04	638.10	271.62	384.52	301.96	263.00	204.19
X2603_29	4.29	5.72	5.77	1787.50	2333.33	2130.77	2182.46	1647.62	190.27	1012.90	794.12	623.33	408.11
X2603_30	1.54	9.87	5.07	1825.00	2200.00	1746.15	1494.74	636.67	266.22	328.39	200.00	143.00	96.35
X2603_31	2.74	18.2	6.75	2471.88	2944.44	2223.08	1828.07	880.95	304.05	493.55	341.18	280.67	198.65
X2603_32	3.48	11.4	3.18	2231.25	2255.56	1630.77	1445.61	671.43	263.51	382.90	297.06	258.00	199.32
X2603_33	2.63	9.9	6.08	1643.75	1844.44	1446.15	1328.07	638.10	359.46	425.81	286.27	232.67	172.97
Upper Mississippi River (Northern)													
X2701_1	3.24	5.87	7.38	245.94	628.89	976.92	1324.56	833.33	491.89	438.71	305.88	234.33	168.92
X2701_2	48.6	3.06	9.49	7187.50	8133.33	6853.85	6280.70	3538.10	939.19	2267.74	2166.67	2236.67	1960.81
X2701_3	5.5	5.32	5.16	1718.75	2522.22	2684.62	3052.63	1923.81	339.19	1067.74	750.98	601.33	420.27
X2701_4	6.42	43.4	31	387.50	621.11	869.23	1192.98	1047.62	570.27	693.55	535.29	483.33	351.35
X2701_5	2.25	12.7	14.2	587.50	733.33	738.46	715.79	340.95	252.70	182.90	123.33	98.67	72.43
X2701_6	4.88	57.7	20.4	4071.88	4377.78	3607.69	3298.25	1533.33	352.70	900.00	596.08	479.33	355.41
X2701_7	1.93	0.651	1.271	26.31	34.22	41.69	54.04	59.52	59.19	63.23	73.73	88.00	79.86
X2701_8	3.72	22.2	11.1	1475.00	1555.56	1430.77	1408.77	804.76	377.03	590.32	456.86	399.67	304.05
X2701_9	0.979	2.68	4.3	1375.00	1044.44	622.31	466.67	163.81	218.92	95.81	56.08	43.93	36.08
X2701_10	6.01	49.7	9.3	2346.88	2455.56	2200.00	2136.84	1290.48	51.62	938.71	784.31	706.67	533.78
X2701_11	0.268	0.168	5.37	605.63	681.11	549.23	480.70	153.81	95.00	75.81	39.61	25.53	17.31
X2701_13	8.14	62.2	37.5	1606.25	1900.00	1907.69	2031.58	1109.52	514.86	687.10	498.04	427.33	339.19
X2701_14	7.26	9.44	5.34	245.31	328.89	476.15	703.51	664.29	514.86	503.55	370.78	315.00	246.35
X2701_15	3.18	69.2	51.7	2381.25	1995.56	1586.92	1454.39	603.81	255.81	338.06	208.04	161.00	123.92
X2701_16	1.092	36.6	28.3	739.69	654.44	620.00	608.77	233.33	269.86	121.29	58.04	37.47	29.19
X2701_17	2.69	92.3	14.6	281.25	622.22	1014.62	1475.44	985.71	574.32	539.03	335.88	243.33	163.51
X2701_18	3.93	19.6	13.57	709.38	912.22	767.69	728.07	411.90	344.59	266.77	201.37	166.33	138.51
X2701_19	27.1	10.38	10.7	693.75	1034.44	1196.92	1331.58	1590.48	263.24	1396.77	1698.04	1843.33	1478.38
X2701_20	1.405	2.22	9.13	194.38	321.11	421.54	482.46	303.81	213.51	171.94	114.12	95.00	73.24
X2701_21	0.567	1.38	1	18.91	24.67	30.38	40.00	30.38	30.14	21.48	14.12	13.37	11.99
X2701_22	1.155	1	11.8	41.56	83.33	140.77	242.11	332.86	267.57	266.45	197.06	150.33	98.78

Sample ID	Lu	^{232}Th	^{238}U	La*	Ce*	Pr*	Nd*	Sm*	Eu*	Gd*	Tb*	Dy*	Ho*
X2701_23	20.5	39.5	16.4	1040.63	1455.56	1638.46	1877.19	1704.76	616.22	1264.52	1005.88	906.67	728.38
X2701_24	0.8	5.25	6.73	308.13	392.22	416.15	385.96	150.00	116.89	72.58	44.12	32.03	26.22
X2701_25	3.59	1.32	2.83	431.25	605.56	783.85	929.82	652.38	424.32	410.97	294.12	232.33	172.43
X2701_26	3.6	4.62	92.6	288.75	363.33	456.92	626.32	545.71	483.78	393.55	267.06	224.67	169.59
X2701_27	2.76	35.8	7.32	1303.13	1877.78	1576.92	1478.95	600.00	670.27	298.39	175.69	128.00	91.22
X2701_30	2.69	11.35	18.6	435.63	646.67	726.15	856.14	631.43	475.68	336.13	246.67	197.67	140.68
X2701_31	0.972	3.08	10.52	91.88	123.78	150.00	174.21	112.38	118.51	81.61	52.35	41.67	34.86
X2701_32	1.55	4.58	14.7	1140.63	2122.22	2315.38	2315.79	1238.10	309.46	664.52	435.29	324.00	210.81
X2701_33	9.86	14	27.4	415.63	536.67	679.23	824.56	719.05	416.22	658.06	643.14	646.67	529.73
X2701_34	7.77	7.88	21.4	90.63	150.00	204.62	305.26	341.90	122.30	385.81	419.61	474.33	428.38
X2701_35	3.23	15.3	2.86	1759.38	2011.11	1561.54	1403.51	590.48	266.22	319.03	202.94	163.67	128.38
X2701_36	0.439	20.8	6.61	687.50	843.33	738.46	650.88	225.24	102.97	99.03	48.04	29.77	22.57
X2701_37	0.74	1.6	0.662	659.38	950.00	960.77	882.46	355.24	186.49	172.90	99.02	66.00	44.46
X2701_38	0.514	1.54	4.54	684.38	913.33	776.92	731.58	288.10	104.19	133.23	72.55	48.07	31.62
X2701_39	4.61	27.9	9.39	2278.13	2466.67	1938.46	1794.74	919.05	350.00	564.52	425.49	373.67	286.49
X2701_40	3.22	8.01	27.3	803.13	1028.89	926.92	947.37	464.29	177.30	299.35	204.12	169.00	135.54
X2701_41	6.93	2.36	13.5	38.44	88.89	187.69	419.30	628.57	209.46	535.48	488.24	465.67	371.62
X2701_42	10.23	13.7	16.6	518.75	645.56	713.85	805.26	703.81	194.59	580.65	531.37	528.00	409.46
X2701_43	7.42	8	9.15	275.00	424.44	546.15	663.16	535.24	470.27	365.81	325.49	325.00	264.32
X2701_44	1.36	32.8	17.6	1306.25	1233.33	969.23	942.11	459.52	443.24	296.45	190.00	147.33	104.19
X2701_45	2.5	34.9	6.78	871.88	1220.00	1169.23	1222.81	673.81	509.46	339.68	213.53	155.33	109.73
X2701_46	1.29	1.88	1.33	1475.00	1611.11	1392.31	1314.04	577.62	215.27	275.16	169.22	121.67	81.76
X2701_47	2.61	17.1	29	289.69	393.33	482.31	582.46	451.43	183.78	308.06	225.88	185.00	140.41
X2701_1	9.5	28.4	19.2	2150.00	1910.00	1930.77	2189.47	1319.05	385.14	1022.58	801.96	716.67	583.78
X2701_2	4.44	3.37	2.68	1371.88	1070.00	886.92	821.05	374.76	236.49	245.48	169.41	144.67	117.16
X2701_3	1.224	60.4	35	3103.13	1657.78	1000.00	726.32	240.95	146.49	148.39	91.57	74.67	56.35
X2701_4	0.91	13.7	2.42	2025.00	1326.67	930.00	768.42	263.33	114.59	136.13	85.29	62.33	48.65
X2701_5	14.34	2.22	11.5	131.56	197.00	269.23	365.79	373.33	217.97	257.10	380.20	528.00	479.73
X2701_6	9.77	5.49	15.49	356.56	360.00	414.62	600.00	760.95	160.41	851.61	823.53	833.33	698.65
X2701_7	2.26	36.4	7.61	3540.63	2644.44	1976.92	1578.95	522.38	210.41	262.58	144.12	97.33	72.03
X2701_8	5.63	0.159	7.46	44.81	87.44	169.23	325.79	511.43	105.14	494.52	552.94	577.33	455.41
X2701_9	1.24	8.63	16.94	170.00	224.67	265.38	339.30	199.52	146.08	113.55	74.71	59.83	45.54
X2701_10	0.598	4.49	3.48	174.06	189.33	210.77	245.09	150.95	108.65	80.32	53.14	40.73	29.05
X2701_11	1.94	6	1.01	2125.00	1948.89	1746.15	1780.70	804.76	248.65	439.35	298.24	226.67	157.70

Sample ID	Lu	^{232}Th	^{238}U	La*	Ce*	Pr*	Nd*	Sm*	Eu*	Gd*	Tb*	Dy*	Ho*
X2701_12	4.71	13.01	3.38	5796.88	4244.44	3423.08	3033.33	1290.48	437.84	712.90	515.69	422.00	306.76
X2701_14	0.526	41.8	7.57	1084.38	912.22	792.31	738.60	265.71	171.62	133.87	72.55	46.10	29.86
X2701_15	3.25	32.8	59.8	718.75	870.00	980.77	1075.44	553.33	314.86	314.19	220.98	190.00	147.16
X2701_16	2.72	6.6	4.45	946.88	876.67	843.08	915.79	423.33	142.70	233.23	160.59	131.00	102.70
X2701_17	2.78	1.48	1.82	76.25	88.22	102.31	152.81	130.48	117.70	125.16	117.25	128.67	117.84
X2701_19	3.3	29.2	20.8	574.69	564.44	540.00	585.96	348.10	124.05	230.65	157.84	139.33	113.92
X2701_20	14.04	2.79	5.93	556.25	573.33	656.15	768.42	733.33	170.27	693.55	762.75	846.67	731.08
X2701_21	3.41	27.6	10.14	1562.50	1514.44	1369.23	1243.86	533.81	267.57	285.16	181.37	143.33	109.86
X2701_22	6.74	3.09	26.8	29.75	71.44	142.85	289.47	630.00	155.41	770.97	956.86	1013.33	741.89
X2701_25	5.03	14.5	8.5	174.06	280.00	460.77	721.05	714.29	264.86	532.26	419.61	338.67	247.30
X2701_27	0.829	19.5	15.9	381.88	404.44	420.00	478.95	237.62	178.38	126.77	70.00	46.97	34.05
X2701_28	6.42	4.04	6.28	140.63	168.56	235.38	396.49	434.29	218.92	383.23	309.80	289.67	239.19
X2701_29	0.548	30.7	8.86	765.63	825.56	868.46	954.39	381.90	258.11	151.61	74.51	42.93	26.76
X2701_30	1.323	0.041	1.65	85.56	158.00	256.92	390.18	268.57	177.30	157.42	116.47	96.67	71.89
X2701_31	1.04	0.33	1.38	13.97	19.89	38.23	82.98	87.14	56.35	76.13	59.02	55.00	44.59
X2701_32	14.12	16.9	5.63	2515.63	2208.89	2174.62	2531.58	1761.90	601.35	1332.26	1201.96	1123.33	877.03
X2701_34	1.067	0.98	6.12	161.25	203.56	262.31	343.86	211.90	109.86	123.23	76.08	58.33	42.16
X2701_36	1.22	44.3	12.64	1446.88	1173.33	876.92	714.04	216.67	204.05	122.58	65.49	47.33	37.16
X2701_37	2.15	5.85	2.53	362.81	886.67	1653.85	2071.93	1057.14	252.70	448.71	308.04	225.67	154.86
X2701_38	14.57	39.8	26.7	1975.00	2988.89	3615.38	4543.86	2785.71	420.27	1719.35	1384.31	1216.67	912.16
X2701_39	11	37	43.5	637.50	738.89	823.08	1038.60	768.57	267.57	574.84	482.35	451.67	360.81
X2701_40	13.72	12.82	11.08	173.13	240.00	345.38	519.30	647.62	266.22	683.87	750.98	790.00	664.86
X2701_41	1.164	4.28	2.19	1509.38	1367.78	1325.38	1412.28	614.29	264.86	289.03	169.41	117.33	78.38
X2701_42	4.04	27.1	10.04	564.69	586.67	620.77	696.49	377.62	178.38	248.39	189.02	175.67	141.62
X2701_43	3.78	33.2	7.47	482.19	534.44	593.08	666.67	413.81	300.00	265.48	199.80	178.00	139.73
X2701_44	1.23	30.3	2.24	3390.63	2955.56	2592.31	2508.77	1152.38	866.22	580.65	394.12	272.33	162.43
X2701_45	0.426	11.46	6.25	2918.75	2377.78	1776.92	1521.05	450.48	221.62	188.39	89.61	50.33	31.89
X2701_46	2.72	30.8	13.8	1203.13	1627.78	1976.92	2326.32	1057.14	516.22	477.74	278.04	187.33	127.16
X2701_47	23.7	8.58	14.9	903.13	1124.44	1530.77	2119.30	2419.05	272.97	2061.29	1707.84	1503.33	1074.32
X2701_48	3.5	1.29	61.3	446.56	695.56	1082.31	1614.04	2319.05	171.22	2316.13	2219.61	1576.67	729.73
Missouri River (Missouri)													
X2703a_1	2.73	18.7	15.98	1131.25	934.44	776.92	663.16	261.43	237.84	168.39	112.94	94.00	80.95
X2703a_2	5.5	26	3.48	3715.63	2343.33	1885.38	1682.46	799.52	389.19	526.13	406.86	341.00	278.24

Sample ID	Lu	^{232}Th	^{238}U	La*	Ce*	Pr*	Nd*	Sm*	Eu*	Gd*	Tb*	Dy*	Ho*
X2703a_3	2.84	22	11.04	3256.25	2137.78	1498.46	1136.84	453.81	226.62	297.74	204.31	167.67	133.51
X2703_1	2.42	6.94	1.01	1037.50	828.89	786.92	807.02	437.14	274.32	262.58	204.90	184.33	144.05
X2703_2	8.52	0.86	7.18	190.63	350.00	614.62	936.84	1428.57	463.51	1164.52	1078.43	1026.67	724.32
X2703_3	4.05	36.6	4.95	2437.50	1806.67	1676.92	1617.54	933.33	531.08	561.29	407.84	357.00	264.86
X2703_4	5.49	33.2	10.87	3325.00	2655.56	2315.38	2133.33	1076.19	329.73	648.39	486.27	451.67	337.84
X2703_5	2.41	47.4	11.79	1956.25	1416.67	1220.77	1101.75	594.76	298.65	350.65	249.22	222.67	159.32
X2703_6	5.65	16.8	2.13	5228.13	3788.89	2938.46	2592.98	1114.29	483.78	612.90	441.18	406.00	300.00
X2703_7	6.12	25.2	5.87	4846.88	3933.33	3638.46	3359.65	1533.33	428.38	878.71	627.45	556.67	389.19
X2703_8	3.89	35	12.31	3775.00	2855.56	2430.77	2168.42	1019.05	463.51	532.26	356.86	311.33	216.22
X2703_9	4.2	9.63	1.57	2634.38	2344.44	1923.08	1833.33	1042.86	704.05	603.23	439.22	396.67	278.38
X2703_10	8.84	31.6	14.9	759.38	977.78	1115.38	1177.19	771.43	367.57	470.97	366.67	371.67	291.89
X2703_11	2.82	8.5	2.87	2393.75	2077.78	1938.46	1726.32	823.81	287.84	432.26	282.35	242.33	167.57
X2703_12	7.63	23.4	6.38	1471.88	1566.67	1353.85	1200.00	631.43	306.76	380.32	292.16	308.00	243.24
X2703_13	11.95	1.39	7.98	593.75	677.78	863.08	1140.35	1247.62	147.70	1032.26	1076.47	1200.00	935.14
X2703_14	4.69	51.8	18.2	4156.25	4188.89	3053.85	2478.95	1138.10	459.46	603.23	407.84	342.00	252.70
X2703_15	0.835	6.33	1.22	628.13	537.78	465.38	450.88	258.10	212.43	155.81	108.43	87.67	60.81
X2703_16	0.613	0.596	0.55	308.13	233.33	175.38	140.70	68.57	77.30	50.65	31.37	26.70	22.84
X2703_17	15.75	30.7	29.4	7343.75	9555.56	7976.92	6438.60	2942.86	502.70	1677.42	1186.27	1013.33	755.41
X2703_18	1.83	11.1	3.37	2618.75	2533.33	1815.38	1438.60	523.81	274.32	281.61	179.41	143.00	105.54
X2703_19	1.82	4.98	3.39	1518.75	1766.67	1569.23	1361.40	586.19	262.16	289.03	186.27	140.33	98.51
X2703_20	5.32	9	10.03	315.94	396.67	431.54	536.84	435.71	264.86	328.71	270.59	260.00	214.86
X2703_21	4.01	321	60.9	13531.25	8722.22	5238.46	3684.21	1371.43	581.08	748.39	382.35	278.00	206.76
X2703_22	6.04	15.7	13.8	603.13	777.78	820.77	910.53	661.90	282.43	419.35	327.45	287.67	235.14
X2703_23	3.81	17.9	4.87	2896.88	3222.22	2438.46	2101.75	938.10	335.14	496.77	354.90	281.00	212.16
X2703_24	2.22	5.11	1.24	3193.75	2766.67	2023.08	1654.39	666.67	525.68	406.45	268.63	207.67	155.81
X2703_25	1.5	0.072	0.02	11.78	20.78	33.31	61.93	123.33	213.51	206.13	232.16	235.67	169.19
X2703_26	2.63	10.28	6.37	1796.88	1766.67	1407.69	1124.56	505.24	268.92	299.03	212.55	185.00	139.32
X2703_27	6.84	3.91	4.41	309.69	473.33	577.69	763.16	601.43	458.11	482.58	419.61	375.33	308.11
X2703_28	4.59	3.78	5.29	640.63	1466.67	1846.15	2350.88	1719.05	175.27	1164.52	931.37	723.33	501.35
X2703_29	2.36	13.22	3.15	1334.38	1311.11	1161.54	1084.21	536.67	327.03	321.61	251.18	202.33	148.78
X2703_30	2.09	4.58	4.24	1590.63	1611.11	1392.31	1277.19	560.95	279.73	306.77	215.88	160.00	111.62
X2703_31	2.7	31.5	9.6	3968.75	3077.78	1976.92	1471.93	528.57	289.19	302.58	203.92	162.00	121.89
X2703_32	4.82	134.4	29.8	1531.25	1717.78	1472.31	1429.82	588.10	658.11	362.90	246.67	187.67	155.54
X2703_33	2.04	212	2.36	20093.75	19444.44	15846.15	13000.00	4114.29	2337.84	1729.03	1017.65	570.00	308.11

Sample ID	Lu	^{232}Th	^{238}U	La*	Ce*	Pr*	Nd*	Sm*	Eu*	Gd*	Tb*	Dy*	Ho*
X2703_34	1.9	24.5	6.51	3409.38	3022.22	1869.23	1435.09	390.95	201.35	206.13	117.84	83.33	62.57
X2703_35	3.2	19.6	11.02	775.00	825.56	726.15	692.98	324.29	158.92	202.58	161.76	138.67	109.86
X2703_36	25.2	8.4	35.9	1790.63	2222.22	2030.77	2114.04	1609.52	371.62	1177.42	1268.63	1193.33	893.24
X2703_37	18.9	7.14	8.2	66.25	85.67	121.54	187.02	296.67	144.86	437.74	627.45	696.67	597.30
X2703_38	2.71	20.5	10.8	2746.88	2611.11	1930.77	1768.42	733.33	393.24	421.29	308.82	236.67	155.00
X2703_1	4.27	34.4	24.4	928.13	716.67	677.69	666.67	308.57	312.16	200.65	134.31	113.00	95.27
X2703_2	4.48	35.5	3.29	3425.00	2244.44	2153.85	2045.61	1100.00	637.84	700.00	492.16	407.33	310.81
X2703_3	6.31	10.67	5.4	514.38	548.89	737.69	1010.53	835.24	356.76	555.48	480.39	434.33	337.84
X2703_4	1.32	4.9	8.87	16.34	13.20	19.31	29.30	36.67	34.73	37.10	33.14	35.03	32.30
X2703_5	2.29	24	12.98	1781.25	968.89	703.85	594.74	221.90	69.05	155.48	102.16	88.33	80.00
X2703_6	2.46	1.8	3.79	643.75	522.22	545.38	580.70	336.19	189.59	221.94	177.65	153.67	120.41
X2703_7	2.87	9.58	2.7	793.75	612.22	616.92	657.89	417.62	260.81	289.68	239.22	209.33	160.54
X2703_8	5.28	25.7	14.9	2209.38	1596.67	1423.08	1294.74	628.57	157.84	392.90	307.84	277.33	233.78
X2703_9	3.89	19.5	2.83	2231.25	1327.78	1205.38	1250.88	735.24	550.00	518.71	421.57	369.67	289.19
X2703_10	3.78	7.25	6.57	58.44	84.56	146.15	248.42	253.33	186.49	196.45	144.51	133.33	113.51
X2703_11	2.95	5.53	4.59	30.13	50.22	84.46	162.11	177.62	137.97	150.65	113.92	102.00	84.59
X2703_12	2.151	4.54	3.23	39.81	39.56	77.31	130.35	139.05	103.11	109.68	85.49	75.37	64.86
X2703_13	6.06	7.21	1.13	890.63	844.44	941.54	1036.84	810.00	329.73	619.03	515.69	456.67	356.76
X2703_14	4.77	47.6	10.63	6040.63	3255.56	2315.38	1847.37	698.57	195.81	422.58	289.22	246.33	202.16
X2703_15	6.01	18.8	2.61	9875.00	6611.11	5553.85	4666.67	1819.05	436.49	958.06	643.14	490.00	359.46
X2703_16	11.37	22.1	5.72	6843.75	4844.44	4384.62	3912.28	1852.38	237.84	1119.35	925.49	833.33	651.35
X2703_17	4.88	15.6	35.9	203.75	321.11	523.08	815.79	852.38	229.73	645.16	533.33	467.00	340.54
X2703_18	5.56	31	37.8	451.88	462.22	496.15	524.56	298.10	202.43	188.39	157.25	146.00	128.24
X2703_19	1.31	1.25	10.9	68.44	71.78	88.46	123.86	103.81	102.30	86.77	67.25	58.67	48.78
X2703_20	2.51	50.8	12.3	1712.50	1231.11	1069.23	1061.40	542.38	302.70	351.61	247.06	220.00	168.92
X2703_21	10.32	0	0.75	65.94	134.22	248.46	436.84	525.71	127.16	458.06	452.94	497.00	427.03
X2703_22	2.1	10.3	4.39	1915.63	1587.78	1645.38	1640.35	804.29	313.51	419.35	270.20	197.67	138.11
X2703_23	1.061	0.011	4.33	791.25	762.22	934.62	1057.89	528.57	359.46	204.19	110.98	72.67	51.89
X2703_24	1.98	14.7	6.78	1368.75	1095.56	1025.38	1031.58	582.86	214.86	376.13	268.63	198.00	140.41
X2703_25	5.51	44.2	15.4	4312.50	3133.33	2546.15	2368.42	1042.86	440.54	587.10	423.53	346.67	281.08
X2703_26	6.97	94	29.9	3703.13	2966.67	2592.31	2275.44	1014.29	450.00	593.55	433.33	366.00	283.78
X2703_27	10.6	0.259	25.5	223.44	272.22	402.31	543.86	709.52	481.08	706.45	900.00	946.67	704.05
X2703_28	3.54	32.1	23.7	2578.13	2100.00	1838.46	1535.09	459.05	331.08	199.03	94.12	53.67	44.05
X2703_29	11.3	21.5	5.3	1965.63	1786.67	1923.08	2185.96	1480.95	614.86	1109.68	888.24	800.00	622.97

Sample ID	Lu	^{232}Th	^{238}U	La*	Ce*	Pr*	Nd*	Sm*	Eu*	Gd*	Tb*	Dy*	Ho*
X2703_30	3.46	27.6	8.02	4025.00	2566.67	2161.54	1970.18	848.57	340.54	450.00	313.14	245.00	181.62
X2703_31	2.53	9.53	5.16	2034.38	1653.33	1692.31	1635.09	722.38	293.24	378.06	236.47	175.33	126.35
X2703_32	4.55	32.9	4.3	2600.00	1882.22	1869.23	2033.33	1195.24	664.86	741.29	529.61	446.67	341.89
X2703_33	7.85	16.28	4.63	3750.00	2614.44	2508.46	2533.33	1418.57	421.49	917.10	714.12	638.00	502.70
X2703_34	8.82	28.5	16	1181.25	993.33	949.23	943.86	539.52	130.81	393.55	316.86	296.67	261.62
X2703_35	5.8	84.7	68.2	4665.63	3077.78	2576.92	2317.54	1080.95	277.03	674.19	509.80	430.33	331.08
X2703_36	2.98	38.4	11.78	3903.13	2207.78	1715.38	1387.72	508.10	248.65	291.61	179.22	144.00	115.00
X2703_37	2.91	38.5	26.9	5109.38	1851.11	1053.85	757.89	256.19	109.73	189.35	121.57	105.00	92.70
X2703_38	11.9	13.1	7.4	1203.13	1226.67	1507.69	1780.70	1623.81	628.38	1348.39	1303.92	1253.33	925.68
X2703_39	1.22	3.18	3.09	3709.38	2433.33	1892.31	1591.23	564.76	109.46	271.29	153.14	97.00	70.95
X2703_40	3.04	12.9	4.88	1137.50	973.33	1100.00	1357.89	847.62	331.08	525.81	374.51	294.00	217.57
X2703_41	3.29	25.4	7.6	2981.25	1955.56	1607.69	1533.33	690.48	444.59	412.90	268.63	199.33	148.65
X2703_42	43	86	51.4	1978.13	2400.00	3061.54	3877.19	3295.24	404.05	2387.10	2215.69	2220.00	1797.30
X2703_43	2.04	24	9.1	2453.13	1243.33	905.38	728.07	271.90	183.78	178.39	108.82	90.00	72.03
X2703_44	4.13	0.97	1.68	247.50	220.00	265.38	314.04	268.57	229.73	242.26	227.25	231.00	191.89
X2703_45	4.57	9.9	1.93	2050.00	1504.44	1530.77	1633.33	857.14	398.65	512.90	405.88	356.33	271.62
X2703_46	3.05	65.8	10.6	6062.50	4844.44	4561.54	4140.35	1571.43	690.54	683.87	431.37	290.00	193.11
X2703_47	33.8	8.9	28	247.50	388.89	696.92	1236.84	1552.38	312.16	1454.84	1547.06	1570.00	1374.32
X2703_48	4.78	81.1	15.9	3175.00	2128.89	1923.08	1826.32	938.57	386.49	562.26	427.45	373.00	285.14
X2703_49	9.02	14.3	11.1	931.25	872.22	1031.54	1235.09	1085.71	378.38	987.10	909.80	963.33	822.97
X2703_50	1.78	22	7.5	2721.88	1700.00	1592.31	1484.21	738.10	370.27	383.87	245.10	167.00	101.35
X2703_51	5.27	44.1	9.2	5156.25	2655.56	1800.00	1540.35	585.71	305.41	361.29	254.90	223.33	193.24
Miss. S. of Illinois, Missouri, and Upper Miss. (not used in study)													
X2704_1	4.49	93.9	38.1	3721.88	3677.78	2861.54	2531.58	1262.86	472.97	642.26	459.22	374.00	270.68
X2704_2	1.507	31.7	2.97	5384.38	4300.00	3469.23	3110.53	1309.52	824.32	584.84	334.12	225.00	140.00
X2704_3	3.42	24.9	17.34	1740.63	1403.33	1306.92	1449.12	863.33	190.81	486.77	348.24	288.33	213.38
X2704_4	8.29	1.82	2.09	1140.63	1308.89	1430.77	1605.26	1471.43	398.65	1000.00	929.41	903.33	693.24
X2704_5	0.245	0.26	0.726	42.59	52.22	63.46	80.18	49.95	33.65	30.45	19.88	15.60	11.66
X2704_6	1.98	38.2	51.7	1059.38	754.44	576.92	512.28	210.95	270.54	130.65	78.43	64.20	56.89
X2704_7	2.05	5.17	3.51	1437.50	1603.33	1611.54	1643.86	870.00	274.86	388.06	254.31	188.67	129.05
X2704_8	3.12	36.3	12.18	3990.63	2844.44	1938.46	1585.96	730.48	303.24	384.84	255.29	205.00	155.54
X2704_9	5.65	0.504	11.4	100.00	150.44	221.77	340.88	540.48	397.30	507.74	574.51	565.00	398.65
X2704_10	4.66	8.52	12.92	1746.88	1372.22	1067.69	901.75	425.71	74.05	240.32	177.25	159.33	136.62

Sample ID	Lu	^{232}Th	^{238}U	La*	Ce*	Pr*	Nd*	Sm*	Eu*	Gd*	Tb*	Dy*	Ho*
X2704_11	4.12	2.04	6.39	445.31	454.44	502.31	626.32	611.43	139.86	430.97	382.35	335.00	262.16
X2704_12	15.97	0.105	5.73	326.25	606.67	871.54	1131.58	1328.57	244.59	916.13	1007.84	1053.33	864.86
X2704_13	20.3	2.93	14.2	604.06	846.67	1075.38	1347.37	1580.95	312.16	1312.90	1421.57	1466.67	1218.92
X2704_14	17.2	7.7	11.3	584.69	873.33	1180.00	1492.98	1780.95	408.11	1432.26	1627.45	1590.00	1117.57
X2704_15	1.333	6.62	3.07	1943.75	1653.33	1422.31	1335.09	585.71	247.84	280.97	176.67	125.67	83.92
X2704_16	1.831	5.73	4.33	1531.25	1380.00	1253.08	1168.42	522.86	255.41	298.39	196.27	152.33	105.68
X2704_17	0.928	47.8	43.1	1393.75	845.56	573.85	480.70	187.62	113.51	123.87	84.71	70.33	51.89
X2704_18	3.79	4.8	1.36	1575.00	1404.44	1402.31	1507.02	814.76	613.51	585.16	445.10	398.00	289.19
X2704_19	7.16	6.74	5.31	1593.75	1947.78	2046.15	2256.14	1490.48	406.76	1106.45	966.67	893.33	647.30
X2704_20	14.71	18.7	34.5	714.06	828.89	952.31	1140.35	1045.71	310.27	1070.97	1005.88	1003.33	802.70
X2704_21	2.87	27.1	10.72	3368.75	3444.44	2761.54	2364.91	938.10	324.32	511.94	339.80	266.33	186.08
X2704_22	1.113	18	5.42	1925.00	1516.67	1240.00	1129.82	481.90	331.08	277.74	164.71	116.33	80.14
X2704_23	2.6	2.4	7.93	150.31	180.78	202.31	246.67	239.52	192.30	235.81	205.69	191.67	147.03
X2704_24	1.8	5.63	2.88	1971.88	1095.56	667.69	496.49	175.24	114.46	125.81	86.27	77.67	64.59
X2704_25	4.14	40.4	18.4	1800.00	1922.22	1453.85	1268.42	518.57	297.30	312.58	220.20	199.33	161.22
X2704_26	3.73	19	6.69	3353.13	3211.11	2369.23	2008.77	750.00	248.65	468.39	331.57	278.67	211.22
X2704_27	1.338	5.45	2.6	413.44	464.44	433.08	410.00	152.86	126.08	96.13	67.65	58.03	48.24
X2704_28	1.366	17.7	9.52	505.31	553.33	477.69	437.02	179.05	94.86	112.90	75.29	64.50	52.70
X2704_29	2.29	4.14	2.57	639.38	698.89	687.69	715.79	440.95	329.73	331.61	258.43	228.00	170.54
X2704_30	0.617	7.83	19.4	478.13	370.00	276.92	242.11	85.24	174.32	53.87	36.08	28.30	21.62
X2704_31	5.07	80.1	27.8	3353.13	3533.33	2930.77	2382.46	1071.43	502.70	600.00	441.18	362.67	270.27
X2704_32	2.84	8.96	3.99	1521.88	1544.44	1323.85	1252.63	660.48	400.00	427.42	328.63	275.33	202.84
X2704_33	11.57	8.85	25.9	771.88	1110.00	1295.38	1384.21	915.71	111.62	588.06	509.80	478.33	394.59
X2704_34	3.3	15.19	6.62	2409.38	1667.78	1079.23	815.79	309.52	219.46	195.16	136.08	119.67	100.81
X2704_35	0.931	0.488	2.83	52.19	68.33	81.15	91.93	64.52	45.00	46.45	41.76	38.23	33.11
X2704_36	1.629	0.648	9.85	360.94	561.11	670.77	803.51	467.14	111.62	256.45	187.84	151.00	110.95
X2704_37	1.443	6.88	4.29	1675.00	1705.56	1439.23	1292.98	616.19	337.97	309.03	200.59	145.67	97.03
X2704_38	4.53	24	48.1	1115.63	1480.00	1377.69	1385.96	687.14	358.11	359.35	265.88	219.67	175.54
X2704_39	7.47	16.31	5.38	2125.00	2076.67	2023.08	1987.72	1347.62	500.00	900.00	743.14	666.00	504.05
X2704_40	22.21	7.8	108.8	859.38	1255.56	1346.15	1512.28	1752.38	85.41	1587.10	1807.84	1876.67	1508.11
Illinois River (Northern)													
X2705_1	3.8	8.4	13.7	352.81	407.78	441.54	440.35	259.05	189.19	148.06	116.86	108.00	91.22
X2705_2	2.78	9.6	3.69	2562.50	2655.56	2092.31	1807.02	780.95	487.84	422.58	303.92	229.33	168.92

Sample ID	Lu	^{232}Th	^{238}U	La*	Ce*	Pr*	Nd*	Sm*	Eu*	Gd*	Tb*	Dy*	Ho*
X2705_3	2.79	0.216	0.085	15.72	18.22	32.62	55.96	133.33	132.84	306.13	427.45	496.00	345.95
X2705_4	1.14	73.5	14.5	2634.38	2988.89	2800.00	2701.75	1442.86	950.00	732.26	405.88	258.00	141.62
X2705_6	30.7	1.54	8.91	868.75	880.00	754.62	657.89	525.24	416.22	510.00	696.08	973.33	943.24
X2705_8	3.85	8.17	1.96	454.06	724.44	850.00	1022.81	802.38	267.57	486.13	349.02	269.33	193.65
X2705_9	0.95	0.367	3.03	89.38	96.67	106.92	128.95	108.10	105.14	89.68	71.76	63.00	48.24
X2705_11	4.34	23.9	18.1	831.25	2155.56	1015.38	998.25	528.57	341.89	329.03	245.10	212.33	174.32
X2705_12	0.725	0.013	0.014	0.41	0.71	1.00	1.53	2.57	2.47	4.42	7.98	12.20	16.08
X2705_13	0.636	1.024	10.23	55.31	80.33	93.08	101.93	71.43	62.57	56.45	39.02	34.03	27.97
X2705_14	2.01	26.1	49.4	1559.38	2100.00	1238.46	1103.51	568.57	106.89	346.13	236.67	177.33	123.51
X2705_15	5.98	75	33.5	4812.50	6688.89	5600.00	3947.37	1538.10	760.81	748.39	462.75	340.00	252.70
X2705_16	25.8	1.23	28	1212.50	2377.78	2384.62	2561.40	2009.52	244.59	1625.81	1596.08	1736.67	1432.43
X2705_18	1.378	2.81	4.35	360.31	456.67	330.77	277.19	154.29	202.70	102.58	73.33	63.33	52.43
X2705_20	1.079	1.43	10.03	14.56	33.89	56.31	87.02	118.10	76.62	105.16	94.90	83.67	62.97
X2705_21	0.382	2.81	1.77	57.81	79.56	107.77	159.47	144.76	111.08	86.13	49.61	32.50	20.95
X2705_22	0.927	11.29	5.54	331.25	418.89	513.85	603.51	318.57	162.57	160.00	95.69	68.10	46.08
X2705_23	10.55	0.208	31.1	314.06	493.33	646.15	791.23	890.48	193.92	783.87	901.96	950.00	740.54
X2705_24	24.6	4.09	46.5	1918.75	3422.22	4230.77	4894.74	3623.81	1132.43	2232.26	1933.33	1766.67	1412.16
X2705_25	0.249	56.7	22.1	247.50	238.78	280.00	289.47	164.29	47.30	86.13	65.29	47.33	30.41
X2705_27	5.84	5.34	26.9	62.69	60.67	59.00	54.39	42.67	127.43	38.55	47.06	61.43	70.68
X2705_29	3.71	4.99	62	396.56	584.44	791.54	996.49	761.43	200.68	496.13	403.14	343.00	242.84
X2705_30	27	2.43	5.85	797.19	945.56	1163.08	1319.30	1365.71	94.86	1019.35	1209.80	1330.00	1089.19
X2705_31	2.88	1.75	9.04	351.88	570.00	790.77	1036.84	809.52	321.62	470.97	347.06	280.00	200.00
X2705_32	6.34	40.3	46.9	1068.75	1324.44	1438.46	1380.70	909.52	418.92	505.16	343.33	266.33	199.86
X2705_33	1.78	1.49	2.02	635.63	563.33	447.69	403.51	157.14	142.03	107.10	65.88	55.23	47.57
X2705_34	2.28	3.54	5.25	127.50	242.22	341.54	452.63	435.71	236.49	295.81	248.24	214.67	158.65
X2705_35	1.89	5.87	33.4	198.75	282.22	338.46	389.47	306.67	267.57	196.77	140.98	114.33	85.41
X2705_36	3.33	0.789	4.33	38.34	60.67	90.08	139.82	187.62	202.70	186.13	181.96	184.00	151.22
X2705_37	4.49	4.06	1.28	2218.75	2844.44	1769.23	1412.28	857.14	556.76	529.03	437.25	390.00	286.49
X2705_38	11.01	1.03	19.3	534.38	1111.11	714.62	673.68	909.52	179.73	816.13	1035.29	1006.67	686.49
X2705_39	2.14	226	58	17593.75	11666.67	6769.23	3491.23	1100.00	490.54	567.74	327.45	240.00	175.68
X2705_40	3.73	8.94	7.67	784.38	1607.78	1384.62	1300.00	657.62	383.78	361.61	268.82	238.00	179.05
X2705_41	12.21	4.19	10.8	540.63	823.33	901.54	957.89	976.19	100.95	709.68	815.69	863.33	670.27
X2705_42	1.71	19.4	5.22	940.63	587.78	401.54	342.11	131.43	111.76	100.00	68.04	55.33	48.65
X2705_44	0.869	10	4.84	409.38	375.56	332.31	329.82	178.57	163.51	115.81	75.49	60.67	47.57

Sample ID	Lu	^{232}Th	^{238}U	La*	Ce*	Pr*	Nd*	Sm*	Eu*	Gd*	Tb*	Dy*	Ho*
X2705_45	4.99	3.81	8.53	43.22	71.78	110.23	165.96	179.52	144.19	148.06	140.78	160.67	148.78
X2705_47	3.58	252	27	17156.25	13933.33	10923.08	8631.58	3442.86	1905.41	1483.87	852.94	540.00	328.38
X2705_48	11.12	0.744	39.9	500.00	796.67	940.00	1019.30	1080.95	91.89	832.26	986.27	1070.00	804.05
X2705_49	3.89	24.8	2.38	1396.88	1817.78	2156.92	2501.75	1442.86	247.30	738.71	517.65	411.00	281.89
X2705_50	2.67	1.53	2.37	450.00	246.67	172.31	153.86	87.62	51.62	71.94	60.59	66.57	61.89
X2705_51	2.28	1.43	6.07	26.44	78.11	157.69	268.42	320.95	221.62	235.16	181.37	155.67	116.76
X2705_52	4.05	4.15	1.007	1721.88	1411.11	1415.38	1521.05	917.14	605.41	582.26	449.02	400.33	288.78
X2705_53	0.304	0.164	3.11	1228.13	1811.11	1700.00	1698.25	866.67	70.95	416.77	215.49	122.67	61.89
X2705_54	0.998	18.9	11.4	1203.13	1477.78	1110.77	808.77	245.24	183.78	130.00	62.75	45.23	32.97
X2705_55	4.7	11.3	22.7	212.50	256.67	283.08	340.35	419.05	328.38	341.94	266.67	251.00	208.11
X2705_56	2.1	2.71	1	5834.38	4766.67	3915.38	3049.12	1138.10	395.95	547.74	328.82	240.00	155.81
X2705_57	3.24	5.44	2.02	1568.75	1588.89	1500.00	1463.16	819.05	539.19	522.58	396.08	348.67	247.30
X2705_58	5.22	71.1	18.6	3262.50	2500.00	2046.15	1791.23	904.76	494.59	550.65	412.16	381.67	285.54
X2705_59	2.41	40	34	600.00	773.33	698.46	663.16	347.62	224.32	207.74	136.27	118.33	92.57
X2705_60	0.143	0.567	0.323	240.00	230.00	200.77	187.89	61.95	42.57	32.58	15.94	10.50	6.95
X2705_1	1.169	7.39	2.73	690.63	680.00	683.08	687.72	342.86	162.84	171.29	102.94	70.67	50.41
X2705_2	4.04	12.99	12.07	205.94	252.22	305.38	371.93	237.62	141.35	160.32	120.00	109.33	95.27
X2705_3	6.03	12.47	9.86	44.88	62.11	118.00	225.26	293.81	217.70	257.74	236.47	239.00	201.76
X2705_4	17.78	3.34	86.1	486.56	578.89	823.85	1082.46	1304.76	140.27	1193.55	1486.27	1586.67	1133.78
X2705_5	2.6	3.44	0.984	965.63	860.00	896.15	1077.19	647.14	452.70	425.48	330.59	284.00	200.27
X2705_6	12.55	100.6	26.8	6465.63	4100.00	2807.69	2152.63	805.24	495.95	533.87	406.86	388.67	339.19
X2705_7	11.33	126.4	55.3	2581.25	3266.67	3638.46	4350.88	2466.67	1832.43	1319.35	884.31	676.00	483.78
X2705_8	2.42	47.9	12.73	1168.75	731.11	570.77	554.39	289.05	169.46	200.00	167.45	153.33	122.30
X2705_9	2.99	15.67	10.55	2634.38	1801.11	1343.85	1185.96	498.10	181.89	295.81	212.94	177.00	137.84
X2705_11	0.72	2.26	12	184.06	124.44	103.08	97.19	51.43	217.57	41.29	29.02	24.50	20.54
X2705_12	10.86	8.03	2.86	3381.25	2814.44	2623.08	2929.82	2009.52	295.95	1490.32	1317.65	1226.67	917.57
X2705_13	6.38	0.279	19.5	293.75	322.22	359.23	436.84	341.43	216.62	318.39	284.12	269.67	232.43
X2705_14	0.634	5.62	1.94	272.81	273.33	280.77	315.79	142.86	111.08	79.68	43.14	31.63	23.78
X2705_15	10.21	10.7	17	278.13	377.78	482.31	607.02	713.33	118.92	626.13	745.10	794.33	624.32
X2705_16	2.176	19.16	6.65	594.38	598.89	680.77	889.47	613.81	336.49	370.97	269.80	212.00	153.65
X2705_17	42.1	84.1	47.2	3418.75	3788.89	4169.23	4898.25	3885.71	199.19	2741.94	2735.29	2696.67	2018.92
X2705_18	10.83	15.55	75.6	2087.50	2322.22	2584.62	2970.18	2100.00	112.16	1274.19	1101.96	968.33	704.05
X2705_19	3.12	3.85	1.22	1187.50	1084.44	1121.54	1296.49	795.71	541.89	516.45	398.82	342.67	246.22
X2705_20	6.24	0.296	5.05	93.44	131.89	184.31	265.79	383.33	179.59	380.97	462.16	442.00	306.22

Sample ID	Lu	^{232}Th	^{238}U	La*	Ce*	Pr*	Nd*	Sm*	Eu*	Gd*	Tb*	Dy*	Ho*
X2705_21	13.74	5.81	4.28	370.94	563.33	872.31	1382.46	1633.33	466.22	1525.81	1939.22	2256.67	1800.00
X2705_22	3.43	31.2	43.2	2003.13	1662.22	1253.08	1108.77	430.00	199.73	245.81	180.39	154.33	124.59
X2705_23	3.13	0.275	6.2	92.19	170.56	366.92	712.28	738.10	196.22	460.32	355.49	290.67	209.32
X2705_24	6.8	30.6	46.3	959.38	721.11	603.08	610.53	332.86	195.27	219.35	172.55	163.67	145.27
X2705_25	6.55	39.3	50.7	1475.00	1514.44	1423.85	1405.26	654.29	510.81	345.16	260.98	219.67	173.92
X2705_26	24.2	29.1	5.76	2796.88	3700.00	4369.23	5228.07	2676.19	1818.92	1735.48	1352.94	1193.33	944.59
Ohio River (Ohio)													
X2801_1	2.68	50.3	8.52	2265.63	2166.67	1715.38	1352.63	569.52	325.68	307.10	230.20	197.67	150.41
X2801_2	5.92	9.7	15.1	1593.75	1755.56	1461.54	1321.05	690.48	178.38	454.84	368.63	348.00	278.38
X2801_3	2.97	6.27	18.6	217.50	330.00	402.31	452.63	340.48	448.65	243.23	172.75	147.00	113.38
X2801_5	4.18	11.15	11.61	3146.88	2488.89	1592.31	1107.02	393.81	198.65	242.26	162.35	146.33	125.27
X2801_6	4.35	0.135	14.3	69.06	116.33	160.00	224.21	245.71	169.32	232.90	219.41	227.67	194.59
X2801_7	5.43	6.29	12.5	226.56	422.22	652.31	866.67	652.38	390.54	400.00	313.73	276.00	218.92
X2801_8	5.56	0.76	1.44	3390.63	3711.11	3053.85	2561.40	1214.29	236.49	709.68	521.57	456.67	341.89
X2801_9	14.07	7.17	9.78	355.94	547.78	763.85	935.09	900.00	344.59	777.42	766.67	830.00	716.22
X2801_10	1.99	6.68	2.84	1034.38	533.33	334.62	260.53	119.52	85.81	91.61	69.80	67.33	59.32
X2801_11	11.9	1.75	14	77.50	190.00	334.62	510.53	580.95	362.16	461.29	456.86	453.33	370.27
X2801_12	18.1	208	40.6	8906.25	6511.11	4415.38	3578.95	1752.38	652.70	1203.23	896.08	800.00	667.57
X2801_14	1.99	0.111	8.51	119.06	247.78	388.46	519.30	386.19	248.65	224.19	165.69	136.67	101.08
X2801_15	1.57	0.249	6.95	83.44	198.89	370.00	542.11	422.38	454.05	222.58	141.76	109.33	77.03
X2801_16	0.97	23.5	26.7	304.38	295.56	250.00	224.56	93.81	139.19	59.03	32.35	24.40	19.86
X2801_17	11.38	0.418	6.72	375.00	526.67	684.62	801.75	995.24	191.89	925.81	1109.80	1086.67	729.73
X2801_18	0.716	0.073	29.8	421.88	775.56	1146.15	1587.72	1895.24	801.35	1461.29	1245.10	813.33	363.51
X2801_19	8.8	14.5	13.4	1187.50	1477.78	1230.77	1108.77	494.76	547.30	332.26	235.29	213.00	177.03
X2801_20	11.36	1.22	3.02	1331.25	1688.89	1900.00	2107.02	2109.52	947.30	1548.39	1631.37	1566.67	1133.78
X2801_21	11.3	12.1	3.95	2415.63	3477.78	3553.85	3789.47	2347.62	1050.00	1432.26	1196.08	1016.67	721.62
X2801_22	0.518	0.069	0.601	11.78	23.67	36.85	62.98	79.52	62.84	61.61	46.27	39.00	29.05
X2801_23	13	2.09	10.5	440.63	648.89	747.69	935.09	1166.67	389.19	1067.74	1250.98	1213.33	854.05
X2801_24	1.98	19.1	7.42	1718.75	610.00	326.92	233.33	91.90	76.35	64.52	50.20	48.33	44.86
X2801_25	23.6	36.7	34.7	197.50	312.22	426.15	608.77	747.62	255.41	764.52	870.59	956.67	820.27
X2801_26	23.6	12.4	74	618.75	1267.78	1507.69	1603.51	1442.86	656.76	996.77	1111.76	1150.00	889.19
X2801_27	2.28	22.3	7.45	781.25	1156.67	1261.54	1180.70	526.67	335.14	249.03	159.41	119.33	89.73
X2801_28	2.77	0.248	6.68	5.16	6.83	10.62	16.91	29.71	53.92	45.81	55.49	70.00	72.97

Sample ID	Lu	^{232}Th	^{238}U	La*	Ce*	Pr*	Nd*	Sm*	Eu*	Gd*	Tb*	Dy*	Ho*
X2801_29	11.4	4.05	3.64	415.94	702.22	973.85	1296.49	1071.43	595.95	706.45	529.41	449.00	377.03
X2801_30	6.86	1.29	54.3	360.63	630.00	906.15	1200.00	1080.95	308.11	751.61	603.92	534.67	382.43
X2801_31	1.5	2.39	1.48	843.75	458.89	309.23	270.18	109.52	111.35	80.65	56.27	52.67	44.19
X2801_32	17.7	7.53	36.6	790.63	1056.67	1023.08	1063.16	595.24	405.41	451.61	374.51	419.67	412.16
X2801_33	2.37	1.43	20.3	521.88	836.67	1010.77	1112.28	752.38	164.05	493.55	396.08	340.33	240.54
X2801_34	4.15	2.49	0.717	50.94	57.44	64.62	79.30	87.62	62.84	89.35	94.51	111.67	105.95
X2801_35	0.136	0.052	0.004	0.25	0.31	0.32	0.37	0.80	0.82	0.87	1.41	2.27	2.59
X2801_36	2.31	2.3	5.6	276.25	346.67	390.00	412.28	270.48	213.51	180.97	131.76	113.00	89.59
X2801_37	0.176	0.097	0.101	26.06	20.00	15.23	13.16	5.05	6.74	5.32	4.51	4.27	4.09
X2801_38	14.2	1.74	16.8	1156.25	2055.56	2476.92	2736.84	1733.33	795.95	1025.81	886.27	816.67	643.24
X2801_39	15.2	46.1	19.6	1250.00	2111.11	2523.08	3035.09	2119.05	1056.76	1335.48	1172.55	1066.67	843.24
X2801_40	1.85	0.073	6.31	64.69	145.11	216.15	322.81	277.62	216.22	189.35	152.55	134.67	103.24
X2801_41	1.87	33.4	20.5	2406.25	2233.33	1653.85	1340.35	553.33	228.38	305.16	198.63	159.00	113.65
X2801_42	2.23	0.977	3.44	98.44	140.33	152.31	169.82	110.48	81.89	78.39	59.80	55.00	51.62
X2801_43	15.2	4.39	22.3	581.25	792.22	961.54	1091.23	980.95	368.92	816.13	790.20	813.33	705.41
X2801_44	2.29	10.5	14.6	1121.88	1055.56	743.08	549.12	224.29	208.11	141.61	96.47	87.67	74.32
X2801_45	2.34	87.7	53.2	3028.13	2588.89	1500.00	1022.81	387.14	158.65	222.26	149.02	130.33	102.84
X2801_46	6.96	126.1	26.3	2312.50	2922.22	2592.31	2417.54	1428.57	185.14	883.87	686.27	611.67	451.35
X2801_1	3.87	21.6	16.5	450.00	543.33	723.08	982.46	642.86	439.19	377.42	252.94	204.33	158.11
X2801_2	2.37	6.97	13.43	2700.00	2065.56	1684.62	1529.82	592.38	164.73	321.94	208.04	156.67	117.84
X2801_3	21.3	0.572	3.73	1131.25	1331.11	1707.69	2280.70	2680.95	339.19	2541.94	2923.53	3026.67	2233.78
X2801_4	11.46	1.49	30.5	40.13	64.56	133.46	302.28	568.10	248.65	812.90	872.55	873.33	654.05
X2801_5	4.11	11.64	5.19	1996.88	825.56	500.00	436.84	193.33	133.92	149.35	110.98	105.67	99.46
X2801_6	37.3	0.729	22.5	250.00	485.56	897.69	1528.07	1714.29	836.49	1390.32	1480.39	1556.67	1345.95
X2801_7	1.201	0.605	5.43	181.56	250.44	308.46	388.07	197.62	118.11	109.03	78.82	65.50	50.27
X2801_8	3.67	0.674	5.52	665.63	720.00	753.85	750.88	382.38	254.05	213.23	180.59	172.00	138.11
X2801_9	0.929	0.044	0.339	0.73	0.98	1.96	4.09	8.05	12.82	14.61	16.88	20.00	21.38
X2801_10	7.17	26.4	7.46	912.50	578.89	506.92	591.23	370.95	149.32	332.26	292.55	297.00	266.22
X2801_11	29.8	84.2	96.7	6675.00	4966.67	3607.69	2938.60	1304.76	312.16	845.16	774.51	803.33	737.84
X2801_12	10.55	0.634	10.37	105.94	115.89	151.54	255.09	364.29	404.05	452.26	484.31	545.67	493.24
X2801_13	2.86	6.6	1.43	1078.13	961.11	1008.46	1136.84	690.48	460.81	456.45	370.59	314.67	225.68
X2801_14	7.91	148.7	14	13187.50	9988.89	8438.46	7333.33	2590.48	1633.78	1183.87	715.69	511.33	363.51
X2801_15	9.41	0.147	3.03	74.69	164.67	325.38	600.00	757.62	667.57	722.58	756.86	780.00	597.30
X2801_16	9.99	0.546	3.42	1125.00	1772.22	2230.77	2675.44	1571.43	722.97	941.94	747.06	670.00	517.57

Sample ID	Lu	^{232}Th	^{238}U	La*	Ce*	Pr*	Nd*	Sm*	Eu*	Gd*	Tb*	Dy*	Ho*
X2801_17	7.66	0.046	12.82	30.69	111.00	280.00	508.77	528.57	240.95	360.97	321.37	309.33	258.11
X2801_18	6.44	0.177	3.27	625.63	1046.67	1550.77	2098.25	1357.14	712.16	806.45	611.76	527.33	386.49
X2801_19	2.55	5.31	7	85.63	116.33	166.15	235.96	194.76	162.30	159.03	130.39	123.00	101.22
X2801_20	14.2	29	26.6	4768.75	3922.22	3615.38	3543.86	1852.38	432.43	1170.97	984.31	903.33	705.41
X2801_21	10.74	0.404	4.94	35.72	45.56	56.77	85.79	105.71	118.11	145.48	188.24	261.67	279.73
X2801_22	0.764	0.489	1.82	123.44	76.11	63.46	64.39	35.10	42.84	26.81	21.57	19.90	17.84
X2801_23	5.02	0.478	8.36	133.75	163.00	231.54	340.35	305.71	131.08	283.87	272.35	278.67	243.11
X2801_24	9.24	17.2	7.42	709.38	992.22	1261.54	1491.23	823.81	429.73	567.74	445.10	415.00	351.35
X2801_25	17.43	2.45	15.68	4200.00	3744.44	3684.62	3894.74	2914.29	285.14	2132.26	1962.75	1790.00	1301.35
X2801_26	11.95	3.43	15.3	117.19	171.11	264.62	471.93	567.14	543.24	561.29	533.33	560.00	487.84
X2801_27	17.2	0.438	19.6	495.00	742.22	1146.92	1814.04	1961.90	533.78	1583.87	1386.27	1233.33	897.30
X2801_28	0.354	6.21	7.19	2750.00	3011.11	3446.15	4140.35	2533.33	632.43	1358.06	780.39	375.67	131.35
X2801_29	7.4	54	14.6	250.63	578.89	947.69	1443.86	1104.76	617.57	751.61	635.29	570.00	431.08
X2801_30	12.33	13.56	6.89	1281.25	1722.22	2346.15	3050.88	2033.33	898.65	1303.23	1058.82	936.67	683.78
X2801_31	17.8	1.51	15	6812.50	5566.67	5469.23	5754.39	3185.71	847.30	2167.74	1805.88	1673.33	1306.76
X2801_32	2.65	4.79	14.82	906.25	507.78	334.62	268.60	137.62	102.84	106.45	99.22	101.67	91.89
X2801_33	2.69	0.954	19.5	695.63	818.89	822.31	750.88	328.10	226.49	165.16	133.14	119.67	96.89
X2801_34	4.57	0.743	0.86	856.25	1038.89	1138.46	1289.47	780.95	152.84	490.32	374.51	335.67	258.11
X2801_35	45.5	12.6	18.9	1284.38	1687.78	2007.69	2363.16	2666.67	71.08	2290.32	2841.18	3043.33	2395.95
X2801_36	10.96	0.78	3.81	1062.50	1134.44	1377.69	1691.23	1176.19	327.03	848.39	798.04	790.00	644.59
X2801_37	0.325	4.35	3.95	3321.88	2866.67	2792.31	3201.75	1814.29	529.73	1016.13	631.37	352.00	136.76
X2801_38	0.893	1.252	35.6	2365.63	2744.44	3092.31	3824.56	3500.00	491.89	2058.06	1168.63	603.67	243.38
X2801_39	10.06	0.195	2.33	14.25	18.36	24.92	35.26	46.33	42.84	57.42	81.96	130.00	169.05
X2801_40	19.4	0.74	8.3	13.13	21.33	35.15	78.07	152.86	135.14	296.45	439.22	616.67	631.08
X2801_41	22.7	53.5	11.92	10031.25	7877.78	7000.00	6649.12	2823.81	981.08	1716.13	1323.53	1150.00	905.41

* Chondrite Normalized McDonough and Sun 1995

Supplementary Table B.3 Trace Element and REE continued along with Apatite Classifications

Sample ID	Er*	Tm*	Yb*	Lu*	Rock Type (Belousova)	Ternary Cat.
Mississippi S. of Red						
X2501_1	53.57	45.84	54.56	56.44	Granitoid	15
X2501_2	207.14	160.63	164.44	116.88	Iron Ore	8
X2501_3	101.90	88.13	98.39	84.69	Granitoid	14
X2501_4	664.29	551.25	541.67	335.63	Dolerite	14
X2501_6	150.95	114.69	116.56	84.06	Iron Ore	9
X2501_7	19.52	15.44	16.61	14.94	Carbonatite	16
X2501_8	985.71	828.13	862.78	568.44	Granite Pematite	10
X2501_9	61.10	43.38	45.61	35.59	Carbonatite	15
X2501_10	90.48	67.81	75.00	58.13	Granitoid	16
X2501_11	51.52	44.47	57.11	63.88	Granitoid	9
X2501_12	81.43	56.28	59.06	42.50	Iron Ore	9
X2501_13	96.19	81.25	98.89	92.81	Granitoid	15
X2501_14	207.62	154.38	166.67	119.38	Iron Ore	8
X2501_15	192.86	150.63	162.22	114.69	Iron Ore	4
X2501_16	35.76	25.38	27.28	20.66	Carbonatite	16
X2501_17	627.14	485.94	515.56	369.69	Granite Pematite	10
X2501_18	311.90	256.25	292.22	228.13	Granite Pematite	11
X2501_19	196.19	136.25	142.22	100.63	Iron Ore	8
X2501_20	116.38	80.31	80.83	56.41	Dolerite	15
X2501_21	29.33	23.78	27.33	24.22	Dolerite	15
X2501_22	470.95	367.19	384.44	284.38	Granite Pematite	12
X2501_23	1314.29	1162.50	1411.11	1325.00	Granite Pematite	10
X2501_24	195.24	170.00	202.78	163.13	Granite Pematite	12
X2501_25	99.05	69.38	74.72	58.75	Carbonatite	15
X2501_26	106.67	74.06	75.61	55.94	Iron Ore	8
X2501_27	606.67	431.88	417.22	295.31	Jacupirangite	6
X2501_28	121.90	106.56	122.78	101.25	Granitoid	9
X2501_29	56.52	41.25	47.39	45.31	Carbonatite	16
X2501_30	91.43	81.25	98.89	94.69	Granitoid	3
X2501_31	191.90	147.19	150.00	109.69	Dolerite	9
X2501_32	389.52	295.94	289.44	200.00	Dolerite	7
X2501_33	280.00	122.19	77.94	50.19	Iron Ore	11
X2501_34	191.90	143.75	143.89	107.81	Iron Ore	9
X2501_35	53.48	42.56	48.94	43.53	Carbonatite	15
X2501_36	159.52	130.31	151.67	135.31	Granitoid	9
X2501_37	90.95	65.94	73.33	58.75	Iron Ore	9
X2501_38	152.86	98.75	95.22	83.13	Granitoid	7
X2501_39	38.10	28.13	36.11	37.50	Granitoid	15
X2501_40	1238.10	1021.88	1123.89	784.38	Granite Pematite	10
X2501_1	598.10	478.13	501.11	405.31	Granitoid	5
X2501_2	202.86	144.38	143.33	105.63	Iron Ore	7
X2501_3	165.24	126.56	128.89	104.06	Granitoid	14
X2501_4	187.14	145.31	151.11	122.19	Dolerite	4
X2501_5	70.24	33.31	25.83	17.78	Carbonatite	16
X2501_6	1514.29	1009.38	878.89	615.63	Iron Ore	10

Sample ID	Er*	Tm*	Yb*	Lu*	Rock Type (Belousova)	Ternary Cat.
X2501_7	1104.76	790.63	730.56	471.88	Carbonatite	10
X2501_8	980.95	915.63	1016.67	678.13	Granite Pematite	10
X2501_9	262.86	200.31	201.11	159.38	Carbonatite	7
X2501_10	353.81	263.44	249.44	186.88	Granitoid	11
X2501_12	477.14	354.69	331.11	243.44	Iron Ore	10
X2501_13	97.14	70.31	71.11	58.13	Granitoid	9
X2501_14	213.33	160.31	164.44	134.69	Iron Ore	4
X2501_16	92.86	82.19	95.00	88.44	Carbonatite	9
X2501_17	52.38	45.00	58.33	68.44	Granite Pematite	9
X2501_18	390.48	300.63	303.89	249.38	Granite Pematite	10
X2501_19	116.67	46.88	29.33	17.56	Iron Ore	14
X2501_20	145.24	129.69	158.89	189.38	Dolerite	7
X2501_21	157.62	97.81	89.44	59.38	Dolerite	16
X2501_22	117.62	98.44	120.00	115.00	Granite Pematite	8
X2501_23	168.57	139.69	158.33	140.63	Granite Pematite	9
X2501_24	85.24	61.25	59.06	46.56	Granite Pematite	8
X2501_25	342.86	293.44	342.78	311.56	Carbonatite	7
X2501_26	86.19	60.00	57.83	46.25	Iron Ore	9
X2501_27	723.81	593.75	597.22	425.94	Jacupirangite	10
X2501_28	42.29	30.44	32.44	31.44	Granitoid	8
X2501_29	22.48	18.84	23.67	26.28	Carbonatite	16
X2501_30	102.38	72.50	71.67	55.63	Granitoid	4
X2501_31	54.29	35.94	33.11	27.41	Dolerite	9
X2501_32	286.19	220.00	239.44	200.94	Dolerite	10
X2501_33	226.67	159.38	150.56	108.75	Iron Ore	13
X2501_34	183.33	138.75	139.44	114.69	Iron Ore	8
X2501_35	57.43	39.94	41.11	34.06	Carbonatite	16
X2501_36	268.57	199.38	193.89	147.19	Granitoid	7
X2501_37	111.90	89.69	93.33	74.38	Iron Ore	15
X2501_38	145.24	120.63	131.67	121.25	Granitoid	14
X2501_39	1228.57	962.50	872.22	568.75	Granitoid	10
X2501_40	36.57	30.25	34.83	34.34	Granite Pematite	8
X2501_41	295.24	210.94	200.00	147.50	Dolerite	7
X2501_42	77.62	52.50	54.17	43.75	Dolerite	9
X2501_43	271.43	203.75	203.89	144.06	Iron Ore	13
X2501_44	51.43	42.81	47.72	46.88	Dolerite	15
X2501_45	190.00	165.31	210.56	237.19	Granitoid	8
X2501_46	244.29	189.06	202.78	170.63	Dolerite	6
X2501_47	814.29	662.50	630.56	450.00	Dolerite	11
X2501_48	128.10	105.94	123.33	128.13	Granitoid	9
X2501_49	1119.05	975.00	1088.89	846.88	Granite Pematite	10
X2501_50	33.24	19.91	17.61	11.38	Carbonatite	16
X2501_51	70.48	52.81	57.50	55.94	Carbonatite	15
X2501_52	1742.86	1931.25	2322.22	1853.13	Granite Pematite	10
X2501_53	193.81	180.31	223.33	228.44	Dolerite	7
X2501_54	538.10	415.63	413.33	321.25	Granite Pematite	10
X2501_55	146.19	118.13	132.22	117.50	Iron Ore	8

Sample ID	Er*	Tm*	Yb*	Lu*	Rock Type (Belousova)	Ternary Cat.
X2501_56	72.86	62.81	65.22	49.69	Carbonatite	16
X2501_57	46.48	33.47	40.06	39.06	Carbonatite	16
X2501_59	157.62	116.88	116.67	84.38	Carbonatite	15
X2501_60	78.57	60.00	67.78	63.44	Lherzolite	8
X2501_61	99.05	86.25	103.89	110.31	Iron Ore	3
X2501_62	88.57	66.56	72.22	61.88	Dolerite	8
Red River (Southwest)						
X2502_1	502.38	452.81	510.56	381.88	Granite Pematite	11
X2502_2	682.86	512.50	502.22	328.13	Granite Pematite	10
X2502_3	1009.52	928.13	1144.44	1106.25	Granite Pematite	10
X2502_4	148.57	149.06	211.67	246.56	Granitoid	6
X2502_5	539.52	381.56	367.78	227.81	Granite Pematite	10
X2502_6	238.57	183.13	192.78	143.13	Iron Ore	3
X2502_7	60.00	44.38	46.06	35.94	Carbonatite	16
X2502_9	914.29	796.88	855.56	565.63	Granite Pematite	10
X2502_1	1466.67	1346.88	1644.44	1431.25	Granite Pematite	10
X2502_2	2519.05	2584.38	2744.44	1975.00	Granite Pematite	10
X2502_4	297.14	296.88	411.67	456.25	Granitoid	6
X2502_5	434.76	390.63	496.11	434.38	Granite Pematite	11
X2502_7	196.67	152.81	165.00	149.06	Carbonatite	4
X2502_8	13.24	9.66	8.89	6.28	Lherzolite	16
X2502_9	436.67	329.38	328.89	264.06	Granite Pematite	6
X2502_10	814.29	671.88	655.56	450.00	Granite Pematite	10
X2502_11	828.57	681.25	688.89	506.25	Granite Pematite	10
X2502_12	115.71	95.00	95.00	84.69	Dolerite	14
X2502_13	395.24	337.50	366.67	353.13	Granite Pematite	10
X2502_14	171.90	153.44	178.33	157.81	Granite Pematite	14
X2502_15	158.10	136.88	166.11	155.31	Granitoid	13
X2502_16	89.52	68.13	69.44	59.06	Carbonatite	16
X2502_17	1200.00	931.25	955.56	718.75	Granite Pematite	10
X2502_18	928.57	821.88	927.78	853.13	Granite Pematite	10
X2502_19	299.05	284.38	351.11	325.00	Dolerite	3
X2502_20	83.81	55.63	56.67	49.06	Dolerite	13
X2502_21	97.62	82.81	100.56	101.56	Iron Ore	7
X2502_22	657.14	562.50	622.22	440.63	Granite Pematite	10
X2502_23	23.00	19.03	24.00	27.72	Carbonatite	16
X2502_24	360.48	282.19	280.00	198.13	Dolerite	8
X2502_25	195.24	190.00	225.56	202.19	Granite Pematite	14
X2502_26	584.76	443.75	466.67	308.13	Granite Pematite	11
X2502_27	129.05	70.31	43.78	26.31	Dolerite	12
X2502_28	1138.10	959.38	1116.67	1190.63	Granitoid	10
X2502_29	133.33	91.56	91.67	67.50	Iron Ore	9
X2502_30	728.57	684.38	822.22	703.13	Dolerite	10
X2502_31	804.76	562.50	539.44	390.63	Larvikite	5
X2502_32	780.95	700.00	755.56	618.75	Iron Ore	5
X2502_33	149.52	118.44	120.00	93.44	Dolerite	15

Sample ID	Er*	Tm*	Yb*	Lu*	Rock Type (Belousova)	Ternary Cat.
X2502_34	62.86	38.13	33.00	28.13	Dolerite	15
X2502_35	59.05	43.44	46.33	39.38	Granitoid	9
X2502_36	262.86	188.75	194.44	151.56	Dolerite	8
X2502_37	255.71	203.44	213.33	178.13	Granite Pematite	12
X2502_38	337.14	230.31	223.89	162.50	Dolerite	6
X2502_39	63.33	51.56	55.00	60.00	Granitoid	15
X2502_40	29.29	23.03	28.61	31.09	Carbonatite	16
X2502_41	108.10	75.63	72.78	58.44	Carbonatite	15
Miss. S. of Arkansas (not used in study)						
X2601a_1	67.62	62.81	80.00	81.56	Granitoid	
X2601a_2	224.29	173.44	174.44	132.50	Iron Ore	
X2601a_3	104.29	31.44	24.06	18.19	Iron Ore	
X2601a_4	59.29	43.13	43.78	31.38	Carbonatite	
X2601a_5	124.76	103.13	101.67	73.44	Iron Ore	
X2601a_6	1157.14	1071.88	1155.56	837.50	Granite Pematite	
X2601a_7	420.95	338.75	332.78	225.00	Granite Pematite	
X2601a_8	106.19	74.06	68.50	52.19	Dolerite	
X2601a_9	261.90	209.38	210.00	162.50	Iron Ore	
X2601a_10	119.52	90.00	101.11	99.69	Iron Ore	
X2601a_11	69.14	56.56	59.39	62.81	Dolerite	
X2601a_12	152.38	114.69	113.89	90.00	Dolerite	
X2601a_13	55.86	49.16	62.00	69.38	Granitoid	
X2601a_14	373.33	276.88	250.00	171.88	Granitoid	
X2601a_15	401.43	330.00	322.78	232.50	Dolerite	
X2601a_16	1009.52	1012.50	1166.67	1003.13	Granite Pematite	
X2601a_17	136.19	109.69	115.56	95.31	Granitoid	
X2601a_19	73.33	37.41	28.00	19.56	Iron Ore	
X2601a_20	13.62	10.28	12.67	15.97	Carbonatite	
X2601a_21	111.90	94.06	109.44	105.31	Iron Ore	
X2601_1	136.67	114.69	137.22	130.00	Iron Ore	
X2601_3	952.38	834.38	950.00	690.63	Granite Pematite	
X2601_5	109.05	83.44	92.78	95.31	Granitoid	
X2601_6	211.90	154.69	162.78	118.13	Dolerite	
X2601_7	761.90	665.63	877.78	965.63	Granite Pematite	
X2601_8	106.67	90.31	113.89	117.50	Dolerite	
X2601_9	173.81	131.25	148.89	149.69	Dolerite	
X2601_10	112.38	92.81	110.56	93.75	Carbonatite	
X2601_11	73.81	51.56	51.94	44.06	Iron Ore	
X2601_12	109.52	76.88	78.89	68.13	Iron Ore	
X2601_13	279.52	199.69	193.33	147.50	Iron Ore	
X2601_14	222.38	182.50	210.00	211.25	Granitoid	
X2601_15	229.52	186.56	215.00	181.56	Larvikite	
X2601_16	418.57	337.50	408.33	434.38	Jacupirangite	
X2601_17	1019.05	806.25	866.67	662.50	Jacupirangite	
X2601_19	633.33	506.25	567.78	493.75	Dolerite	
X2601_20	159.52	120.94	138.33	110.63	Iron Ore	

Sample ID	Er*	Tm*	Yb*	Lu*	Rock Type (Belousova)	Ternary Cat.
X2601_22	809.52	581.25	588.89	425.00	Granite Pematite	
X2601_23	55.71	35.94	36.00	27.84	Carbonatite	
X2601_24	170.95	130.94	136.67	113.44	Iron Ore	
X2601_25	23.62	21.06	26.94	34.38	Granitoid	
X2601_26	113.33	80.31	83.33	65.00	Iron Ore	
X2601_27	152.86	109.69	110.00	83.44	Dolerite	
X2601_28	150.95	140.31	170.00	171.25	Granitoid	
X2601_29	2038.10	1793.75	1955.56	1412.50	Granite Pematite	
X2601_30	89.52	76.88	83.89	66.88	Carbonatite	
X2601_31	1076.19	921.88	1038.89	737.50	Granite Pematite	
X2601_32	466.67	431.25	486.11	390.63	Iron Ore	
X2601_33	85.71	64.69	73.44	68.13	Iron Ore	
X2601_34	292.86	197.81	181.11	110.94	Dolerite	
X2601_35	85.24	60.00	59.94	47.19	Dolerite	
X2601_36	114.29	95.31	116.67	119.69	Granitoid	
X2601_37	253.33	180.63	183.33	135.94	Dolerite	
X2601_38	100.48	71.25	72.78	59.69	Dolerite	
X2601_39	303.33	283.44	362.22	362.19	Granitoid	
X2601_40	492.86	437.50	508.89	418.75	Granite Pematite	
X2601_41	190.00	140.63	132.22	100.00	Granite Pematite	
X2601_42	28.29	21.97	24.06	23.75	Carbonatite	
X2601_43	84.76	69.69	73.33	63.13	Granitoid	
X2601_45	71.43	61.88	71.67	65.94	Granitoid	
Arkansas River (Southwest)						
X2602_1	55.48	41.81	47.72	47.06	Carbonatite	16
X2602_2	682.38	473.44	417.22	288.44	Iron Ore	5
X2602_3	924.29	611.25	597.22	489.38	Granite Pematite	10
X2602_4	423.81	365.31	414.44	402.50	Jacupirangite	6
X2602_5	90.67	84.38	98.89	100.31	Granitoid	8
X2602_6	542.86	485.63	546.67	510.94	Granite Pematite	11
X2602_7	851.43	837.50	951.67	728.13	Granite Pematite	10
X2602_8	462.38	408.75	416.11	340.31	Granite Pematite	10
X2602_9	107.62	91.25	101.56	103.75	Granitoid	1
X2602_10	1128.57	900.00	816.67	606.25	Granite Pematite	10
X2602_11	165.24	149.06	160.56	156.88	Granitoid	7
X2602_12	228.10	183.75	168.33	127.19	Dolerite	13
X2602_13	638.57	656.25	750.00	737.50	Granite Pematite	10
X2602_15	151.43	133.75	139.44	119.06	Dolerite	8
X2602_16	73.52	73.44	86.17	90.94	Granitoid	14
X2602_17	3861.90	3809.38	3950.00	3006.25	Granite Pematite	10
X2602_20	339.05	280.63	283.89	219.06	Granitoid	6
X2602_21	357.14	263.13	278.89	210.94	Dolerite	7
X2602_22	9.48	6.75	7.89	8.44	Carbonatite	16
X2602_24	276.67	188.13	203.89	150.31	Larvikite	8
X2602_25	501.90	290.00	295.56	198.75	Granite Pematite	10
X2602_26	470.00	310.63	296.11	172.50	Dolerite	10

Sample ID	Er*	Tm*	Yb*	Lu*	Rock Type (Belousova)	Ternary Cat.
X2602_27	308.10	240.31	297.78	240.63	Iron Ore	3
X2602_28	57.19	44.69	60.28	60.94	Carbonatite	15
X2602_29	1185.71	1000.00	1161.11	809.38	Granite Pematite	10
X2602_30	733.33	592.19	725.00	625.94	Granitoid	11
X2602_31	923.81	665.63	682.22	427.81	Granite Pematite	10
X2602_32	130.95	93.13	103.89	80.00	Iron Ore	8
X2602_33	490.95	321.25	336.11	239.06	Jacupirangite	2
X2602_34	233.33	159.69	172.78	125.00	Dolerite	9
X2602_35	132.86	100.94	120.00	96.88	Iron Ore	4
X2602_37	651.90	494.69	542.22	397.50	Jacupirangite	2
X2602_38	39.76	31.31	38.11	32.50	Carbonatite	9
X2602_40	845.71	621.88	632.22	472.81	Granite Pematite	10
X2602_41	54.19	40.63	49.67	47.19	Carbonatite	16
X2602_42	1347.62	1046.88	1027.78	678.13	Dolerite	10
X2602_43	41.71	37.94	49.94	50.84	Granite Pematite	14
X2602_44	716.19	522.81	516.67	403.13	Granite Pematite	10
X2602_45	697.62	580.00	620.00	445.94	Granite Pematite	10
X2602_46	833.33	656.25	670.00	462.50	Granite Pematite	10
X2602_47	550.00	380.31	389.44	285.63	Granite Pematite	10
X2602_48	642.86	568.75	646.11	534.38	Granitoid	5
X2602_49	520.48	375.63	338.33	225.94	Dolerite	10
X2602_50	55.33	40.50	46.72	46.09	Granitoid	8
X2602_51	56.95	53.75	69.67	75.00	Granitoid	8
X2602_52	76.48	56.56	56.06	40.50	Dolerite	15
X2602_1	263.33	211.56	232.22	195.00	Carbonatite	6
X2602_2	430.00	414.38	499.44	408.75	Iron Ore	10
X2602_3	118.10	92.19	102.61	86.56	Granite Pematite	7
X2602_4	1442.86	1000.00	933.33	656.25	Jacupirangite	11
X2602_5	151.90	116.88	126.67	103.75	Granitoid	8
X2602_6	1480.95	1184.38	1183.33	771.88	Granite Pematite	10
X2602_7	106.67	75.00	74.89	55.72	Granite Pematite	15
X2602_8	437.62	323.13	325.00	229.69	Granite Pematite	2
X2602_9	439.05	337.19	327.78	212.19	Granitoid	10
X2602_10	981.43	699.06	700.00	523.75	Granite Pematite	5
X2602_11	196.19	162.19	188.89	181.25	Granitoid	7
X2602_12	52.62	36.88	39.78	38.50	Dolerite	16
X2602_13	266.67	188.44	188.33	136.56	Granite Pematite	13
X2602_14	237.62	198.75	225.56	217.50	Granitoid	6
X2602_15	267.14	253.13	336.67	361.56	Dolerite	12
X2602_16	1000.00	825.00	878.89	671.88	Granitoid	10
X2602_17	693.81	551.56	565.00	460.63	Granite Pematite	10
X2602_19	617.62	488.44	509.44	389.69	Granite Pematite	11
X2602_20	165.71	114.38	113.28	83.75	Granitoid	15
X2602_21	176.67	151.88	180.56	162.81	Dolerite	14
X2602_22	109.24	95.31	120.56	125.63	Carbonatite	14
X2602_23	944.76	868.75	931.11	643.75	Granite Pematite	10
X2602_24	44.14	37.50	48.44	56.88	Larvikite	16

Sample ID	Er*	Tm*	Yb*	Lu*	Rock Type (Belousova)	Ternary Cat.
X2602_25	112.86	98.75	124.44	138.75	Granite Pematite	14
X2602_26	518.10	442.19	531.67	530.94	Dolerite	11
X2602_27	111.43	79.38	78.22	60.63	Iron Ore	15
X2602_28	224.76	155.94	147.78	113.44	Carbonatite	6
X2602_29	127.14	114.38	128.89	108.13	Granite Pematite	14
X2602_30	191.43	140.31	148.89	117.50	Granitoid	15
X2602_31	114.29	81.88	88.22	96.56	Granite Pematite	8
X2602_32	510.48	405.63	445.00	395.31	Iron Ore	11
X2602_33	2085.71	1646.88	1655.56	1212.50	Jacupirangite	10
X2602_34	483.81	403.44	461.11	434.06	Dolerite	10
X2602_35	206.19	166.56	181.67	154.69	Iron Ore	3
X2602_36	1547.62	1265.63	1316.67	900.00	Granite Pematite	10
X2602_37	34.81	27.56	33.33	33.56	Jacupirangite	9
X2602_38	104.29	78.44	92.89	92.81	Carbonatite	16
X2602_39	990.48	815.63	827.78	540.63	Granite Pematite	10
X2602_40	540.48	478.75	521.67	378.75	Granite Pematite	12
X2602_42	11.24	8.56	10.28	10.19	Dolerite	16
X2602_44	59.05	48.75	57.22	59.69	Granite Pematite	15
Miss. S. of Ohio (not used in study)						
X2603_1	114.29	86.56	86.11	65.63	Iron Ore	
X2603_2	1509.52	1134.38	1011.11	712.50	Granite Pematite	
X2603_3	103.33	82.81	88.06	72.19	Dolerite	
X2603_4	680.95	587.50	661.11	506.25	Granite Pematite	
X2603_5	597.62	481.25	520.00	358.75	Granite Pematite	
X2603_6	92.38	66.88	72.61	68.13	Dolerite	
X2603_7	160.48	110.94	106.11	80.94	Iron Ore	
X2603_8	82.90	55.34	53.33	40.72	Dolerite	
X2603_9	498.57	372.19	390.00	279.69	Granite Pematite	
X2603_10	373.81	309.06	335.56	262.81	Iron Ore	
X2603_12	51.57	40.31	46.33	35.00	Dolerite	
X2603_13	115.71	79.06	81.11	68.13	Granitoid	
X2603_14	211.43	144.38	139.44	99.38	Iron Ore	
X2603_15	431.90	324.06	294.44	197.50	Dolerite	
X2603_17	190.48	141.88	144.44	112.50	Iron Ore	
X2603_18	39.81	28.69	33.00	28.72	Carbonatite	
X2603_19	971.43	762.50	787.22	559.38	Granite Pematite	
X2603_20	140.48	101.25	97.94	75.63	Lherzolite	
X2603_21	80.95	72.19	87.39	90.00	Granitoid	
X2603_22	1271.43	1225.00	1416.67	1109.38	Dolerite	
X2603_23	188.10	155.63	172.22	145.31	Granitoid	
X2603_24	24.38	21.69	27.11	29.38	Carbonatite	
X2603_25	152.86	140.63	176.67	181.88	Granitoid	
X2603_26	200.48	160.31	172.78	141.56	Dolerite	
X2603_27	80.00	59.06	66.67	55.94	Carbonatite	
X2603_28	193.81	158.75	176.11	149.06	Granitoid	
X2603_29	305.71	203.44	188.89	134.06	Iron Ore	

Sample ID	Er*	Tm*	Yb*	Lu*	Rock Type (Belousova)	Ternary Cat.
X2603_30	82.86	58.75	60.44	48.13	Iron Ore	
X2603_31	173.81	124.38	121.67	85.63	Iron Ore	
X2603_32	180.00	141.88	145.00	108.75	Dolerite	
X2603_33	147.14	111.88	111.11	82.19	Iron Ore	
Upper Mississippi River (Northern)						
X2701_1	147.14	112.19	120.56	101.25	Granitoid	14
X2701_2	2042.86	1796.88	1966.67	1518.75	Jacupirangite	5
X2701_3	350.48	238.13	225.00	171.88	Granitoid	5
X2701_4	322.38	246.56	250.56	200.63	Granitoid	12
X2701_5	68.10	60.63	75.00	70.31	Granitoid	15
X2701_6	305.71	207.50	198.33	152.50	Granitoid	2
X2701_7	79.90	71.56	75.17	60.31	Dolerite	16
X2701_8	254.29	168.13	158.89	116.25	Iron Ore	14
X2701_9	36.43	29.38	33.72	30.59	Granitoid	4
X2701_10	447.62	308.13	273.89	187.81	Iron Ore	5
X2701_11	15.48	10.09	10.33	8.38	Carbonatite	16
X2701_13	317.62	252.50	277.78	254.38	Granitoid	6
X2701_14	230.48	187.19	213.33	226.88	Granite Pematite	14
X2701_15	122.86	93.75	105.56	99.38	Granitoid	4
X2701_16	27.71	21.00	26.28	34.13	Granitoid	8
X2701_17	138.10	98.13	101.11	84.06	Lherzolite	16
X2701_18	135.24	110.31	123.89	122.81	Granitoid	7
X2701_19	1376.19	1128.13	1172.22	846.88	Granite Pematite	10
X2701_20	66.67	50.00	54.78	43.91	Granitoid	15
X2701_21	13.00	13.56	16.56	17.72	Carbonatite	16
X2701_22	78.57	54.06	50.56	36.09	Carbonatite	16
X2701_23	704.76	568.75	673.89	640.63	Granitoid	10
X2701_24	25.38	20.41	25.00	25.00	Carbonatite	16
X2701_25	157.14	121.25	132.22	112.19	Dolerite	15
X2701_26	147.62	113.13	122.22	112.50	Granitoid	13
X2701_27	93.33	77.50	87.78	86.25	Granitoid	15
X2701_30	127.14	95.94	103.89	84.06	Granitoid	13
X2701_31	33.14	26.69	30.44	30.38	Carbonatite	16
X2701_32	155.24	89.38	74.44	48.44	Granitoid	7
X2701_33	504.76	390.63	383.33	308.13	Granite Pematite	10
X2701_34	419.05	336.25	319.44	242.81	Granite Pematite	10
X2701_35	126.19	98.75	111.67	100.94	Dolerite	8
X2701_36	20.52	13.41	14.44	13.72	Carbonatite	9
X2701_37	37.52	26.28	27.67	23.13	Carbonatite	16
X2701_38	29.90	19.69	20.44	16.06	Carbonatite	9
X2701_39	255.24	190.63	193.89	144.06	Iron Ore	7
X2701_40	126.19	94.38	101.28	100.63	Granitoid	7
X2701_41	341.90	271.25	279.44	216.56	Granite Pematite	12
X2701_42	399.05	344.69	395.56	319.69	Granite Pematite	11
X2701_43	261.43	233.13	273.89	231.88	Granite Pematite	11
X2701_44	83.33	55.00	50.83	42.50	Granitoid	8

Sample ID	Er*	Tm*	Yb*	Lu*	Rock Type (Belousova)	Ternary Cat.
X2701_45	99.52	76.88	87.78	78.13	Granitoid	15
X2701_46	70.95	49.28	49.89	40.31	Dolerite	9
X2701_47	126.19	93.75	98.33	81.56	Granitoid	13
X2701_1	518.10	354.38	340.00	296.88	Granitoid	5
X2701_2	118.10	107.81	138.33	138.75	Jacupirangite	8
X2701_3	50.95	40.66	45.78	38.25	Granitoid	4
X2701_4	42.19	30.94	31.67	28.44	Granitoid	8
X2701_5	477.62	465.63	595.00	448.13	Granitoid	10
X2701_6	610.95	430.00	402.22	305.31	Granitoid	10
X2701_7	72.86	56.56	71.39	70.63	Dolerite	3
X2701_8	400.00	290.31	265.00	175.94	Iron Ore	12
X2701_9	43.52	35.34	40.83	38.75	Granitoid	16
X2701_10	26.29	19.94	21.28	18.69	Iron Ore	16
X2701_11	132.86	86.88	82.78	60.63	Carbonatite	3
X2701_12	273.33	203.13	206.11	147.19	Larvikite	3
X2701_14	25.24	16.31	19.44	16.44	Granite Pematite	16
X2701_15	135.24	103.75	114.44	101.56	Granitoid	13
X2701_16	99.05	80.94	93.33	85.00	Granitoid	7
X2701_17	121.90	99.06	106.67	86.88	Lherzolite	14
X2701_19	111.90	90.94	106.67	103.13	Granite Pematite	7
X2701_20	717.14	590.63	622.78	438.75	Granitoid	10
X2701_21	109.52	90.94	112.22	106.56	Carbonatite	7
X2701_22	580.00	381.25	325.00	210.63	Carbonatite	10
X2701_25	217.14	164.69	180.56	157.19	Dolerite	12
X2701_27	30.67	22.94	27.33	25.91	Granitoid	16
X2701_28	227.62	186.25	214.44	200.63	Granite Pematite	12
X2701_29	23.43	16.63	17.72	17.13	Carbonatite	16
X2701_30	62.10	46.94	49.22	41.34	Granitoid	16
X2701_31	43.38	35.63	37.00	32.50	Carbonatite	16
X2701_32	773.81	586.56	601.67	441.25	Granitoid	5
X2701_34	40.19	31.41	37.61	33.34	Granite Pematite	16
X2701_36	36.43	27.72	35.00	38.13	Carbonatite	4
X2701_37	135.71	95.94	97.78	67.19	Carbonatite	13
X2701_38	800.00	600.00	607.78	455.31	Carbonatite	11
X2701_39	352.86	308.75	386.67	343.75	Iron Ore	11
X2701_40	619.05	490.63	519.44	428.75	Granitoid	10
X2701_41	65.48	45.16	47.06	36.38	Granite Pematite	9
X2701_42	142.86	123.75	147.78	126.25	Granite Pematite	13
X2701_43	136.67	118.75	135.56	118.13	Granite Pematite	14
X2701_44	119.05	70.94	61.17	38.44	Granitoid	15
X2701_45	28.62	16.34	17.61	13.31	Granitoid	9
X2701_46	115.24	88.13	101.11	85.00	Dolerite	15
X2701_47	980.95	868.75	977.78	740.63	Granitoid	10
X2701_48	402.86	212.50	166.67	109.38	Iron Ore	10
Missouri River (Missouri)						
X2703a_1	83.05	68.13	79.06	85.31	Granitoid	8

Sample ID	Er*	Tm*	Yb*	Lu*	Rock Type (Belousova)	Ternary Cat.
X2703a_2	265.24	203.44	208.89	171.88	Dolerite	8
X2703a_3	129.52	99.69	102.50	88.75	Granitoid	4
X2703_1	132.38	102.50	95.56	75.63	Dolerite	15
X2703_2	590.48	409.38	365.00	266.25	Granite Pematite	10
X2703_3	237.14	175.63	168.89	126.56	Lherzolite	16
X2703_4	311.43	237.50	223.89	171.56	Iron Ore	8
X2703_5	140.95	104.06	100.56	75.31	Carbonatite	15
X2703_6	279.52	219.69	222.78	176.56	Dolerite	4
X2703_7	348.57	259.38	248.33	191.25	Larvikite	2
X2703_8	197.62	147.19	148.89	121.56	Iron Ore	8
X2703_9	241.43	184.38	185.00	131.25	Dolerite	15
X2703_10	287.62	257.50	297.78	276.25	Granitoid	12
X2703_11	150.95	115.00	113.89	88.13	Dolerite	8
X2703_12	247.62	219.38	256.67	238.44	Granitoid	7
X2703_13	866.67	640.63	569.44	373.44	Granite Pematite	10
X2703_14	230.48	177.19	177.78	146.56	Iron Ore	4
X2703_15	51.81	36.31	35.39	26.09	Lherzolite	16
X2703_16	20.86	16.91	18.67	19.16	Carbonatite	16
X2703_17	695.24	555.00	600.00	492.19	Granitoid	2
X2703_18	93.81	71.56	68.33	57.19	Carbonatite	9
X2703_19	88.10	65.00	67.50	56.88	Dolerite	9
X2703_20	204.76	162.81	180.56	166.25	Granitoid	13
X2703_21	194.29	140.63	152.22	125.31	Larvikite	4
X2703_22	229.52	187.19	207.78	188.75	Granitoid	13
X2703_23	196.67	150.00	156.11	119.06	Iron Ore	8
X2703_24	129.05	91.25	89.44	69.38	Dolerite	9
X2703_25	133.33	84.38	70.94	46.88	Dolerite	16
X2703_26	125.71	100.31	103.33	82.19	Iron Ore	8
X2703_27	283.33	224.69	246.11	213.75	Iron Ore	12
X2703_28	374.76	238.13	211.67	143.44	Iron Ore	11
X2703_29	130.48	95.00	98.33	73.75	Dolerite	15
X2703_30	98.10	72.81	82.28	65.31	Dolerite	9
X2703_31	111.90	88.44	100.00	84.38	Iron Ore	8
X2703_32	146.67	118.75	149.44	150.63	Granitoid	7
X2703_33	235.24	114.06	106.11	63.75	Jacupirangite	1
X2703_34	61.14	46.25	59.78	59.38	Granitoid	3
X2703_35	105.24	87.19	107.22	100.00	Granitoid	7
X2703_36	876.19	837.50	1055.56	787.50	Granitoid	11
X2703_37	586.67	525.63	686.67	590.63	Granite Pematite	10
X2703_38	130.48	96.88	111.11	84.69	Iron Ore	8
X2703_1	104.29	90.31	118.33	133.44	Dolerite	7
X2703_2	270.00	195.94	190.56	140.00	Granite Pematite	9
X2703_3	303.81	247.81	242.22	197.19	Lherzolite	13
X2703_4	34.29	28.03	34.94	41.25	Iron Ore	16
X2703_5	78.57	64.38	68.06	71.56	Carbonatite	4
X2703_6	115.71	91.25	93.89	76.88	Dolerite	15
X2703_7	147.14	111.56	115.00	89.69	Larvikite	15

Sample ID	Er*	Tm*	Yb*	Lu*	Rock Type (Belousova)	Ternary Cat.
X2703_8	228.57	182.19	196.67	165.00	Iron Ore	6
X2703_9	257.14	189.06	169.44	121.56	Dolerite	16
X2703_10	112.38	96.56	110.00	118.13	Granitoid	12
X2703_11	88.57	73.13	86.11	92.19	Dolerite	12
X2703_12	62.43	53.03	61.00	67.22	Granitoid	14
X2703_13	319.05	239.38	230.56	189.38	Granite Pematite	13
X2703_14	195.71	162.81	173.89	149.06	Iron Ore	1
X2703_15	326.19	246.88	243.33	187.81	Lherzolite	3
X2703_16	608.10	484.38	481.67	355.31	Carbonatite	2
X2703_17	285.71	213.44	204.44	152.50	Granitoid	12
X2703_18	135.71	127.50	160.00	173.75	Carbonatite	13
X2703_19	46.10	34.13	35.83	40.94	Dolerite	16
X2703_20	141.90	104.06	102.22	78.44	Granitoid	15
X2703_21	457.14	418.75	440.00	322.50	Larvikite	10
X2703_22	110.48	78.13	77.22	65.63	Granitoid	8
X2703_23	48.00	35.69	39.94	33.16	Iron Ore	16
X2703_24	112.86	80.31	77.78	61.88	Dolerite	8
X2703_25	270.95	212.50	213.33	172.19	Dolerite	4
X2703_26	271.43	226.88	243.89	217.81	Iron Ore	7
X2703_27	600.00	496.88	491.67	331.25	Iron Ore	11
X2703_28	54.29	60.94	89.44	110.63	Iron Ore	4
X2703_29	566.67	434.38	445.56	353.13	Dolerite	5
X2703_30	165.24	123.13	130.94	108.13	Dolerite	4
X2703_31	117.62	87.50	91.67	79.06	Iron Ore	8
X2703_32	294.29	207.81	197.22	142.19	Granitoid	15
X2703_33	448.57	329.06	320.56	245.31	Jacupirangite	7
X2703_34	260.95	221.88	272.22	275.63	Granitoid	5
X2703_35	292.86	220.94	226.67	181.25	Granitoid	3
X2703_36	111.43	91.88	104.44	93.13	Granitoid	4
X2703_37	93.76	78.00	90.33	90.94	Granite Pematite	3
X2703_38	800.00	575.00	521.11	371.88	Iron Ore	11
X2703_39	63.95	46.25	45.00	38.13	Dolerite	3
X2703_40	179.05	129.38	131.67	95.00	Iron Ore	15
X2703_41	140.95	109.38	119.44	102.81	Granitoid	8
X2703_42	1714.29	1581.25	1755.56	1343.75	Larvikite	10
X2703_43	67.62	53.44	59.44	63.75	Granitoid	4
X2703_44	187.62	146.88	153.89	129.06	Dolerite	15
X2703_45	252.38	182.19	188.33	142.81	Dolerite	9
X2703_46	169.05	124.38	126.11	95.31	Larvikite	4
X2703_47	1333.33	1203.13	1316.67	1056.25	Granite Pematite	10
X2703_48	260.48	194.06	193.33	149.38	Iron Ore	8
X2703_49	704.76	478.13	392.78	281.88	Iron Ore	11
X2703_50	84.76	61.25	65.56	55.63	Iron Ore	8
X2703_51	201.90	166.88	185.00	164.69	Iron Ore	4
Miss. S. of Illinois, Missouri, and Upper Miss. (not used in study)						
X2704_1	237.14	180.63	190.56	140.31	Iron Ore	

Sample ID	Er*	Tm*	Yb*	Lu*	Rock Type (Belousova)	Ternary Cat.
X2704_2	115.71	74.06	68.39	47.09	Lherzolite	
X2704_3	179.52	131.25	130.56	106.88	Granitoid	
X2704_4	605.24	450.31	403.33	259.06	Dolerite	
X2704_5	10.00	7.25	7.57	7.66	Carbonatite	
X2704_6	58.00	48.41	53.72	61.88	Granitoid	
X2704_7	111.43	84.69	86.39	64.06	Dolerite	
X2704_8	142.38	114.06	118.89	97.50	Iron Ore	
X2704_9	330.00	271.25	267.78	176.56	Granite Pematite	
X2704_10	141.43	135.00	161.67	145.63	Granitoid	
X2704_11	228.57	183.75	179.44	128.75	Granitoid	
X2704_12	857.62	765.63	751.67	499.06	Granite Pematite	
X2704_13	1171.43	978.13	927.78	634.38	Granite Pematite	
X2704_14	957.14	806.25	834.44	537.50	Granite Pematite	
X2704_15	71.29	51.78	54.06	41.66	Dolerite	
X2704_16	91.14	65.22	70.72	57.22	Iron Ore	
X2704_17	45.57	31.50	36.11	29.00	Iron Ore	
X2704_18	241.90	160.31	168.33	118.44	Dolerite	
X2704_19	535.71	355.00	356.67	223.75	Iron Ore	
X2704_20	709.52	490.00	551.67	459.69	Granite Pematite	
X2704_21	163.33	109.06	121.11	89.69	Iron Ore	
X2704_22	68.48	43.06	47.33	34.78	Carbonatite	
X2704_23	131.05	90.00	102.56	81.25	Granite Pematite	
X2704_24	64.33	49.59	65.00	56.25	Carbonatite	
X2704_25	158.10	124.06	158.33	129.38	Iron Ore	
X2704_26	192.86	133.44	158.89	116.56	Iron Ore	
X2704_27	48.33	35.03	44.67	41.81	Dolerite	
X2704_28	49.76	37.06	46.17	42.69	Granitoid	
X2704_29	146.19	94.38	101.67	71.56	Dolerite	
X2704_30	20.24	13.78	18.83	19.28	Carbonatite	
X2704_31	242.38	178.75	205.56	158.44	Iron Ore	
X2704_32	168.57	117.19	126.67	88.75	Dolerite	
X2704_33	390.48	344.06	435.00	361.56	Granitoid	
X2704_34	105.71	88.75	115.00	103.13	Iron Ore	
X2704_35	31.57	25.91	29.89	29.09	Dolerite	
X2704_36	96.24	70.94	68.72	50.91	Granitoid	
X2704_37	78.76	57.97	59.33	45.09	Dolerite	
X2704_38	168.10	147.50	170.00	141.56	Granitoid	
X2704_39	439.05	328.13	319.44	233.44	Iron Ore	
X2704_40	1371.43	1068.75	991.67	694.06	Granite Pematite	
Illinois River (Northern)						
X2705_1	99.52	94.38	123.89	118.75	Granitoid	14
X2705_2	150.48	112.50	115.00	86.88	Dolerite	8
X2705_3	260.00	179.38	154.44	87.19	Dolerite	14
X2705_4	107.14	58.75	53.56	35.63	Lherzolite	15
X2705_6	1038.10	1037.50	1255.56	959.38	Granite Pematite	10
X2705_8	175.24	138.44	151.67	120.31	Dolerite	13

Sample ID	Er*	Tm*	Yb*	Lu*	Rock Type (Belousova)	Ternary Cat.
X2705_9	45.24	35.63	38.06	29.69	Dolerite	14
X2705_11	165.24	139.38	158.33	135.63	Granitoid	13
X2705_12	21.24	19.66	23.39	22.66	Carbonatite	16
X2705_13	25.81	19.19	21.06	19.88	Granitoid	16
X2705_14	102.86	73.13	77.78	62.81	Iron Ore	8
X2705_15	235.24	193.13	227.22	186.88	Jacupirangite	3
X2705_16	1371.43	1115.63	1177.78	806.25	Granitoid	10
X2705_18	51.33	41.53	47.50	43.06	Granitoid	14
X2705_20	57.14	42.81	43.78	33.72	Granite Pematite	14
X2705_21	16.90	12.25	13.44	11.94	Carbonatite	16
X2705_22	40.10	30.16	32.56	28.97	Carbonatite	16
X2705_23	654.76	504.69	486.67	329.69	Granite Pematite	10
X2705_24	1300.00	1018.75	1061.11	768.75	Jacupirangite	14
X2705_25	23.24	15.19	12.83	7.78	Carbonatite	16
X2705_27	100.10	126.25	183.89	182.50	Granite Pematite	14
X2705_29	206.67	150.00	151.39	115.94	Granitoid	11
X2705_30	1128.57	1090.63	1250.00	843.75	Granite Pematite	10
X2705_31	170.48	126.56	125.56	90.00	Granitoid	13
X2705_32	191.43	167.50	210.00	198.13	Granitoid	6
X2705_33	47.67	38.56	48.94	55.63	Dolerite	15
X2705_34	138.57	101.88	97.22	71.25	Granitoid	13
X2705_35	76.67	60.31	66.83	59.06	Granitoid	16
X2705_36	139.05	117.50	127.78	104.06	Granite Pematite	14
X2705_37	256.19	195.63	202.22	140.31	Dolerite	7
X2705_38	594.29	506.25	538.33	344.06	Iron Ore	10
X2705_39	167.62	120.31	115.56	66.88	Larvikite	4
X2705_40	168.57	135.00	147.22	116.56	Granitoid	15
X2705_41	645.24	540.63	571.67	381.56	Granite Pematite	10
X2705_42	45.90	39.06	48.33	53.44	Granitoid	8
X2705_44	44.57	30.03	30.06	27.16	Granitoid	9
X2705_45	170.95	161.88	195.00	155.94	Granite Pematite	12
X2705_47	269.05	167.81	166.11	111.88	Lherzolite	9
X2705_48	712.86	543.75	522.22	347.50	Granite Pematite	10
X2705_49	243.81	170.94	166.11	121.56	Dolerite	7
X2705_50	70.33	66.25	84.61	83.44	Dolerite	13
X2705_51	105.71	80.63	83.44	71.25	Granite Pematite	14
X2705_52	249.52	185.63	177.22	126.56	Dolerite	7
X2705_53	40.62	17.22	14.67	9.50	Dolerite	4
X2705_54	34.52	25.81	30.83	31.19	Carbonatite	9
X2705_55	200.48	164.06	175.56	146.88	Granite Pematite	12
X2705_56	138.57	95.00	92.78	65.63	Larvikite	3
X2705_57	211.43	149.69	144.44	101.25	Dolerite	7
X2705_58	271.90	215.63	220.00	163.13	Iron Ore	15
X2705_59	92.38	71.88	81.11	75.31	Granitoid	7
X2705_60	6.38	4.50	4.84	4.47	Carbonatite	16
X2705_1	47.19	36.25	41.28	36.53	Granitoid	9
X2705_2	100.95	94.69	123.89	126.25	Dolerite	13

Sample ID	Er*	Tm*	Yb*	Lu*	Rock Type (Belousova)	Ternary Cat.
X2705_3	200.95	177.81	206.67	188.44	Dolerite	12
X2705_4	949.52	748.44	793.89	555.63	Lherzolite	10
X2705_5	165.24	113.44	110.22	81.25	Dolerite	13
X2705_6	354.76	320.00	402.78	392.19	Granite Pematite	2
X2705_7	440.00	347.81	395.00	354.06	Jacupirangite	14
X2705_8	113.00	87.19	91.50	75.63	Dolerite	6
X2705_9	129.52	104.06	112.78	93.44	Dolerite	4
X2705_11	20.57	16.50	19.72	22.50	Granitoid	15
X2705_12	778.57	539.06	493.33	339.38	Carbonatite	5
X2705_13	218.10	168.13	194.44	199.38	Granitoid	11
X2705_14	21.48	15.25	17.11	19.81	Iron Ore	16
X2705_15	576.67	469.69	472.78	319.06	Jacupirangite	10
X2705_16	132.38	92.19	86.83	68.00	Granitoid	13
X2705_17	1885.71	1637.50	1838.89	1315.63	Granitoid	10
X2705_18	620.48	469.06	471.11	338.44	Granitoid	5
X2705_19	199.05	138.44	133.11	97.50	Dolerite	7
X2705_20	260.00	225.00	256.67	195.00	Granite Pematite	11
X2705_21	1414.29	799.69	617.78	429.38	Carbonatite	10
X2705_22	122.38	101.56	118.89	107.19	Carbonatite	3
X2705_23	177.14	129.38	128.33	97.81	Granite Pematite	14
X2705_24	161.43	156.25	201.67	212.50	Jacupirangite	7
X2705_25	177.62	166.25	217.78	204.69	Carbonatite	6
X2705_26	879.52	710.63	810.56	756.25	Jacupirangite	5
Ohio River (Ohio)						
X2801_1	139.05	109.69	115.00	83.75	Lherzolite	15
X2801_2	262.38	216.56	233.89	185.00	Granitoid	6
X2801_3	104.76	83.44	93.89	92.81	Granitoid	14
X2801_5	132.38	121.88	145.00	130.63	Granitoid	8
X2801_6	187.14	151.88	161.67	135.94	Granite Pematite	12
X2801_7	210.00	174.38	193.89	169.69	Granitoid	12
X2801_8	305.71	224.38	228.33	173.75	Dolerite	
X2801_9	690.48	556.25	570.00	439.69	Granite Pematite	10
X2801_10	62.33	50.94	58.17	62.19	Dolerite	8
X2801_11	381.43	345.31	421.11	371.88	Granite Pematite	10
X2801_12	657.14	537.50	594.44	565.63	Larvikite	2
X2801_14	87.62	67.81	74.44	62.19	Granitoid	14
X2801_15	67.14	50.31	56.11	49.06	Iron Ore	16
X2801_16	19.81	17.25	22.17	30.31	Carbonatite	15
X2801_17	607.14	487.50	503.89	355.63	Granite Pematite	10
X2801_18	155.24	50.94	35.28	22.38	Iron Ore	12
X2801_19	182.86	167.19	233.89	275.00	Granitoid	7
X2801_20	933.33	640.63	563.89	355.00	Dolerite	10
X2801_21	619.05	450.00	462.78	353.13	Jacupirangite	5
X2801_22	24.29	18.28	19.50	16.19	Carbonatite	16
X2801_23	723.81	575.00	583.33	406.25	Granite Pematite	10
X2801_24	49.00	44.69	55.56	61.88	Iron Ore	1

Sample ID	Er*	Tm*	Yb*	Lu*	Rock Type (Belousova)	Ternary Cat.
X2801_25	871.43	818.75	944.44	737.50	Granite Pematite	10
X2801_26	861.90	828.13	1000.00	737.50	Granite Pematite	10
X2801_27	83.81	67.19	77.22	71.25	Granitoid	15
X2801_28	81.90	79.38	94.44	86.56	Carbonatite	16
X2801_29	362.86	302.50	350.56	356.25	Dolerite	11
X2801_30	328.57	251.56	266.11	214.38	Granitoid	11
X2801_31	44.86	37.81	46.00	46.88	Carbonatite	15
X2801_32	467.14	437.81	541.11	553.13	Granitoid	11
X2801_33	192.38	123.44	107.22	74.06	Iron Ore	14
X2801_34	115.24	107.81	126.11	129.69	Dolerite	13
X2801_35	3.77	3.63	4.84	4.25	Lherzolite	16
X2801_36	80.48	63.44	74.44	72.19	Granitoid	15
X2801_37	4.19	3.66	4.61	5.50	Carbonatite	16
X2801_38	623.81	540.63	579.44	443.75	Granitoid	11
X2801_39	780.95	600.00	620.00	475.00	Jacupirangite	11
X2801_40	89.05	69.69	71.11	57.81	Granitoid	16
X2801_41	101.43	72.81	72.22	58.44	Granitoid	4
X2801_42	54.81	47.19	60.56	69.69	Dolerite	14
X2801_43	666.67	537.50	560.00	475.00	Granite Pematite	10
X2801_44	80.95	68.75	78.33	71.56	Granitoid	7
X2801_45	102.86	86.88	97.22	73.13	Iron Ore	3
X2801_46	400.95	295.63	289.44	217.50	Granitoid	6
X2801_1	144.76	114.69	132.78	120.94	Lherzolite	14
X2801_2	110.00	83.13	89.89	74.06	Granitoid	4
X2801_3	1723.81	1156.25	1027.78	665.63	Granitoid	10
X2801_4	570.95	465.31	492.22	358.13	Granite Pematite	10
X2801_5	102.38	90.31	117.78	128.44	Granitoid	4
X2801_6	1404.76	1287.50	1483.33	1165.63	Granite Pematite	10
X2801_7	47.76	40.34	44.78	37.53	Granitoid	15
X2801_8	140.00	118.75	136.67	114.69	Dolerite	6
X2801_9	23.71	21.97	27.39	29.03	Granite Pematite	16
X2801_10	261.43	210.00	233.89	224.06	Dolerite	6
X2801_11	829.05	837.50	1062.22	931.25	Granite Pematite	6
X2801_12	481.43	384.69	399.44	329.69	Larvikite	10
X2801_13	187.14	129.38	126.11	89.38	Dolerite	13
X2801_14	336.19	255.63	288.33	247.19	Granitoid	4
X2801_15	525.71	416.56	413.89	294.06	Iron Ore	11
X2801_16	470.00	363.44	386.11	312.19	Carbonatite	11
X2801_17	253.81	227.81	273.33	239.38	Granite Pematite	12
X2801_18	333.81	251.25	257.78	201.25	Iron Ore	12
X2801_19	95.71	76.25	82.94	79.69	Granitoid	16
X2801_20	653.81	518.13	551.67	443.75	Dolerite	6
X2801_21	329.05	330.00	398.33	335.63	Jacupirangite	12
X2801_22	19.52	17.59	21.94	23.88	Carbonatite	16
X2801_23	228.57	179.06	182.78	156.88	Granite Pematite	12
X2801_24	351.43	285.00	316.11	288.75	Iron Ore	11
X2801_25	1100.00	781.25	730.56	544.69	Granite Pematite	5

Sample ID	Er*	Tm*	Yb*	Lu*	Rock Type (Belousova)	Ternary Cat.
X2801_26	470.48	393.75	442.78	373.44	Granite Pematite	12
X2801_27	790.48	637.50	693.33	537.50	Granitoid	10
X2801_28	59.48	12.56	15.11	11.06	Carbonatite	3
X2801_29	383.81	264.69	267.22	231.25	Dolerite	12
X2801_30	599.05	459.69	500.56	385.31	Granitoid	11
X2801_31	1171.43	840.63	788.33	556.25	Carbonatite	5
X2801_32	92.86	82.19	93.72	82.81	Granitoid	7
X2801_33	99.05	87.50	101.11	84.06	Iron Ore	8
X2801_34	230.95	179.06	185.56	142.81	Dolerite	5
X2801_35	2266.67	1881.25	1972.22	1421.88	Lherzolite	10
X2801_36	592.38	454.06	454.44	342.50	Granitoid	11
X2801_37	64.24	18.75	16.83	10.16	Carbonatite	3
X2801_38	129.52	51.25	46.00	27.91	Granitoid	2
X2801_39	239.05	265.94	352.78	314.38	Jacupirangite	12
X2801_40	709.52	684.38	793.33	606.25	Granitoid	10
X2801_41	849.52	675.00	756.11	709.38	Granitoid	7

* Chondrite Normalized McDonough and Sun 1995

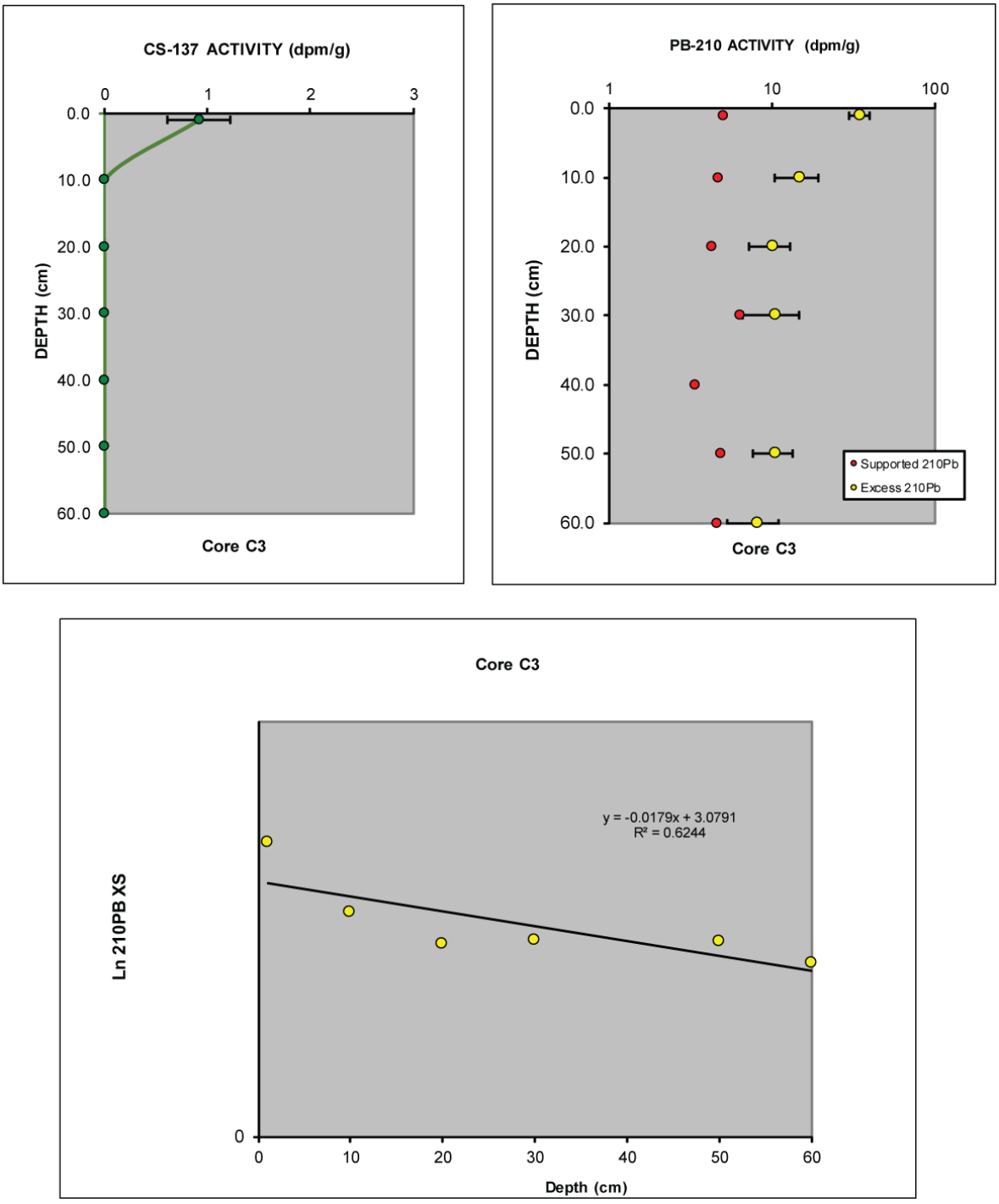

Supplemental Figure C. 1 Cross plots showing 137Cs and 210Pb calculations for dating in the core.

Supplementary Table C. 1 Core and Modern River Nd and Sr Isotope Data

Sample	87Sr/86Sr	143Nd/144Nd	Epsilon Nd	Depth (cm)
C3-1	0.725751181	0.512075	-10.98	10
C3-2	0.724688147	0.512090	-10.69	30
C3-3	0.724884264	0.512097	-10.55	40
C3-4	0.724128798	0.512113	-10.24	60
C3-5	0.724091177	0.512148	-9.56	66
C3-6	0.725066015	0.512123	-10.05	90
C3-7	0.724414154	0.512131	-9.89	113
C3-8	0.724641258	0.512108	-10.34	119
C3-9	0.724626915	0.512118	-10.14	140
C3-10	0.723807989	0.512110	-10.30	167
C3-11	0.723801565	0.512131	-9.89	200
C3-12	0.723740619	0.512117	-10.16	231
C3-13	0.72253604	0.512183	-8.88	250
C3-14	0.721784155	0.512142	-9.68	276
C3-15	0.723261727	0.512156	-9.40	291
C3-16	0.723478104	0.512142	-9.68	309
C3-17	0.724160	0.512133	-9.85	340
C3-18	0.72429619	0.512149	-9.54	365
C3-19	0.723374658	0.512133	-9.85	385
C3-20	0.724311652	0.512125	-10.01	410
C3-21	0.72358872	0.512162	-9.29	440
C3-22	0.723319019	0.512152	-9.48	463
C3-23	0.725126821	0.512162	-9.29	480
C3-24	0.724852414	0.512148	-9.56	489
South of Red	0.726496262	0.512091	-10.67	lat 30.98 lon-91.66
Red River	0.727298015	0.512165	-9.23	lat 31.21 lon -92.09
South of Arkansas	0.728882048	0.512062	-11.24	lat 35.51 lon -91.16
Arkansas River	0.726262146	0.512099	-10.51	lat 33.91 lon -91.25
South of Ohio	0.723443767	0.512104	-10.42	lat 36.95 lon -89.11
Upper Mississippi	0.725870704	0.511973	-12.97	lat 39.72 lon -91.35
Missouri River	0.722657507	0.512121	-10.09	lat 38.69 lon -90.66
South of Missouri	0.724720	0.512068	-11.12	lat 38.54 lon -90.25

Sample	87Sr/86Sr	143Nd/144Nd	Epsilon Nd	Depth (cm)
Illinois River	0.728380	0.512009	-12.27	lat 39.15 lon -90.62
Ohio River	0.732646494	0.512046	-11.55	lat 37.12 lon -88.13

Core to depth of 5m w __cm of compaction

NBS987 std 87Sr/86Sr=0.710240

JNdi-1 std 143Nd/144Nd=0.512104

CURRICULUM VITAE

Brittney Anne Gregory
75 Oak St. Mobile Al. 36608
email: brikkagr84@gmail.com

Education

2011 M. S. Geography, The University of North Texas Thesis title: Geologic and Lithic Analysis of the Red River Cache. Dr. Reid Ferring, advisor

2006 B. A. Applied Anthropology, University of North Texas

2019: PhD Geology and Geophysics, Louisiana State University

Professional Work Experience

2010-present Consulting geomorphologist-geoarchaeologist.

2008-2010 Teaching Assistant, Department of Geography, University of North Texas.

2006 Wenas Creek Mammoth Project (Dr. Pat Lubinski, Central Wahington Univeristy).

Regional Experience: Texas Rivers and Streams including the Guadalupe, San Antonio, Trinity, Colorado, and Brazos. Paleoindian coastal sites in Florida, Chihuahuan Desert including Fort Bliss, Trans-Pecos, and Lower Pecos. Southern Great Plains and periphery with work in South Eastern New Mexico and the Canadian Breaks. Loess landscapes on the Columbian Plateau in Central Washington and Idaho.

Research interests: Geoarchaeology, geomorphology, paleoenvironmental reconstruction, and fluvial geology.

Publications, Journal Articles, and Chapters in Edited Books

Rink, W. J., J. S. Dunbar, G. Doran, C.D. Frederick and B. Gregory
2012 Geoarchaeological investigations and OSL dating evidence in an Archaic and Palaeoindian at the Helen Blazes Site (8BR27), Brevard County, Florida. Florida Anthropologist 65(1-2): 87-107.

Contract and Project Reports

W. Nicholas Trierweiler, Brittney Gregory, Charles Frederick, and Jon Dowling
2013 Geoarcheological Investigations of the Henderson Street Borrow Pit in the Trinity River Floodplain, Tarrant County, Texas. Ammaterra Environmental, Inc. Report No. 44, Texas Antiquities Permit No. 6381. Austin, Texas

Quigg, J. Michael, Paul M. Matchen, Charles D. Frederick, Robert A. Ricklis, Brittney Gregory, David Maki and Mark Bateman, with contributions by J. Phil Dering, Jeffery R. Ferguson, Michael D. Glascock, Michelle Hamilton, Bruce L. Hardy, Mary E. Malainey, Linda Perry, David G. Robinson, M. Steven Shackley, Grant Smith, M. Kate Spradley, J. Byron Sudbury, Daniel J. Wescott, and Barbara Winsborough
2013 Long View (41RB112): Data Recovery of Two Plains Village Period Components In Roberts County, Texas. Volume I. TRC Project No. 174542, Texas Antiquities Committee Permit No. 3721. Austin, Texas.

Brittney Gregoryand Charles D. Frederick
2012 Geoarchaeological Observations From the Wharton Levee Project. In The Archaeological Survey of the Proposed Wharton Levee System in the City of Wharton, Wharton County (Draft Report), by Somers, B., D. Barnes, K. Ellzey. Manuscript submitted to Submitted to U.S. Corps of Engineers, Fort Worth District, Contract No. W9126G-09D-0067 Delivery Order 0058. Gulf South Research Corporation, Baton Rouge, Louisiana.

Hatfield, Virginia, Charles D. Frederick, Brittney Gregory, and Karl W. Kibler
2012 Archeological and geoarchaeological Investigations for the new Baylor University Football Stadium in Waco, McLennan County, Texas. Technical Report 88, Prewitt and Associates, Inc. Austin, Texas

Weinstein, Richard A., Charles D. Frederick, Timothy K. Perttula, Brittney Gregory, and Jennifer A. Kelly
2012 Archaeological and Geological Investigations at Site 41HM61, Hamilton County, Texas: Interim Report. Coastal Environments, Inc., Corpus Christi, Texas.

Frederick, C. D., Brittney Gregoryand Phillip Shelley
2011 Geomorphology. In The Boot Hill Site (LA 32229): An Oasis in the Desert, Eddy County, New Mexico, edited by Marie E. Brown, pp.77-98. TRC Environmental Inc., Albuquerque, New Mexico.

Frederick, Charles D. and Brittney Gregory
2010 Geoarchaeological Reconnaissance of the XS Ranch, Bastrop County Texas. Appendix B in Thornton, Meg, T. Miller, and M. Doty Freeman, Phase I Archeological Investigations of Portions of the XS Ranch Property, Bastrop County, Texas, USACE No: 2008-280. ACI consulting, Austin Texas.